



# Utilisation de la détection cohérente pour les systèmes de transmission optique à 40 GB/s ET 100 GB/s

Oriol Bertran Pardo

## ► To cite this version:

Oriol Bertran Pardo. Utilisation de la détection cohérente pour les systèmes de transmission optique à 40 GB/s ET 100 GB/s. Optique / photonique. Télécom ParisTech, 2010. Français. NNT: . pastel-00676633

HAL Id: pastel-00676633

<https://pastel.hal.science/pastel-00676633>

Submitted on 5 Mar 2012

**HAL** is a multi-disciplinary open access archive for the deposit and dissemination of scientific research documents, whether they are published or not. The documents may come from teaching and research institutions in France or abroad, or from public or private research centers.

L'archive ouverte pluridisciplinaire **HAL**, est destinée au dépôt et à la diffusion de documents scientifiques de niveau recherche, publiés ou non, émanant des établissements d'enseignement et de recherche français ou étrangers, des laboratoires publics ou privés.



Alcatel-Lucent



# Thèse

présentée pour obtenir le grade de Docteur  
de Télécom ParisTech

Spécialité : **Électronique et Communications**

Oriol Bertran-Pardo

On coherent detection for optical  
transmissions at 40 Gb/s and 100 Gb/s

Soutenue le 10 septembre 2010 devant le jury composé de

A. Bononi      Président

G. Bosco      Rapporteurs

P. Emplit

A. Bononi      Examinateurs

G. Rekaya

S. Bigo      Co-directeurs de thèse

Y. Jaouen

S. Gosselin      Invité



*Para chuaki, tete y mucho-mucho.*

*Cuatro excelentes compañeros de viaje*



*No te quedes inmóvil  
al borde del camino  
no congeles el júbilo  
no quieras con desgana  
no te salves ahora  
ni nunca  
no te salves  
no te llenes de calma  
no reserves del mundo  
sólo un rincón tranquilo  
no dejes caer los párpados  
pesados como juicios  
no te quedes sin labios  
no te duermas sin sueño  
no te pienses sin sangre  
no te juzgues sin tiempo*

*pero si  
pese a todo  
no puedes evitarlo  
y congelas el júbilo  
y quieras con desgana  
y te salvas ahora  
y te llenas de calma  
y reservas del mundo  
sólo un rincón tranquilo  
y dejas caer los párpados  
pesados como juicios  
y te secas sin labios  
y te duermes sin sueño  
y te piensas sin sangre  
y te juzgas sin tiempo  
y te quedas inmóvil  
al borde del camino  
y te salvas  
entonces  
no te quedes conmigo.*

*(Mario Benedetti, No te salves)*



*Quan surts per fer el viatge cap a Itaca,  
has de pregar que el camí sigui llarg,  
ple d'aventures, ple de coneixences.  
Has de pregar que el camí sigui llarg,  
que siguin moltes les matinades  
que entraràs en un port que els teus ulls ignoraven,  
i vagis a ciutats per aprendre dels que saben.*

*Tingues sempre al cor la idea d'Itaca.*

*Has d'arribar-hi, és el teu destí,  
però no forcis gens la travessia.*

*És preferible que duri molts anys,  
que siguis vell quan fondegis l'illa,  
ric de tot el que hauràs guanyat fent el camí,  
sense esperar que et doni més riqueses.*

*Itaca t'ha donat el bell viatge,  
sense ella no hauries sortit.*

*I si la trobes pobra, no és que Itaca  
t'hagi enganyat. Savi, com bé t'has fet,  
sabràs el que volen dir les Itaques.*

*Més lluny, heu d'anar més lluny  
dels arbres caiguts que ara us empresonen,  
i quan els haureu guanyat  
tingueu ben present no aturar-vos.*

*Més lluny, sempre aneu més lluny,  
més lluny de l'avui que ara us encadena.*

*I quan sereu deslliurats  
torneu a començar els nous passos.*

*Més lluny, sempre molt més lluny,  
més lluny del demà que ara ja s'acosta.*

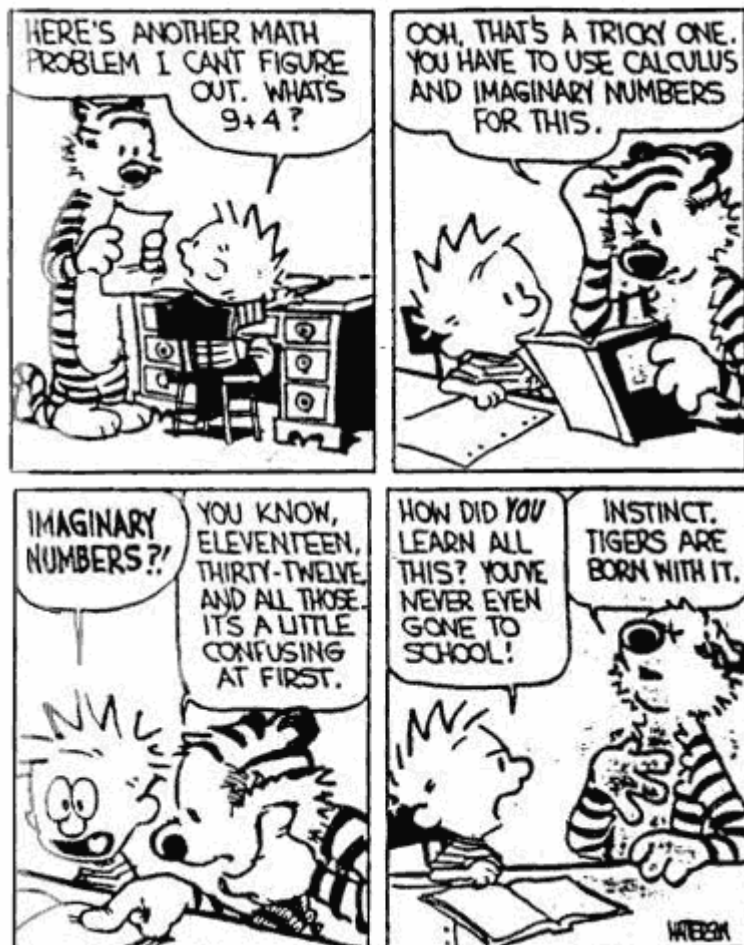
*I quan creieu que arribeu, sapigueu trobar noves sendes.*

*Bon viatge per als guerrers  
que al seu poble són fidels,  
afavoreixi el Déu dels vents  
el velam del seu vaixell,  
i malgrat llur vell combat  
tinguin plaer dels cossos més amants.*

*Omplin xarxes de volguts estels  
plens de ventures, plens de coneixences.*

*Bon viatge per als guerrers  
si al seu poble són fidels,  
el velam del seu vaixell  
afavoreixi el Déu dels vents,  
i malgrat llur vell combat  
l'amor ompli el seu cos generós,  
trobin els camins dels vells anhels,  
plens de ventures, plens de coneixences.*

*(Lluis Llach, El viatge a Itaca)*



« hai voluto la bicicletta, adesso pedala... »



# Contents

ACKNOWLEDGEMENTS.....	1
RÉSUMÉ .....	5
FOREWORD .....	19
LIST OF ACRONYMS AND SYMBOLS.....	23
LIST OF ACRONYMS.....	23
LIST OF SYMBOLS.....	26
CHAPTER 1. THE FIBRE-OPTIC TRANSMISSION CHANNEL.....	29
1.1. LINEAR TRANSMISSION EFFECTS.....	30
1.1.1 <i>Fibre attenuation</i> .....	30
1.1.2 <i>Chromatic dispersion</i> .....	32
1.1.3 <i>Polarisation mode dispersion</i> .....	35
1.1.4 <i>Polarisation dependent loss</i> .....	37
1.2. NONLINEAR TRANSMISSION EFFECTS .....	39
1.2.1 <i>Kerr effect</i> .....	39
1.2.2 <i>Self-phase modulation</i> .....	41
1.2.3 <i>Cross-phase modulation</i> .....	43
1.2.4 <i>Four wave mixing</i> .....	45
1.2.5 <i>Intra-channel cross-phase modulation and four-wave mixing</i> .....	46
1.2.6 <i>Cross-polarisation modulation</i> .....	47
1.2.7 <i>Nonlinear phase noise</i> .....	49
1.2.8 <i>Non-elastic scattering effects</i> .....	51
1.3. SUMMARY .....	52
CHAPTER 2. FIBRE-OPTIC COMMUNICATION SYSTEMS .....	55
2.1. TRANSMITTERS AND DIRECT-DETECTION RECEIVERS .....	56
2.1.1 <i>General transmitter and receiver aspects</i> .....	56
2.1.2 <i>On-off keying</i> .....	60
2.1.3 <i>Phase modulation formats</i> .....	62
2.1.4 <i>Return-to-zero pulse-shaping</i> .....	70
2.2. POLARISATION DIVISION MULTIPLEXING.....	72

2.2.1 Transmitter scheme .....	73
2.2.2 Noise sensitivity.....	75
2.3. WAVELENGTH DIVISION MULTIPLEXING .....	76
2.4. LOSS COMPENSATION .....	78
2.4.1 Erbium doped fibre amplifiers.....	78
2.4.2 Distributed Raman amplification.....	80
2.4.3 Optical signal to noise ratio evolution.....	82
2.4.4 Trade-off between noise and nonlinearities .....	84
2.5. CHROMATIC DISPERSION COMPENSATION .....	85
2.6. A LABORATORY TOOL: THE RECIRCULATING LOOP .....	87
2.7. SUMMARY .....	88
<b>CHAPTER 3. COHERENT DETECTION: THE COME-BACK.....</b>	<b>90</b>
3.1. RECEIVER SENSITIVITY .....	92
3.2. POLARISATION DIVERSITY COHERENT MIXER .....	94
3.3. DIGITAL SIGNAL PROCESSING ASSOCIATED TO COHERENT DETECTION .	98
3.4. SUMMARY .....	105
<b>CHAPTER 4. 40-GB/S SYSTEMS.....</b>	<b>106</b>
4.1. 40 GB/S PDM-QPSK .....	107
4.1.1 Experimental set up.....	108
4.1.2 Impact of polarisation multiplexing .....	109
4.1.3 Tolerance to intra and inter-channel nonlinearities.....	110
4.1.4 Containing inter-channel nonlinearities in WDM transmission...	111
4.2. 40 GB/S PDM-BPSK .....	115
4.2.1 Experimental set up and noise sensitivity .....	115
4.2.2 Impact of cross nonlinearities.....	116
4.2.3 Further insight on inter-channel nonlinearities: interplay between nonlinearities and PMD.....	119
4.2.4 Impact of dispersion map.....	123
4.3. COMPARISON AND SUMMARY.....	124
<b>CHAPTER 5. 100-GB/S SYSTEMS.....</b>	<b>127</b>
5.1. PDM-QPSK: WHY IS IT SUITABLE FOR 100 GB/S AND NOT FOR 40 GB/S?	128
5.1.1 Experimental set up.....	128
5.1.2 Nonlinear tolerance evolution with the symbol rate .....	128

5.2. UPGRADING LEGACY SYSTEMS .....	130
5.2.1 Experimental set up.....	130
5.2.2 Tolerance to nonlinear effects in homogenous WDM systems ....	132
5.2.3 Impact of inter-channel effects in hybrid WDM systems.....	133
5.2.4 Containing inter-channel nonlinearities in hybrid WDM systems	
135	
5.2.5 Further insight on XPolM: required number of channels .....	137
5.3. INTERPLAY BETWEEN NONLINEARITIES AND LUMPED PMD.....	139
5.3.1 Experimental set up.....	139
5.3.2 Impact of nonlinear effects.....	140
5.3.3 Impact of PMD in linear regime .....	140
5.3.4 Impact of PMD in nonlinear regime.....	141
5.4. INCREASING THE REACH OF 100 GB/S PDM-QPSK.....	143
5.5. SUMMARY AND FIELD TRIAL .....	145
<b>OUTLOOK AND CONCLUSIONS .....</b>	<b>149</b>
<b>APPENDICES .....</b>	<b>153</b>
A. BIT ERROR RATIO AND Q <sup>2</sup> FACTOR.....	153
B. CAPACITY INCREASE OF UNREPEATED SUBMARINE SYSTEMS USING 100 GB/S COHERENT PDM-QPSK.....	155
B.1 Experimental set up.....	155
B.2 Results.....	156
B.3 Summary .....	157
<b>BIBLIOGRAPHY .....</b>	<b>159</b>
<b>PUBLICATIONS .....</b>	<b>177</b>
AS FIRST AUTHOR .....	177
AS CO-AUTHOR .....	178



# **Acknowledgements**

*(un día cualquiera...)*

- 06.14 – suena el despertador. radio, ducha, desayuno, mochila. rer, bus. (suerte de los especialistas secundarios).
- 08.10 – llego al despacho. todo está en calma, silencioso, estático. curioso momento éste...
- 08.16 – patrice, le maître qui vient d’Okinawa, arrive le premier. comme d’habitude avec un grand sourire. quel plaisir travailler avec des gens comme ça qui gardent la bonne humeur tout le temps et qui ont toujours une (*i bonne?*) blague pour remonter le moral des troupes.
- 08.31 – mamá me envía un mail. “hola hijo, qué tal?”. siempre tan extensa. “muy bien y vosotros?”. “muy bien quim libra hoy e iremos a dar una vuelta esta tarde por cambrils. que tengas un buen día.”. “pasáoslo muy bien!”
- 08.59 – «¡¡HOMBRE!!» se sente nel corridoio. dopo sta esclamazione arriva la persona. alberto llega con su energía característica. lo que ayer a última hora eran solamente intuiciones en nuestras mentes, hoy son ecuaciones claras y comprensibles. y pensar que un día osó decir que habíamos aprendido mucho juntos! (si consideramos que él ha aportado el 99.99% contra 0.01% yo, quizá sea verdad...).
- 09.36 – maintenant c'est le tour de jérémie. il arrive avec sa veste de golfeur. avant de poser ses affaires il me dit une phrase caractéristique : “j’ai réfléchi à ce nous dissons hier et je pense que nous pourrions faire...”. il s’arrête jamais de réfléchir. alehop ! le point bloquant est parti et nous pouvons continuer nos manips.
- 09.59 – je croise jean pierre au couloir. à la place de bonjour, j’ai un sourire de taquinerie. et penser que j’ai été à l’autre bout de monde pour représenter bell labs!

10.01 – je suis au laboratoire. haïk entre dans la pièce. “tu te la donnes à wimbledon ? ”. psg ont perdu hier mais je me souviens de mon ananas... comme le gens dissent souvent, on a toujours besoin d'un petit haïk. il est vraiment pris aujourd’hui, la gestion du brevet n'a pas l'air facile. néanmoins, et comme toujours, il a dix minutes pour me donner un coup de main. ainsi nous serons en mesure de comparer ce qui est comparable.

10.38 – max entra en el laboratorio. “chi lascia la strada vecchia per la nuova, sa quel che lascia e non sa quel che trova”

10.41 – ummmmm... l'équipement du labo n'est pas suffisant pour la manip. j'appelle bruno (allez toulouse). c'est ok, il pourra nous donner un coup de main la semaine prochaine. nous en rediscussions dans l'après-midi.

11.50 – el temps passa molt ràpid quan s'està al laboratori. és hora d'anar a jugar a frisbee. per ser més seriosos, direm anar a jugar a ultimate. *l'ultimate est un sport qui se joue à 7 contre 7 et dans lequel gagne toujours gab.*

11.51 – en parlant de gab, il rentre au laboratoire. aux articles que nous voulions faire, il faut seulement ajouter une démo, une manip pour soutenir la business division et demain nous avons une audioconf pour laquelle il faut faire les slides avec les résultats d'avant-hier, qui d'ailleurs étaient un peu surprenants... par ailleurs, d'après lui, je dois changer de téléphone. il ne comprend pas comment j'arrive à supporter celui-ci. nous partons au firsbee.

12.15 – Thierry nous attend avec les clefs du vestiaire. aujourd’hui nous sommes nombreux. 2 équipes. d'un côté, gabriel, clemens, philippe, pascal, adrian, richard, francesco et la guest star : yann. de l'autre, laurent, jérémie, olivier, mathieu, yvan, ln, seb, arnaud, oriol. domage que sophie ne vient plus. afin de ne pas rompre la statistique, l'équipe de gab gagne.

13.00 – la mail de max. destinatarios: la belle cecile, marie, verónica, frais, donato, y un servidor. sólo faltaría marco.

*dans un premier temps il semblait s'agir d'une erreur d'estimation mais après avoir eu la confirmation des experts de l'observatoire de port royale à paris, une jolie ville dans la banlieue de massy, maintenant nous pouvons vous confirmer que c'est bien vendredi !*

*la découverte de [REDACTED] à long island ne nous empêchera pas de boire [REDACTED] notre cocktail préféré [REDACTED].*

*D'ailleurs, [REDACTED]*

*[REDACTED] on sait très bien [REDACTED] !*

*-8 hours...*

*Max*

*(ndr: ciertos elementos del mail han sido suprimidos para salvaguardar la integridad de las personas afectadas).*

- 14.06 – le fait d'avoir vue ln ce midi m'a fait penser que je n'ai pas des nouvelles de francis, nadine, pom-pom ni romanus. il faudra que je les appelle pour qu'ils viennent manger à la maison.
- 14.30 – réunion avec la business division. moment pour pouvoir discuter avec bruno, mathieu et christine, jean paul, dominique, hans, philippe & co.
- 15.36 – no sé ben bé perquè, però avui penso en la iaia. segur que li hagués agradat venir-me a veure a paris... bé, què hi farem? trucaré a valls aquest cap de setmana.
- 15.59 – vuelvo a cruzarme con max, “hai voluto la bicicletta? adesso, pedala!”. ¡qué filósofo!
- 16.02 – laurent passe me chercher pour prendre un café. ces moments de pause font du bien. on parle de tout, de frisbee et de gestion de projets européens.
- 17.20 – miro el móvil. *ochentaydós* mensajes. creo que éstos están fatal. bajo a casa en dos semanas pero me gustaría estar allí esta noche. hay cena. nada especial, sólo una cena entre amigos.
- 17.21 – recibo un mail de tete. “¿a qué hora llegas dentro de dos semanas?”. “a las 22.30. ¿será demasiado tarde? me gustaría cenar con el piti en barcelona”. como siempre, la respuesta: “ningún problema. te venimos a buscar dragón y yo, y vamos a cenar a barcelona con vosotros. ¿facturas maleta?” fácil. ¿para qué complicarse?
- 17.29 – “je pense que la journée va bientôt finir. elle est même déjà finie. je suis désolé mais je ne peux plus rien faire pour vous... ” à demain, patrice !
- 17.41 – nous allons soumettre un article bientôt. seb arrive avec les corrections. il y en a une d'inadmissible. j'ai écrit ‘in this paper, we study’ et j'aurais dû écrire ‘in this paper, we investigate’. heureusement qu'il y a quelqu'un rigoureux dans les parages ! Besides, we have good news. we have a jury: g. bosco, g. rekaya, a. bononi, p. emplit, s. gosselin, y. jaouen and s. bigo. thank you all for your time and attention!
- 18.36 – apareix fresc al laboratori. s'adona que els posters estan lleugerament torts. no diu res. podrà dormir? ha trobat com fer glaçons transparents, “vechio, ho letto un blog che...” ho provarem aquest cap de setmana amb una mica de half-half. ¿porqué últimamente cada vez que lo veo suena “la caja del diablo”?
- 20.02 – nous partons. jérémie m'amène au rer des baconnets. nous avons des problèmes pour sortir du site. il faudra qu'un jour nous demandions l'autorisation pour pouvoir sortir tard du site...
- 20.58 – entro en el patio de casa. hay luz en el piso. llamo a la ventana. me dirijo hacia la puerta. huele deliciosamente, marie está en casa. la puerta se abre. aparecen una sonrisa cálida y unos ojos alegres. ¡qué gozada! abrazo. beso. cruzo el umbral de la puerta. las preocupaciones se quedan fuera. cierro la puerta.
- “je pense que la journée va bientôt finir. elle est même déjà finie. je suis désolé mais je ne peux plus rien faire pour vous... ”*

*ha sido “un buen día”*

je saisis également cette opportunité pour remercier mes directeurs de thèse, yves et ghaya, ainsi que jean pierre et sébastien de m'avoir permis faire ma thèse dans ce cadre.

finalement, je tiens à remercier spécialement et explicitement les deux personnes les plus importantes pour moi pendant ces trois ans. la première est la personne grâce à laquelle j'ai plus appris. la deuxième, la personne qui m'a apporté la paix et l'équilibre nécessaire pour profiter au maximum de cette expérience. ces personnes sont jérémie renaudier et marie *waka-waka* guibert. moltíssimes gràcies a tots dos, us en dec una!

# Résumé

La transmission des données sur fibre optique a révolutionné le monde des télécommunications et a joué un rôle majeur dans l'avènement de l'ère de l'information en offrant des solutions permettant de soutenir l'explosion de la demande en bande passante induite par le développement de l'Internet et l'introduction du « world wide web ». Les estimations actuelles prévoient encore une augmentation soutenue du trafic de données de l'ordre de 50% par an pour les dix prochaines années.

Les fournisseurs de télécommunications emploient les systèmes de communication par fibre optique dans la plupart des réseaux dorsaux, régionaux et métropolitains pour répondre à ce besoin de capacité. Les systèmes de communication par fibre optique n'ont pas cessé d'évoluer depuis la première démonstration commerciale, transportant des données téléphoniques réelles, menée par la compagnie « General Telephone and Electronics » le 22 avril 1977. Différentes innovations clefs ont permis de surmonter progressivement les obstacles rencontrés, telles que :

- l'introduction des fibres monomodes,
- l'invention des amplificateurs à fibre dopée Erbium (EDFA) qui a permis le déploiement efficace des systèmes multiplexés en longueur d'onde (WDM),
- l'utilisation des codes correcteurs d'erreurs (FEC)
- et aussi, les techniques de gestion de dispersion chromatique.

Typiquement, les distances de transmission dans les réseaux métropolitains, régionaux et dorsaux sont de moins de 300 km, entre 300 et 1000 km, et plus de 1000 km, respectivement. Le travail de thèse décrit dans ce manuscrit se concentre sur les systèmes longue distance utilisés pour les réseaux dorsaux. La norme aujourd'hui dans les systèmes longue distance terrestres est d'utiliser des fibres monomodes, du multiplexage en longueur d'onde (WDM) avec un espacement spectral de 50 GHz entre canaux, lesquels sont simultanément amplifiés par un amplificateur optique

(typiquement EDFA), de la gestion de dispersion et des codes correcteurs d'erreurs. Ces systèmes peuvent généralement transporter jusqu'à 80 ou 100 canaux multiplexés en longueur d'onde, ce nombre étant principalement limité par la bande passante restreinte des amplificateurs optiques actuels.

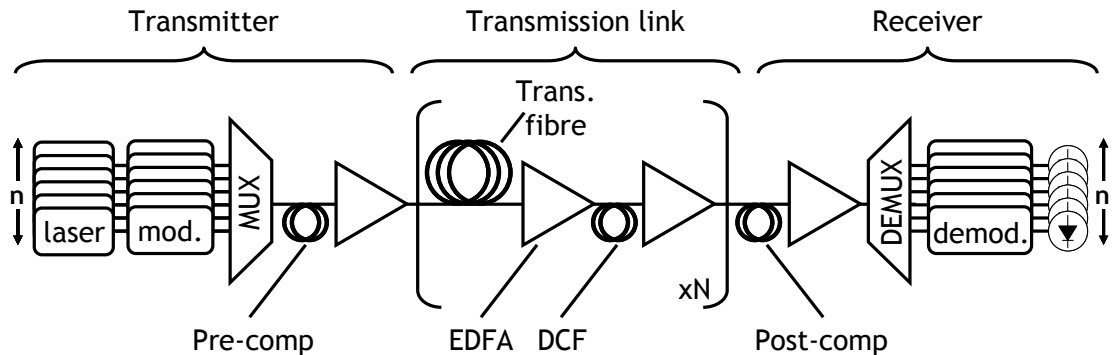


*Fig. a: Configuration typique des systèmes de communication par fibre optique longue distance.*

La modulation de l'intensité de la lumière combinée avec la détection directe a été la technique de référence pour les systèmes commerciaux de transmission par fibre optique jusqu'à récemment. Cette option combine des émetteurs et des récepteurs rentables avec une qualité de transmission suffisante pour des transmissions allant jusqu'à 10 Gb/s. Néanmoins, pour répondre à la demande incessante d'augmentation de la capacité, des débits plus élevés sont nécessaires, à savoir 40 et 100 Gb/s. Le défi est que la transmission par fibre optique devient généralement de plus en plus difficile avec l'augmentation du débit par canal car le rapport signal à bruit optique (OSNR) requis en fin de liaison augmente tandis que la robustesse face aux effets physiques (linéaires) de propagation, tels que la dispersion chromatique et la dispersion modale de polarisation (PMD), se réduit sévèrement. Dans ce contexte, de nombreuses études ont porté sur la modulation par déplacement de phase (PSK) combinée avec de la détection (directe-) différentielle durant les dix dernières années. Néanmoins, la tolérance aux effets linéaires de propagation est restée une des contraintes majeures pour le déploiement commercial. Ainsi, une solution en rupture, permettant d'augmenter la capacité totale transmise tout en étant robuste vis-à-vis des effets linéaires de propagation, a été nécessaire.

Parfois, les nouvelles solutions ne viennent pas de découvertes vraiment récentes mais de l'association innovante de technologies existantes. En effet, la détection cohérente optique fut proposée dans les années 1980 pour améliorer la sensibilité du récepteur. À cette époque, aucune pré-amplification optique n'était employée en amont du récepteur et la performance était principalement limitée par le bruit thermique des photodiodes et amplificateurs électriques. Ainsi, un oscillateur local beaucoup plus puissant que le signal permettait une amplification cohérente. Néanmoins, le développement des amplificateurs EDFA comme préamplificateur optique causa le déclin de l'intérêt pour la détection cohérente. Il a fallu attendre les progrès récents en électronique ultra-rapide, surtout en convertisseurs analogique-numérique, et le traitement du signal pour que la détection cohérente se révèle comme l'un des outils les plus puissants pour réaliser des transmissions optiques à haut débit.

En effet, les récepteurs cohérents fournissent l'amplitude, la phase et la polarisation du champ optique ce qui permet de profiter de l'excellente sensibilité au bruit optique associé à la détection homodyne, comme l'illustre la Fig. b, avec les avantages supplémentaires du traitement de signal avancé. Plus de détails concernant ce sujet et la définition du facteur  $Q^2$  (ou  $Q^2$  factor) sont mentionnés dans le Chapitre 3 et l'Annexe A, respectivement.

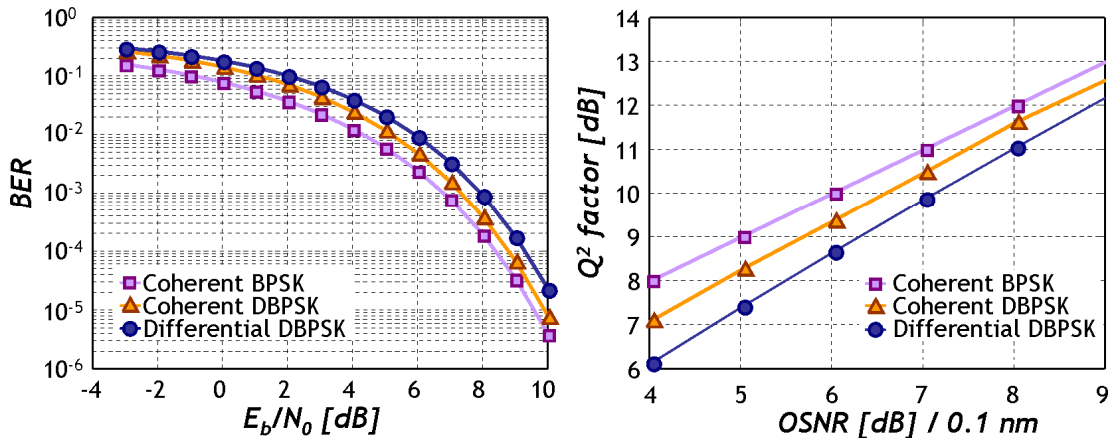


*Fig. b: Comparaison de la sensibilité au bruit d'un signal BPSK à 21.4 Gb/s détecté dans un détecteur cohérent ▲ avec et ■ sans décodage différentiel et ● détecté dans un récepteur différentiel avec décodage différentiel.*

Grâce aux techniques avancées de traitement de signal numérique, les récepteurs cohérents offrent aussi la possibilité d'opérer avec des oscillateurs locaux non-verrouillés en fréquence et de compenser les effets de propagation linéaires ce qui rend les transmissions à haut débit possibles. Parmi ces effets linéaires de transmission se trouvent la dispersion chromatique (CD) et la dispersion modale de polarisation (PMD), par exemple.

De plus, les récepteurs cohérents permettent la détection des signaux multiplexés en polarisation (PDM) sans aucun composant supplémentaire au niveau du récepteur. En comparaison aux signaux classiques qui portent l'information sur une seule polarisation, les signaux multiplexés en polarisation doublent l'efficacité spectrale, c'est-à-dire le nombre de bits par Hertz, car ils portent des informations indépendantes sur chacune des deux polarisations orthogonales du champ optique. D'un autre point de vue, les signaux multiplexés en polarisation permettent de diviser par deux le débit symbole par rapport aux signaux utilisant une seule polarisation, pour un même débit binaire.

En plus des effets linéaires de propagation et du bruit optique, les systèmes optiques peuvent être limités aussi par des effets non-linéaires de propagation provenant principalement de l'effet Kerr. Les dégradations causées par ces effets non-linéaires peuvent dépendre du débit binaire, du format de modulation et de la technique de détection. En effet, l'interaction entre les signaux multiplexés en polarisation et les effets non-linéaires peut être différente de celle des signaux classiques (utilisant une seule polarisation) dû au fait que les deux tributaires de polarisation peuvent interagir non-linéairement au long de la propagation, comme le montre l'exemple de la figure suivante :

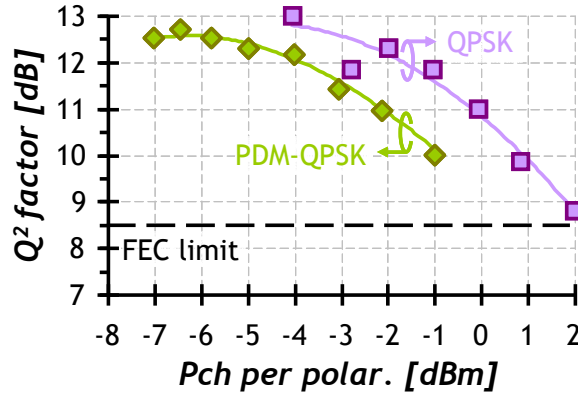


Fig. c: Tolérance aux effets non-linéaires intra-canaux après une propagation de 1600 km à travers de fibres monomode standard (SSMF).  $\blacksquare$  QPSK à 20 Gb/s et  $\blacklozenge$  PDM-QPSK à 40 Gb/s. Le débit symbole des deux types de signaux est le même : 10 Gbaud. L'OSNR est fixé dans le récepteur pour obtenir approximativement la même performance quand la transmission est principalement limitée par le bruit optique, c'est-à-dire, à puissances faibles.

Par ailleurs, la majorité des opérateurs ne prévoit pas de déployer des réseaux spécifiques pour les signaux portant les nouveaux débits de 40 et 100 Gb/s. Au contraire, ils demandent que les signaux aux nouveaux débits soient compatibles avec les réseaux existants conçus pour des signaux à 10 Gb/s. Leur motivation est de répondre progressivement à la croissance prévue du trafic d'environ 50% par an mentionnée auparavant. En conséquence, un scénario réaliste et probable pour la mise à niveau des réseaux actuels à 10 Gb/s est d'insérer progressivement des canaux à des débits supérieurs parmi des canaux à 10 Gb/s et de les faire se propager ensemble sur des liens conçus pour opérer à 10 Gb/s, avec espacement entre canaux de 50 GHz et gestion de dispersion. Ainsi, les paramètres clefs pour déterminer la pertinence d'une solution pour mettre à jour les systèmes actuels seront la tolérance aux distorsions linéaires (dispersion chromatique, PMD et le filtrage étroit) et la cohabitation correcte avec des canaux existants à 10 Gb/s modulés en intensité (OOK, on-off keying) avec non-retour à zéro (NRZ).

La première partie de ce manuscrit, constituée par les chapitres 1 et 2, traite de la fibre optique en tant que canal de transmission et des principes des systèmes de communication longue distance par fibre optique. Dans ces deux chapitres, je décris la fibre optique en tant que milieu physique de propagation ainsi que la structure des systèmes de transmission longue distance basés sur la détection cohérente, utilisant des signaux modulés en phase et multiplexés en polarisation.

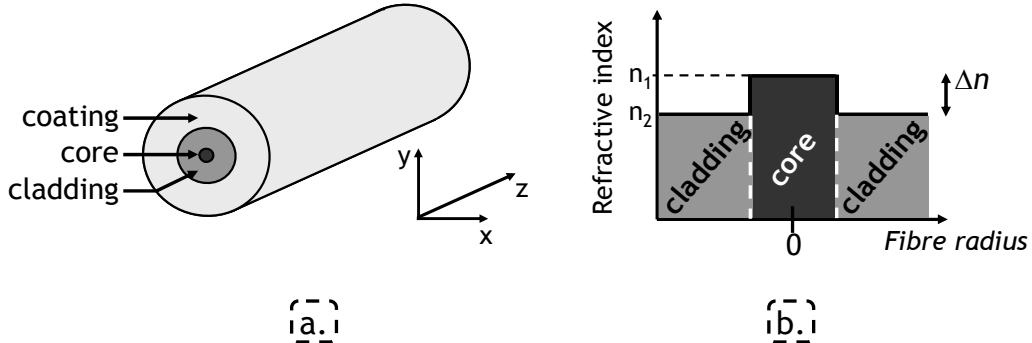


Fig. d : (a) Schéma d'une fibre optique et (b) profil d'indice de réfraction.

Dans le chapitre 1, je discute des principaux effets physiques de propagation, linéaires et non-linéaires, dans le cadre des systèmes de transmissions longue distance utilisant le multiplexage de polarisation. Dans le chapitre 2, j'explique les considérations générales des émetteurs et récepteurs basés sur la détection directe, y compris les formats de modulation considérés tout au long de ce manuscrit. Le chapitre 2 est également consacré aux différentes techniques utilisées dans les systèmes typiques de longue distance telles que le multiplexage en longueur d'onde, la compensation périodique des pertes et la gestion de la dispersion. De même, je discute dans ce chapitre des principes de multiplexage de polarisation et de la structure de l'émetteur. De plus, j'illustre la sensibilité au bruit optique des signaux multiplexés en polarisation à travers de résultats expérimentaux, comme le montre la figure suivante présentant une comparaison entre un signal multiplexé en polarisation et un signal portant l'information sur une seule polarisation.

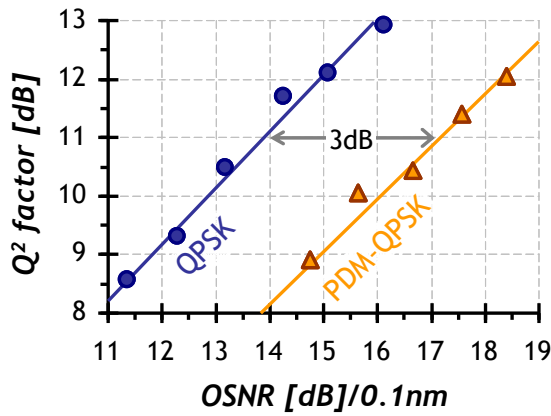
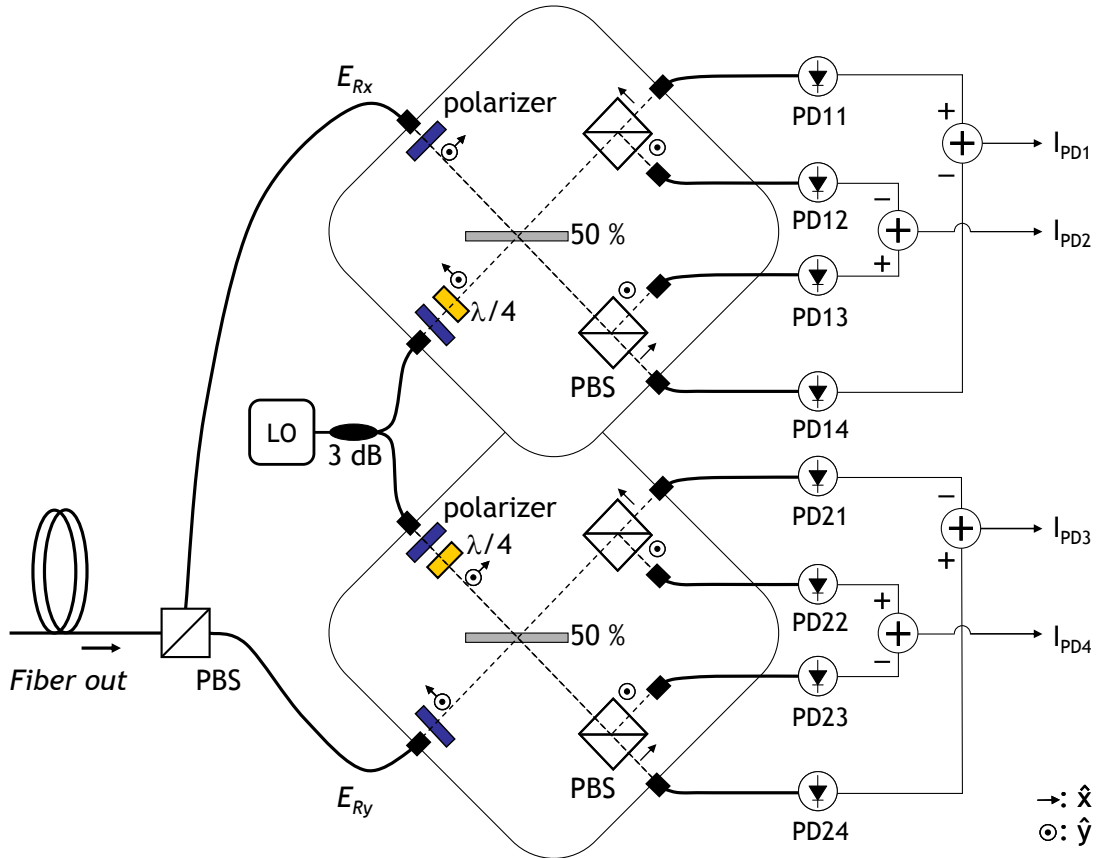


Fig. e: Sensibilité au bruit d'un signal ● QPSK à 56 Gb/s et un signal ▲ PDM-QPSK à 112 Gb/s. Le débit symbole des deux signaux est le même, 28 Gbaud.

Dans le chapitre 3, la deuxième partie du manuscrit, je décris le mélangeur cohérent et les algorithmes que j'ai utilisés pendant ma thèse, illustrés dans la Fig. f et la Fig. g, respectivement.



*Fig. f: Schéma d'une réalisation d'un récepteur cohérent à diversité de polarisation.  
C'est un récepteur cohérent de ce type que j'ai utilisé au long de mes travaux de recherche.*

Le récepteur cohérent fournit les composantes en phase et en quadrature (le long des deux polarisations de la lumière) résultant du battement entre le signal modulé et l'oscillateur local (qui n'est pas verrouillé en fréquence) :

$$\begin{cases} I_{PD1} = I_{PD11} - I_{PD14} \propto \frac{1}{\sqrt{2}} \sqrt{P_{Rx} P_{LO}} \cos(\Delta\omega \cdot t + \phi_{Rx}(t) + \phi'_{nx}(t)) \\ I_{PD2} = I_{PD13} - I_{PD12} \propto \frac{1}{\sqrt{2}} \sqrt{P_{Rx} P_{LO}} \sin(\Delta\omega \cdot t + \phi_{Rx}(t) + \phi'_{nx}(t)) \\ I_{PD3} = I_{PD24} - I_{PD21} \propto \frac{1}{\sqrt{2}} \sqrt{P_{Ry} P_{LO}} \cos(\Delta\omega \cdot t + \phi_{Ry}(t) + \phi'_{ny}(t)) \\ I_{PD4} = I_{PD22} - I_{PD23} \propto \frac{1}{\sqrt{2}} \sqrt{P_{Ry} P_{LO}} \sin(\Delta\omega \cdot t + \phi_{Ry}(t) + \phi'_{ny}(t)) \end{cases}$$

où  $I_{PDmn}$  sont les photocourants fournis par les photodiodes,  $\Delta\omega = (\omega_s - \omega_{LO}) = 2\pi\Delta f$  est la différence entre les fréquences porteuses du signal émis et de l'oscillateur local,  $P_{Rx}$  et  $P_{Ry}$  sont les puissances du champ le long des deux polarisations ( $\hat{x}$  et  $\hat{y}$ ) à l'entrée des mélangeurs cohérents,  $P_{LO}$  est la puissance de sortie de l'oscillateur local,  $\phi_{Rx}(t)$  et  $\phi_{Ry}(t)$  sont les phases modulées du signal reçu, et  $\phi_{nx}(t)$  et  $\phi_{ny}(t)$  représentent le bruit de phase sur les deux polarisations de la lumière. Les composantes en phase et en quadrature du battement entre le signal et l'oscillateur local sont transformées dans le domaine électrique par quatre photodiodes équilibrées

et traitées numériquement hors ligne dans un ordinateur. L'algorithme de traitement du signal est composé des différents blocs représentés sur la Fig. g.

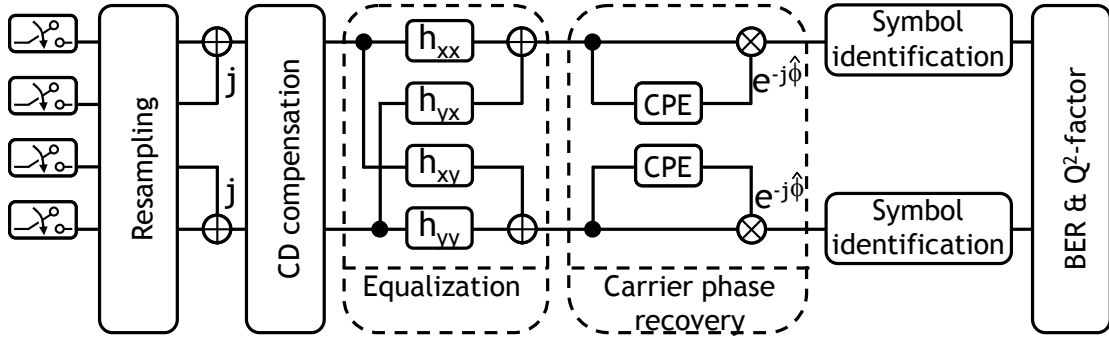


Fig. g: Traitement de signal numérique réalisé dans un récepteur cohérent.

Tout d'abord, l'algorithme compense numériquement la dégradation du signal causée par la dispersion, comme le montre la Fig. h.

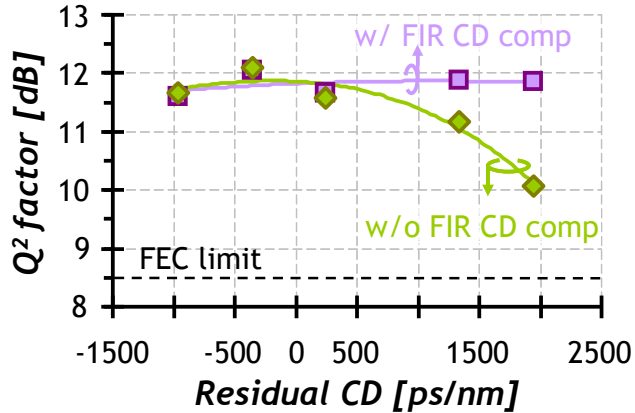
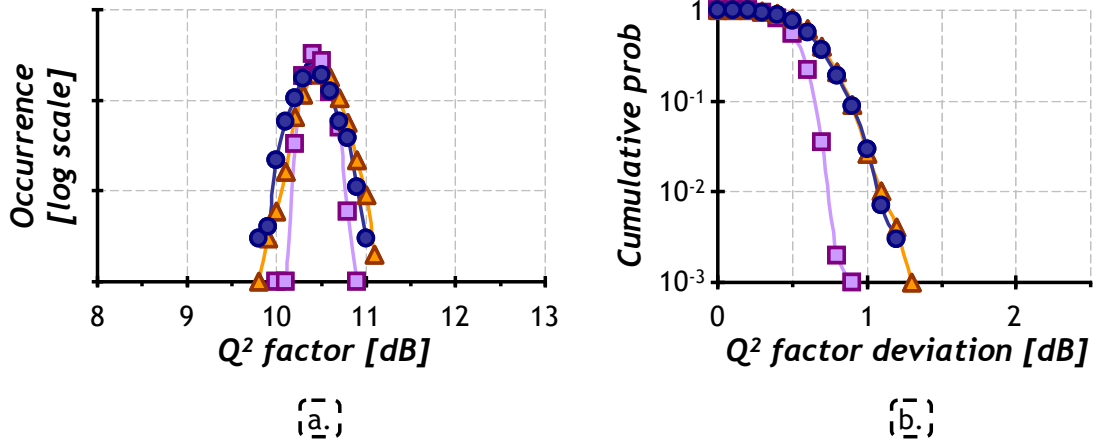


Fig. h: Dépendance de la performance d'un signal PDM-QPSK à 40 Gb/s en fonction de la dispersion chromatique résiduelle  $\blacksquare$  avec et  $\blacklozenge$  sans l'application d'un filtre à réponse impulsionnelle (FIR) dédié à la compensation de la dispersion chromatique, placé avant l'égaliseur.

Ensuite, il démultiplexe les tributaires de polarisation tout en égalisant le signal. L'égaliseur est continuellement mis à jour afin de suivre les perturbations du canal, comme par exemple la PMD (Fig. i).



*Fig. i: Dépendance de la performance en fonction de la PMD pour un signal PDM-QPSK à 100 Gb/s. (a) Distribution des  $Q^2$  factor, and (b) probabilité cumulée (b) avec une PDM de □ <1 ps, ● 8 ps et ▲ 20 ps.*

La dernière étape de l'algorithme, appelée estimation de la fréquence et la phase de la porteuse, consiste à verrouiller en fréquence et en phase l'oscillateur local et le signal reçu. En compensant les décalages de fréquence et de phase entre le signal et l'oscillateur local, cette opération relâche grandement les contraintes de réalisation pratique de la détection cohérente en permettant l'opération avec un oscillateur local non verrouillé en fréquence.

Les chapitres 4 et 5 constituent la dernière partie de ce manuscrit. Dans ces deux chapitres, je discute de la combinaison de signaux modulés en phase et multiplexés en polarisation pour la prochaine génération des systèmes de communication longue distance par fibre optique aux débits de 40 et 100 Gb/s. Le chapitre 4 est dédié à l'étude de l'insertion des canaux à 40Gb/s dans les systèmes actuels conçus pour et transportant des canaux 10 Gb/s modulés en intensité avec du NRZ. Dans ce contexte, nous étudions et comparons deux solutions différentes à 40 Gb/s : les signaux multiplexés en polarisation modulés par déplacement de phase quaternaire (PDM-QPSK) et les signaux multiplexés en polarisation modulés par déplacement de phase binaire (PDM-BPSK). Les deux solutions présentent les avantages d'avoir une excellente tolérance au bruit et aux effets linéaires de propagation grâce à la détection cohérente. En conséquence, l'investigation se centre sur leur tolérance aux effets non-linéaires de propagation. La Fig. j montre la tolérance aux effets non-linéaires de propagation pour un signal PDM-QPSK à 40 Gb/s dans trois configurations différentes : monocanale (sgle ch), WDM avec 80 canaux PDM-QPSK à 40 Gb/s multiplexés en longueur d'onde avec une grille 50 GHz (WDM homog.) et WDM avec 79 canaux modulés en NRZ à 10 Gb/s et un canal PDM-QPSK à 40 Gb/s inséré au milieu.

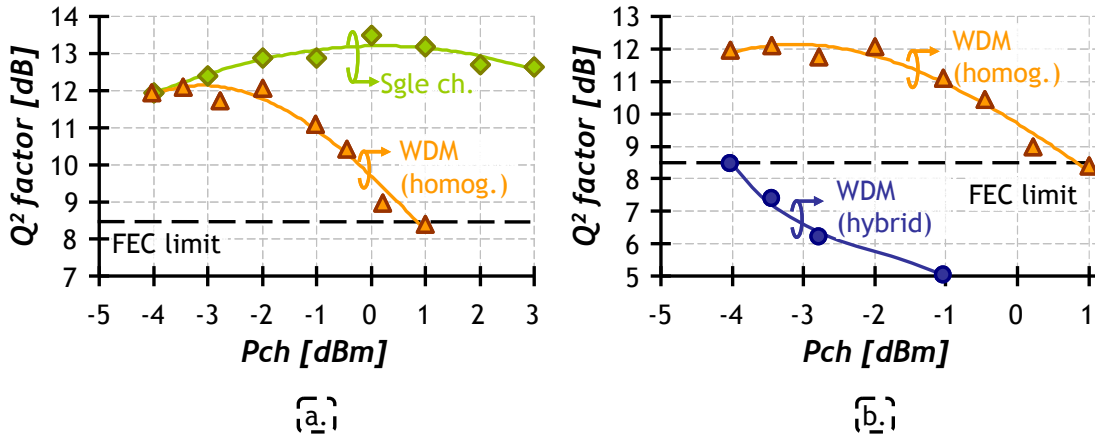


Fig. j: Tolérance aux effets non-linéaires de propagation des signaux PDM-QPSK à 40 Gb/s après 1600 km de SSMF. ♦ Configuration monocanal, ▲ configuration WDM homogène comprenant des canaux PDM-QPSK à 40 Gb/seulement et ● configuration WDM hybride comprenant un mélange des canaux PDM-QPSK à 40 Gb/s et NRZ à 10 Gb/s. Le débit symbole de tous les canaux est 10 Gbaud.

Après avoir identifié que les dégradations plus sévères proviennent des effets non-linéaires générés par les canaux voisins NRZ à 10 Gb/s, nous portons une attention particulière aux systèmes dits hybrides. Dans ces systèmes, plusieurs canaux à débit plus élevé (à savoir 40 ou 100 Gb/s) sont progressivement insérés dans les systèmes conçus pour les canaux NRZ à 10 Gbit/s. Ainsi, les canaux à débit plus élevé peuvent être distordus par les effets non-linéaires générés par les canaux NRZ à 10 Gb/s qui se propagent en même temps dans la même fibre. Cette thèse démontre que dans cette configuration la solution PDM-BPSK à 40Gb/s est plus robuste que la solution PDM-QPSK à 40 Gb/s vis-à-vis des effets générés par les canaux NRZ à 10 Gb/s, comme le montre la Fig. k.

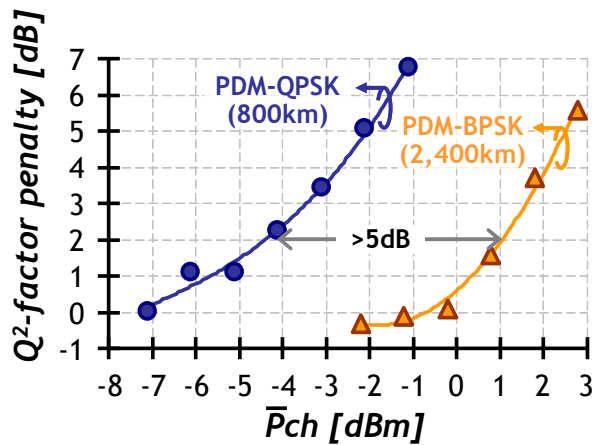


Fig. k: Comparaison de la tolérance aux effets non-linéaires générés par les canaux NRZ à 10 Gb/s se propageant en même temps à travers d'une fibre à faible dispersion au milieu de la bande C (1546.52 nm). ● PDM-BPSK et ▲ PDM-QPSK à 40 Gb/s. Pour cette figure, la puissance est normalisée prenant en compte les différents portés : 800 km pour PDM-QPSK and 2400 km pour PDM-BPSK.

Le chapitre 5 à son tour discute de la tolérance aux effets non-linéaires des signaux PDM-QPSK, ici à 100 Gb/s. Nous démontrons que les canaux 100 Gb/s PDM-QPSK sont compatibles avec l'espacement spectral standard de 50 GHz tout en permettant une augmentation de la capacité totale transmise d'un facteur 10 par rapport aux systèmes actuels à 10 Gb/s. Nous portons un intérêt spécial à l'évolution de l'impact des effets non-linéaires lorsque le débit augmente de 40 à 100 Gb/s et nous démontrons que cette évolution diffère de celle des systèmes classiques basés sur la détection directe. Comme le montre la Fig. 1, le seuil non-linéaire (NLT), c'est-à-dire, la puissance à partir de laquelle les dégradations non-linéaires deviennent dominantes, augmente avec le débit. Autrement dit, les signaux PDM-QPSK deviennent plus tolérants aux effets non-linéaires de propagation quand leur débit augmente.

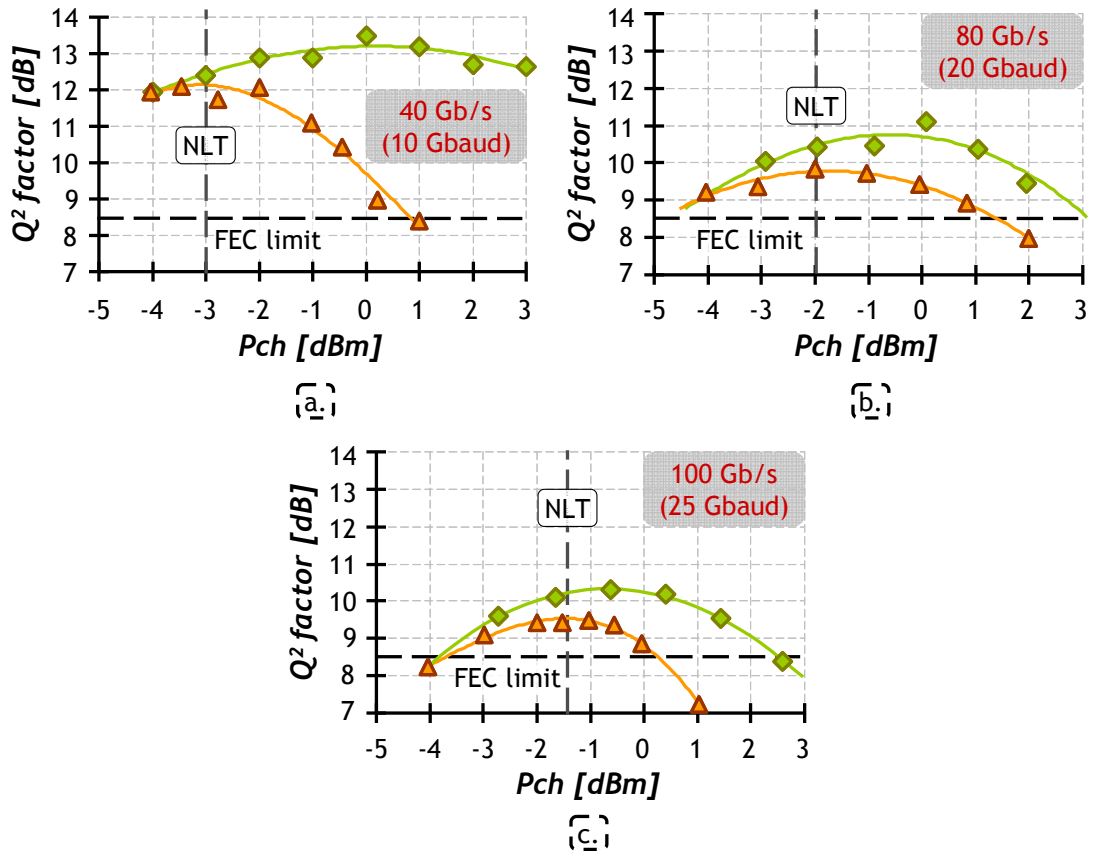


Fig. 1: Tolérance aux effets non-linéaires des signaux PDM-QPSK à (a) 40 Gb/s, (b) 80 Gb/s (c) and 100 Gb/s dans des configurations  $\blacklozenge$  monocanal et  $\blacktriangle$  WDM homogène après 1600 km de SSMF.

Je discute également dans les chapitres 4 et 5 des investigations que j'ai proposées, mises en places et réalisées expérimentalement à propos de l'interaction entre la dispersion modale de polarisation (PMD) et les effets non linéaires. Je montre que le résultat de l'interaction entre la PMD et les effets non-linéaires dans les systèmes cohérents multiplexés en polarisation peut différer de ceux des systèmes classiques (employant une seule polarisation) avec modulation d'intensité et détection directe. Ces investigations démontrent que le résultat de cette interaction se révèle plus complexe que la simple addition de l'impact de ces deux effets physiques séparément.

Contrairement aux systèmes existants où l'effet de la PMD est toujours pénalisant, nous prouvons que la PMD s'avère souvent être bénéfique dans les systèmes cohérents en réduisant les pénalités causées par les non-linéarités lorsqu'elle est distribuée. En effet, les résultats de la Fig. m montrent que l'effet de la PMD peut induire une amélioration de la distribution de  $Q^2$  factor non seulement en termes de valeur moyenne mais aussi en termes de largeur de la distribution, comme pour le cas NRZ-PDM-BPSK. En revanche, la PMD n'affecte quasiment pas la performance dans le cas du iRZ-PDM-BPSK.

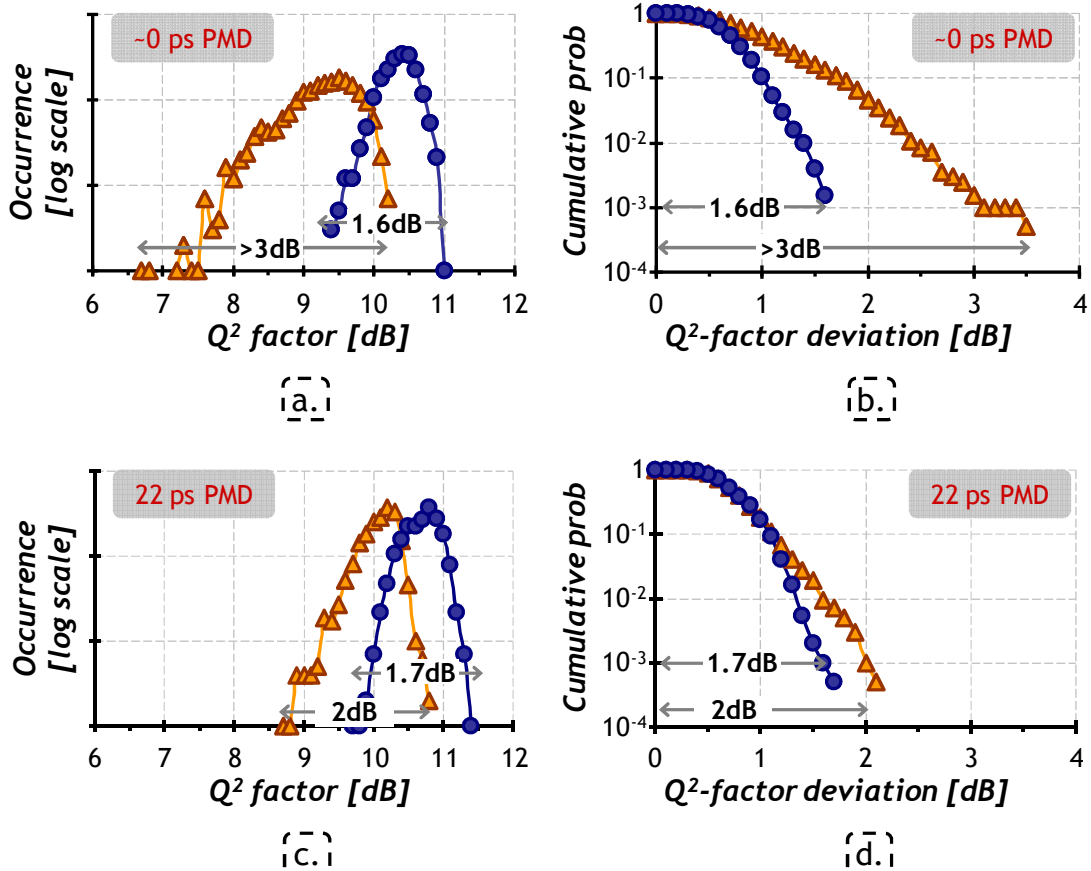


Fig. m: (a,c) Distribution des  $Q^2$  factor, and (b,d) probabilité cumulée avec une PDM de 0 ps (a,b) et 22 ps (c,d) pour les signaux  $\blacktriangle$  NRZ-PDM-BPSK et  $\bullet$  iRZ-PDM-BPSK à 40 Gb/s après 4000 km de SSMF dans une configuration WDM homogène.

En revanche, quand la PMD est localisée, elle peut augmenter la dégradation causée par lesdites non-linéarités en fonction de l'endroit où elle a lieu. Les résultats de la Fig. n illustrent que la présence de PMD en début de ligne (dans ce cas précis, au niveau du transmetteur) peut augmenter l'impact pénalisant des effets non-linéaires de propagation, par exemple en augmentant le nombre d'occurrence de résultats en dessous de la moyenne, c'est-à-dire, en élargissant la distribution des facteurs  $Q^2$ . Au contraire, quand la PMD est localisée en bout ligne (au niveau du récepteur), la PMD n'interagit pas avec les effets non-linéaires de propagation et n'augmente pas les pénalités introduites par ceux-ci.

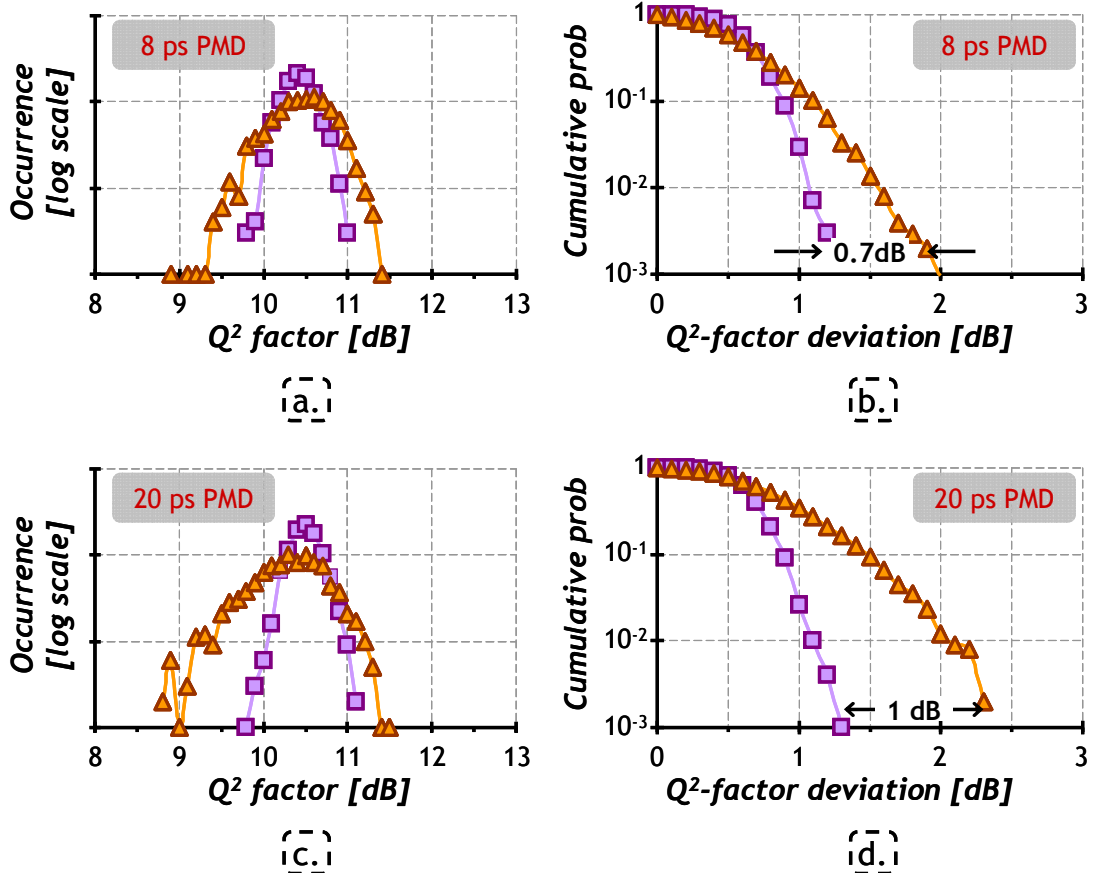
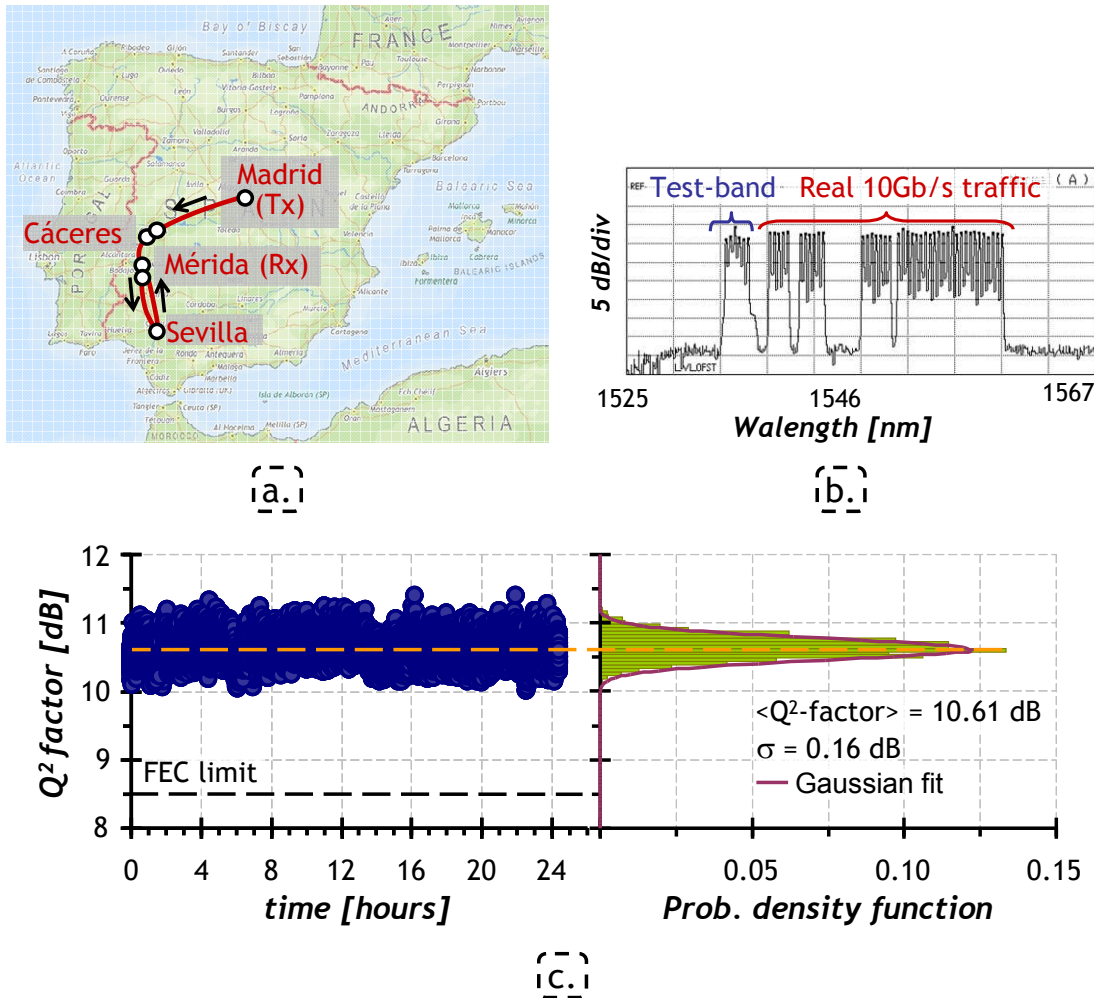


Fig. n: (a, c) Distribution des  $Q^2$  factor, et (b, d) probabilité cumulée (b, d) avec une PDM de 8 ps et (c, d) 20 ps, quand la PMD est placée au niveau du ▲ transmetteur ou au niveau du □ récepteur.

Finalement, comme preuve de l'intérêt porté par les opérateurs aux technologies à 100 Gb/s, le chapitre 5 contient aussi les résultats d'un essai de terrain que nous avons mené récemment sur le réseau de Telefónica en Espagne montrant le potentiel des technologies cohérentes pour moderniser les réseaux existants. J'ai participé activement à la réussite de cet essai de terrain aussi bien concernant le déploiement et la mise en place du système que la réalisation des mesures.



*Fig. o: Essai terrain sur les équipements Alcatel-Lucent installés de Telefónica comprenant une distance de 1088 km entre Madrid-Sevilla-Mérida. Le lien est composé de fibres SSMF, amplificateurs EDFA et 5 noeuds optiques. (a) situation géographique, (b) allocation du spectre (portant des données réelles), (c) évolution du  $Q^2$ -factor durant plus de 24 heures et fonction de densité de probabilité.*

De plus, nous avons proposé, pour la première fois (à notre connaissance), d'utiliser les avantages de la détection cohérente combinés avec des signaux modulés en phase pour augmenter la capacité totale des systèmes sous-marins sans répéteur. A cet effet, l'*Appendix B* décrit la première démonstration expérimentale de transmission de canaux PDM-QPSK à 100 Gb/s sur des systèmes sans répéteurs. J'ai mené cette expérience conjointement avec des collègues de *Alcatel-Lucent Submarine Networks*.

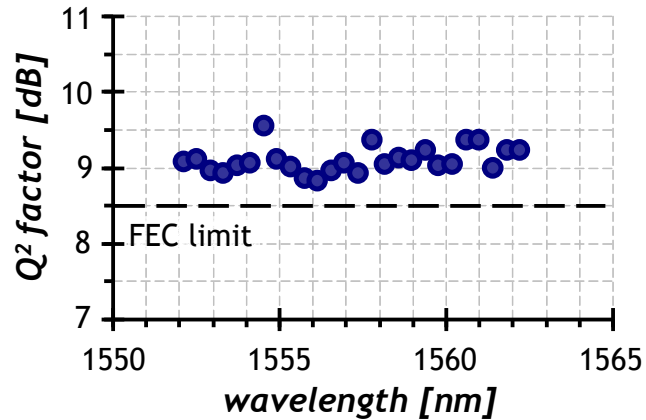


Fig. p: Performance mesurée pour les 26 canaux après 401 km de transmission sans répéteur.

Les résultats présentés dans ce manuscrit ont été obtenus essentiellement grâce à des recherches expérimentales. La plupart de ces résultats ont déjà été publiés et présentés en tant qu'articles dans des revues scientifiques et des conférences internationales. Ces articles, dont je suis auteur ou co-auteur, sont répertoriés dans la dernière section du manuscrit appelée *Publications*.

# **Foreword**

Ever since the development of the internet and the introduction of the world wide web (www), the demand for data capacity has increased exponentially. Current predictions foresee indeed a long term traffic growth of about 50% per year [1], driven by heavy-content applications such as *Youtube*, *Skype*, *Google earth*, *Facebook*, and *video-on-demand services*, for example. The data transmission over optical fibre has revolutionised the telecommunication landscape and has played a major role in the advent of the information age.

Telecommunication providers employ fibre-optic communication systems for most of the backbone, regional and metropolitan transmission links in order to respond to this need for capacity. Fibre-optic communications systems have not stopped evolving since the first commercial demonstration of live telephone traffic over optical fibre on 22 April, 1977, carried out by the General Telephone and Electronics company. Different key enablers have progressively contributed to overcome the encountered bottlenecks such as the introduction of single mode fibres, the invention of optical Erbium-doped fibre amplifiers (EDFA) allowing the efficient deployment of wavelength division multiplexing (WDM), the utilisation of forward error correction (FEC), and the arrival of chromatic dispersion management techniques. Typically, the transmission distances in the metropolitan, regional and backbone networks are less than 300 km, between 300 and 1,000 km, and more than 1,000 km, respectively. This thesis focuses on these *long-haul* fibre-optic systems used in backbone networks. Today's standard long-haul terrestrial systems employ single mode fibres, WDM with 50-GHz channel spacing, optical amplification, dispersion management and forward error correction. Due to the limited bandwidth of current optical amplifiers, these systems carry typically up to 80 or 100 WDM channels.

Until recently, simple intensity modulation of light combined with direct detection has been the choice for commercial optical transmission systems. This option combines cost-effective transmitter and receiver structures with a sufficient transmission performance enabling the realisation of 10-Gb/s long-haul transmission systems. Nevertheless, to keep responding to the ceaseless increasing demand for

capacity, higher bit rates per channel are required, namely 40 Gb/s and 100 Gb/s. The challenge is that fibre-optic transmission becomes generally more difficult with the increasing bit rate since the requirements on the end of link optical signal-to-noise ratio (OSNR) increases whereas the robustness against linear transmission impairments, namely chromatic dispersion and polarisation mode dispersion (PMD), is drastically decreased. In this context, phase shift keying (PSK) modulation formats using (direct) differential detection have been widely studied over the last decade. However, the tolerance to linear impairments remains one of the major concerns for their field deployment. Therefore, a disruptive solution allowing the capacity increase while being robust against linear impairments is required.

Sometimes, disruptive solutions do not come from really new discoveries but from the innovative association of available technologies. Thus, optical coherent detection was firstly proposed in the 1980's to improve receiver sensitivity. At that time, no optical pre-amplification was used in front of the receiver and the detection was mostly limited by the thermal noise of the photodiodes and electrical amplifiers. Hence, a local oscillator much more powerful than the signal allowed for coherent amplification. However, the development of the EDFA as an optical pre-amplifier implied the decline of the interest on coherent detection. It was not until the recent advances in digital signal processing and high speed electronics, especially in analog-to-digital-converters, that coherent detection has revealed as one of the most powerful tools to achieve high-speed optical transmissions. By providing access to the amplitude, the phase and the polarization of the optical field, coherent receivers enjoy the excellent sensitivity to optical noise associated with homodyne detection with the added benefits of advanced digital signal processing. Thus they offer the possibility to operate with unlocked local oscillators and to compensate for linear impairments making high bit rate transmissions possible. Moreover, digital coherent receivers allow detecting polarisation division multiplexed (PDM) signals without any extra component at the receiver side. In comparison to singly-polarised signals, PDM can double the spectral efficiency, i.e. the number of bits transmitted per second per Hertz, as it modulates independent data onto each of the two orthogonal polarisations of the optical field. Besides, PDM halve the symbol rate with respect to singly-polarised signals for a given bit rate.

On top of linear fibre effects and optical noise, optical communication systems may be limited by nonlinear fibre effects stemming mainly from the Kerr effect. The penalties caused by nonlinearities may depend on channel bit rates, modulation formats and detection techniques. Hence, the behaviour against nonlinearities of polarisation-multiplexed signals detected with coherent receivers may differ from that of current (singly-polarised) intensity-modulated direct-detected schemes, due to the fact the two modulated polarisation tributaries may interact nonlinearly along the transmission, for example. Besides, most of carriers do not intend to build specific networks from scratch for the new data rates and they require the future upgrade at higher bit rate to be compatible with their (legacy) 10-Gb/s networks. Their motivation is to smoothly respond to the predicted traffic growth of about 50% per year mentioned above. Therefore, one likely scenario for upgrading 10-Gb/s infrastructures is to progressively insert higher bit rate channels among other 10-Gb/s ones and propagate them through links designed for 10-Gb/s operation with 50-GHz channel spacing. Hence, the key parameters to determine the suitability of one

solution for overlaying existing 10-Gb/s legacy networks will be its tolerance to linear distortions (chromatic dispersion, PMD and narrow filtering) and the correct cohabitation with co-propagating 10-Gb/s non-return-to-zero on-off keying (NRZ-OOK) channels.

The first part of this thesis, constituted by Chapter 1 and 2, treats the fibre-optic transmission channel and fibre-optic communication systems for long-haul distances. In these two chapters, I give a fresh look at the optical fibre as a physical transport medium and at the structure of long-haul transmission in the light of coherent systems using phase-modulated polarisation-multiplexed signals. In Chapter 1, I discuss the principal linear and nonlinear impairments in long-haul transmissions using polarisation multiplexing. In Chapter 2, I review general considerations of transmitters and direct-detection receivers including the modulation formats considered throughout this thesis. Chapter 2 deals also with different techniques used in typical long-haul systems such as wavelength division multiplexing, periodic loss compensation and dispersion management. Likewise, I discuss in this chapter the principles of polarisation multiplexing and the transmitter structure. In addition I also illustrate the noise sensitivity of polarisation-multiplexed signals through experimental results.

In Chapter 3, the second part of this thesis, I describe the coherent mixer and the algorithms I have used during this thesis. The coherent receiver supplies the in-phase and quadrature components (along the two polarisations of the light) of the beating between the signal and the unlocked local oscillator. These components are transformed into the electrical domain by four balanced photodiodes and processed off-line in a computer. The algorithm realises digital chromatic dispersion compensation, equalisation and polarisation demultiplexing. The equaliser is continuously updated so as to follow channel perturbations. Moreover, the last stage of the algorithm, named carrier frequency and phase estimation, is able to compensate for frequency and phase mismatches between the signal and the local oscillator, allowing thus the operation with an unlocked local oscillator. I report also in Chapter 3 experimental results where I show the excellent tolerance of digital coherent receivers against linear transmission impairments, namely chromatic dispersion and PMD.

Finally, the last part of the thesis is formed by Chapters 4 and 5. I treat in this two chapters the combination of phase-modulated polarisation-multiplexed signals and digital coherent receivers for the next generation of ultra-long haul systems at 40 Gb/s and 100 Gb/s. Chapter 4 focuses on the upgrade of legacy 10-Gb/s systems to 40 Gb/s. In this context, we investigate and compare two different solutions, namely 40 Gb/s PDM-Quaternary-PSK (PDM-QPSK) and PDM-Binary-PSK (PDM-BPSK). Both solutions benefit from the excellent tolerance to linear impairments brought by coherent detection. Our investigation therefore mainly concerns their tolerance to nonlinearities. Having identified that the dominant nonlinearities come from co-propagating 10-Gb/s NRZ channels, we pay especial attention to hybrid systems. In these systems, several channels at higher bit rate (namely 40 or 100 Gb/s) are progressively inserted in wavelength slots originally designed for NRZ channels at 10 Gb/s and co-propagated together with 10 Gb/s NRZ channels. Hence, higher bit rate channels could suffer from (cross) nonlinearities stemming from co-propagating 10-Gb/s NRZ-OOK channels limiting their

performance. Chapter 5 in turn deals with the tolerance of PDM-QPSK against nonlinearities, now at 100 Gb/s. We demonstrate that 100 Gb/s PDM-QPSK is compatible with standard 50-GHz channels and allows a tenfold increase of the total transmitted capacity compared to current 10-Gb/s NRZ systems. We particularly investigate the evolution of the impact of nonlinear effects when increasing the bit rate from 40 to 100 Gb/s.

I also report in Chapter 4 and 5 investigations on the interplay between PDM and nonlinear effects that I proposed, designed and conducted. I show that the effect of the interplay between PMD and nonlinearities in PDM coherent systems may differ from current (singly-polarised) intensity-modulated direct-detected systems. Moreover, we demonstrate that the effect of this interplay reveals more complex than the simple addition of the effect of both effects separately.

As a proof of the carriers' interest onto 100-Gb/s technologies, Chapter 5 also reports the results of a field trial we have recently conducted on Telefónica's network in Spain. I have actively participated in the success of this field trial deploying the set up and performing the measurements together with other colleagues from the business unit.

In addition, we propose for the first time, to best of our knowledge, to increase the transmitted capacity of unrepeatered submarine systems by taking full advantage of coherent detection combined with polarisation-multiplexing and multilevel modulation formats. Hence, I report, in Appendix B, the first experimental demonstration, of coherent 100 Gb/s PDM-QPSK over an unrepeatered transmission link. I have conducted this experiment together with the colleagues from *Alcatel-Lucent Submarine Networks*.

The results presented in this manuscript have been primarily obtained through experimental investigations. Most of these results have been already published and presented in different peer-reviewed journal articles and conference contributions which I have authored or co-authored. These articles are listed in the last section of the manuscript named *Publications*.

# *List of acronyms and symbols*

## *List of acronyms*

<b>ADC</b>	analog to digital converter
<b>AMI</b>	alternating mark inversion
<b>Apol</b>	alternate polarisation
<b>ASK</b>	amplitude shift keying
<b>ASE</b>	amplified spontaneous emission
<b>AWG</b>	arrayed waveguide grating
<b>AWGN</b>	additive white Gaussian noise
<b>BER</b>	bit error rate
<b>BPSK</b>	binary phase shift keying
<b>CD</b>	chromatic dispersion
<b>CMA</b>	constant modulus algorithm
<b>CPE</b>	carrier phase estimation
<b>CRZ</b>	chirped-return-to-zero
<b>CSRZ</b>	carrier-suppressed return-to-zero
<b>CW</b>	continuous wave
<b>DBPSK</b>	differential binary phase shift keying
<b>DCF</b>	dispersion compensating fibre
<b>DEMUX</b>	demultiplexer
<b>DFB</b>	distributed feedback laser
<b>DGD</b>	differential group delay
<b>DML</b>	direct modulated laser
<b>DPSK</b>	differential phase shift keying
<b>DQSPK</b>	differential quaternary phase shift keying
<b>DSF</b>	dispersion shifted fibre
<b>EAM</b>	electro-absorption modulator
<b>ECL</b>	external cavity laser

<b>EDFA</b>	erbium doped fibre amplifiers
<b>FEC</b>	forward error correction
<b>FIR</b>	finite impulse response
<b>FSR</b>	free spectral range
<b>FWM</b>	four wave mixing
<b>GVD</b>	group velocity dispersion
<b>IFWM</b>	intra-channel cross-phase modulation
<b>ISD</b>	information spectral density
<b>ISI</b>	inter-symbol interference
<b>IXPM</b>	intra-channel cross phase modulation
<b>ITU</b>	international telecommunication union
<b>LMS-DD</b>	least mean squares decision-directed
<b>LSPS</b>	loop synchronous polarisation scrambler
<b>MUX</b>	multiplexer
<b>MZM</b>	Mach-Zendher modulator
<b>NF</b>	noise figure
<b>NLPN</b>	nonlinear phase noise
<b>NLT</b>	nonlinear threshold
<b>NZDSF</b>	non-zero dispersion shifted fibre
<b>OFDM</b>	frequency division multiplexing
<b>OSA</b>	optical spectrum analyser
<b>OSNR</b>	optical signal to noise ratio
<b>PBC</b>	polarisation beam combiner
<b>PBS</b>	polarisation beam splitter
<b>PDM</b>	polarisation division multiplexing
<b>PLL</b>	phase-locked loop
<b>PMD</b>	polarisation mode dispersion
<b>PM-DL</b>	polarisation maintaining delay line
<b>PMF</b>	polarisation maintaining fibre
<b>POLMUX</b>	polarisation multiplexed
<b>PolSK</b>	polarisation shift keying
<b>PRBS</b>	pseudo-random bit sequences
<b>PSBT</b>	phase shaped binary transmission

<b>PSCF</b>	pure silica core fibre
<b>PSD</b>	power spectral density
<b>PSP</b>	principal state of polarisation
<b>QAM</b>	quadrature amplitude modulation
<b>QPSK</b>	quaternary phase shift keying
<b>RDPS</b>	residual dispersion per span
<b>ROADM</b>	reconfigurable optical add and drop multiplexer
<b>RZ</b>	return-to-zero
<b>SBS</b>	stimulated Brillouin scattering
<b>SE</b>	spectral efficiency
<b>SER</b>	symbol error ratio
<b>SNR</b>	signal to noise ratio
<b>SOA</b>	semiconductor optical amplifiers
<b>SOP</b>	state of polarisation
<b>SPM</b>	self-phase modulation
<b>SRS</b>	stimulated Raman scattering
<b>SSMF</b>	standard single mode fibre
<b>ULH</b>	ultra-long haul
<b>WDM</b>	wavelength division multiplexing
<b>WSS</b>	wavelength selective switch
<b>XPM</b>	cross phase modulation
<b>XPolM</b>	cross-polarisation modulation

## List of symbols

$\langle \cdot \rangle$	ensemble average
$\alpha$	attenuation coefficient
$\beta$	mode-propagation constant
$\lambda$	optical wavelength
$\lambda_0$	zero-dispersion wavelength
$\gamma$	nonlinear coefficient
$\Phi_{NL}$	nonlinear induced phase modulation
$\eta_{sh}$	shot noise
$\omega$	angular frequency
$A_{eff}$	effective fibre area
$B$	birefringence
$B_{ref}$	reference bandwidth
$c$	speed of light in the vacuum ( $c=2.99792 \cdot 10^8$ m/s)
$d_{12}$	walk-off parameter
$d_{min}$	minimum Euclidian distance
$D$	dispersion factor
$D'$	dispersion factor slope
$f$	frequency
$F$	noise factor
$g_R$	Raman gain coefficient
$G$	gain (amplifier)
$G_{eff}$	effective Raman gain
$G_{ON/OFF}$	on-off Raman gain
$h$	Planck's constant ( $6.626068 \cdot 10^{-34}$ J·s)
$I$	in-phase component
$I_{PD}$	photocurrent
$L$	fibre length
$L_B$	polarisation beat length
$L_D$	normalised dispersion length
$L_{eff}$	effective fibre length

$L_w$	walk-off length
$n$	refractive index
$N_o$	noise power spectral-density
$Np$	neper unit
$N_{spans}$	number of spans in the transmission line
$n_0$	linear refractive index
$n_2$	nonlinear refractive index
$\text{NF}$	noise figure
$n_g$	group refractive index
$n_{sp}$	spontaneous emission factor
$P$	power
$P_{\text{ch}}$	power per channel
$P_{\text{error}}$	error probability
$P_{\text{error\_d}}$	error probability of differentially-decoded sequence
$Q$	quadrature component
$R$	photodiode responsivity
$R_b$	bit rate
$r$	analog received signal
$\hat{s}$	estimated sequence
$\hat{s}_d$	estimated differentially-decoded sequence
$t$	time
$T_s, T_o$	symbol period
$v_g$	group velocity
$v_p$	phase velocity
$V_{\text{pp}}$	peak-to-peak voltage
$V_\pi$	characteristic voltage of a modulator
$z$	transmission distance



# Chapter 1. The fibre-optic transmission channel

In the telecommunications landscape, optical fibres are massively used as a physical medium to transfer information from one point to another by means of an optical signal. Optical fibres are cylindrical nonlinear dielectric waveguides commonly made of silica glass. Since Kao and Hockham proposed their use for telecommunications at optical frequencies in 1966 [2], they have not stopped to evolve [3]. The most common structure consists of three concentric cylindrical sections: the core, the cladding and the coating, as depicted in Fig. 1.1-a. The light is confined within the core through total internal reflexion thanks to a difference between refractive indexes of the core and the cladding [4]. The core refractive-index of silica fibres is  $n_1 \sim 1.48$  whereas the refractive index of the cladding,  $n_2$ , is between 0.2 and 3% lower, as shown in Fig. 1.1-b. This difference between the refractive indexes can be achieved either by increasing the refractive index of the silica within the core, through Germanium-Oxide ( $GeO_2$ ) doping, or by reducing the refractive index of the cladding, through fluoride ( $F$ ) doping.

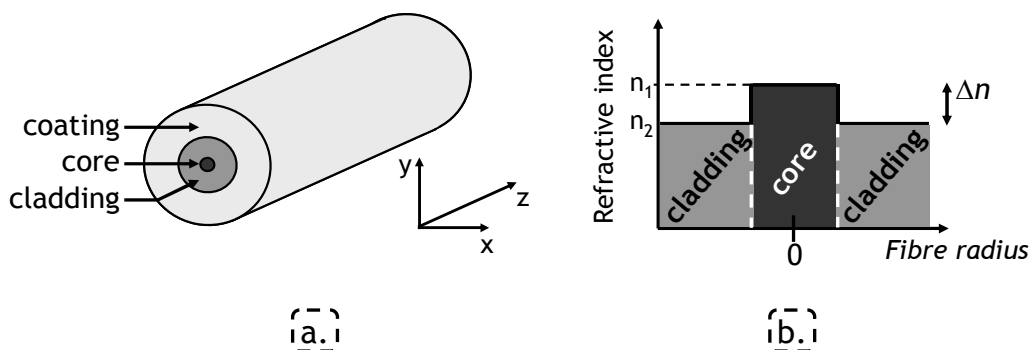


Fig. 1.1: (a) Optical fibre scheme and (b) refractive index profile.

Depending on the number of existing modes of propagation, one can talk about single-mode (one mode) or multi-mode (several modes) fibres. The number of modes supported by an optical fibre at a given wavelength depends on its design parameters, namely it scales with the core radius and the difference of refractive index between the core and the cladding. Single-mode fibres are the most widely used today, avoiding thus detrimental pulse broadening induced by intermodal dispersion. The most commonly employed fibre for telecommunications purposes is standard single-mode fibre (SSMF). The radius of its core is 4.5 µm which ensures single-mode transmission in the telecommunications bandwidth around 1550 nm. The core of SSMF is doped with  $GeO_2$ . Since this doping slightly increases fibre losses, better attenuation characteristics can be obtained by doping the cladding with fluoride [5].

In this chapter, the principal impairments for long-haul transmissions are discussed. They are divided into linear and nonlinear effects, according to whether they are independent of the signal power or not. The former group is composed of fibre attenuation, chromatic dispersion, polarisation mode dispersion and polarisation dependent loss. Nonlinear effects comprise Kerr-effect related impairments (such as self and cross-phase modulation, four-wave mixing, intra-channel cross-phase modulation and four-wave mixing, cross-polarisation modulation), as well as nonlinear phase noise and non-elastic scattering effects (such as stimulated Raman and Brillouin scattering).

## 1.1. Linear transmission effects

### 1.1.1 Fibre attenuation

Fibre loss is one of the main limiting aspects of the optical communications systems, as discussed in section 2.4. As in any other physical medium except the vacuum, when an optical signal propagates through an optical fibre its power is attenuated due to absorption and scattering loss. The power of the optical signal  $P(z)$ , in [W], decreases exponentially along the propagation, as shown in Fig. 1.2, following the equation:

$$P(z) = P_0 \cdot \exp(-\alpha z) \quad (1.1)$$

where  $P_0$  is the injected power in the fibre in [W],  $z$  is the distance in [km] and  $\alpha$  is the attenuation coefficient in [ $Np/km$ ]. For practical reasons, the attenuation is commonly expressed in [ $dB/km$ ]. Both values are related by

$$\alpha [dB/km] = 10 \cdot \log_{10} (\exp(\alpha [Np / km])) \approx 4.343 \cdot \alpha [Np / km] \quad (1.2)$$

The attenuation suffered by the propagating signal depends on its frequency (or wavelength) as shown in Fig. 1.3. The wavelength,  $\lambda$ , and the frequency,  $f$ , of a spectral component are related by

$$\lambda = \frac{c}{f} \quad (1.3)$$

where  $c$  is the speed of light in the vacuum,  $c=2.9979 \cdot 10^8$  m/s. Two fundamental loss mechanisms govern the attenuation profile of an optical fibre: Rayleigh scattering and intrinsic absorption of the  $SiO_2$  [1][4]. The former results from imperfections of the

silica such as microscopic fluctuations in the material density created in the manufacturing process. These imperfections imply a fluctuation in the refractive index causing scattering. Since the distance between these imperfections is significantly smaller than the wavelength of the light, shorter wavelengths are more attenuated than longer ones [6]. For wavelengths longer than 1600 nm, the harmonic resonances of the optical signal with the silica molecules that make up the glass become dominant causing the intrinsic absorption of the  $SiO_2$ .

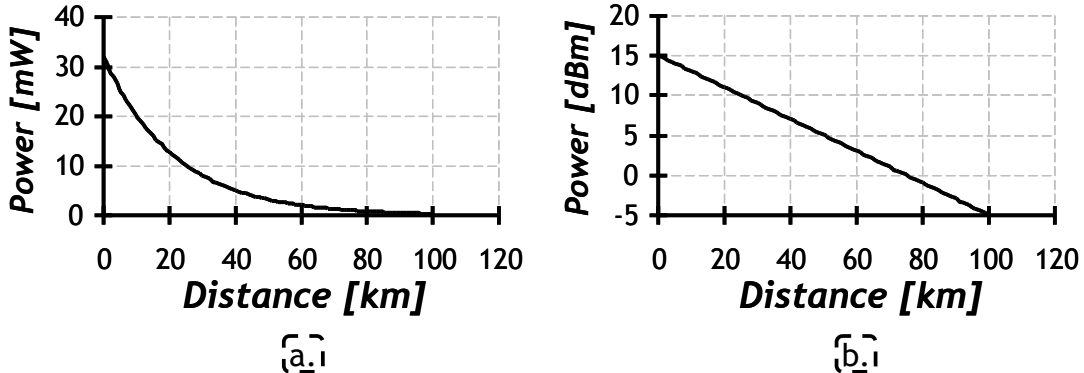


Fig. 1.2: Power profile of an optical signal propagating over an optical fibre with an attenuation of 0.2 dB/km as a function of the distance (a) in [mW] and (b) [dBm].

Apart from these two mechanisms, a peak of attenuation is observed at 1.39  $\mu$ m which corresponds to the absorption of the  $OH^-$  ions. Nevertheless, it can be nearly eliminated by reducing the concentration of hydroxyl ( $OH^-$ ) ions in the core of the optical fibre [5][7][8]. This absorption peak separates two low-loss regions historically used for optical-fibre transmissions located around 1300 nm and 1550 nm. More precisely, the telecommunication standardization sector of the international telecommunication union (ITU-T) defined six bands for transmission using single-mode fibre [9]: the O, E, S, C, L and U-band, as seen in Fig. 1.3. Although the attenuation is lower in the C-band, former transmissions were done in the O-band (around 1300 nm) because of the light sources available at that time. Advances in the opto-electronic components have allowed realizing transmissions around the C-band (around 1550 nm) where the minimum of attenuation is located. This value is typically around 0.2 dB/km and can be as low as 0.148 dB/km [10]. As a comparison, the attenuation of electrical cables is in the range of 100 and 1000 dB/km (for signals with carriers lower than 100 MHz) [11] whereas the conventional window glass shows an attenuation approximately of 100 dB/km.

Most of today's transmissions use the C-band, nevertheless the bandwidth can be enlarged by using the long-wavelength band, L-band (around 1590 nm) to increase the transmission capacity and/or the number of transmitted wavelength channels. A total of approximately 160 wavelength channels can be transmitted on a 50-GHz grid when combining both bands [12].

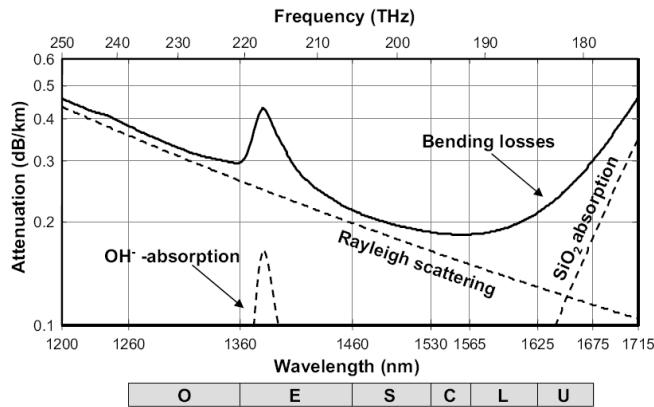


Fig. 1.3: Fiber attenuation dependence on the wavelength and frequency.

Although fibre loss is small, it remains one of the main limiting aspects for optical communications systems. Hence optical signal must be reamplified along the transmission link to increase the maximum reachable distance, as discussed in section 2.4.

### 1.1.2 Chromatic dispersion

Chromatic dispersion (CD) refers to the wavelength dependence of the fibre refractive index which implies a phase-shift between the different spectral components along the transmission translated by a pulse broadening in time domain. This causes inter-symbol interference (ISI) and therefore limits the maximum reach achievable of optical transmission systems without chromatic dispersion management (see section 2.5).

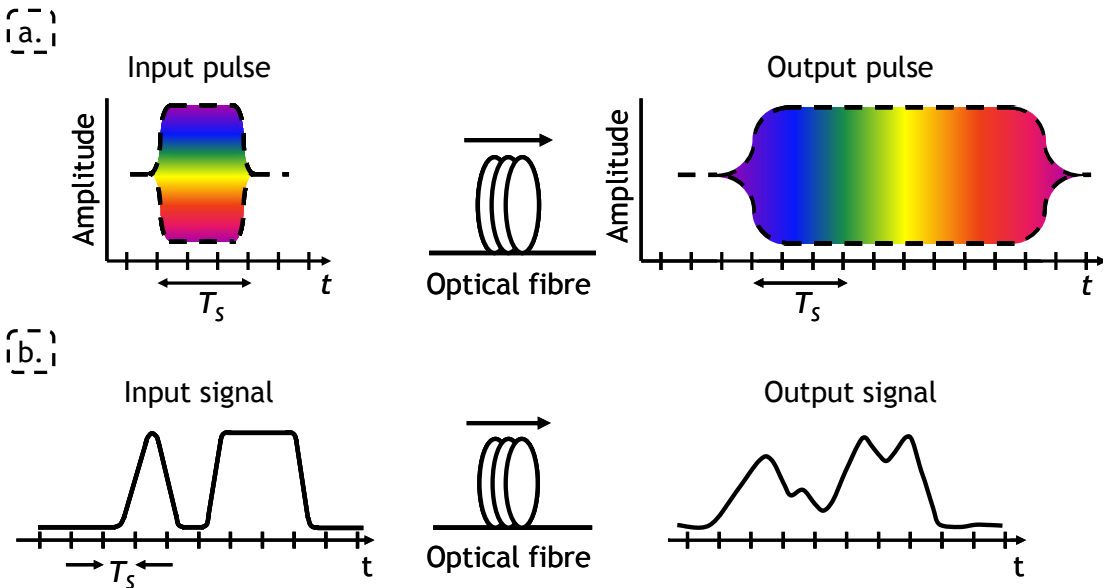


Fig. 1.4: (a) Schematic representation of the effect of a chromatic dispersive fibre (neglecting the effect of the attenuation) over a single impulsion and (b) over a sequence of symbols.

The speed of light travelling in an optical fibre, as in any other dielectric material, is lower than  $c$  and may be frequency dependent. The phase velocity,  $v_p$ , of any spectral component of a wave which propagates over an optical fibre is:

$$v_p(\omega) = \frac{c}{n_0 + \delta n(\omega)} \quad (1.4)$$

where  $\omega = 2\pi f$  is the angular frequency in [rad/s] and  $n_0 + \delta n(\omega)$  is the refractive index of the fibre which is larger than 1. The dependency of the refractive index on the angular frequency is known as material dispersion. The effect of the dispersion can be described by considering the mode-propagation constant [13],  $\beta$ , which is related to the phase velocity by :

$$\beta(\omega) = \frac{\omega}{v_p} = [n_0 + \delta n(\omega)] \frac{\omega}{c} \quad (1.5)$$

Expanding equation (1.5) in Taylor series with respect to the central frequency,  $\omega_0$ , gives:

$$\beta(\omega) \approx \beta_0 + \beta_1(\omega - \omega_0) + \frac{1}{2}\beta_2(\omega - \omega_0)^2 + \frac{1}{6}\beta_3(\omega - \omega_0)^3 + \dots \quad (1.6)$$

where  $\beta_i$  is the  $i$ -th derivative of the propagation constant with respect to the angular frequency.

$$\beta_i = \left. \frac{\partial^i \beta}{\partial \omega^i} \right|_{\omega=\omega_0} \quad (1.7)$$

$\beta_0$  in [ $km^{-1}$ ] implies a constant phase-shift whereas  $\beta_1$  in [ $ps/km$ ] is related to the envelope propagation speed also called group velocity, which is defined by  $v_g = 1/\beta_1$ . Therefore a group index is also defined as  $n_g = c/v_g$ . The second order derivative corresponds to the acceleration of the spectral components in the pulse and is responsible of the pulse broadening in time domain.  $\beta_2$  is called group velocity dispersion (GVD) and is expressed in [ $ps^2/nm$ ]. Finally,  $\beta_3$  in [ $ps^3/nm$ ] is the GVD slope and expresses the variation of GVD as a function of the angular frequency.

From a fibre-optic transmission systems point of view, it is more common to use the dispersion factor,  $D$ , and its slope,  $D'$ , which are wavelength dependent and are related to  $\beta_2$  and  $\beta_3$  by:

$$\begin{aligned} D &= \frac{\partial \beta_1}{\partial \lambda} = -\frac{2\pi c}{\lambda^2} \beta_2 \\ D' &= \frac{\partial D}{\partial \lambda} = \frac{4\pi c}{\lambda^3} \left( \beta_2 + \frac{\pi c}{\lambda} \beta_3 \right) \end{aligned} \quad (1.8)$$

$D$ , and  $D'$  are expressed in [ $ps/(nm \cdot km)$ ] and [ $ps/(nm^2 \cdot km)$ ]. Apart from material dispersion, another dispersive effect existing in single-mode fibres is waveguide dispersion. Waveguide dispersion is related to the fact that the wave is not perfectly confined within the core and therefore a fraction of the field propagates through the cladding [14]. Since cladding and core have different refractive indexes, the part of the field propagating through the core and through the cladding travel at different velocities causing thus dispersion. Zero dispersion is obtained at the wavelength  $\lambda_0$ , called zero-dispersion wavelength, in which the influence of material and waveguide dispersion are equal but with opposite sign. A different dispersive-regime is observed on each side of  $\lambda_0$  as see in Fig. 1.5.

- When  $D < 0$ , i.e.  $\beta_2 > 0$ , we talk about “normal” regime. In this case, short-wavelength spectral-components travel at a lower group velocity than longer ones.
- In contrast, when  $D > 0$ , i.e.  $\beta_2 < 0$ , we talk about “anomalous” regime. Here, long-wavelength spectral-components travel at a lower group velocity.

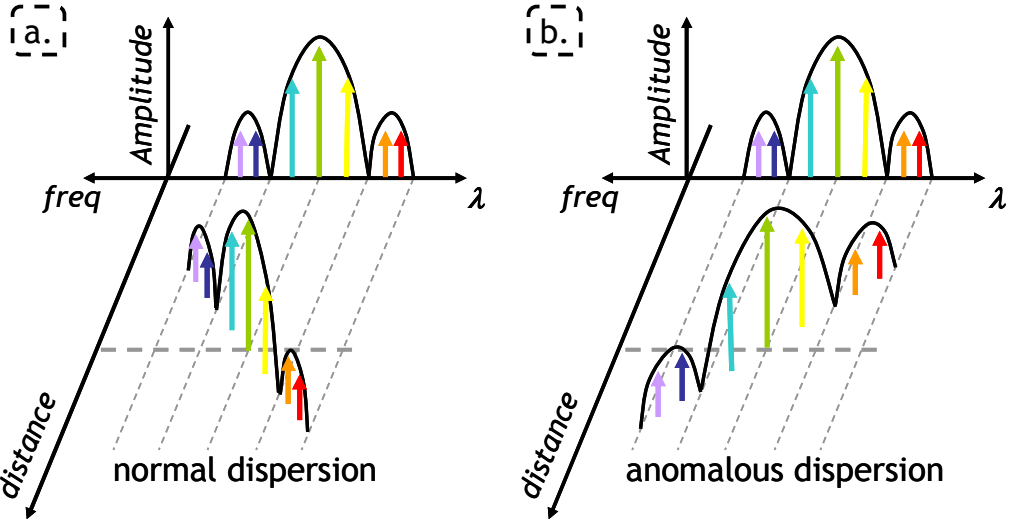


Fig. 1.5: Schematic representation of both (a) normal and (b) anomalous dispersion regime.

The pulse spreading in time domain may cause ISI in fibre-optic transmission systems. Normalized dispersion length,  $L_D$ , characterizes the distance after which a Gaussian pulse of initial width  $T_0$  broadens by a factor of  $\sqrt{2}$  [15] due to the GVD:

$$L_D = \frac{T_0^2}{|\beta_2|} \quad (1.9)$$

$T_0$  is inversely proportional to data symbol-rate. As it can be clearly appreciated, the tolerance to dispersion scales therefore with the inverse of the square of the symbol rate.

The magnitude of waveguide dispersion depends on parameters of the structure of the fibre such as the difference of refractive index between the core and cladding or the radius of the core. Consequently, specific fibre-design is realised in order to obtain different dispersion characteristics. Standard single mode fibres (SSMF) have a zero-dispersion wavelength around 1320 nm [16] and a dispersion coefficient of 17 ps/(nm·km) at 1550 nm with a slope of 0.057 ps/(nm<sup>2</sup>·km).  $\lambda_0$  can be shifted to longer wavelengths (near or within the C band) by increasing the magnitude of waveguide dispersion. Thus, dispersion shifted fibres (DSF) and non-zero dispersion shifted fibres (NZDSF) have been developed [13]. DSF shows a zero-dispersion wavelength at 1550 nm whereas for NZDSF there is no unique standard and each fibre manufacturer develops their own fibre, for example: Alcatel *TeraLight<sup>TM</sup>*, Corning *LEAF<sup>TM</sup>* and Lucent *TrueWave<sup>TM</sup>*. Nevertheless, in general, NZDSF have a zero-dispersion wavelength around 1450 nm and a dispersion of between 2 and 8 ps/(nm·km) approximately at 1550 nm.

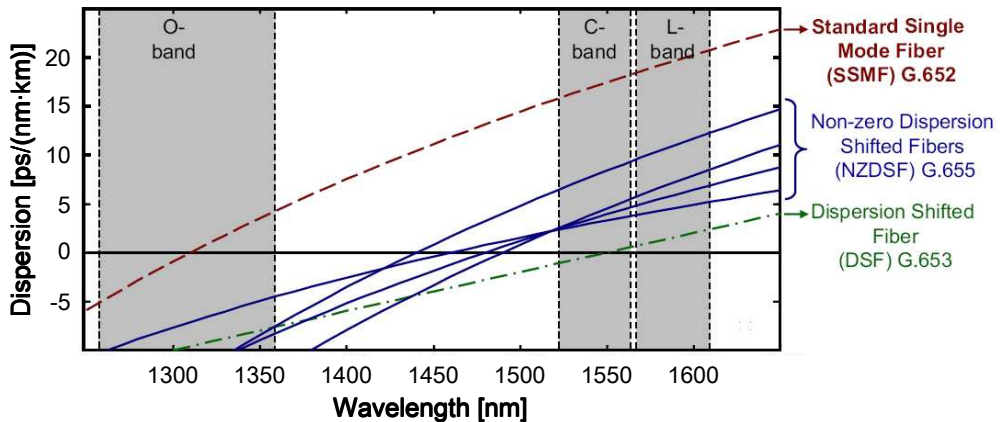


Fig. 1.6: Dispersion dependence on the wavelength

A fibre with negative dispersion in the C-band and negative slope can be created by using a complex refraction index. Such kind of fibres is commonly used in long-haul transmissions in order to compensate for the cumulated dispersion and is known as dispersion compensating fibre (DCF). Different types of DCF exist with different dispersive characteristics. The most widely used DCF compensates for the dispersion and the slope of the SSMF and have a dispersion around  $-170 \text{ ps}/(\text{nm}\cdot\text{km})$  and a matched slope following the same ratio between both dispersions.

### 1.1.3 Polarisation mode dispersion

Polarisation mode dispersion (PMD) arises from the birefringence of the fibre, i.e. the dependence of the refractive index on the signal polarisation. However before talking about PMD, differential group delay (DGD) should be introduced. An arbitrarily-polarised optical wave can be represented as the linear superposition of two orthogonally polarised modes. In ideal fibres, the propagation properties of the two modes are identical due to the cylindrical symmetry of the waveguide. Nevertheless, real fibres contain some amount of asymmetry owing to an accidental loss of circular symmetry during the manufacturing process and/or caused by external forces in handling or cabling or by temperature conditions. Therefore the symmetry axes of the fibre are no longer equal and the propagation of both modes is not exactly the same leading to birefringence  $B$  and a difference in group velocity  $\Delta\beta_1$  [15]:

$$B = \frac{c}{\omega_0} |\beta_s - \beta_f| = |n_s - n_f| \quad (1.10)$$

where  $\beta_s$  and  $\beta_f$  are the propagation constants of the slow and fast modes respectively provided the refractive indexes verify  $n_s > n_f$ . The difference between mode-propagation constants implies a periodic change in the polarisation of the light with period  $L_B = \lambda / B$  in [km] when the signal is coupled into the fibre in between both orthogonal axes as well as a delay between the modes propagating over the different axes:

$$\Delta t = \left| \frac{L}{v_{gs}} - \frac{L}{v_{gf}} \right| = L |\beta_{1,s} - \beta_{1,f}| \quad (1.11)$$

where  $1 / \beta_{1,S}$  and  $1 / \beta_{1,F}$  are the group velocities of the slow and fast modes, respectively. Fig. 1.7-a depicts the effect of the PMD in the time domain over a fibre with constant birefringence. Two pulses sent at the same time over the slow and the fast axes respectively are delayed by an amount  $\Delta t$  after a given distance. This amount  $\Delta t$  in [ps] is known as DGD or first-order PMD. This effect can cause pulse broadening or even a split into two different pulses.

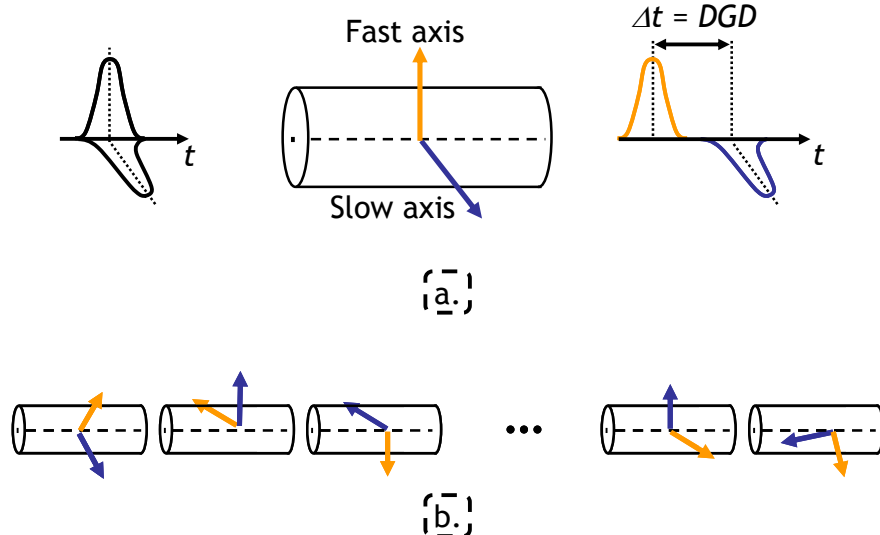


Fig. 1.7: (a) Time-domain effect of first order PMD or DGD over a fibre with constant birefringence and (b) schematic representation of a real fibre model as a concatenation of infinitesimal birefringent sections randomly coupled.

Polarisation maintaining fibres (PMF) verify the hypothesis that birefringence and DGD can be considered constant along the length and time. A large asymmetry between both birefringence axes is induced during the fabrication process of these fibres so as asymmetry caused by external forces and temperature can be neglected. In contrast, fibre constraints, and consequently birefringence, vary randomly with distance and time due to environmental changes in standard transmission fibres. DGD is therefore a stochastic process and PMD is indeed defined as its mean value [17]. Standard optical fibre can be modelled as a concatenation of infinitesimal randomly coupled birefringent sections, as seen in Fig. 1.7-b. Considering this concatenation, there is an input state of polarisation (SOP) for which the output SOP remains unchanged. This input SOP is known as principal state of polarisation (PSP). In PMF, the PSP corresponds to the birefringence axes. The DGD at the output of a standard fibre is the result of the contribution of every infinitesimal birefringent section and can be modelled by a Maxwellian probability density function as shown by Poole et al. [18], so as:

$$P(\Delta t) = \frac{32}{\pi} \cdot \frac{\Delta t^2}{\langle \Delta t \rangle^3} \cdot \exp\left(-\frac{4}{\pi} \cdot \frac{\Delta t^2}{\langle \Delta t \rangle^2}\right) \quad (1.12)$$

where  $\langle \cdot \rangle$  denotes the average and  $\Delta t$  is the DGD. This distribution is represented in Fig. 1.8 for a 43 ps PMD fibre measured during 6 months. One can easily deduce that it is difficult to guarantee permanently the correct operation of a fibre-based communications system since there is a non-zero probability of having a very large DGD. However, one can guarantee that the DGD will not exceed a given value

during more than a certain fraction of time per year which is called system outage probability (by assuming that DGD is an ergodic process over one year). A commonly accepted value for this fraction of time is 5 minutes per year or, in other words, an out-of-service probability of  $1 \cdot 10^{-5}$ .

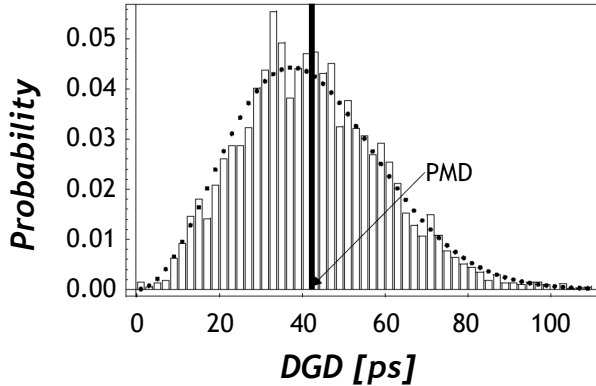


Fig. 1.8: Statistical distribution of measured DGD of a fibre with 43 ps PMD over 6 months [19].

For PMF, PMD is equivalent to DGD and scales linearly with the length, whereas for standard transmission fibres, PMD scales with the root-mean-square of the length due to the random orientation of the birefringent waveplates that constitute them. Thus, the PMD coefficient, in  $[ps/\sqrt{km}]$ , multiplied by the square root of the fibre length L, gives the total PMD value of the fibre link. The physical units of the PMD coefficient indicate that the maximum tolerable amount of PMD decreases linearly with the increasing symbol rate, R, whereas the maximum reach limited by the PMD scales quadratically with R. Modern optical fibres have a PMD value in the order of  $0.05 ps/\sqrt{km}$  [20] while older already installed ones may have a much higher PMD coefficient.

It has to be noted that when along the transmission link there are points with high local PMD, the model of infinite small consecutive birefringent sections randomly coupled does not apply. This local PMD can be caused by thermal conditions or mechanical vibrations of roads or railroads for example. In this case the outage probability may depend on the optical frequency and the Maxwellian model may lead to an overestimation of the outage probability [21][22].

#### 1.1.4 Polarisation dependent loss

Another polarisation effect stemming from the asymmetry of the fibre is polarisation-dependent loss (PDL). PDL refers to the fact that the two orthogonal polarisation modes suffer different attenuation during propagation. The PDL of a given component is usually expressed as the ratio between the maximum and the minimum power transitivity in decibels [23][24]:

$$PDL = 10 \cdot \log_{10} \left( \frac{T_{\max}}{T_{\min}} \right) \quad (1.13)$$

It is mainly introduced by optical components such as optical isolators or amplifiers. PDL is therefore randomly distributed and translates into signal power

fluctuations depending on the random evolution of the SOP. These power fluctuations cause OSNR variations and depolarisation when PDL axes are not aligned with the birefringence axes since PSPs, or more properly fibre eigenmodes, are no longer orthogonal to each other.

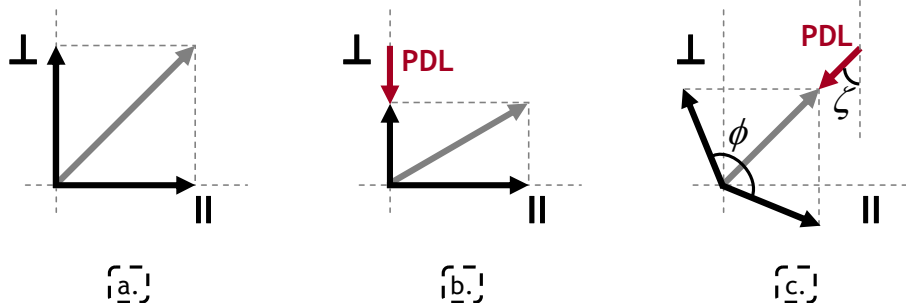


Fig. 1.9: PDL effect, (a) reference signal without PDL, (b) PDL aligned with polarisation axes and (c) PDL with an angle  $\zeta = \pi / 4$  with respect to polarisation axis.

The impact of PDL can be stronger in systems exploiting SOP to transmit information as for example polarisation division multiplexed (PDM) systems (described in section 2.2) which encodes information in both polarisation tributaries (parallel and perpendicular) [25][26]. Consider one isolated PDL element. When its axis is aligned with the polarisation tributaries of the PDM signal, PDL further attenuates one of the two polarisation tributaries compared to the other, as depicted in Fig. 1.9-b. This translates in a different OSNR for each polarisation tributary, degrading hence the total performance. In contrast, PDL results not only in a loss of OSNR but also in depolarisation of the signal when there is an angle,  $\zeta$ , between the PDL axis and the polarisation tributaries. I find that the resulting angle between parallel and perpendicular tributary,  $\phi$ , is:

$$\phi = \frac{\pi}{2} + \tan^{-1} \left( \sqrt{PDL'} \tan \zeta \right) - \tan^{-1} \left( \frac{1}{\sqrt{PDL'}} \tan \zeta \right) \quad (1.14)$$

where  $PDL' = \sqrt{T_{\max} / T_{\min}}$  is the linear PDL. Other expressions leading to the same result can be found in the literature [25].

At the output of the PDL element, polarisation tributaries are no longer orthogonal, as illustrated in Fig. 1.9-c. This translates in crosstalk between polarisation tributaries at the receiver side if a polarisation beam splitter (PBS) with orthogonal axes is used. This effect is maximum when the angle between the PDL axis and the polarisation tributaries is  $\zeta = \pi/4$ , which results in an angle:

$$\phi = 2 \tan^{-1} \left( \sqrt{PDL'} \right) \quad (1.15)$$

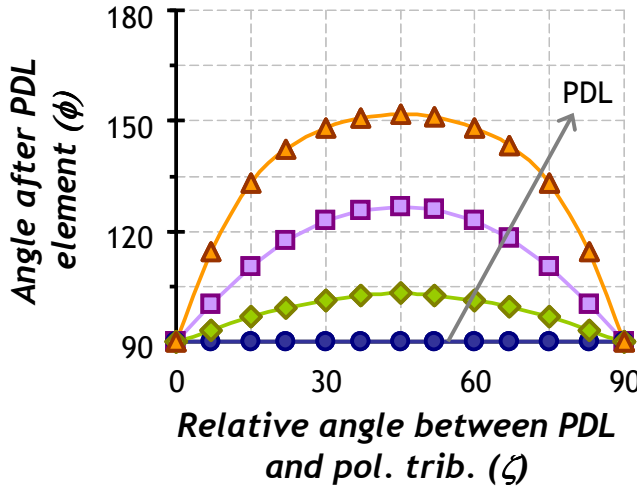


Fig. 1.10: Evolution of the angle between the two (originally orthogonal) polarisation tributaries at the output of a PDL element ( $\phi$ ) versus the relative angle between PDL and polarisation axis ( $\zeta$ ) for different PDL values: ● 0 dB, ◆ 1 dB, ■ 3 dB and ▲ 6 dB.

## 1.2. Nonlinear transmission effects

### 1.2.1 Kerr effect

Kerr effect is the main cause of the nonlinear distortions experienced by the optical signal in WDM transmissions. Indeed, Kerr effect creates changes in the refractive index of the material in response to an electromagnetic field depending on its optical power  $|E|^2$  [14]:

$$\tilde{n}(\omega, |E|^2) = n_0(\omega) + n_2 \frac{|E|^2}{A_{\text{eff}}} \quad (1.16)$$

where  $A_{\text{eff}}$  is the effective core area of the fibre in  $[m^2]$ ,  $n_0(\omega)$  is the linear contribution of the refractive index and  $n_2$  is the nonlinear one in  $[m^2/W]$ . The typical value of  $n_2$  for silica is around  $2.5 \cdot 10^{-20} m^2/W$  and is weakly dependent on the type of fibre. On the contrary, the effective area strongly depends on fibre parameters such as the core radius and the core-cladding index difference and critically influences the strength of the Kerr effect. Effective area is defined by [15]:

$$A_{\text{eff}} = \frac{\left( \iint |F(x, y)|^2 dx dy \right)^2}{\iint |F(x, y)|^4 dx dy} \quad (1.17)$$

where  $F(x, y)$  is modal distribution for the fundamental fibre mode. Typically,  $A_{\text{eff}}$  can vary in the range 20–100  $\mu\text{m}^2$  in the 1500– $\mu\text{m}$  region depending on the fibre design.

The propagation of a signal along a sufficiently long randomly birefringent transmission fibre including attenuation, chromatic dispersion and nonlinearities is described by the modified nonlinear Schrödinger equation (NLSE) [27]:

$$\frac{\partial E}{\partial z} = - \underbrace{\frac{\alpha}{2} E}_{\text{attenuation}} - \underbrace{\frac{i}{2} \beta_2 \frac{\partial^2 E}{\partial T^2}}_{\text{dispersion}} + \underbrace{\frac{1}{6} \beta_3 \frac{\partial^3 E}{\partial T^3}}_{\text{dispersion slope}} + \underbrace{i\gamma |E|^2 E}_{\text{Kerr nonlinearities}} \quad (1.18)$$

where  $E$  represents the envelope of the optical field,  $z$  is the distance,  $\alpha$  is the attenuation coefficient in  $[Np/km]$ ,  $T = t - \beta_1 \cdot z$  is the time measured in a retarded frame and  $\gamma$  is the nonlinear coefficient in  $[1/(W \cdot km)]$ , defined as:

$$\gamma = \frac{8}{9} \cdot \frac{2\pi}{\lambda} \cdot \frac{n_2}{A_{\text{eff}}} \quad (1.19)$$

The factor of 8/9 in the nonlinear coefficient has been verified experimentally [28][29]. It has to be noted that the factor of 8/9 becomes 1 in fibres with constant birefringence, such as PMF. The strength of the Kerr effect is proportional to the optical signal power  $|E|^2$ . Therefore, the impact of Kerr effect is stronger over the first kilometres of the fibre since the optical power decreases exponentially along the transmission length, as seen in equation (1.1). This first part of the fibre is known as the high power region and is upper-bounded by the effective length,  $L_{\text{eff}}$ . The effective length corresponds to the integration of the normalized power over the fibre length:

$$L_{\text{eff}} = \int_0^L \exp(-\alpha z) dz = \frac{1 - \exp(-\alpha L)}{\alpha} \quad (1.20)$$

where  $L$  is the total length of the fibre and  $\alpha$  is the attenuation coefficient in  $[Np/km]$ . For example, the effective length of 100 km of SSMF, with an attenuation coefficient of 0.2 dB/km, is 21.5 km.

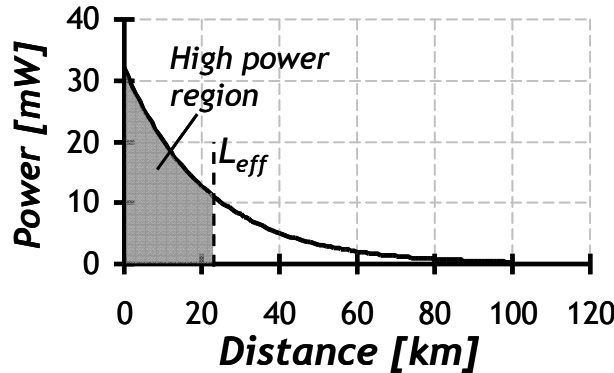


Fig. 1.11: Power profile of an optical signal propagating over 100 km of optical fibre with an attenuation of 0.2 dB/km as a function of the distance.

The main nonlinear impairments stemming from Kerr effect can be divided in two categories namely *intra*-channel and *inter*-channel effects. Intra-channel refers to nonlinearities occurring within a wavelength channel itself whereas inter-channel effects originate from the interaction between different wavelength channels. Both types of effects can be in turn broken down into more elementary nonlinearities arising either from signal-signal interactions or from the interplay between the optical signal field and the noise, mainly amplified spontaneous emission (ASE), as seen in Fig. 1.12.

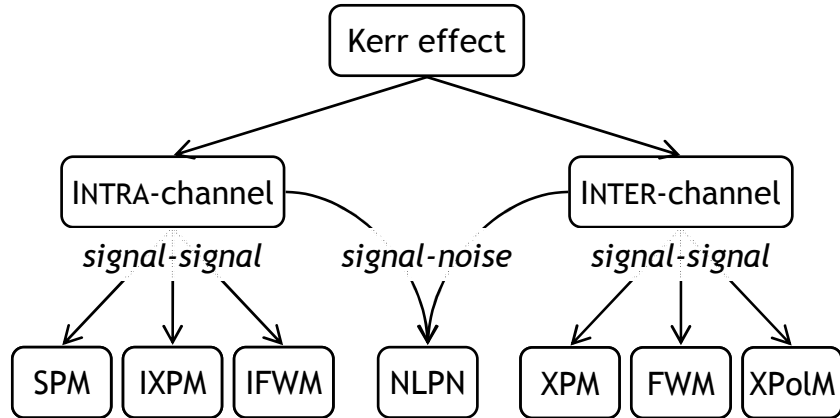


Fig. 1.12: Classification of nonlinearities in optical fibres. Intra-channel and inter-channel stand for nonlinearities occurring within or between WDM channels, respectively.

### 1.2.2 Self-phase modulation

An electromagnetic field propagating through the optical fibre modifies the refractive index depending on its own instantaneous power, according to equation (1.16). This momentaneous variation of the refractive index translates into a phase shift of the optical signal known as self-phase modulation (SPM). The impact of SPM can be studied through NLSE, equation (1.18), neglecting the influence of chromatic dispersion, i.e.  $\beta_2 = \beta_3 = 0$ :

$$\frac{\partial E}{\partial z} = - \underbrace{\frac{\alpha}{2} E}_{\text{attenuation}} + \underbrace{i\gamma |E|^2 E}_{\text{Kerr nonlinearities}} \quad (1.21)$$

The solution of this equation is:

$$E(z, T) = E(0, T) \cdot \exp\left(-\frac{\alpha z}{2}\right) \cdot \exp(i\Phi_{NL}(z, T)) \quad (1.22)$$

where  $E(0, T)$  is the field amplitude at  $z=0$  and  $\Phi_{NL}$  is the SPM-induced phase modulation, defined as:

$$\Phi_{NL}(z, T) = \gamma \cdot |E(0, T)|^2 \cdot \frac{1 - \exp(-\alpha z)}{\alpha} \quad (1.23)$$

The maximum of  $\Phi_{NL}$  is obtained at the centre of the pulse ( $T=0$ ) after the propagation over the length of the fibre,  $L$ , corresponding to:

$$\Phi_{NL,\max} = \gamma \cdot P_0 \cdot L_{eff} \quad (1.24)$$

Unlike chromatic dispersion, the SPM-induced phase shift is time varying since different parts of the pulse have different intensity. Thus, it also implies a nonlinear frequency shift,  $\delta\omega$ :

$$\delta\omega(T) = -\frac{\partial \Phi_{NL}}{\partial T} \quad (1.25)$$

The time dependence of  $\delta\omega$  is referred to as frequency chirping. As shown in Fig. 1.13, the signal frequency components is shifted towards lower frequencies (red shift) at the raising edge of the pulse whereas it is shifted towards higher frequencies (blue shift) during the falling one. Thus SPM may broaden the spectrum since new frequency components can be generated as the pulse propagates over the fibre making the signal less tolerant to narrow optical filtering [23].

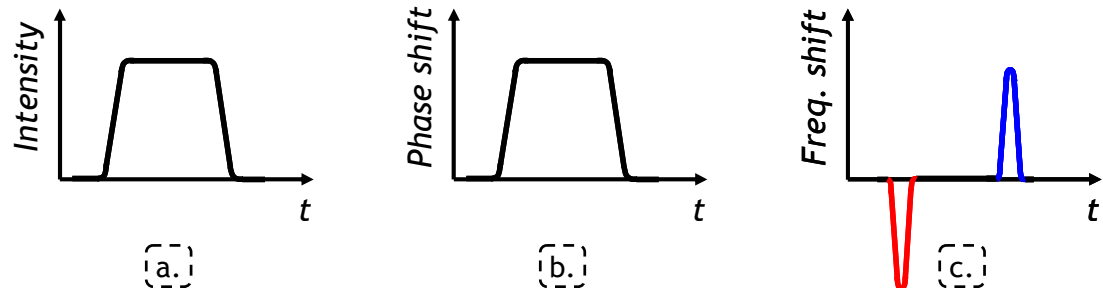


Fig. 1.13: (a) Temporal variation of pulse intensity, (b) SPM-induced phase and (c) frequency shift.

SPM translates into amplitude signal distortion through the interplay with chromatic dispersion. Nonlinearly-shifted frequency-components do not propagate at the same speed due to chromatic dispersion. When two pulse components with different frequency overlap, they interfere leading to nonlinear amplitude distortions, contrary to chromatic dispersion which induces a linear phase shift. As an example, Fig. 1.14 shows the impact of SPM onto a 10 Gb/s non-return-to-zero (NRZ) signal after a propagation over 200 km of SSMF with the chromatic dispersion fully compensated. It can be clearly observed a deformation of the signal over the edges of the pulses for the highest power per channel.

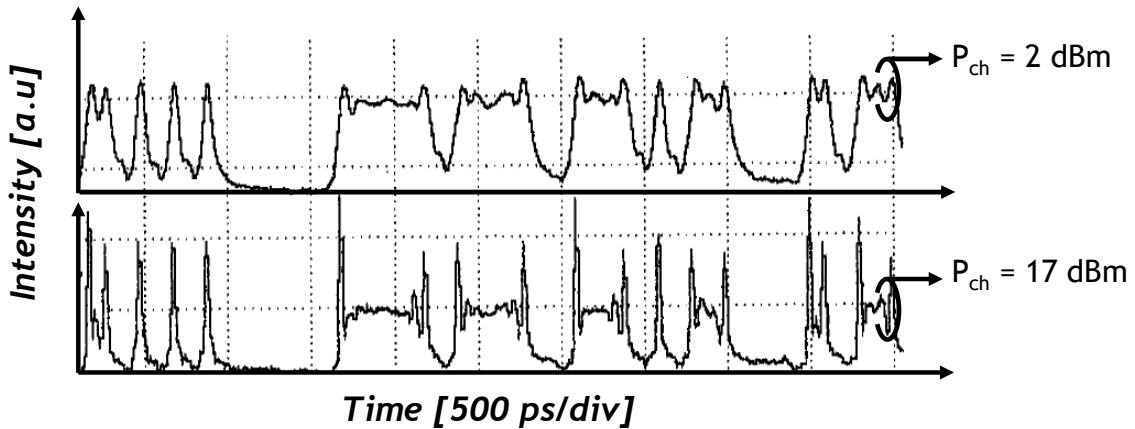


Fig. 1.14: Temporal variation of SPM-induced phase and frequency shift.

Nonetheless, the nonlinear chirp may be beneficial in specific cases, such as soliton propagation. The SPM-induced chirp can compensate the dispersion-induced pulse broadening in the anomalous regime of the SSMF. Thus, the SPM compress the pulse to compensate for the effect of dispersion. The shape of the pulse remains consequently unchanged (except for the attenuation) during the transmission, as first demonstrated by Mollenauer et. al. in 1980 [30]. Nevertheless, the practical implementation is not straightforward. The attenuation breaks the balance between SPM and chromatic dispersion which implies relatively small amplifier spacing,

around 50 km increasing the cost of the system. On the other hand, interactions between co-propagating channels strongly limit the reach in a WDM system.

### 1.2.3 Cross-phase modulation

Similarly to SPM, cross-phase modulation (XPM) arises from the dependence of the refractive index on the optical power. However, contrary to SPM, XPM depends on the power of other co-propagating WDM channels. XPM can be studied through NLSE, equation (1.18), considering two co-propagating channels,  $E_1$  and  $E_2$ . Neglecting both the influence of chromatic dispersion and the SOP-dependent terms, one can write NLSE as:

$$\frac{\partial E_k}{\partial z} = - \underbrace{\frac{\alpha}{2} E_k}_{\text{attenuation}} + \underbrace{i\gamma(|E_k|^2 + B|E_{3-k}|^2)E_k}_{\text{Kerr nonlinearities}} \quad (1.26)$$

where  $k = 1, 2$ ; and  $B$  is equal to 3/2 for fibres with randomly varying birefringence and after averaging over input signals SOPs [31]. In contrast,  $B$  depends on the difference in polarisation between both channels for linearly birefringent fibres, as PMF. In these fibres,  $B$  is equal to 2 when both channels have the same polarisation whereas it is equal to 2/3 when they are orthogonally polarised. The effective area can be indeed considered equal for both channels. The term  $B|E_{3-k}|^2$  depends on the power of the co-propagating channel and is the responsible of XPM. Since  $B$  can be as high as 2, XPM is potentially twice as effective as SPM for the same intensity.

Nonlinear phase modulation induced by XPM is obtained through equation (1.26), likewise for SPM. For the common case of random varying birefringence fibres, and after averaging over the co-propagating channel SOP:

$$\Phi_{NL,k}(z, T) = \gamma \cdot \left( |E_k(0, T)|^2 + \frac{3}{2} |E_{3-k}(0, T)|^2 \right) \cdot \frac{1 - \exp(-\alpha z)}{\alpha} \quad (1.27)$$

Consider the absence of chromatic dispersion. The effect of XPM is very close to SPM, with different strength, when the pulses of both wavelength channels overlap each other. In contrast, when the pulses at different wavelengths are only partially aligned the impact of the XPM is more detrimental since a part of the pulse is nonlinearly phase shifted while the other is not.

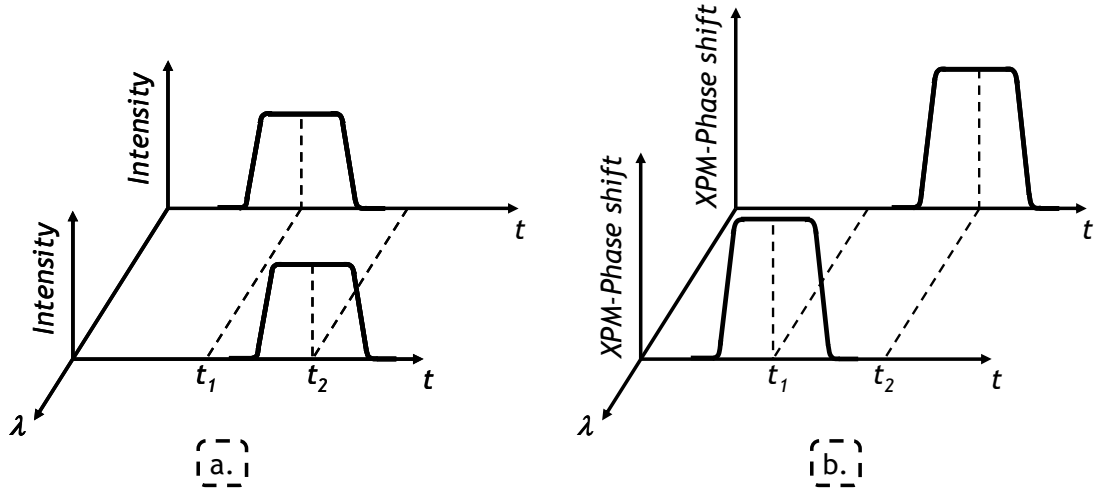


Fig. 1.15: (a) Temporal variation of the intensity of co-propagating pulses and (b) XPM-induced phase shift.

The interplay between XPM and chromatic dispersion translates the nonlinear phase shift into amplitude distortions. Besides, XPM scales with wavelength channel spacing and dispersion. One defines the walk-off length,  $L_w$ , as the distance in [m] for which two co-propagating pulses (at  $\lambda_1$  and  $\lambda_2$ ) are shifted by one symbol period,  $T_s$  [14]:

$$L_w = \frac{T_s}{|d_{12}|} \quad (1.28)$$

where  $d_{12}$  is the walk-off parameter in [ $s/m$ ], defined as:

$$d_{12} = \frac{1}{v_{g1}} - \frac{1}{v_{g2}} \approx D \cdot \Delta\lambda_{12} \quad (1.29)$$

with  $D$  is the dispersion parameter,  $\Delta\lambda_{12}$  is the wavelength separation between the two channels,  $\Delta\lambda_{12} = |\lambda_1 - \lambda_2|$ , and  $1/v_{g1}$  and  $1/v_{g2}$  are the group velocities of both channels. The faster two pulses walk-off, the bigger is the walk-off parameter and the smaller is the XPM-induced phase shift variance [32][33]. As it can be seen, the XPM-induced penalties can be reduced by increasing the dispersion factor and/or the wavelength separation [34]. Moreover, as the walk-off length scales with the symbol period, the impact of the XPM becomes smaller as the symbol rate increases for a given modulation format.

The XPM effect has been explained here for two wavelength channels transmission. However in WDM systems in which  $N$  wavelength channels are multiplexed, one channel is perturbed by the other  $N-1$  channels carrying different data and propagating at different velocities due to chromatic dispersion. This results in a very complex phase modulation depending on different parameters such as: dispersion, channel spacing, modulation format, or data and polarisation alignment, for example.

### 1.2.4 Four wave mixing

Four-wave mixing (FWM) is the phenomenon through which two or more frequency components interact nonlinearly to generate new frequency components. Likely to SPM and XPM, FWM is generated by the intensity-dependent refractive index of the silica [35]. In quantum-mechanical terms, FWM occurs when two or more photons are annihilated and new photons at different frequencies are created such that the net energy and momentum are conserved during the parametric interaction [15]. Stringent phase matching between different spectral components involved in the process is required to achieve high efficiencies.

Three photons at frequencies  $f_1$ ,  $f_2$  and  $f_3$  can be annihilated with simultaneous creation of a single photon at frequency  $f_4 = f_1 + f_2 - f_3$ . Therefore, FWM can generate third frequency harmonic if  $f_1 = f_2 = f_3$ , or frequency conversion otherwise. The phase matching required between the different frequency components for the FWM process is very difficult to satisfy in fibre optic transmissions and consequently the efficiency is low. The most efficient and thereby most observed variant of FWM occurs when two photons at  $f_1$  and  $f_2$  transfer their energy to two other photons at  $f_3$  and  $f_4$  so as:

$$f_1 + f_2 = f_3 + f_4 \quad (1.30)$$

The phase matching condition in this case is [15]:

$$n_1 \cdot f_1 + n_2 \cdot f_2 = n_3 \cdot f_3 + n_4 \cdot f_4 \quad (1.31)$$

where  $n_i$  are the refractive indexes at  $f_i$ . This requirement is easier to satisfy when  $f_1 = f_2$ . Thus, a couple of photons at  $f_1$  generate two photons at  $f_3$  and  $f_4$ . This specific case is referred to as degenerate FWM.

According to this mechanism, two wavelength multiplexed channels at  $f_1$  and  $f_2$  will create FWM products at  $f_3 = 2f_1 - f_2$  and  $f_4 = 2f_2 - f_1$ , as seen in Fig. 1.16. This effect can be significantly detrimental in WDM systems where channels are regularly-spaced and the FWM-generated products results into cross-talk from other co-propagating channels.

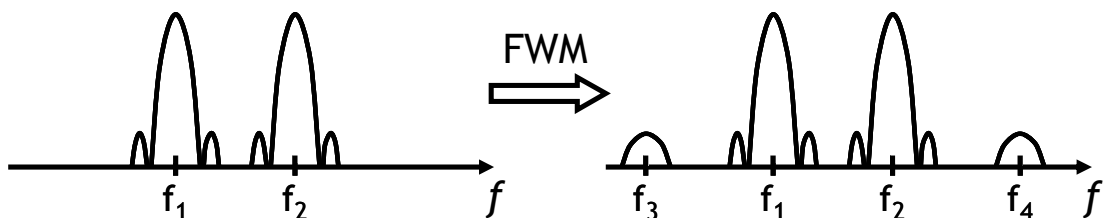


Fig. 1.16: New frequency components generation through FWM

FWM efficiency strongly depends on the phase matching of the involved spectral-components. Thereby, high chromatic dispersion can drastically reduce the impact of FWM. The phase velocity of each spectral component is different due to dispersion and consequently the phase matching is only satisfied during a short time. At the same time, higher symbol-rate signals are more tolerant to FWM than lower ones since they are further impacted by chromatic dispersion.

### 1.2.5 Intra-channel cross-phase modulation and four-wave mixing

Intra-channel cross-phase modulation (IXPM) and four-wave mixing (IFWM) are the analogue of XPM and FWM (discussed in sections 1.2.3 and 1.2.4) for distortions caused and suffered by a wavelength channel itself. The principles of IXPM and IFWM are the same as XPM and FWM. Nevertheless, the nonlinear distortions of the pulse arise no longer from co-propagating wavelength channels but from other pulses at the same wavelength that have been broadened by chromatic dispersion, as shown in Fig. 1.17-a-b.

Chromatic dispersion broadens time pulses, as seen in section 1.1.2. Hence a number of consecutive pulses overlap (Fig. 1.17-b) creating time-varying intensity fluctuations. These fluctuations are responsible of IXPM-induced phase shifts through Kerr effect which are translated into time jitter once chromatic dispersion is compensated (Fig. 1.17-c) [36][37], as shown in Fig. 1.17.

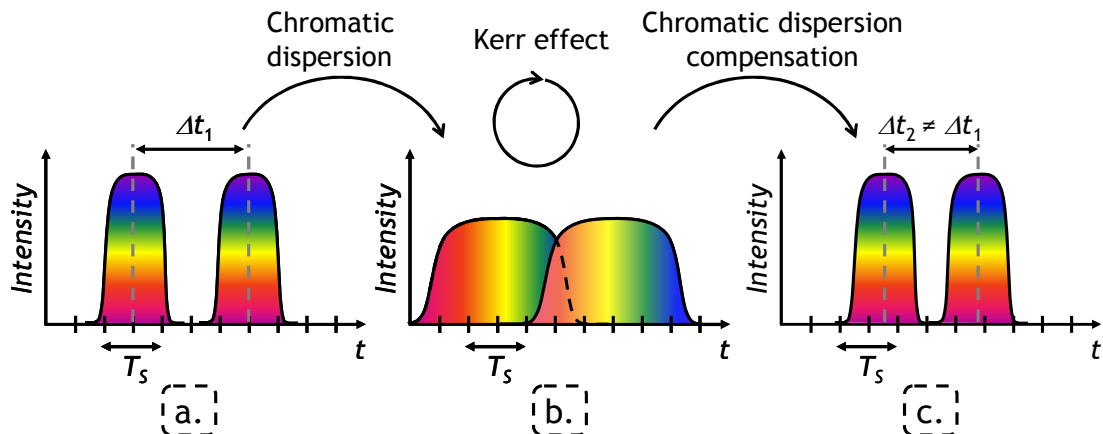


Fig. 1.17: Principle of intra-channel XPM.

The mechanisms behind IFWM are similar to IXPM but the consequences are much different. IFWM leads to an energy transfer between two consecutive pulses generating new pulses known as “ghost” or “shadow pulses” [37]. To illustrate such effect, one can consider a return-to-zero (RZ) signal carrying the sequence “0 1 1 0”, as seen in Fig. 1.18-a. Pulses corresponding to “1” are spread due to chromatic dispersion (Fig. 1.18-b). They then overlap and interact nonlinearly through Kerr effect generating two four-wave mixing products (Fig. 1.18-c). As a consequence, two shadow pulses appear where there should be no intensity once chromatic dispersion is compensated (Fig. 1.18-d) [37][38]. This effect is evidently most important in intensity-modulated signals as light is observed where zero-intensity should be.

Intra-channel XPM and FWM are particularly important for transmissions at symbol rates beyond 40 Gb/s over high dispersive fibre such as SSMF, known as pseudo-linear regime [37][38]. Nevertheless, their impact can be reduced using a symmetric transmission link in terms of chromatic dispersion. This can be done by splitting the chromatic dispersion between the transmitter and the receiver [39] or by mid-link optical phase conjugation [40][41].

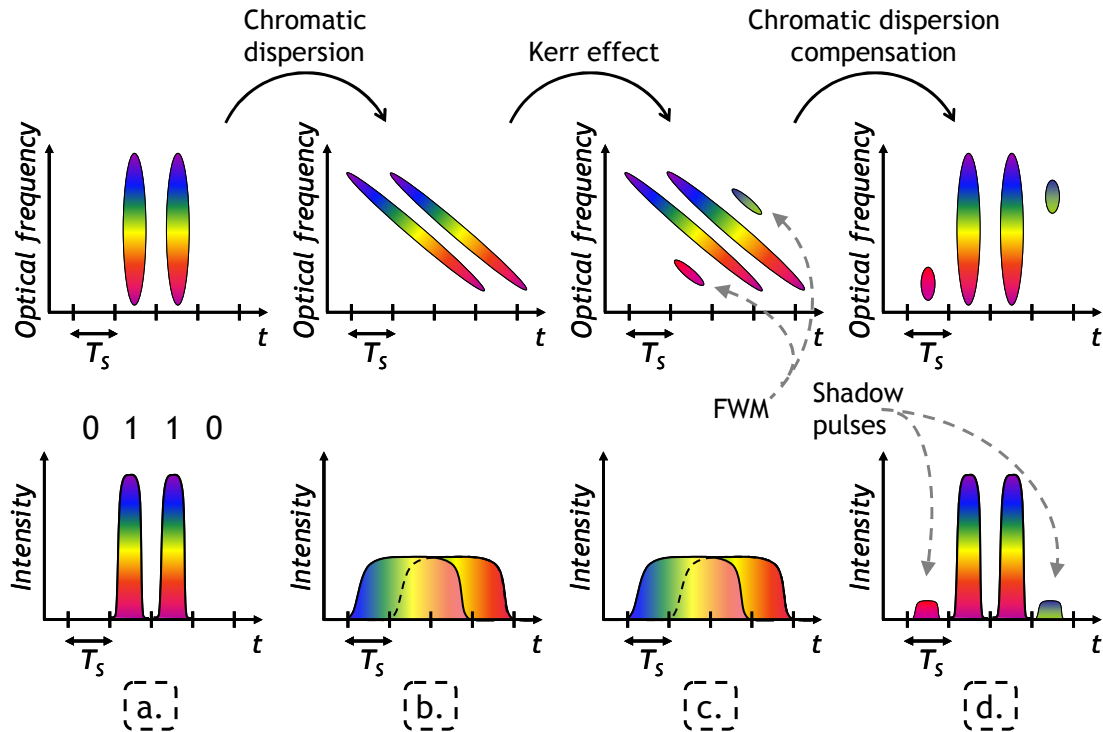


Fig. 1.18: Principle of intra-channel FWM (after [38])

### 1.2.6 Cross-polarisation modulation

Cross-polarisation modulation (XPolM) refers to the SOP scattering of the field due to a different nonlinear induced phase-shift onto each of the polarisations components of the field caused by co-propagating channels. It arises from Kerr effect like the other nonlinear effects. XPolM can be studied through the coupled NLSE in its vector form neglecting the influence of chromatic dispersion [31]. Consider the field evolution of one channel propagating at  $\lambda_1$ ,  $\underline{E}_1$ , surrounded by other co-propagating channels at  $\lambda_n$ :

$$\frac{\partial \underline{E}_1}{\partial z} = i\gamma \exp(-\alpha z) \left\{ \underbrace{s_{01}\sigma_0}_{SPM} + \underbrace{\frac{3}{2} \sum_{n \neq 1} s_{0n}\sigma_0}_{\text{"scalar" XPM}} + \underbrace{\frac{1}{2} \sum_{n \neq 1} s_n^T \sigma}_{XPolM} \right\} \underline{E}_1 \quad (1.32)$$

where  $\underline{E}_n = \exp(-\alpha z)(E_{xn} \ E_{yn})^T$  is the two dimensional complex vector which describes the optical field of the  $n$ -th wavelength channel in Jones space,  $\underline{\sigma} = (\sigma_1 \ \sigma_2 \ \sigma_3)^T$  is the Pauli-matrices vector, the Pauli matrices being:

$$\sigma_0 = \begin{pmatrix} 1 & 0 \\ 0 & 1 \end{pmatrix} \quad \sigma_1 = \begin{pmatrix} 1 & 0 \\ 0 & -1 \end{pmatrix} \quad \sigma_2 = \begin{pmatrix} 0 & 1 \\ 1 & 0 \end{pmatrix} \quad \sigma_3 = \begin{pmatrix} 0 & -i \\ i & 0 \end{pmatrix} \quad (1.33)$$

$\underline{s}_n = (s_{1n} \ s_{2n} \ s_{3n})^T$  is the three-dimension Stokes vector of unit length indicating the polarisation of the field:

$$\underline{s} = E^+ \underline{\sigma} E = \begin{pmatrix} \underline{E}^+ \underline{\sigma}_1 \underline{E} \\ \underline{E}^+ \underline{\sigma}_2 \underline{E} \\ \underline{E}^+ \underline{\sigma}_3 \underline{E} \end{pmatrix} \quad (1.34)$$

where ‘+’ denotes the conjugate transpose. The components of  $\underline{s}$  are the Stokes parameters:

$$\begin{cases} s_{0n} = |E_{xn}|^2 + |E_{yn}|^2 \\ s_{1n} = |E_{xn}|^2 - |E_{yn}|^2 \\ s_{2n} = 2 \operatorname{Re} \{E_{xn}^* E_{yn}\} \\ s_{3n} = 2 \operatorname{Im} \{E_{xn}^* E_{yn}\} \end{cases} \quad (1.35)$$

The first and second terms of the right part of equation (1.32) correspond to the SPM and XPM described in sections 1.2.2 and 1.2.3 respectively. XPM-term is denoted as “scalar” in contrast to the last term which does depend on the SOP of the field. The SPM and scalar-XPM terms are independent of the SOP, as it can be observed. They imply the same amount of nonlinear phase-shift into both polarisations and consequently do not change the SOP. In contrast, XPolM induces different phase-shift onto each polarisation components,  $E_{x1}$  and  $E_{y1}$ , which results in a change of the relative phase difference between them which in turn changes the SOP

In order to explicitly observe the evolution of each of the polarisation components, one can decouple the equation (1.32) using equations (1.33) and (1.35). For two linearly-polarised channels,  $\underline{E}_1$  and  $\underline{E}_2$ , this leads to the following expressions:

$$\begin{aligned} \frac{\partial E_{x1}}{\partial z} &= i\gamma' \left\{ \underbrace{\left( |E_{x1}|^2 + |E_{y1}|^2 \right)}_{SPM} E_{x1} + \underbrace{\frac{3}{2} \left( |E_{x2}|^2 + |E_{y2}|^2 \right)}_{\text{"scalar" XPM}} E_{x1} + \dots \right. \\ &\quad \left. \dots + \frac{1}{2} \underbrace{\left[ \left( |E_{x2}|^2 - |E_{y2}|^2 \right) E_{x1} + 2(E_{x2} E_{y2}^*) E_{y1} \right]}_{XPolM} \right\} \\ \frac{\partial E_{y1}}{\partial z} &= i\gamma' \left\{ \underbrace{\left( |E_{x1}|^2 + |E_{y1}|^2 \right)}_{SPM} E_{y1} + \underbrace{\frac{3}{2} \left( |E_{x2}|^2 + |E_{y2}|^2 \right)}_{\text{"scalar" XPM}} E_{y1} + \dots \right. \\ &\quad \left. \dots + \frac{1}{2} \underbrace{\left[ \left( |E_{y2}|^2 - |E_{x2}|^2 \right) E_{y1} + 2(E_{x2}^* E_{y2}) E_{x1} \right]}_{XPolM} \right\} \end{aligned} \quad (1.36)$$

The nonlinear coefficient is normalized to take into account the losses and considering the constant birefringence of the fibre, such that

$$\gamma' = \gamma \cdot \exp(-\alpha z) \quad (1.37)$$

The very last term of the XPolM contribution can be considered as FWM-like effect between the X and Y components of the pump and the X and Y components of the reference signal. Although the total amount of energy within the channel is constant (except by fibre losses), both polarisation components exchange energy through such FWM term which potentially induces a larger relative phase-shift difference between the two polarisations.

Some of the terms of equation (1.36) can be clustered together, leading to a more compact expression:

$$\begin{aligned}\frac{\partial E_{x1}}{\partial z} &= i\gamma' \left\{ \left( |E_{x1}|^2 + |E_{y1}|^2 \right) E_{x1} + \left( 2|E_{x2}|^2 + |E_{y2}|^2 \right) E_{x1} + (E_{x2}E_{y2}^*)E_{y1} \right\} \\ \frac{\partial E_{y1}}{\partial z} &= i\gamma' \left\{ \left( |E_{x1}|^2 + |E_{y1}|^2 \right) E_{y1} + \left( 2|E_{y2}|^2 + |E_{x2}|^2 \right) E_{y1} + (E_{y2}E_{x2}^*)E_{x1} \right\}\end{aligned}\quad (1.38)$$

As an example of the XPolM effect, consider the two linearly-polarised co-propagating channels, such that  $E_{x1} = E_{y1} = E_1 / \sqrt{2}$ , and  $E_{x2} = E_2$  and  $E_{y2} = 0$ . The nonlinear phase shift induced onto the  $E_{x1}$  component is then greater by a factor of 2/3 compared to the  $E_{y1}$  component. The picture is much more complex in WDM systems where N wavelength channels are multiplexed. In these systems, one channel is perturbed by the other N-1 channels carrying different data, propagating at different velocities and with different SOP. This results in very complex SOP variations induced by nonlinear phase modulation.

Because the SOP variation depends on the intensity fluctuations of co-propagating channels, it results in a noise-like SOP scattering and, hence, depolarisation. XPolM is especially detrimental in systems relying on polarisation-sensitive receivers contrary to conventional polarisation-insensitive detection. Nonlinear XPolM creates sudden changes of the SOP of the signal that are possibly faster than the speed of the polarisation tracking done in polarisation-sensitive receivers [42]. Thus, in polarisation-sensitive receivers, these changes in SOP may be translated into amplitude fluctuations further deteriorating the performance, whereas they would not affect the performance of a polarisation-insensitive receiver.

### 1.2.7 Nonlinear phase noise

Amplified spontaneous emission (ASE) causes power fluctuations between pulses which results, through Kerr effect, in different nonlinear induced phase shifts for different pulses. This different induced phased shift is known as nonlinear phase noise (NLPN). Nonlinear phase shift was firstly described by Gordon and Mollenauer in 1990 [43].

Consider a binary phase shift keyed (BPSK) signal. In the absence of ASE noise, all the pulses/symbols contain the same energy and the SPM-induced phase shift is thus the same for all symbols. Nevertheless, when ASE noise is added to the optical signal, each pulse randomly interferes constructively or destructively with the ASE causing power fluctuations for each symbol. To illustrate the effect of NLPN consider the constellation diagram of a BPSK signal in which the symbols correspond to 0 and  $\pi$ . The distribution of symbols is isotropically broadened in the complex

plane due to the interaction between ASE and optical signal, as seen in Fig. 1.19-a. The SPM-induced nonlinear phase shift experienced by each symbol along the transmission is different as it varies with the symbol power. Hence, the nonlinear phase shift experienced by more powerful symbols is larger than that of less powerful symbols. This causes the typical NLPN-induced “ying-yang” shape in the constellation diagram Fig. 1.19-b. Different methods have been proposed to combat NLPN as semiconductor optical amplifiers (SOA) based attenuation compensation [44] or phase conjugation [45].

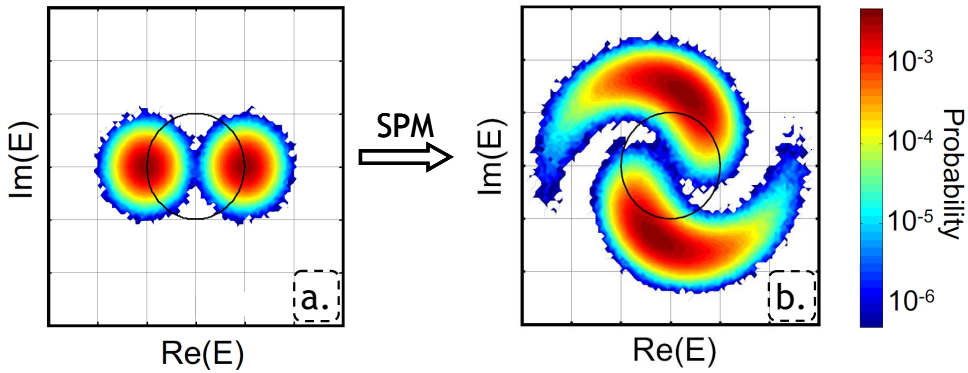


Fig. 1.19: Effect of NLPN onto a BPSK signal

The correlation between the symbol power and the nonlinear phase shift may be exploited to reduce degradations by SPM-induced NLPN at the receiver end. The principle is to apply a different phase shift (opposite to the SPM) for each symbol and proportional to the optical power; which can be done optically [46][47] or electronically [48]. However, NLPN is also induced by XPM. In that case, the amplitude of the pulses carried by co-propagating channels depends on the interferences between the ASE noise and the optical signal which in turn enhances or reduces the strength of XPM-induced nonlinear phase shift. XPM-induced NLPN is much more difficult to compensate compared to SPM since there is no correlation between the channel power and the nonlinear phase shift experienced. Nevertheless, recent studies demonstrate that XPM-induced NLPN can be mitigated without knowing data carried by each neighbouring WDM channels through appropriate post-processing [49].

The strength of NLPN depends on the OSNR, the chromatic dispersion and the symbol rate [48][50]. For high OSNR, the ASE power is not large enough to make a significant contribution on the nonlinear phase shift and the NLPN influence is reduced. On the other hand, for high dispersive fibres (or high symbol rates), the power in a symbol period varies rapidly along the transmission which averages the influence of NLPN. Consequently, the tolerance to NLPN increases with the symbol rate [50] (for a given modulation format) as the OSNR requirements are also higher and the impact of chromatic dispersion is higher as well.

### 1.2.8 Non-elastic scattering effects

Stimulated Raman scattering (SRS) and stimulated Brillouin scattering (SBS) are two significant nonlinear effects which do not arise from Kerr effect contrary to previous ones. The origin of these two effects is found in the interaction of the optical field with the silica molecules of the optical fibre. They are referred to as non-elastic scattering effects in opposition to elastic ones such as Rayleigh scattering.

#### a) Stimulated Raman scattering

When a photon collides with a molecule of silica, it is normally scattered by Rayleigh scattering. The scattered photon then has the same energy as the incident one (elastic scattering) and no energy is therefore transferred to the silica molecule. However, a partial transfer of energy from the photon to the molecule occurs for a small fraction of collisions between photons and silica molecules ( $\sim 10^{-6}$ ). This is known as Raman scattering or Raman effect and is referred to as non-elastic since the energy of the scattered photon is lower than that of incident one. The silica molecule moves to a higher-energy vibrational state through the absorption of a fraction of energy of the incident photon whereas a lower frequency (higher wavelength) photon is generated. The scattered photon/wave is referred to as Stokes photon/wave [15]. Stimulated emission through SRS only occurs when the power is above a critical value (SRS threshold). SRS threshold depends not only on the power of the optical field but also on the type of fibre [51]. Above this threshold the amplification at longer wavelengths scales exponentially with the power of the shorter wavelengths. The maximum efficiency of SRS power transfer is found around 13.2 THz ( $\sim 100$  nm) away from the original frequency. This effect can be exploited to build Raman amplifiers. Raman amplification is further discussed in section 2.4.2.

The same Raman gain that is beneficial for making amplifiers can be detrimental for WDM systems since it may result in unwanted crosstalk between different channels. In this case, a fraction of the energy of the shorter wavelength (higher frequency) channels is transferred to the longer wavelength (lower frequency) channels and can result in a time averaged [52] and in a bit-dependent SRS crosstalk [53]. The former results in a gain-tilt in the WDM spectrum, as depicted in Fig. 1.20. This gain-tilt can be reduced by employing gain-tilt filters or dynamic gain equalisers (DGE). Bit-dependent SRS crosstalk in turn behaves similarly to XPM and its impact is therefore relatively small for fibres with high chromatic dispersion (or signals with high symbol rate). Anyhow, the input power per channel in (repeatered) long-haul optical transmission systems is generally lower than the SRS threshold and therefore SRS-induced impairments are normally not substantial.

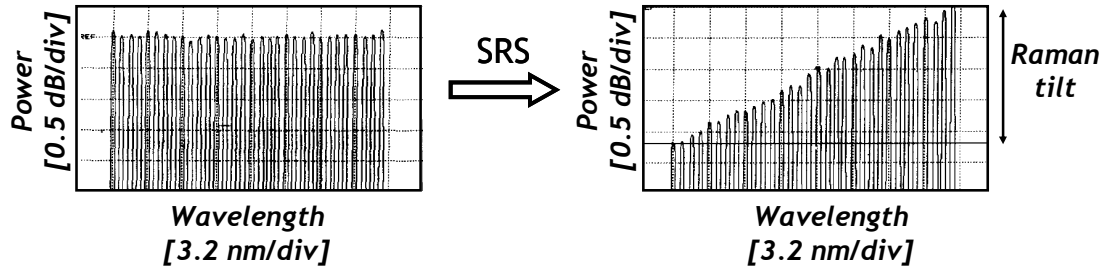


Fig. 1.20: Effect of stimulated Raman scattering onto a WDM multiplex.

### b) Stimulated Brillouin scattering

The mechanisms behind stimulated Brillouin scattering (SBS) are close to SRS. Nevertheless, stimulated Brillouin scattering arises from the interaction between photons and acoustical phonons. An optical wave propagating over an optical fibre generates an acoustic wave through the process of electrostriction. This acoustic wave in turn modulates periodically the refractive index of the fibre which results in a reflexion grating. The incident light is then scattered through Bragg diffraction. As a result, a Stokes wave propagating backwards, counter-directionally to the optical signal at longer wavelength is generated. The frequency downshift caused by SBS ( $\sim 10$  GHz or  $\sim 0.08$  nm) is much lower than SRS. The power reflected by SBS scales exponentially with the power of the incident field above the SBS threshold. SBS threshold depends on the spectral width of the incident field and its lowest value ( $\sim 1$  mW) is obtained for a continuous-wave (CW) or slowly modulated (pulses larger than  $1\ \mu\text{s}$ ) incident field. The efficiency of SBS is strongly reduced when using short pulses ( $<10$  ns) or phase-modulated signals [15]. Indeed, SBS can be neglected in transmission systems relying on phase-modulation beyond 1 Gb/s.

## 1.3. Summary

Fibre impairments distort the signal and therefore reduce the system performance. They can be classified into linear effects, which are independent of the power, and nonlinear effects, whose strength depends on the power of the optical field. Main linear impairments are fibre losses, chromatic dispersion, polarisation mode dispersion and polarisation dependent loss. On the other hand, nonlinear effects arise either from Kerr-effect or from non-elastic scattering effects or even from the interaction between optical noise and Kerr-related impairments. Nonlinearities can be in turn divided into intra-channel and inter-channel effects. When the nonlinear effect is suffered and caused by the same channel, it is referred to as intra-channel effect in opposition to inter-channel effects which are caused by co-propagating channels. Main intra-channel effects are SPM, intra-channel XPM and FWM, SPM-induced NLPN and stimulated Brillouin scattering; whereas main inter-channel effects are XPM, XPolM, XPM-induced NLPN and stimulated Raman scattering.

For a given modulation format, the tolerance to linear impairments generally decreases with the increasing symbol rate. The trend of the tolerance to nonlinear effects is much harder to establish since it depends on channel bit rates, modulation formats, link characteristics and detection techniques. Fig. 1.21 presents the results of

an extensive numerical study, showing the most important nonlinearity that limits transmission of on-off keying (OOK) channels as a function of the fibre dispersion and the channel symbol rate (lower x-axis). The spectral efficiency considering 100-GHz channel spacing is also plotted (upper x-axis). The transmission distance is 2000 km, and nonlinear interactions between signal and noise are neglected. The bit rate is equivalent to the symbol rate here as OOK is a binary modulation.

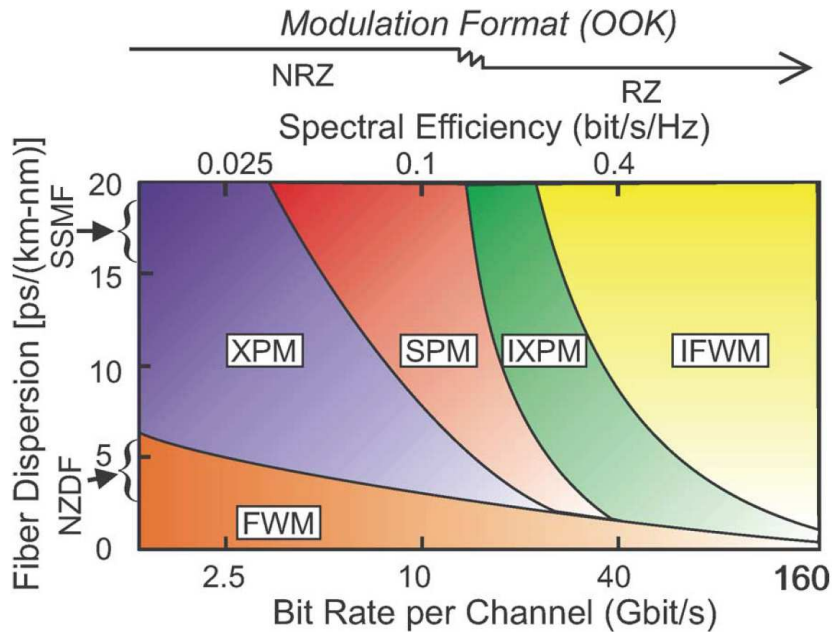


*Fig. 1.21: Significance of nonlinear impairments in WDM systems with 100-GHz channel spacing for different channel bit rates of OOK modulation formats [54] (courtesy of Dr. P.J. Winzer).*

As a general trend, it can be observed that inter-channel nonlinearities dominate at lower bit rates and lower dispersion coefficients whereas intra-channel nonlinearities are particularly important at high channel bit rates. This is mainly due to the fact that at low bit rates and/or low chromatic dispersion the walk-off length is large and pulses of co-propagating channels interact during a significant time inducing a higher nonlinear phase-shift. Moreover, the phase matching conditions required for FWM are easier to satisfy under these conditions. In contrast, for high bit rates and/or high chromatic dispersion, the walk-off length is short and the pulses of co-propagating channels do not interact for long time. For high bit rates, however, pulses are shorter and the spectrum wider. Therefore the impact of chromatic dispersion is more important: pulses overlap over a large number of consecutive pulses with significant energy and intra-channel nonlinearities become then dominant. A similar reasoning could be conducted for a given bit rate combined with a higher dispersion.



# *Chapter 2. Fibre-optic communication systems*

The goal of fibre-optic communication systems is to bring the information sent by a transmitter to a receiver by means of an optical transmission link with an acceptable quality. Many different optical communication systems exist depending on their geographical extension, such as for instance access, metro and long-haul systems. This thesis focuses on optical systems for long-haul distances, i.e. longer than 1,000 km. As any other communication system, long-haul optical communication schemes are composed of a transmitter, a receiver and a transmission channel or link, as depicted in Fig. 2.1. Transmitters transform the electrical information into the optical domain. Information propagates through an optical transmission link up to the receiver. Once at the receiver side, the information is transformed from the optical back into the electrical domain.

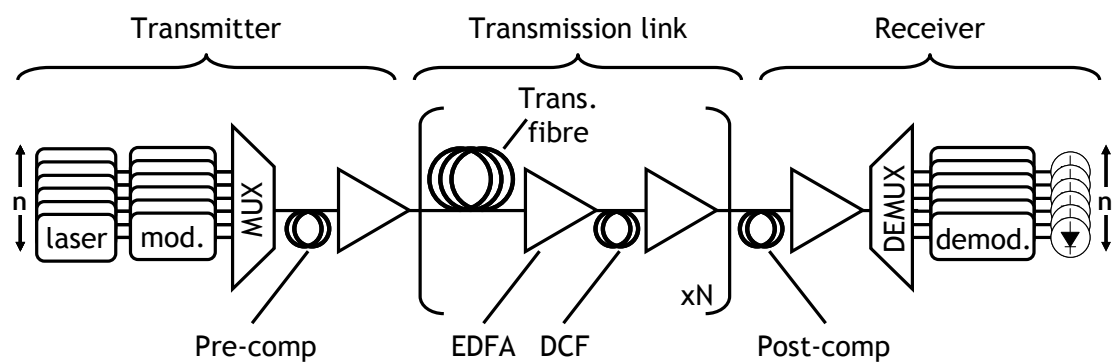


Fig. 2.1: Configuration of a long-haul transmission system

This chapter deals with several relevant aspects of long-haul transmission systems. It is divided in six sections. First of all, section 2.1 reviews general considerations of transmitters and direct-detection receivers. Section 2.1 also comprises the use of forward error correction in optical communications and the most commonly used modulation formats. Section 2.2 discusses the principle of polarisation multiplexing as well as the transmitter scheme and optical noise sensitivity of polarisation-multiplexed systems. Wavelength division multiplexing (WDM), periodic loss compensation and dispersion management are treated in section 2.3, section 1.1 and section 2.5, respectively. Finally, section 2.6 describes the recirculating loop used in laboratory experiments.

## **2.1. Transmitters and direct-detection receivers**

Optical transmission links consist of cascaded fibre spans with optical amplifiers in-between. They can be considered as a physical medium allowing the transmission of information from a point to another by means of an optical signal. Most optical transmission link are bi-directional using different fibres for each direction. Thereby, optical transmitters and receivers are usually combined within a single module, referred to as transponder. Many different modulation formats have been proposed to encode the information [54]. Each modulation format has its advantages and disadvantages and in general it cannot be said that a single modulation format is superior to all others in all aspects.

This section treats the most conventional principles of optical modulation, the structure of direct-detected receivers and the use of forward error correction to relax the constraints of optical transmission systems. Besides, the three different modulation formats used in this thesis are discussed namely on-off keying (OOK), binary phase shift keying (BPSK) and quaternary phase shift keying (QPSK).

### **2.1.1 General transmitter and receiver aspects**

#### *a) Optical modulation*

The main function of an optical transmitter is to convert the electrical data into the optical domain. This can be achieved by different means namely: direct modulated lasers (DML), electro-absorption modulators (EAM), Mach-Zehnder modulators (MZM) or phase modulators. An optical modulator should have the following five properties in order to efficiently realize high-speed modulations: 1) a large electro-optical bandwidth; 2) a low optical insertion loss; 3) a high extinction ratio (defined as the ratio between the power on a ‘1’ and the power on a ‘0’ in OOK modulation); 4) wavelength independence; and 5) it should not induce any frequency chirp.

DMLs are the simplest option to modulate an optical signal. The principle consists of directly modulating the pump current of the laser diode which translates in turn into a modulation of the emitted optical power. They are cost-effective, compact and supply a high output power. Transmissions up to 40 Gb/s employing

DML have been demonstrated [55][56]. Nevertheless, directly modulating the pump current at high data rates results into a degraded extinction ratio and induces frequency chirp, i.e. an undesired phase modulation [19]. The frequency chirp therefore broadens the spectrum, and thus the signal becomes more sensitive to chromatic dispersion. Besides, DML's electro-optical bandwidth is relatively small. Consequently, DMLs are not suitable for high-speed long-haul WDM systems in practice and they are mostly used in access and metro networks. Cascading CW lasers and external modulators is preferable for high-speed WDM long-haul systems. Electro-absorption modulators (EAM) are semiconductor-based components whose transfer function depends on the applied voltage. The absorption provided by an EAM is maximal for high voltages and minimal for low ones. Thus, EAM modulates the CW laser output by means of the electrical data signal applied to it. EAMs can provide a higher electro-optical bandwidth and a lower frequency chirp behaviour than DMLs [57] and are easy to integrate on the same optical substrate as the CW laser. Nevertheless, the transfer function of EAM strongly depends on the wavelength, they have a poor extinction ratio ( $<10$  dB) and their insertion loss is relatively high ( $\sim 10$  dB). EAMs are not widely used in long-haul WDM systems due to these three key disadvantages. One possible approach to modulate the phase of the signal is to use phase modulators. An ideal phase modulator modifies only the phase of the field while keeping the amplitude constant. However, phase modulators are not normally used in practice due to two main shortcomings: 1) transient chirp due to limited bandwidth, which limits the speed of the phase changes, and 2) the fact that any drive-waveform imperfections get directly mapped onto the optical phase, thus potentially degrading performance [58].

In most practical long-haul high-speed transmission systems, external modulation is realized by cascading a CW distributed feedback (DFB) laser with a Mach-Zehnder modulator (MZM). The MZM, first proposed by Ernst Mach [59] and Ludwig Zehnder [60], is an interferometer composed of two 3-dB couplers and two waveguides (arms) with equal length, as depicted in Fig. 2.2-a. Thus, half of the energy of the light at the input of the modulator propagates through each waveguide. Each arm comprises an electro-optical cell which induces a phase-shift into the optical signal depending on the applied voltage (drive voltage). By playing with the value of drive voltages, a certain phase difference between the signals along each arm can be achieved. This phase difference is translated into amplitude fluctuations once the signals at the end of each arm interfere, constructively or destructively, through the second 3-dB coupler.

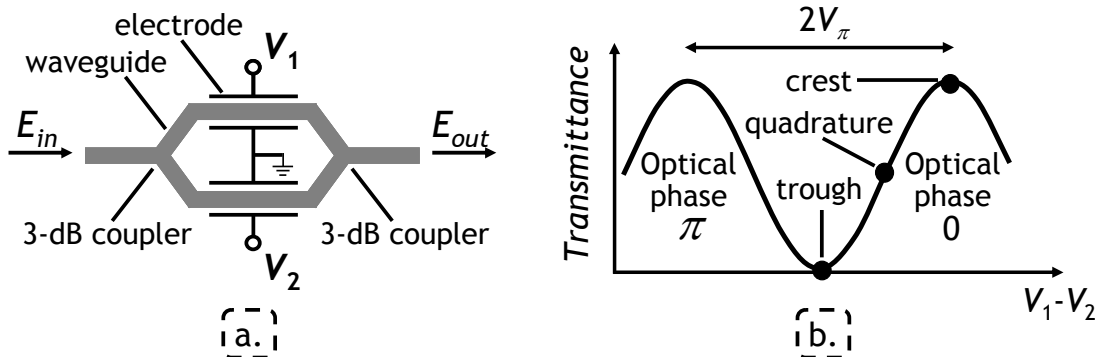


Fig. 2.2: (a) Mach-Zehnder modulator (Z-cut, push-pull) scheme and (b) transfer function

Fig. 2.2 depicts the input-output characteristic of a MZM which is analytically given by:

$$E_{out} \propto E_{in} \cos\left(\pi \frac{V_1 - V_2}{2V_\pi}\right) \quad (2.1)$$

where  $E_{in}$  and  $E_{out}$  are the fields at the input and at the output of the modulator, respectively;  $V_1$  and  $V_2$  are the voltages applied to the first and second arm, respectively; and  $V_\pi$  is the voltage which induces a phase shift of  $\pi$  at the output of one arm of the interferometer. Consequently,  $2V_\pi$  corresponds to the voltage difference between  $V_1$  and  $V_2$  which induces a phase shift of  $\pi$  at the output of the interferometer.  $V_\pi$  is also the value of drive voltage corresponding to a change from constructive interference to destructive interference. A modulator in which both arms are modulated separately, often with  $V_1 = -V_2$ , is referred to as push-pull whereas if both waveguides are coupled together it is called single drive. Two main types of modulators exist depending on the orientation of the  $LiNbO_3$  crystal axes to the waveguides and electrodes namely Z-cut and X-cut modulators [61]. Z-cut modulators require push-pull drive to generate chirp-free signals whereas with X-cut single drive is used. Z-cut modulators have a slightly lower (10 to 20%)  $V_\pi$  compared to X-cut. Push-pull modulators in turn require half drive-voltage compared to X-cut. A typical value of  $V_\pi$  is  $\sim 2.5$  V for (state of the art)  $LiNbO_3$  MZM modulators. Broadband electrical amplifiers (drivers) are used to amplify the electrical data signal to the operating voltage of the modulator. Since there is a trade-off between the output voltage and the amplifier bandwidth, Z-cut modulators are more attractive than X-cut for high-speed operation although two electrical amplifiers are needed. Compared to EAM, MZM are more suitable for long-haul systems since they exhibit large bandwidth (up to  $\sim 35$  GHz), low insertion loss ( $\sim 5$  dB), high extinction ratio ( $>20$  dB), they are nearly wavelength independent and can be designed to be almost chirp-free. On the other hand, many different modulation formats can be generated thanks to a MZM, including intensity and phase modulation as discussed in sections 2.1.2 and 2.1.3. Unlike with phase modulators, when using MZMs any remaining drive-waveform imperfections are only translated into the optical intensity variations, but the phase information is left intact. Besides, MZM can be used to perform return-to-zero (RZ) pulse carving, i.e. to convert a non-return-to-zero (NRZ) signal into RZ, as discussed in section 2.1.4.

*b) Direct-detection optical receivers*

At the receiver end, information is converted from the optical to the electrical domain by means of photodiodes. The electrical bandwidth of the photodiode-electrical current-to-voltage converter chain is typically about 70% of the symbol rate, and is followed by a clock recovery unit to synchronise the receiver with the incoming digital signal in order to sample at the correct instant within the symbol period. However, some actions must be realized before opto-electrical conversion in order to optimise the quality of the electrical detected data. Given an incident optical field,  $E$ , a photodiode supplies a photocurrent, which is expressed in Amperes [A] as:

$$I_{PD}(t) = R \cdot |E(t)|^2 + \eta_{sh}(t) \quad (2.2)$$

where  $R$  is the photodiode responsivity in [A/W], and  $\eta_{sh}(t)$  is the shot noise associated with the DC value of the photodetected current. The photocurrent is proportional to the optical signal power and therefore no phase information is extracted from the incident field. In case of a phase-modulated optical signal, it is mandatory then to optically demodulate the signal before opto-electrical conversion to extract any phase information carried by the optical field, as discussed in section 2.1.3. In practice, optical demodulation translates phase fluctuations into power variations allowing a correct detection in the electrical domain. On the other hand, chromatic dispersion considerably influences BER performance. Therefore, residual chromatic dispersion should be optimised to obtain the best performance after opto-electrical conversion. For systems where residual dispersion is nearly the same for all wavelength channels, such as SSMF-based systems, compensation can be performed jointly onto all channels before demultiplexing, as illustrated in Fig. 2.1. In contrast, per-channel compensation is required for systems with strong wavelength-dependent residual dispersion, such as systems relying on NZ-DSF.

*c) Forward error correction*

A transmission is considered “error-free” when BER is smaller than  $10^{-13}$  after propagation. However, the quality of the signal at the receiver end is usually too poor to ensure error-free reception in long-haul systems. This is the reason why forward error correction (FEC) is employed in modern transmission systems. Used in copper-wire radio communication since the 1960s, the application of FEC for the fibre-optic communication systems was not reported until 1988 by Grover [62]. It should be stretched that on shorter distances and lower speed transmissions the fibre-optic channel is almost ideal compared with the traditional copper-based channel. The principle of FEC is to add redundant information bits within the transmitted signal and to exploit them at the receiver side to detect and correct errors. This extra transmitted information are referred to as FEC overhead and the highest pre-FEC BER that can be corrected to a BER below  $10^{-13}$  after FEC is typically known as FEC limit or threshold. FEC coding is typically preceded by data interleaving in order to disperse possible channel error bursts, such as those induced by PMD [63] by a matched data de-interleaver placed before FEC decoding, so as to obtain an independent error distribution within the received sequence.

Different FECs with different characteristics are standardised by the telecommunication standardization sector of the ITU [64]. For ultra long-haul

submarine transmissions, FECs with 25% overhead is sometimes employed leading to a FEC limit of  $1.31 \cdot 10^{-2}$  as referenced in ITU-T G.975.1-I.7 [64]. However, one of today's most widely used FEC for optical systems is referenced in ITU-T G.975.1-I.9 [64]. It consists of two interleaved extended Bose-Chaudhuri-Hocquenghem BCH(1020,988) codes with a ten times iterative-decoding. Such FEC requires 7% overhead and the FEC limit is  $4 \cdot 10^{-3}$ , corresponding to a  $Q^2$  factor about 8.5 dB (the relation between BER and  $Q^2$  factor is defined in section A). This means that any transmission resulting in a BER below  $4 \cdot 10^{-3}$  can be considered as error-free. This is the FEC considered in the rest of the thesis. Mizuochi [65] gives an overview of FEC in fibre-optic systems where more advanced FECs are also discussed.

### 2.1.2 On-off keying

For decades, the non-return-to-zero (NRZ) on-off keying (OOK) modulation format has been the format of choice for commercial optical transmission systems. More commonly simply referred to as NRZ, it is the most simple and intuitive existing modulation format. An optical NRZ signal is indeed the replica of the binary electrical sequence in the optical domain. A '0' is coded with weak optical-field power (ideally null) whereas a '1' is coded with high power. OOK is a particular case of amplitude shift keying (ASK) as the information is directly encoded in the amplitude of the optical field. Fig. 2.3-a illustrates the constellation diagram of an NRZ signal. The constellation diagram represents the complex envelope of the signal as a two-dimensional scatter diagram in the complex plane at symbol sampling instants (usually the centre of the symbol period). It displays thus the possible symbols that may be used by a given modulation scheme as points in the complex plane. The constellation diagram depicted here assumes ideal extinction ratio in optical modulation and is normalised w.r.t. the square root of average power of the optical signal  $\langle E^2 \rangle = 1/2 \cdot |E(1)|^2 + 1/2 \cdot |E(0)|^2 = 1/2 \cdot |E(1)|^2$ . As it can be observed, the amplitude is null for symbols corresponding to an electrical binary '0' whereas it is  $\sqrt{2}$  for '1' symbols, with a constant phase on the symbol. The Euclidian distance, i.e. the straight line distance between two points in a plane, is closely related to the bit error ratio (BER). Indeed, the BER as a function of the minimum Euclidian distance between symbols,  $d_{\min}$ , is given by [66]:

$$BER = Q \left( \sqrt{\frac{d_{\min}^2}{2N_0}} \right) \quad (2.3)$$

where  $N_0 / 2$  is the power-spectral density, in [ $W/Hz$ ], assuming additive white Gaussian noise (AWGN) and the Q-function is:

$$Q(x) = \frac{1}{\sqrt{2\pi}} \int_x^\infty \exp\left(-\frac{t^2}{2}\right) dt = \frac{1}{2} \operatorname{erfc}\left(\frac{x}{\sqrt{2}}\right) \quad (2.4)$$

for  $x \geq 0$  and  $\operatorname{erfc}(x)$  is the complementary error function defined in Appendix A. OOK signals have therefore a bit error rate given by:

$$BER = Q \left( \sqrt{\frac{|E(1)|^2}{N_0}} \right) \quad (2.5)$$

Fig. 2.3-b shows the power spectral density (PSD) as function of optical frequency normalized with respect to the bit rate. The spectrum of an NRZ-OOK signal is composed, as for most modulation formats, of a main lobe surrounded by side lobes, which are half wide. The spectral width of the main lobe from zero to zero is referred to as the bandwidth of the format. For NRZ-OOK signals, the main lobe width is twice the symbol rate from zero to zero, while the 3-dB bandwidth equals the symbol rate. The spectrum has a strong spike at the carrier frequency, which contains half of the optical power, and is referred to as the carrier.

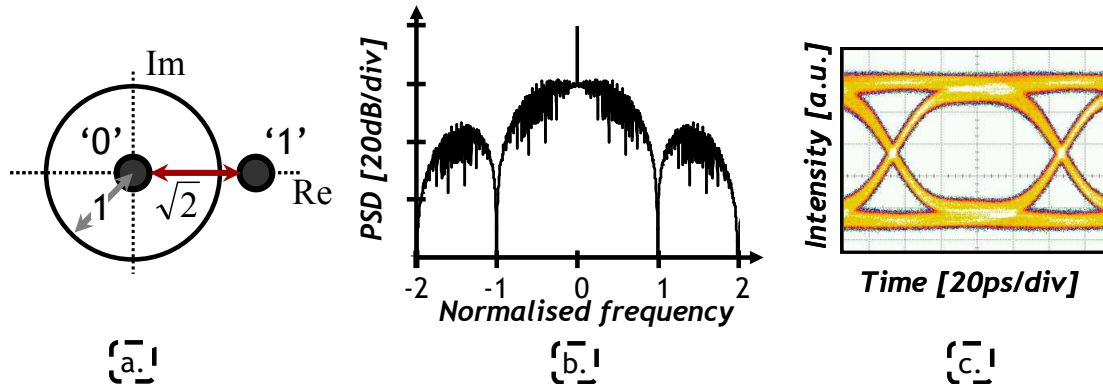


Fig. 2.3: NRZ-OOK, (a) constellation diagram normalised w.r.t. the square root of average power of the optical signal, i.e.  $\sqrt{\langle E^2 \rangle}$ , (b) simulated spectrum with frequency normalised with respect to the bit rate, and (c) experimental eye diagram of an optical 10-Gb/s signal.

For long-haul transmissions, NRZ is usually generated by means of a CW-DFB laser followed by a MZM, as depicted in Fig. 2.4-a. The bias voltage of the MZM is set at the quadrature point and is driven from minimum to maximum transmittance, as shown in Fig. 2.4-b. The electrical drive signal requires therefore a peak-to-peak amplitude of  $V_\pi$ . The modulation rate of electrical data corresponds to the bit rate ( $R_b$ ) as NRZ is a binary format. At the receiver side, a single photodiode converts the signal from the optical into the electrical domain and an electrical circuit integrates the photocurrent over a given time allowing and then performs a threshold decision: this is shown as a slicer in Fig. 2.4-a a threshold decision. The clock recovery unit is incorporated in the slicer module.

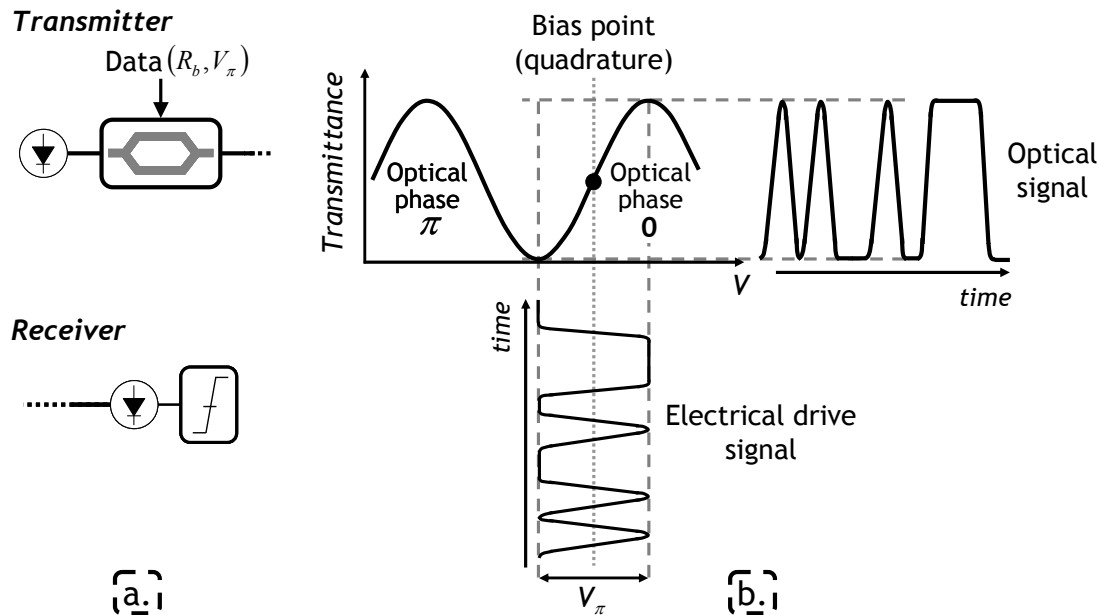


Fig. 2.4: NRZ-OOK, (a) transmitter and receiver schemes and (b) MZM operation.

NRZ-OOK has the advantages of being easy, and thus cheap, to generate and detect. Nevertheless, its noise sensitivity and nonlinear tolerance are relatively poor. Return-to-zero (RZ) pulse-shaped OOK (RZ-OOK) can improve the noise sensitivity in direct detection schemes by  $\sim 1$  dB compared to NRZ (as the optical filter is better matched to the RZ rather than to the NRZ spectrum) and enhance the tolerance to nonlinearities [67] and PMD [68][69]. The main drawbacks of RZ-OOK are a more complex transmitter scheme and its broader spectrum (depicted in Fig. 2.12) compared to NRZ. Thereby, RZ-OOK tolerance to residual chromatic dispersion is lower than that of NRZ-OOK [69] due to its broader spectrum. The generation of RZ pulse-shaping is discussed in section 2.1.4. One particular configuration is carrier-suppressed return-to-zero (CSRZ) which results in a  $180^\circ$  phase change between consecutive symbols. Thus, half of the ‘1’ symbols have a phase 0 whereas the other half have a phase of  $\pi$ . As a consequence, the strong spike at the frequency carrier vanishes, as seen in Fig. 2.12-c. Another scheme consists of adding a specific amount of phase modulation, or chirp, to the RZ-OOK signal. This is referred to as chirped RZ-OOK (CRZ) and requires three modulators: one for data modulation, another for RZ pulse carving and the third for additional phase modulation. The spectrum of CRZ is broader than RZ-OOK but it can be used for ultra long-haul transmissions thanks to its higher robustness against nonlinearities [70][71].

### 2.1.3 Phase modulation formats

Unlike intensity modulation, phase modulation formats code the information on the phase of the signal while ideally keeping a constant power profile. As stated in section 2.1.1a), MZMs are normally used also for generating optical phase-modulated signals in long haul transmission systems. At the receiver side, phase modulated signals require being optically demodulated before opto-electrical conversion because photodiodes are inherently insensitive to the optical phase. Thus phase information carried by the signal translates into power fluctuations detectable by photodiodes. This implies specific receiver schemes for phase modulated signals.

### a) Differential binary phase shift keying

Binary phase shift keying (BPSK) consists of encoding the binary electrical information within two different phase levels of the optical signal corresponding to a phase of ‘0’ and ‘ $\pi$ ’. As it is a phase modulation, it needs to be optically demodulated before being converted into the electrical domain. Although coherent homodyne detection is the optimal scheme in terms of sensitivity, it is up to now not commonly used due to its cost and complexity. Optical demodulation is normally achieved through a Mach-Zehnder delay-interferometer (MZDI), whose differential delay is equal to the symbol period [58]. Thus, one performs self-homodyne demodulation where role of the local oscillator is played by the preceding received symbol. The extracted phase information corresponds therefore to the phase difference between the signal and the signal itself delayed by 1 symbol period. Hence, the name differential receiver. In such configuration, information is encoded in the phase difference between consecutive symbols, and not in the absolute phase. The association of differentially-encoded BPSK together with differential reception is known as differential BPSK (DBPSK) or more simply differential PSK (DPSK).

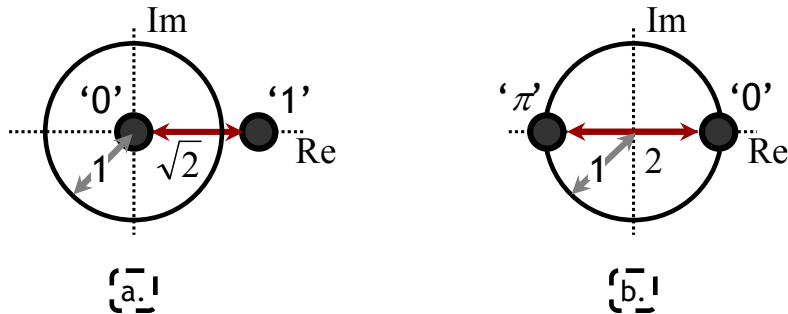


Fig. 2.5: (a) Constellation diagram of a NRZ-OOK and (b) a BPSK signal. Both constellations have the same average optical power.

One of the main advantages of BPSK with respect to OOK is its better noise sensitivity. Intuitively, this can be understood by comparing the signal constellations for OOK and BPSK, as shown in Fig. 2.5. BPSK constellation diagram, illustrated in Fig. 2.5-b, is normalised with respect to the square root of average power of the optical signal  $\langle E^2 \rangle = 1/2 \cdot |E(0)|^2 + 1/2 \cdot |E(\pi)|^2 = |E(\pi)|^2$  as it is the OOK constellation (explained for Fig. 2.3-a). For BPSK, both symbols have the same amount of energy but different phase either ‘0’ or ‘ $\pi$ ’. Therefore, for the same total average optical power the minimum Euclidian distance between symbols increases by  $\sqrt{2}$  for BPSK compared to OOK at equal average power. This translates into a 3-dB lower required OSNR for a given BER, since in the linear propagation regime BER scales with the square of the minimum Euclidian distance between symbols [66], according to equation (2.3).

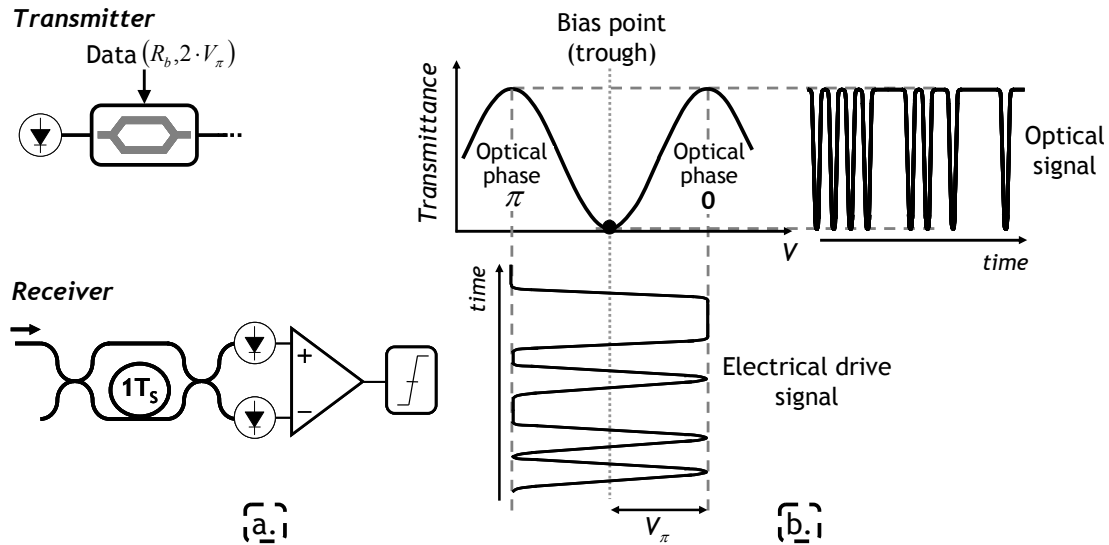


Fig. 2.6: BPSK, (a) transmitter and differential receiver schemes and (b) MZM operation.

The most commonly used DPSK transmitter scheme consists of a CW laser followed by a MZM, as for OOK and is shown in Fig. 2.6-a. The MZM here is biased in the trough of the characteristic curve and the drive-signal swing is  $2 V_\pi$ , i.e. twice the voltage needed for OOK. Therefore, the MZM switches between two crests points, which results in phase changes of  $\pi$ , as shown in Fig. 2.6-b. Using a MZM instead of a phase modulator allows achieving exactly a phase difference of  $\pi$  between symbols. Nevertheless, it induces intensity fluctuations (dips) when moving from a phase 0 to  $\pi$  or vice versa. These dips can be appreciated in the experimental eye diagram depicted in Fig. 2.7-a. Their width is related to the electro-optical bandwidth of the modulator and the electrical driver. The optical bandwidth of a BPSK signal is the same as an OOK since both result from a binary modulation by means of a drive signal at a frequency equal to the symbol rate. Nevertheless, BPSK spectrum does not have the strong carrier neither its harmonics present in OOK, as it can be seen in Fig. 2.7-b, since the average amplitude is zero. As for OOK, DPSK can be combined with RZ pulse carving (discussed in section 2.1.4) which permits to reduce the impact of receiver shortcomings. This leads to modulation formats such as return to zero DPSK (RZ-DPSK) or carrier-suppressed return-to-zero DPSK (CSRZ-DPSK). The name CSRZ-DPSK is given as an analogue of OOK case and it is also sometimes referred to as 66% RZ-DPSK [58]. Unlike OOK, there is no suppression of spike but merely an inversion of the logic.

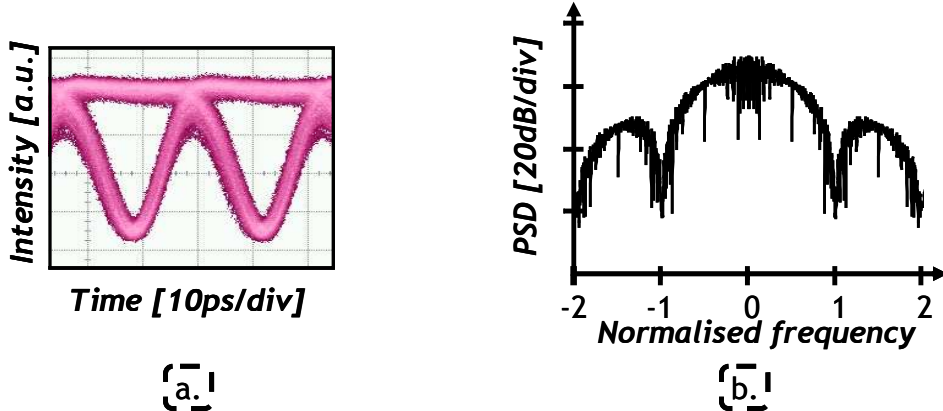


Fig. 2.7: BPSK, (a) experimental eye diagram of an optical 40-Gb/s signal and (b) simulated spectrum with frequency normalised with respect to the bit rate.

Since DPSK relies on differential detection, logical data need to be pre-coded before modulating optical signal such that at the receiver side the transmitted sequence is recovered. A DPSK pre-coder can be implemented through the operation:

$$p[k] = \overline{d[k] \oplus p[k-1]} \quad (2.6)$$

where  $d[k]$  is the bit  $k$  of the input sequence,  $p[k]$  is the pre-coded sequence,  $\oplus$  represents the exclusive OR operation and the top line represents the NOT operation.

At the receiver side, a Mach-Zehnder delay-interferometer optically demodulates the signal before opto-electronic conversion, as shown in Fig. 2.6-a. Different technologies can be used to build a MZDI such as for example with a fibre-optic tuneable delay-line [72], in free space [73], with fibre Bragg-gratings [74] or in InP [75]. In any case, the principle of a MZDI is very close that of a MZM. The difference, here, is that the length of the two arms differs by one symbol period. Hence, the incoming optical signal is split in two copies, one of them is delayed by one symbol period,  $T_s$ , and they are finally recombined. Pulse  $k$  therefore interferes with the pulse  $k-1$ . MZDI have two outputs ports, labelled as constructive and destructive, respectively. One can write the field at the output of each port as:

$$\begin{aligned} u_c(t) &= \frac{1}{2} [r(t) + r(t - T_s)] \\ u_d(t) &= \frac{1}{2} [r(t) - r(t - T_s)] \end{aligned} \quad (2.7)$$

where subscripts  $c$  and  $d$  stand for constructive and destructive ports respectively and  $r(t)$  is the optical field at the input of the receiver. For the constructive port, constructive interference occurs when there is no phase difference between fields whereas destructive interference takes place when there is phase difference of  $\pi$ . The opposite is true for the destructive port. In practice, the phase offset between both consecutive pulses is sometimes actively fine-tuned to ensure it is zero when combining both fields. The frequency response of both ports is periodic with a 3-dB bandwidth of  $1/(2 \cdot T_s)$  and a free spectral range (FSR) of  $1/T_s$  [58][76]. However, MZDI can be designed with a FSR of 50 GHz, so that a single MZDI is able to demodulate any selected channel of a standard WDM comb with a 50-GHz grid.

The output signals from both ports carry the same information (but inverted) and therefore, detecting either only the constructive or destructive output is in theory sufficient to recover data (at the expense of certain noise-sensitivity degradation). This is referred to as single-ended detection. The combination of both signals through balanced detection is required to obtain the improvement of  $\sim 3$  dB compared to OOK and to increase the tolerance against narrow filtering [77]. In balanced detection, two photodiodes convert the optical field into the electrical domain. Afterwards, the electrical currents are fed into a differential amplifier after which a signal centred around 0 V is obtained.

The use of interferometric detection in DPSK has the advantage of yielding a lower-complexity receiver with respect to a coherent receiver, but requires a higher OSNR to obtain the same performance of coherent homodyne detection. Coherent homodyne detection benefits from an optical-noise-free reference signal supplied by the local oscillator; whereas the reference in differential detection is the preceding (noisy) symbol. In particular, differential detection requires 0.6 dB higher OSNR for a  $10^{-3}$  BER (see Fig. 3.4). Another option to demodulate DPSK signals is to replace MZDI by optical discriminator filters [78]. This results in a simpler receiver but induces a loss in sensitivity.

A particular application of MZDI is the generation of either duobinary or alternating mark inversion (AMI) signals. Here, a standard DPSK transmitter is followed by a MZDI to demodulate either the constructive (duobinary) or the destructive (AMI) component. Duobinary is especially interesting due to its high tolerance to narrow optical filtering [79]. However, these applications are out of the scope of this manuscript. An extensive work on this subject was realised by M. Lefrançois [11].

### *b) Differential quaternary phase shift keying*

Quaternary phase shift keying (QPSK) is a multilevel phase modulation format. Similar to BPSK, QPSK encodes the information in the phase of the signal; however, QPSK uses four states, or symbols, instead of two. QPSK encodes two bits in each symbol, namely one “in phase” and one “in quadrature”. The symbol rate, or baud rate, of the QPSK signal is therefore half the bit rate, i.e. half the symbol rate of BPSK and OOK. QPSK signals are naturally more tolerant against chromatic dispersion, PMD and narrow filtering than BPSK signals (at the same bit rate) since the tolerance to these effects decreases with the spectral width, and hence with the symbol rate [79]. QPSK needs optical demodulation before photodetection as does DPSK. This is achieved with by means of a differential-receiver-based scheme. As so, information is encoded in the phase difference between consecutive symbols. Thus, taking ‘00’ as a reference, a phase shift of 0,  $\pi/2$ ,  $\pi$ , and  $3\pi/2$  corresponds to the symbols ‘00’, ‘01’, ‘11’ and ‘10’ (having used a Gray-coding in the bit mapping). Differentially-encoded QPSK paired with differential detection is known as differential QPSK (DQPSK).

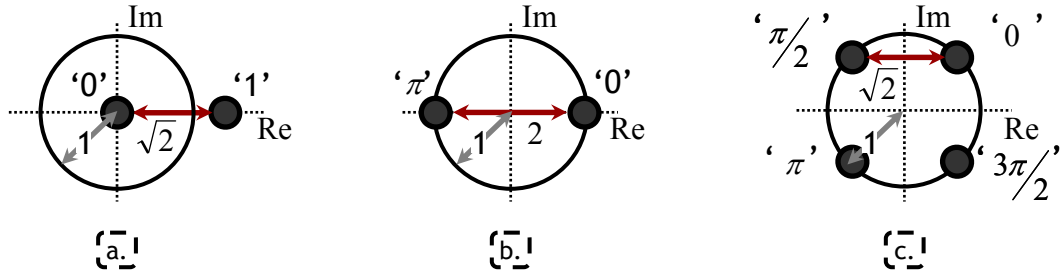


Fig. 2.8: Constellation diagram of a (a) NRZ-OOK, (b) BPSK and (c) QPSK signal.  
The three constellations have the same average optical power.

QPSK format exhibits the same sensitivity as BPSK for a given bit rate. This can be understood directly from the signal constellations visualized in Fig. 2.8. The QPSK constellation is represented with an arbitrary  $\pi/4$  phase offset. All constellations are normalized with respect to the square root of average power of the optical signal, which for QPSK is:  $\langle E^2 \rangle = 1/4 \cdot \sum_{k=1}^4 |E[k\pi/2]|^2 = |E(\pi/2)|^2$ . OOK and

BPSK normalisation is described in sections 2.1.2 and 2.1.3a). All QPSK symbols have the same energy but different phases. For the same total average optical power, the minimum Euclidian distance between QPSK symbols decreases by  $\sqrt{2}$  compared to BPSK. This results in a 3-dB higher required OSNR for a given symbol error ratio (SER), which scales with the square of the minimum Euclidian distance between symbols. The relation between BER and SER, considering Gray code to encode symbols, is [66]:

$$BER = \frac{SER}{K} \quad (2.8)$$

where  $K$  represents the number of bits per symbol. For QPSK signals,  $BER = 2 \cdot SER/2$ , where the multiplicative factor 2 comes from the fact that QPSK symbols have two next-neighbours at the minimum Euclidian distance. Therefore, QPSK also requires a 3-dB higher OSNR than BPSK for a given BER at equal symbol rate (where QPSK symbols have the energy of BPSK symbols). However, QPSK is normally used at half the symbol rate of BPSK to obtain the same bit rate. Therefore, QPSK pulses are twice longer and have twice the energy of BPSK and one obtains the same OSNR requirements for the two formats. In practice, the sensitivity of DQPSK is slightly lower than DPSK due to practical implementation of the differential receiver.

DQPSK can be either built through a serial modulator structure (a MZM followed by a phase modulator) [80] or a parallel modulator structure [81]. The most widely used is the parallel scheme, referred to as nested Mach-Zehnder structure, comprising two MZMs in parallel with a  $\pi/2$  phase-shift between their outputs. It was introduced by Griffin et al. [81] and is depicted in Fig. 2.9-a. The output of the CW laser is fed into the super MZM where it is split into two tributaries (in-phase and quadrature). Each tributary is modulated through a different MZM biased in the trough with a drive signal at a frequency of half the bit rate and a swing of  $2 V_\pi$ . Each MZM hence generates a DPSK signal. Finally, the QPSK signal is obtained by means of the interference of both BPSK signals with an appropriate phase shift of  $\pi/2$  (or  $-\pi/2$ ), which is induced by a calibrated phase shifter. Thus two independent

electrical binary sequences at a rate half the total bit rate feed the MZM. This fact brings the advantage of using electrical drivers with half the bandwidth compared to DPSK (at equal bit rate) although the number of electrical signals is doubled. The eye diagram, depicted in Fig. 2.10-a, shows a double intensity dip corresponding to a phase switch of  $\pi/2$  (mid level) and  $\pi$  (lowest level). The optical QPSK bandwidth is half the one of BPSK since its baud rate is half the bit rate, as shown in Fig. 2.10-b, which increases the tolerance to narrow filtering. One can generate return-to-zero DQPSK (RZ-DQPSK) by cascading a DQPSK modulator (either parallel or serial) and a MZM carver, as discussed in section 2.1.4 [80][82]. RZ pulse carving improves the noise sensitivity (due to practical implementation) and the tolerance to optical filtering [54].

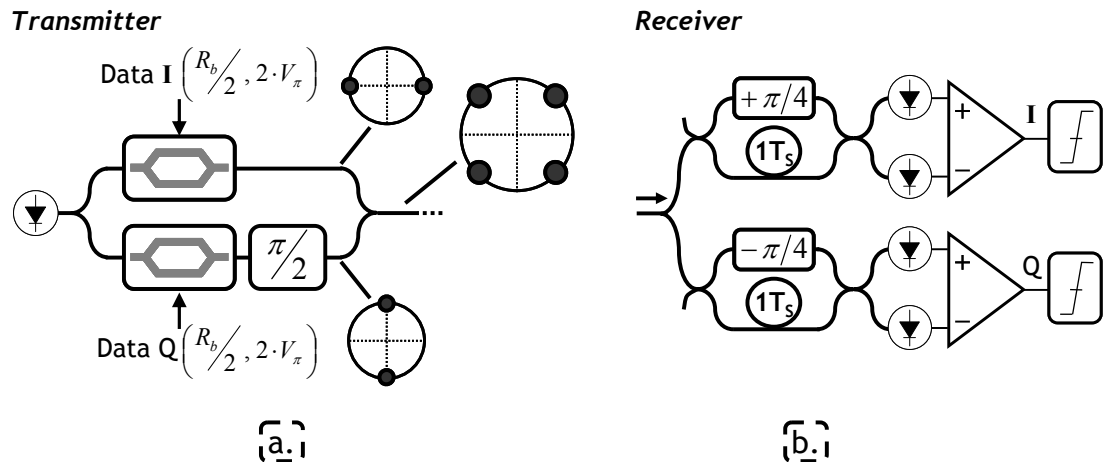


Fig. 2.9: QPSK, (a) transmitter and (b) differential receiver schemes.

Logical data need to be pre-coded before modulating the optical signal such that after differential detection the original data are recovered, as explained for DPSK. A DQPSK pre-coder can be implemented through the operation [83]:

$$I[k] = \overline{(i[k] \oplus q[k])} (i[k] \oplus I[k-1]) + (i[k] \oplus q[k]) (q[k] \oplus Q[k-1]) \quad (2.9)$$

$$Q[k] = \overline{(i[k] \oplus q[k])} (q[k] \oplus Q[k-1]) + (i[k] \oplus q[k]) (q[k] \oplus I[k-1])$$

where  $i[k]$  and  $q[k]$  are the odd and even bits of the input sequence, respectively;  $I[k]$  and  $Q[k]$  are the pre-coded sequences fed into the MZMs,  $\oplus$  represents the exclusive OR operation,  $+$  represents the OR operation and the top line represents the NOT operation.

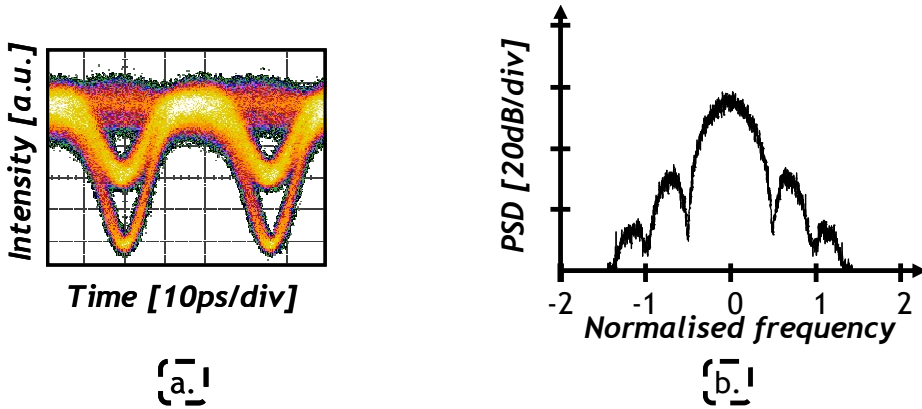


Fig. 2.10: QPSK, (a) experimental eye diagram of an optical 28-Gbaud signal and (b) simulated spectrum with frequency normalised with respect to the bit rate.

At the receiver side, two MZDI<sup>s</sup> convert the information encoded in phase into the amplitude domain. The in-phase and quadrature component of the DQPSK signal are detected by adjusting the phase difference between the arms of the MZDI<sup>s</sup> to  $+\pi/4$  and  $-\pi/4$ , respectively. The MZDI<sup>s</sup> have a periodic frequency response with 3-dB bandwidth of  $1/(2 \cdot T_s)$  and a FSR of  $1/T_s$  [84], where  $T_s$  is the symbol period. 4 photodiodes are required for balanced detection of DQPSK since each MZDI has a constructive and destructive output. The fields at the output of each photodiode, for a received optical signal  $r(t) = r_0 \exp[i\Phi(t)]$ , can be written as:

$$\begin{aligned} |u_c^{I/Q}(t)|^2 &\propto \left| \frac{1}{2} \left[ r(t) \cdot \exp\left(\pm i\pi/4\right) + r(t - T_s) \right] \right|^2 = |r_0|^2 \left| \cos\left(\frac{\Delta\Phi(t)}{2} \pm \frac{\pi}{8}\right) \right|^2 \\ |u_d^{I/Q}(t)|^2 &\propto \left| \frac{1}{2} \left[ r(t) \cdot \exp\left(\pm i\pi/4\right) - r(t - T_s) \right] \right|^2 = |r_0|^2 \left| \sin\left(\frac{\Delta\Phi(t)}{2} \pm \frac{\pi}{8}\right) \right|^2 \end{aligned} \quad (2.10)$$

where subscripts  $c$  and  $d$  stand for constructive and destructive ports respectively for the in-phase ( $I$ ) and quadrature ( $Q$ ) components, and  $\Delta\Phi(t) = \Phi(t) - \Phi(t - T_s)$ . ‘+’ and ‘-’ signs correspond to  $I$  and  $Q$  respectively. These photocurrents are subsequently fed into two distinct differential amplifiers after which one obtains the following currents:

$$\begin{aligned} \hat{I}(t) &\propto \left| \cos\left(\frac{\Delta\Phi(t)}{2} + \frac{\pi}{8}\right) \right|^2 - \left| \sin\left(\frac{\Delta\Phi(t)}{2} + \frac{\pi}{8}\right) \right|^2 = \cos\left(\Delta\Phi(t) + \frac{\pi}{4}\right) \\ \hat{Q}(t) &\propto \left| \cos\left(\frac{\Delta\Phi(t)}{2} - \frac{\pi}{8}\right) \right|^2 - \left| \sin\left(\frac{\Delta\Phi(t)}{2} - \frac{\pi}{8}\right) \right|^2 = \sin\left(\Delta\Phi(t) + \frac{\pi}{4}\right) \end{aligned} \quad (2.11)$$

Thus, phase differences of 0 and  $\pi$  are demodulated as two positive and two negative currents, respectively.  $\Delta\Phi(t) = +\pi/2$  in turn results into a negative value of  $\hat{I}(t)$  and positive value of  $\hat{Q}(t)$  and vice versa for a  $-\pi/2$  phase shift. Apart MZDI, other techniques to demodulate DQPSK signals are possible such as InP-based star-couplers [85] and 90° hybrids [86] or narrow optical filters [84].

The main advantage of (D)QPSK compared to binary modulation formats is the higher tolerance against linear effects, namely chromatic dispersion, PMD and optical filtering. Thanks to its compact spectrum, DQPSK can improve the

information spectral density (ISD) of WDM systems, i.e. increase the number of transmitted bits per Hertz. In typical 10-Gb/s WDM systems with 50-GHz grid, the ISD is 0.2 b/s/Hz. Up to 1.6 b/s/Hz have been reported at 21.4 Gb/s on a 12.5-GHz grid [87] and at 85.6 Gb/s on a 50-GHz grid [88] using single polarisation DQPSK. When propagating over meshed networks designed with 50-GHz grid, optical signals travel through different optical filters with a 3-dB bandwidth of around 47 GHz. This results in a narrower equivalent filtering function. Apart from the equivalent bandwidth, the filter centre frequency of all filters may not be the same due to temperature variations or aging. Thus, the total equivalent filtering function may be narrower than expected and asymmetric. 43 Gb/s DQPSK is well suited for optical meshed networks since it is more tolerant to narrow filtering [89] and to filtering detuning [90] than DPSK. DQPSK is more robust against chromatic dispersion and PMD than binary modulation formats due its lower symbol rate. The tolerance to chromatic dispersion scales quadratically with symbol period whereas the tolerance to PMD scales linearly, as discussed in section 1.1. DQPSK has however about twice the PMD tolerance and three times (instead of four) the tolerance to chromatic dispersion of binary modulation formats [79].

Compared to BPSK, the angular distance between QPSK constellation symbols is halved:  $\pi/2$  instead of  $\pi$ . QPSK is therefore inherently more sensitive to (linear and nonlinear) phase distortions, especially those coming from cross phase modulation [91]. One particular but important consideration is the impact of 10 Gb/s NRZ-OOK co-propagating channels. This normally occurs when upgrading transmission systems carrying 10 Gb/s NRZ-OOK channels with 43 Gb/s DQPSK. Co-propagating 10 Gb/s NRZ channels limit the performance and the maximum reach of 43 Gb/s DQPSK. In order to reduce their impact, one can think about two options: either lowering the operating power of 10-Gb/s channels (which reduces the amount of induced XPM) or increasing the frequency spacing between both types of channels (which reduces the efficiency of induced XPM). Nevertheless, both options are difficult to realise, sometimes impossible, since the former may result in a decrease of the reach of 10-Gb/s channels (as discussed in section 1.1) and the second would imply a limitation of the total transmitted capacity and a loss of network flexibility. 10-Gb/s system upgrades are a critical issue for the deployment of 40 Gb/s DQPSK and have therefore been widely studied [92][93][94][95][96].

### 2.1.4 Return-to-zero pulse-shaping

The behaviour of an optical signal may differ whether an RZ pulse shaping is applied, as introduced in section 2.1.2. RZ pulse shaping can indeed increase the tolerance of OOK signals to PMD [68][69] or even to nonlinearities [67][70]. RZ pulse shaping is potentially combined with different modulation formats such as differential phase shift keying (DPSK) [58][69] or quaternary phase shift keying (QPSK) [80][91] for example. However, the spectrum broadens when applying a RZ-over-modulation (as shown in Fig. 2.12) and the transmitter becomes more complex as extra components are required (the receiver remains almost unchanged most of the times). RZ pulse carving is normally performed by means of an extra MZM, as depicted in Fig. 2.11-a.

Three different duty cycles, 33%, 50% and 66%, can be generated by tuning the MZM drive and bias voltages as well as the frequency of the drive signal. The MZM is driven by a sinusoidal drive signal for the three duty cycles. 33% and 66%

are obtained by driving the MZM with a signal at a frequency half the symbol rate and a drive voltage of  $2 \cdot V_\pi$  but with different bias points: the crest for 33% and the trough for the 66%. 50% duty cycle in turn is obtained by driving the MZM with a signal biased on the quadrature point, at a frequency equal to the symbol rate and with a drive voltage of  $V_\pi$ . Fig. 2.11-b synthesises the values of these three parameters for each duty cycle.

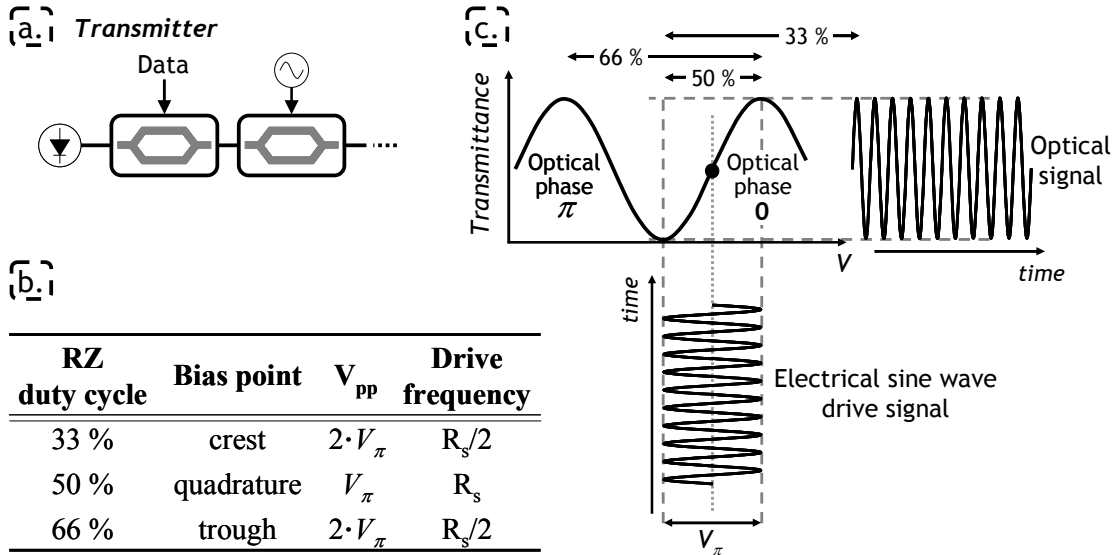


Fig. 2.11: RZ pulse shaping, (a) transmitter scheme, (b) drive signal parameters ( $R_s$  is the symbol rate), and (c) example of MZM operation for 50% duty cycle.

The shorter the pulses are, the broader the spectrum of the optical signal becomes, as illustrated in Fig. 2.12 for OOK signals. 33% and 50% duty cycles modulate only the amplitude. In contrast, 66% results in both an amplitude modulation and a phase modulation, since a phase shift of  $\pi$  is induced between consecutive symbols. When applied to OOK signals, this results in the suppression of the strong component at the frequency carrier, as seen in Fig. 2.12-c and is therefore referred to as carrier suppressed RZ (CSRZ).

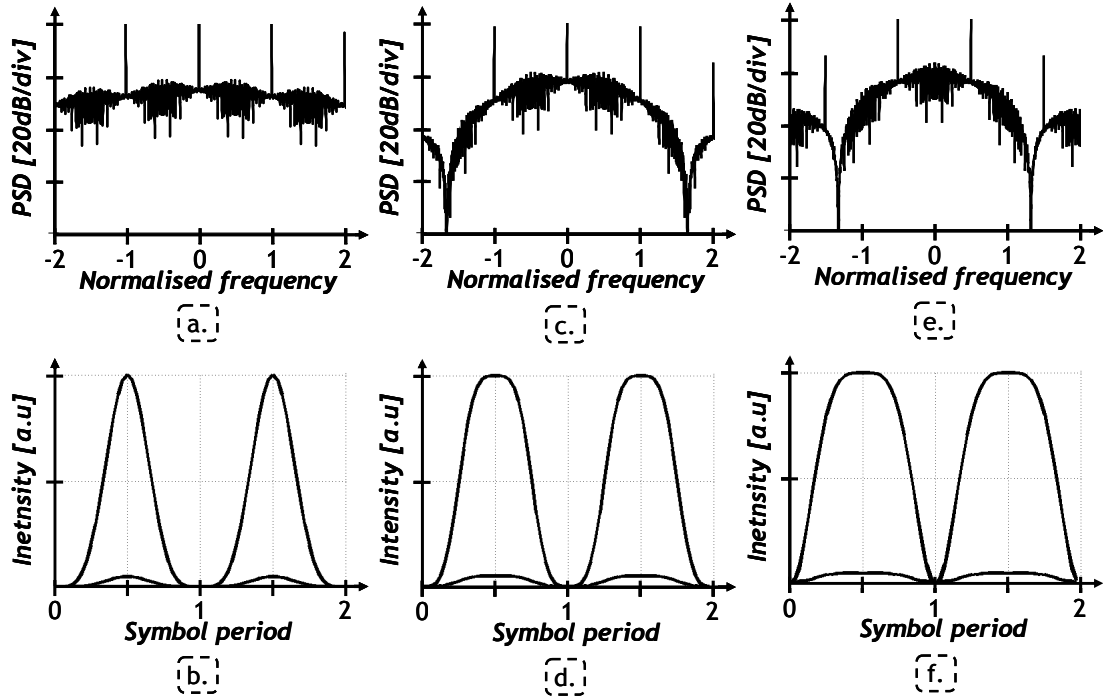


Fig. 2.12: Simulated spectra and eye diagrams of (a,b) 33%, (c,d) 50%, and (e,f) 66% RZ-OOK (after [11] ). The frequency is normalised with respect to the bit rate.

## 2.2. Polarisation division multiplexing

Polarisation division multiplexing (PDM) consists of encoding one independent tributary in each of the two orthogonal polarisations of the optical field. PDM, sometimes referred to as polarisation multiplexed (POLMUX) or dual-polarisation, has attracted only modest attention so far compared to OOK, DPSK or DPQSK due to the relatively complex required receiver. Nevertheless, recent advances in electronics allow robust reception thanks to coherent detection and advanced signal processing. Paired with coherent detection and digital signal processing, discussed in Chapter 3, PDM opens a wide and exciting range of possibilities to increase the robustness against linear effects and the spectral efficiency of optical transmission systems.

The discussion of preceding sections was limited to modulation formats employing either the intensity or the phase of the optical field to encode information. Nevertheless, another degree of freedom exists: the polarisation of the light. Different modulation formats use polarisation in order to transmit information such as alternate polarisation (Apol) and polarisation shift keying (PolSK). PolSK was first proposed by R. Calvani et al. in 1986 [97] and first demonstrated by E. Dietrich et al. in 1987 [98]. It relies on coding the information directly in the SOP and can lead to high spectral efficiency. Nevertheless it requires very complex transmitters and receivers. G. Evangelides et al. first proposed in 1992 polarisation multiplexing for ultra-long haul soliton transmissions [99]. Polarisation multiplexing was combined together with time multiplexing, so as the polarisation of consecutive symbols was alternated (hence the name Apol). This potentially improves the tolerance to nonlinearities but does not increase the spectral efficiency with respect to binary modulation formats (due to time-multiplexing of both polarisation tributaries).

After the first demonstration of PDM [99], it was used (without time-multiplexing) to increase the bit rate of single channel transmissions [100][101][102]. Later on, PDM has been applied to increase the spectral efficiency and the total transmitted capacity of WDM systems. Using PDM, A. Chraplyvy et al. demonstrated the first 1-Tb/s transmission in 1996 [103], and in 2001, K. Fukuchi et al [104] and S. Bigo et al. [105] demonstrated the first 10-Tb/s transmissions. More recently, in 2009, A. Sano et al have achieved the record transmitted capacity of 69 Tb/s[106] using PDM and optical coherent detection.

The possibility of multiplexing two independent tributaries in the polarisation domain comes indeed naturally if one considers the two degenerate polarisation modes of an optical fibre. Since both polarisations are transmitted simultaneously, PDM allows doubling the spectral efficiency because of doubling the symbol period compared to singly-polarised formats. Transmission fibres have random birefringence as discussed in section 1.1.3. Therefore, PDM must be detected through a polarisation sensitive receiver able to demultiplex the received signal. This is a remarkable difference with respect to receivers described in preceding sections which rely only on the intensity and the phase of the signal. Polarisation sensitive receivers can be realized in the optical [99] or the electrical domain. This thesis focuses on the second group which combines optical coherent detection with digital signal processing, which actually perform demultiplexing, as discussed in Chapter 3.

### 2.2.1 Transmitter scheme

Fig. 2.10 illustrates the scheme of a PDM transmitter. The light from the laser is split into two copies through a 3-dB coupler. Each copy is sent into a distinct modulator driven with different electrical data. Finally, a polarisation beam combiner (PBC) recombines the output of both modulators onto the two polarisations of the PDM channel. Polarisation tributaries are referred to as either parallel/orthogonal or X/Y tributaries. One may use two lasers, one per polarisation tributary, instead of one. Nevertheless, this option is less cost-effective and therefore is rarely used. All the components used in the PDM generation process must be polarisation maintaining to ensure correct operation.

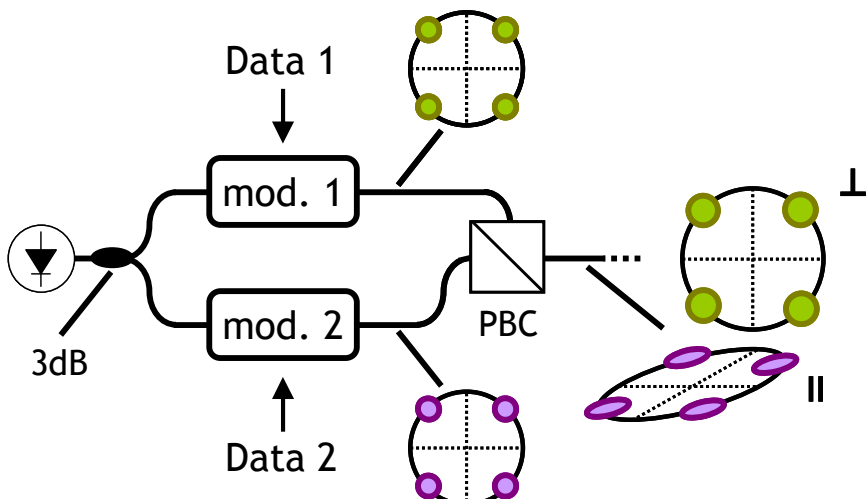


Fig. 2.13: PDM transmitter scheme. Constellation diagrams correspond to a PDM-QPSK signal.

The bit rate of each polarisation tributary is half the total bit rate of the PDM signal. Hence, the symbol rate of PDM signals is half the symbol rate of singly-polarised signals for a given total bit rate. This is depicted in Fig. 2.14 for a PDM-QPSK signal. Consequently, the required bandwidth of opto-electronic devices as well as the drive frequency of modulators is also halved with respect to single-polarisation transmitters which is a remarkable property of PDM transmitters over single-polarisation transmitters. On the other hand, PDM generation requires almost the double of components.

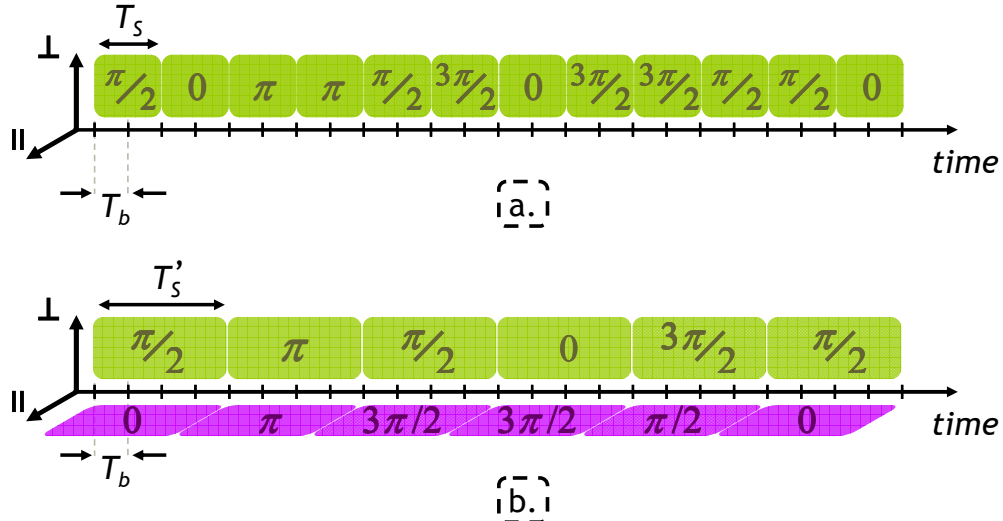
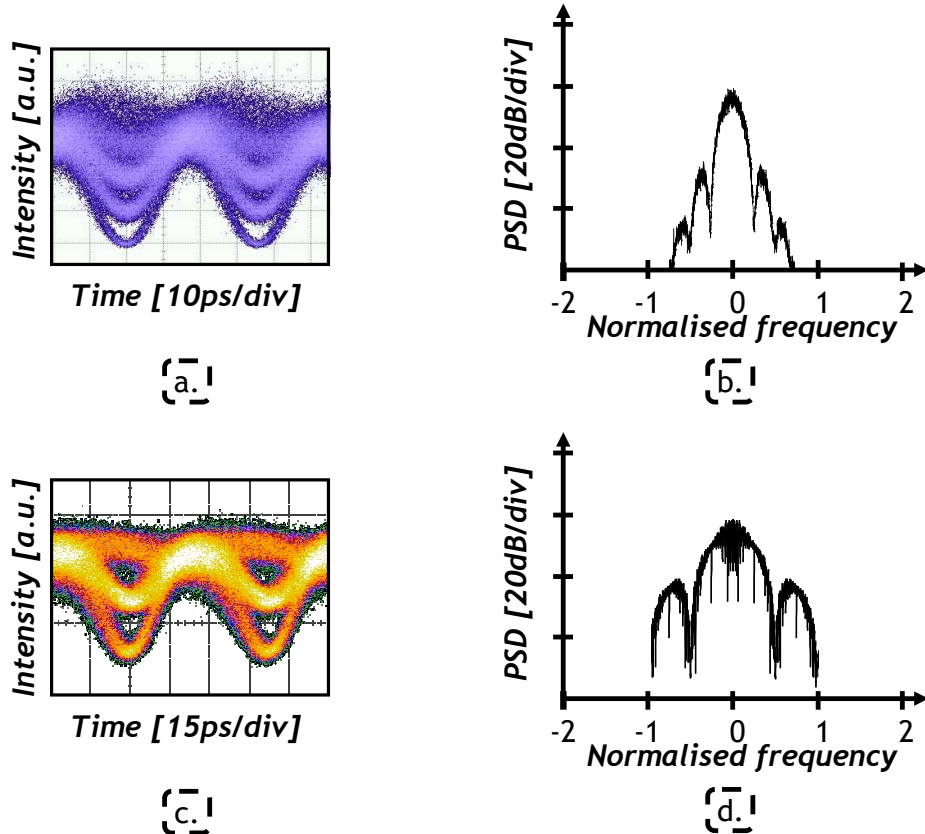


Fig. 2.14: Representation of the same transmitted sequence (a) with QPSK and (b) with PDM-QPSK at the same bit rate ( $1/T_b$ ).

Like RZ pulse carving, PDM can be combined with different modulation formats such as BPSK [107], QPSK [108] or 16 quadrature amplitude modulation (QAM) [109]. It is also possible to pair PDM with multi carrier formats such as orthogonal frequency division multiplexing (OFDM) [110]. It is out of the scope of this thesis to deeply study and compare all the possibilities. This manuscript focuses on the application of two of these options, namely PDM-QPSK and PDM-BPSK. The symbol rate of PDM-QPSK is a quarter of the bit rate (it encodes 4 bits per symbol) whereas the symbol rate of PDM-BPSK is half the bit rate (as it encodes 2 bits per symbol). Fig. 2.15 shows the experimental eye diagrams of PDM-BPSK and PDM-QPSK as well as the simulated spectra, in which the frequency is normalised with respect to the bit rate. Compared to singly-polarised signals (Fig. 2.7-a and Fig. 2.10-a), additional levels appear in the eye diagram as a result of sum of the intensities of the two polarisation tributaries when switching from one symbol to another.

The optical bandwidth of PDM signals is halved with respect to signals employing only one polarisation (for equal total bit rate). This fact, as explained in section 1.1 and in section 2.1.3b) for QPSK, enhances the tolerance of PDM signals against linear effects, namely chromatic dispersion, PMD and narrow filtering. From another point of view, when operating at the same symbol rate, polarisation multiplexing allows doubling the bit rate while keeping almost unchanged the tolerance to linear impairments [111]. On the contrary, tolerance against nonlinearities decreases, in general, with the application of PDM due to nonlinear interactions between both polarisations [112] and to the lower symbol rate which

makes signals more sensitive against cross nonlinearities [50], as discussed in Chapter 1.



*Fig. 2.15: Experimental eye diagrams of an optical (a) 28-Gbaud PDM-QPSK and (c) a 21.4-Gbaud PDM-BPSK signal. And simulated spectrum with frequency normalised with respect to the bit rate of (b) 28-Gbaud PDM-QPSK and a (d) 21.4-Gbaud PDM-BPSK signal.*

### 2.2.2 Noise sensitivity

PDM does not induce a loss in noise sensitivity compared to singly-polarised signals (at the same bit rate) as both polarisation fields are orthogonal. It is the possible to separately represent the two tributaries as illustrated in Fig. 2.16. PDM indeed doubles the bits per symbol with respect to a singly polarised signal. All constellations are normalized with respect to the square root of average power of the optical field:  $\langle E \rangle^2 = \langle E_x \rangle^2 + \langle E_y \rangle^2$ , where  $\langle E_x \rangle^2$  and  $\langle E_y \rangle^2$  are the average optical power of the parallel and perpendicular polarisation tributaries. The minimum Euclidian distance between PDM symbols is reduced by a factor  $\sqrt{2}$  for the same average optical power. This implies a 3-dB higher required OSNR for a given SER for PDM signals since it scales with the square of the minimum distance between symbols. Nevertheless, considering that PDM doubles the number of bits per symbols and according to equation (2.8), singly-polarised and PDM signals theoretically require the same OSNR for a given BER, provided PDM symbols have twice the energy of singly-polarised signal symbols. This condition is achieved when the symbol rate of PDM signals is half the symbol rate of singly polarised signals (PDM pulses are then twice longer) achieving in both cases the same total bit rate.

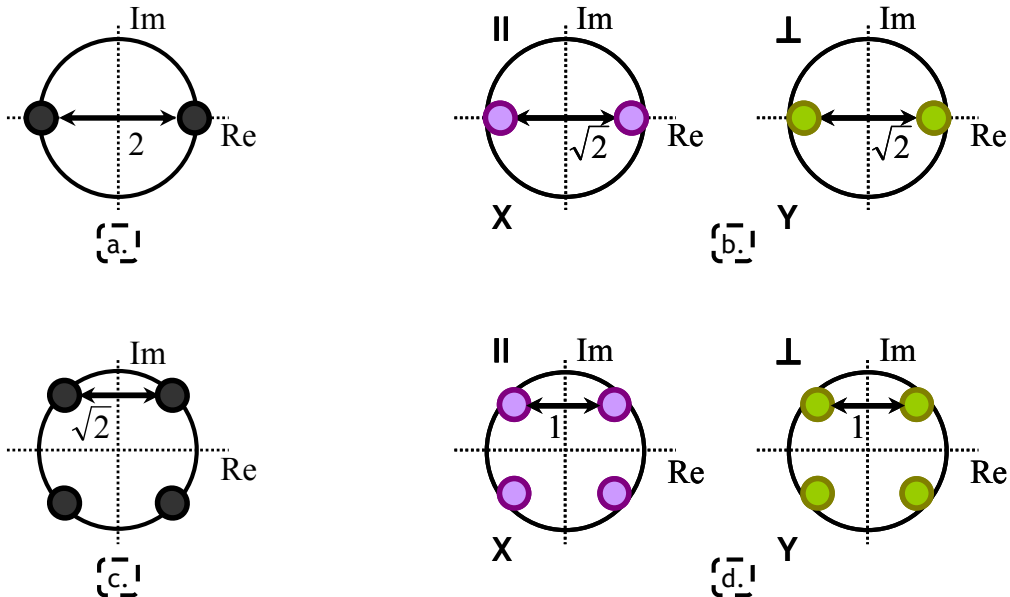


Fig. 2.16: Constellation diagram of a (a) BPSK, (b) PDM-BPSK, (c) QPSK and (d) PDM-QPSK signals. All constellations have the same average optical power.

One finds 3-dB higher OSNR requirement for a given BER for PDM signals when PDM is used to double the bit rate compared to singly-polarised signals. Fig. 2.17 shows the optical noise sensitivity of 56 Gb/s QPSK and 112 Gb/s PDM-QPSK measured in back to back with the polarisation-diversity coherent receiver described in Chapter 3. Results are depicted in terms of  $Q^2$  factor, discussed in appendix A, as a function of the OSNR. Experimental results demonstrate here that PDM-QPSK requires 3 dB higher OSNR than QPSK, at the same baud rate (28 Gbaud here), in back-to-back and in the linear propagation regime.

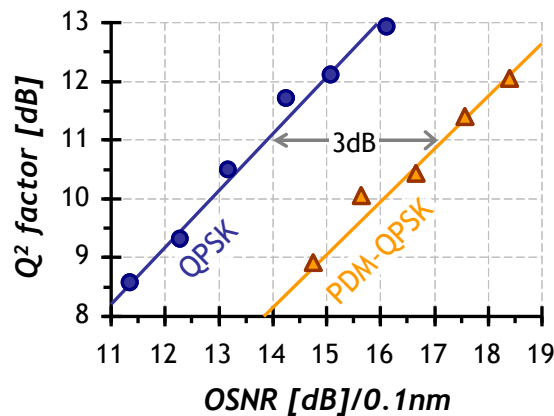


Fig. 2.17: Optical noise sensitivity of ● 56 Gb/s QPSK and ▲ 112 Gb/s PDM-QPSK. The symbol rate of both signals is 28 Gbaud.

## 2.3. Wavelength division multiplexing

In wavelength division multiplexed (WDM) systems, lightwaves emitted by different laser sources at different wavelengths are independently modulated and simultaneously propagated over the same optical fibre [23]. Therefore, a WDM link transports a large amount of data by multiplexing various optical signals with lower

capacity. Each modulated signal at a different wavelength is referred to as a channel of the multiplex. The total capacity of the system is thereby the addition of the individual capacities of each channel. The benefit of WDM is not only to increase the total capacity transmitted within an optical fibre but also to reduce the cost per bit.

As discussed in section 1.1.1, ITU defines the bands of interest for optical telecommunications and the frequency spacing between channels [9], referred to as frequency grid. Common channel spacings are 100 GHz and 50 GHz. Nowadays, most of optical transmissions use the C band, where around 80 channels can be multiplexed within a 50-GHz grid, as shown in Fig. 2.18. Hence, current WDM systems can carry a total capacity of about either 0.8 or 3.2 Tb/s, using either 10 or 40 Gb/s channels, respectively. However, the bandwidth can be enlarged by using the L band. Approximately 160 wavelength channels can be transmitted combining C and L bands on a 50-GHz grid [12], doubling hence the total transmitted capacity. One sees easily the huge interest of optical amplification, explained in the following section, for WDM systems. If optical amplifiers had not been invented, one would be forced at each amplifying site to: demultiplex wavelength all channels, convert individually each channel into the electrical domain, regenerate each electrical signal separately, and convert them again in the optical domain and re-multiplex them. In contrast, optical amplifiers enhance the power of all the optical signals of the multiplex at once independently of the modulation format and the bit rate (different amplifiers are actually used in the C and L band normally).

Information spectral density (ISD), also referred as spectral efficiency (SE), is often used a figure of merit of WDM systems. Expressed in [ $\text{bit/s/Hz}$ ], ISD is defined as the ratio between the channel bit rate and the channel frequency spacing. Therefore, it is meaningless to report the ISD of single channel transmissions, although it is sometimes reported in the literature. ISD is also referred in terms of percentage. Current deployed systems exhibit a ISD between 0.2 b/s/Hz and 0.8 Gb/s/Hz (or 20% and 80%), obtained by multiplexing on a 50-GHz grid 10 and 40 Gb/s channels, respectively. Next generation of optical systems will rely on 40 and 100 Gb/s while keeping unchanged the channel spacing. Therefore, their ISD will be between 0.8 and 2 b/s/Hz.

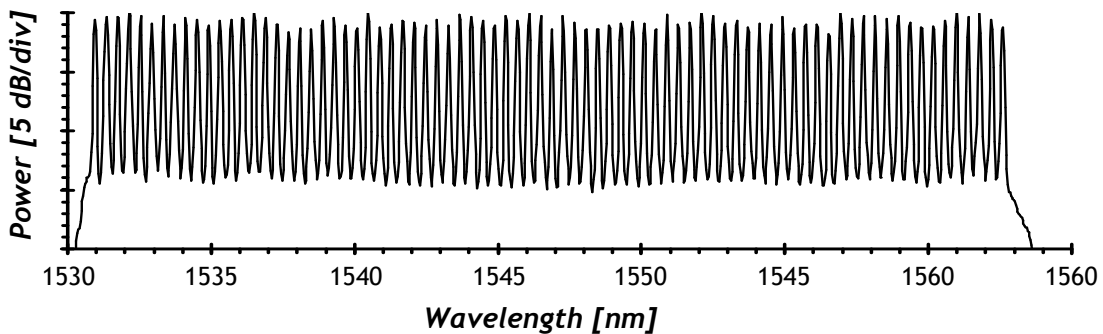


Fig. 2.18: Experimental spectrum of 80 channels (modulated with 40 Gb/s PDM-QPSK) multiplexed in the C band with 50-GHz channel spacing.

In practice, modulated wavelength channels need to be filtered individually before being combined in order to minimize linear cross-talk. Optical signals are aggregated by means of a wavelength multiplexer (MUX). This is often realised

through arrayed waveguide grating (AWG), which also performs channel filtering [13][113]. AWG have typically a 50 or 100-GHz channel spacing. Thus, optical filter interleavers are often used to alternately multiplex different frequency-combs in order to increase the WDM channel density. At the receiver side, one can use the same component to extract the desired channel in the multiplex as it is a reciprocal device.

## 2.4. Loss compensation

Optic fibre is a low loss transmission medium, as discussed in section 1.1.1. Nevertheless, fibre attenuation has been the most limiting factor in long-distance optical communication systems until the invention of optical amplifiers in 1980's. Nowadays, long haul optical systems incorporate periodic optical amplification in order to compensate fibre loss and to amplify the whole WDM multiplex at once achieving long transmission distances. Thus, the transmission link itself consists of consecutive fibre spans separated by optical amplifiers, as depicted in Fig. 2.1. Optical amplifiers amplify the weak input signal from the previous span and launch it again into the next span at high power. The span length varies depending on system configuration (namely type of fibre and amplification); however, most of the terrestrial systems use spans between 50 and 100 km.

### 2.4.1 Erbium doped fibre amplifiers

Erbium doped fibre amplifiers (EDFA) are the most widely used nowadays and have been introduced by E. Desurvire et al. [114] and R. J. Mears et al. [115] in 1987. They consist of a single-mode fibre doped with Erbium ( $\text{Er}^{3+}$ ) ions which is pumped by one or more pump lasers, as illustrated in Fig. 2.19-a. The mechanism behind EDFA amplification is stimulated emission, which was first described by Einstein in 1917 [116] and is schematised in Fig. 2.20. E. Desurvire gives a detailed overview of EDFAs in [117][118].

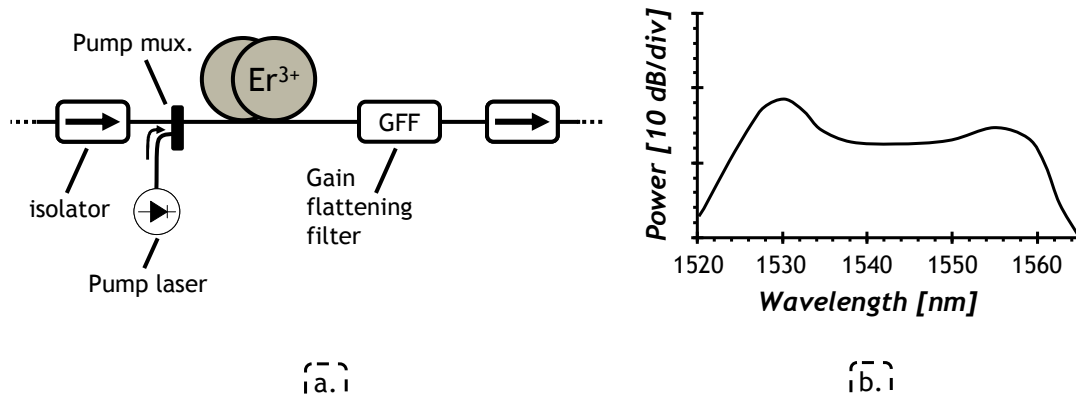


Fig. 2.19: (a) Scheme and (b) typical gain spectrum of a C-band EDFA.

Optical amplification actually takes place in the Erbium-doped fibre, whose length is typically around 10 m. This fibre can be co and counter-directionally pumped. However, in order to achieve higher output powers both pumpings can be combined. The input signal and the CW pumps are combined through pump multiplexers to minimise insertion loss as much as possible. One usually employs optical isolators to prevent back reflections (going into the link and into the Erbium

doped fibre). The typical gain spectrum of a C-band EDFA is shown in Fig. 2.19-b. It exhibits a maximum around 1530 nm. Consequently, a gain flattening filter is usually inserted within the amplifier structure to compensate the non-flat spectrum gain. The optical power at the output of the amplifier,  $P_{out}$ , is given by:

$$P_{out} = G \cdot P_{in} \quad (2.12)$$

where  $G$  is the gain of the amplifier and  $P_{in}$  is the optical power at the input of the amplifier.

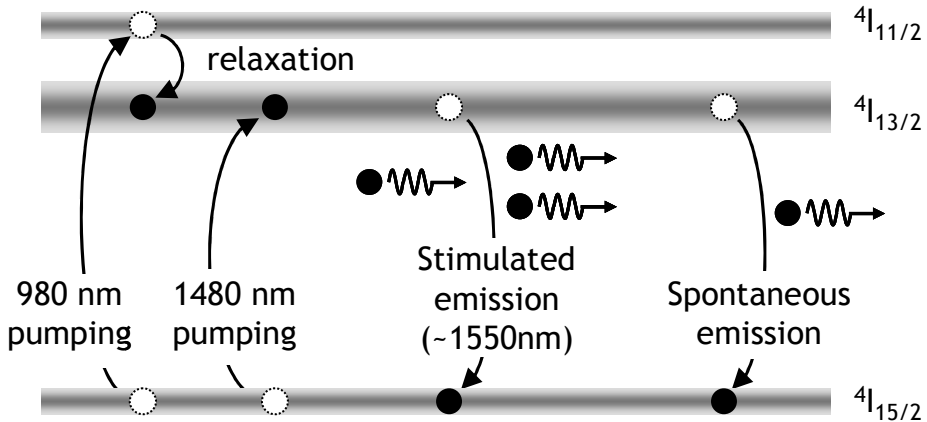


Fig. 2.20: Energy level diagram of an EDFA.

The population inversion required for optical amplification is realised by pump lasers either at 980 nm or 1480 nm corresponding to Erbium absorption bands. The energy levels depicted in Fig. 2.20 are not discrete but rather a manifold due to the non-crystalline nature of the silica. This is known as Stark effect and explains why amplification takes place in a wavelength band instead of at a single wavelength [117]. When pumping is realised at 980 nm, ions are firstly excited to a higher energy level,  $^4I_{11/2}$ , and from there, they quickly transfer ( $<1\text{ }\mu\text{s}$ ) to the level  $^4I_{13/2}$  (relaxation) without generating any photon. Then, the incoming signal induces the generation of new photons (with its same frequency and polarisation) through stimulated emission. The lifetime of excited ions in  $^4I_{13/2}$  ( $>10\text{ ms}$ ) is orders of magnitude higher than the typical symbol periods of modulated optical signals ( $<0.1\text{ ns}$ ). Thus optical amplifiers are insensitive to variations in the envelope of incoming signals. Apart from stimulated emission, spontaneous emission is ineluctable. Spontaneously-emitted photons are decorrelated from the incoming signal and have an arbitrary frequency and polarisation. These photons are subsequently amplified via stimulated emission leading to amplified spontaneous emission (ASE). In the end, ASE results into noise added to the signal which degrades the OSNR, as discussed in section 2.4.3. The ASE introduced by an optical amplifier is characterised by the noise factor ( $F$ ) which is the ratio between the (linear) OSNR at the input and at the output of the amplifier, as defined by H. A. Haus [119]:

$$F = \frac{OSNR_{in}}{OSNR_{out}} \quad (2.13)$$

The noise factor is often expressed in [ $\text{dB}$ ]. In this case, it is referred to as noise figure (NF):

$$NF = 10 \cdot \log_{10} (F - 1) \quad (2.14)$$

The total noise factor of a chain of amplifiers with noise factor  $F_n$  and gain  $G_n$  is obtained by means of Frij's formula:

$$F = F_1 + \frac{F_2 - 1}{G_1} + \frac{F_3 - 1}{G_1 G_2} + \dots + \frac{F_n - 1}{G_1 G_2 G_3 \dots G_{n-1}} \quad (2.15)$$

One obtains a lower noise figure with 980 nm pumping. Nevertheless, the power efficiency of 1480 nm pumping is higher as there is no (non-radiative) relaxation transfer and one obtains a larger number of ions for the same amount of pump power. The typical EDFA structure used in long-haul systems is a dual-stage amplifier with a DCF in-between to periodically compensate for chromatic dispersion, as shown in Fig. 2.1. This is also the amplifier structure considered in most of the work of this thesis. Both stages are co-directionally pumped at 980 nm in order to keep the NF as low as possible. In practice, C-band EDFA have a NF between 4 and 6 dB and supply around 20 dBm of output power. L-band EDFA amplification requires a lower Erbium ion population inversion and thus a larger doped fibre length ( $\sim 100$  m). As a consequence, a single EDFA cannot amplify C and L band at the same time and two different amplifiers are required.

### 2.4.2 Distributed Raman amplification

Apart from EDFA amplification, stimulated Raman scattering (SRS) can be used to achieve optical amplification, as mentioned in section 1.2.8. Amplification is achieved by propagating a powerful CW pump signal. Unlike EDFA which relies on discrete amplification, Raman amplifiers use transmission fibre as amplification medium and amplification is therefore distributed. Using SRS to amplify optical signals was first proposed by Stolen et al. in 1972 [120] and demonstrated by Hegarty et al. in 1985 [121].

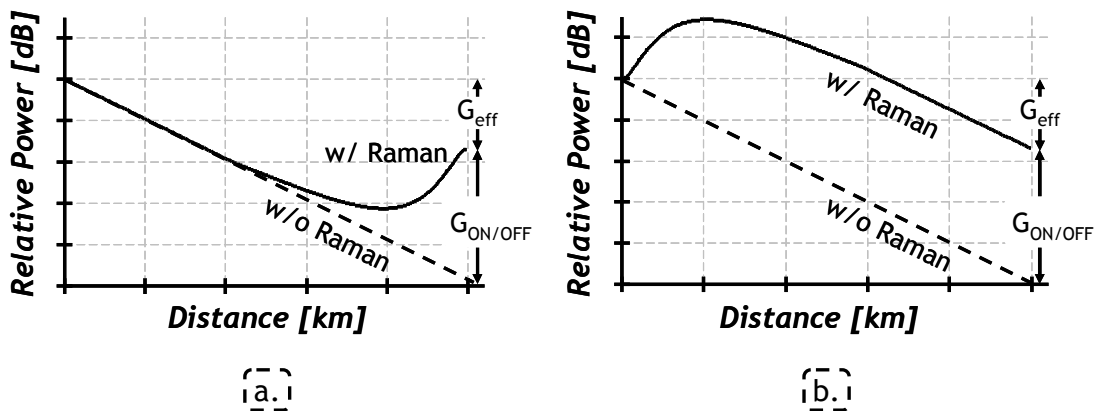


Fig. 2.21: Power profile of an optical signal amplified by means of (a) backward and (b) forward-pumped Raman amplification.

Two different Raman amplifiers exist depending on the direction of the pump: forward (pump co-propagates with the signal) and backward (pump counter-propagates with respect to the signal) amplifiers. The signal power profile for both configurations is depicted in Fig. 2.21. Raman amplification is more commonly used in backward configuration in which the pump is inserted at the end of the

transmission link to increase the power at the input of the next amplifier. The power of the optical pump,  $P_p(z)$ , and of the signal,  $P_s(z)$ , as a function of the distance,  $z$ , are given by [122]:

$$\begin{cases} P_p(z) = P_p(L) \cdot \exp(-\alpha_p(L-z)) \\ P_s(z) = P_s(0) \cdot \exp(-\alpha_s z) \cdot \exp\left(\frac{g_R}{A_{eff}} \frac{P_p(L)}{\alpha_p} [\exp(-\alpha_p(L-z)) - \exp(-\alpha_p L)]\right) \end{cases} \quad (2.16)$$

where  $P_p(L)$  is the power in [ $W$ ] of the counter-propagating Raman pump launched at the end of the transmission fibre ( $z=L$ ),  $\alpha_p$  and  $\alpha_s$  in [ $Np/km$ ] represent the attenuation fibre coefficient at the pump and signal wavelengths;  $g_R$  is the Raman gain coefficient in [ $m/W$ ],  $A_{eff}$  is the effective mode area defined in equation (1.17). For co-propagating Raman amplifiers in turn:

$$\begin{cases} P_p(z) = P_p(0) \cdot \exp(-\alpha_p z) \\ P_s(z) = P_s(0) \cdot \exp(-\alpha_s z) \cdot \exp\left(\frac{g_R}{A_{eff}} \frac{P_p(0)}{\alpha_p} [1 - \exp(-\alpha_p z)]\right) \end{cases} \quad (2.17)$$

where  $P_p(0)$  is the power in [ $W$ ] of the counter-propagating Raman pump launched at the beginning of the transmission fibre ( $z=0$ ). The gain of a Raman amplifier is defined as the ratio between the power at the link output with and without Raman amplification. It is referred to as on-off gain ( $G_{ON/OFF}$ ) and for both configurations is given by:

$$G_{ON/OFF} = \exp\left(\frac{g_R}{A_{eff}} \frac{P_p}{\alpha_p} [1 - \exp(-\alpha_p z)]\right) \quad (2.18)$$

where  $P_p$  is the maximum pump power for both configurations. Another measure of Raman gain is given by the ratio between the signal power at the input,  $P_s(0)$ , and at the output,  $P_s(L)$ , of the link. It is referred to as effective gain ( $G_{eff}$ ) and is given by:

$$G_{eff} = \frac{P_s(0)}{P_s(L)} \quad (2.19)$$

All-Raman amplification is normally done by combining forward and backward pumps. Raman amplifiers exhibit two main advantages over EDFA. First of all, Raman amplification is distributed as the amplification medium is the transmission fibre, whereas EDFA is a discrete amplification. Therefore, the minimum power along the link is higher for Raman amplification which translates in a better noise figure. Sometimes in the literature, the noise figure of Raman amplifiers is not expressed according to equation (2.14) but in terms of *effective* noise figure which compares systems with and without Raman amplification [122]. The effective noise figure of Raman amplifiers is defined as the noise figure that EDFA-only amplifiers should have in order to achieve the same OSNR at the end of the link as the one obtained with Raman amplification. It can give negative values [122][123] unlike noise figure defined in equation (1.12). Another advantage of Raman amplification is the wider amplification bandwidth compared to EDFA [122]. The

3-dB gain bandwidth of a Raman amplifier is approximately 25 nm but it can be extended using multiple pumps to 100 nm [124]. Nonetheless, Raman amplification presents also two main drawbacks which make its practical deployment difficult. The first one is the price. Raman amplifiers are significantly more expensive than EDFA since they require much higher power pumps. Furthermore, high pump power can cause skin and eyes injuries and optical connectors can easily burn due to dirt or dust. Therefore, special safety precautions must be taken when using/deploying these pump lasers.

One particular application of Raman amplification is the so-called hybrid EDFA/Raman amplifiers. This configuration consists of one backward Raman amplifier, which partially compensates span loss followed by one EDFA which compensates the remaining part. Hybrid EDFA/Raman amplifiers give a better OSNR at the end of the link than EDFA-only amplification since the minimum power along the link is increased, as seen in Fig. 2.21-a. The effective noise figure of these amplifiers is very low and can also achieve negative values allowing an extension of the maximum reach of optical systems [125].

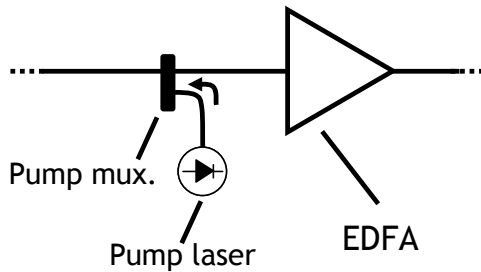


Fig. 2.22: Scheme of a hybrid EDFA/Raman amplifier.

### 2.4.3 Optical signal to noise ratio evolution

The ASE added by optical amplifiers degrades the signal and, consequently, system performance (reducing in turn the feasible reach). The amount of ASE noise added within the signal is given by the signal to noise ratio (OSNR). The OSNR is defined as the ratio between the signal power,  $P_{signal}$ , and the power of ASE,  $P_{ASE}$  [117][36]:

$$OSNR = \frac{P_{signal}}{P_{ASE}} = \frac{P_{signal}}{2 \cdot N_{ASE} \cdot B_{ref}} \quad (2.20)$$

where  $P_{signal}$  and  $P_{ASE}$  are expressed in [W]. One can also give the OSNR in terms of noise power spectral density per polarisation mode,  $N_{ASE}$ , which is expressed in [W/Hz]. OSNR is usually normalised to a certain reference bandwidth,  $B_{ref}$  in [Hz]. The reference bandwidth historically considered corresponds to measure-bandwidth of the optical spectrum analyser (OSA), i.e. 0.1 nm. The power spectral density is assumed constant in the reference bandwidth since the amplification spectrum of an EDFA is smooth. The factor ‘2’ results from the two orthogonal polarisation modes of the optical field. The power spectral density of a single EDFA is given by [117]:

$$N_{ASE} = n_{sp} \cdot h \cdot f_o \cdot (G - 1) \quad (2.21)$$

where  $n_{sp}$  is the spontaneous emission factor,  $h$  is Planck's constant ( $6.626068 \cdot 10^{-34} \text{ J}\cdot\text{s}$ ), and  $f_0$  is the reference frequency in [Hz]. The noise factor an EDFA is given by:

$$F = \frac{\frac{P_{signal}^{in}}{h \cdot f_0 B_{ref}}}{GP_{signal}^{in} / [h \cdot f_0 B_{ref} G + 2n_{sp} \cdot h \cdot f_0 \cdot (G - 1)]} = 1 + \frac{2n_{sp} \cdot (G - 1)}{G} \quad (2.22)$$

where  $P_{signal}^{in}$  is the signal power at the input . In the high gain region ( $G \gg 10$ ), the noise factor can be approximated by  $F - 1 \approx 2 n_{sp}$ . This demonstrates that even a perfect amplifier,  $n_{sp} = 1$ , has a noise figure of 3 dB. Assuming that all the spans have the same span loss and all the amplifiers are equal, the ASE noise after a transmission along  $N_{spans}$  spans is:

$$P'_{ASE} = N_{spans} \cdot P_{ASE} \quad (2.23)$$

Combining equations (2.20), (2.21), (2.22), and (2.23), the OSNR after amplification can be expressed by:

$$OSNR = \frac{P_{signal}^{out}}{[G(F - 1) - 1] h f_0 B_{ref} N_{spans}} = \frac{GP_{signal}^{in}}{(GF - 1) h f_0 B_{ref} N_{spans}} \quad (2.24)$$

where  $P_{signal}^{in}$  and  $P_{signal}^{out}$  are the signal power at the input and at the output of the amplifiers, respectively. According to equation (2.24), the OSNR decreases with the amplifier gain for a constant output power. In other words, the higher amplifier gain is required, the more ASE is added during the amplification process. Low power signals require higher amplification gain. Thereby, the lower the power is at the input at the amplifiers, the lower the OSNR is at the end of the link.

One can express equation (2.24) in a simpler way in dB by considering spans loss of more than 16 dB where  $(G/F-1)-1$  can be approximated to  $G/F-1$ . Besides, the term  $10 \log_{10}(h f_0 B_{ref})$  is approximately 58 dBm when  $\lambda_0 \approx 1550 \text{ nm}$  and  $B_{ref} = 12.5 \text{ GHz}$ , i.e 0.1 nm.

$$\begin{aligned} OSNR &\approx 10 \log_{10} \left( \frac{P_{signal}^{in}}{(F-1)h f_0 B_{ref} N_{spans}} \right) = \\ &= 58 \text{ dBm} + P_{signal}^{in} [\text{dBm}] - NF - 10 \log_{10}(N_{spans}) \end{aligned} \quad (2.25)$$

OSNR decreases logarithmically along the link with the number of amplifiers (or spans), as shown in Fig. 2.23. In contrast, OSNR improves with amplifiers output power, which increases the power at the input of the next amplifier. However, the amplifiers output power is upper-bounded by degradations induced by nonlinear impairments. A trade-off exists between OSNR achieved at the end of the link and nonlinearities generated along the transmission line, as discussed in section 2.4.4. Besides, one can improve the OSNR at the end of the link by reducing the span loss or improving the NF. This can be achieved either by reducing the distance between amplifiers or by using hybrid EDFA/Raman amplification.

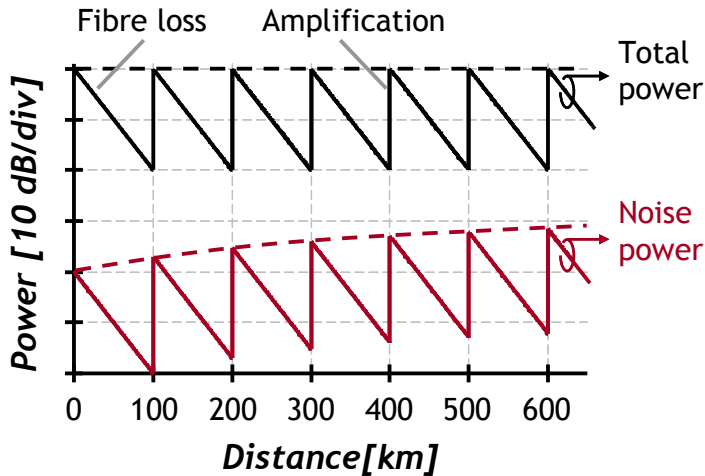


Fig. 2.23: Evolution of total power and noise power as a function of the distance for a system relying in discrete amplification.

#### 2.4.4 Trade-off between noise and nonlinearities

On top of linear fibre effects, optical transmission systems are limited by optical noise and nonlinearities. One must find a trade-off between these two limitations in order to optimise the behaviour of the system. Performance is limited by optical noise for low values of launch power per channel ( $P_{ch}$ ). Therefore, it improves with the increasing  $P_{ch}$  along with OSNR, as seen in Fig. 2.24-a. Nevertheless, beyond a certain value of  $P_{ch}$ , referred to as nonlinear threshold (NLT), nonlinearities become dominant and performance is degraded with the increasing power. The NLT is thus the power corresponding to the optimum of performance. NLT value depends on system parameters such as modulation format, bit rate, dispersion map, type of fibre or type of amplification, for example. It characterises the system determining the maximum power that can be launched at the input of each span.

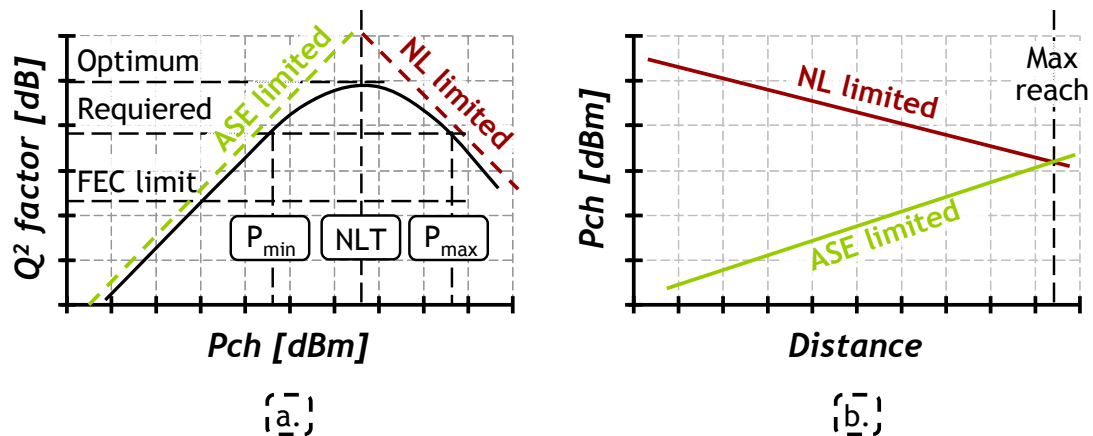


Fig. 2.24: (a) Evolution of performance as function of power per channel and (b) tolerable power range as function of the distance.

The most important feature of a digital transmission system is the ability to operate with a sufficient small bit error rate (BER). At the beginning of life of an optical transmission system, extra margins are defined to allow for the system to age. The required performance depends therefore on the FEC considered and additional

extra margins. It can be lower than the optimal value. Thus, optical noise and nonlinearities delimit the minimum ( $P_{\min}$ ) and the maximum ( $P_{\max}$ ) allowable launched power within the line, respectively, as shown in Fig. 2.24.

On the other hand, the OSNR is degraded along the transmission line for a given value of output amplifier power, as discussed in the preceding section. The impact of nonlinearities in turn becomes greater with the distance as signal suffers from nonlinear distortions at each span. Consequently, performance gets worse and the difference between the maximum and the minimum allowable reduces with the distance, as schemed in Fig. 2.24-b. The maximum distance of a system is therefore reached when the required performance meet the optimal one.

## 2.5. Chromatic dispersion compensation

Chromatic dispersion accumulates along the transmission line, causes inter-symbol interference (ISI) and therefore limits the maximum reach achievable of optical transmission systems without chromatic dispersion management. Besides, chromatic dispersion is strongly related with different nonlinear effects arising from Kerr effect, as discussed in section 1.2. One of the most powerful and most widely used techniques to reduce the impact of fibre nonlinearities is thereby the optimisation of dispersion mapping, referring to the precise placement of dispersion-compensating fibre in optical networks.

WDM cross nonlinear effects are stronger in fibres with zero chromatic dispersion and consequently fibres with non zero dispersion are preferable for WDM transmissions. Thus, accumulated chromatic dispersion must be compensated for in order to properly decode the information carried by the signal. Different methods have been proposed to achieve this goal namely: dispersion compensating fibres (DCF) [126][127], fibre-Bragg gratings [128], (electronic) pre-distortion [129] and optical nonlinear phase conjugation [130]. Periodical compensation is often preferable over full compensation at the transmitter or the receiver side in order to minimise the interplay between chromatic dispersion and nonlinear effects. Today's conventional systems use periodically discrete dispersion compensation through DCF, as illustrated in Fig. 2.1. DCF were first proposed by Lin et al. in 1980 [131] and first demonstrated by Dugan et al in 1992 [132]. They have a negative chromatic dispersion at 1550 nm between -200 and -100 ps/nm/km depending on the type of in-line fibre they are associated with. DCF allow WDM wavelength-independent compensation and, in general, dispersion slope matching between transmission fibre and DCF. However, nonlinear effects are important within DCF as the effective is relatively small. Therefore, DCF are placed in-between a dual stage EDFA and the power at its input is normally set at least 5 dB lower than the launched power into the transmission fibre.

Type of fibre	$D_{1550\text{nm}}$ [ps/(nm·km)]	$A_{\text{eff}}$ [ $\text{nm}^2$ ]	$n_2$ [ $10^{-20}\text{m}^2/\text{W}$ ]
SSMF	17	80	2.6
Teralight	8	65	2.7
LEAF	4.25	72	2.7
DSF	0	55	2.7
DCF	[-200,-100]	20	3

Fig. 2.25: Characteristics of principal fibres used in transmission systems, according to [133]. These values do not take into account the 8/9 factor present in equation (1.19)

One can visualise the course of the dispersion along a transmission line using a dispersion map. It gives the cumulated chromatic dispersion as a function of the transmission distance. A dispersion map has normally three degrees of freedom: the pre-compensation (realised at the transmitter side), the in-line under-compensation or residual dispersion per span (RDPS), and the post-compensation (realised at the receiver side). Fig. 2.26 depicts dispersion maps with different values of pre-compensation (a) and different values of residual dispersion per span (b). One talk about increasing, decreasing or flat dispersion map when the value of residual dispersion per span is positive, negative and null, respectively. Post-compensation is adjusted to optimise BER performance and does not necessarily correspond to the value leading to null dispersion at the end of the link. Pre-compensation and RDPS are in turn designed to minimise intra-channel [134][135] and inter-channel [136] nonlinear effects. Optimal dispersion map for WDM transmissions depends on the different system parameters such as type of fibre, spacing grid, modulation format or channels symbol rate. In that respect, many numerical [137][138][139][140][141] and experimental [136] [142][143] studies have been reported concerning its optimisation.

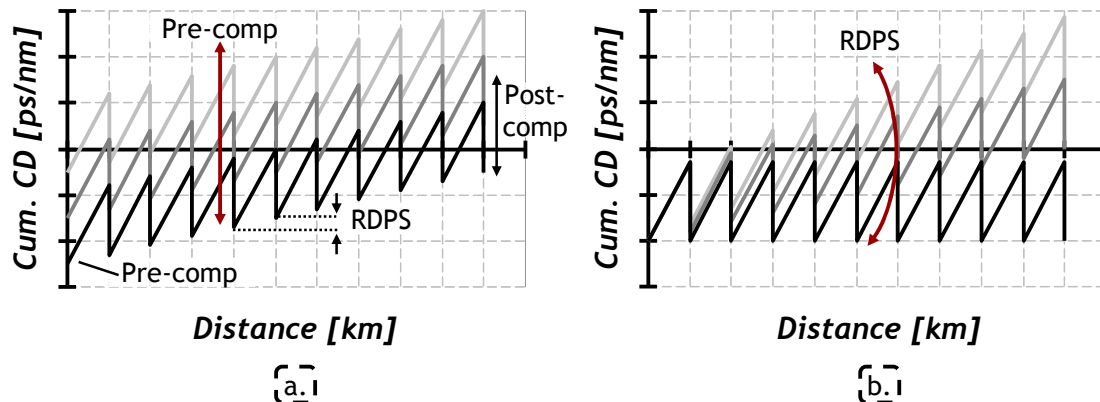


Fig. 2.26: Dispersion map (a) for different dispersion pre-compensation values and (b) for different residual dispersion per span (RDPS).

As seen in Fig. 1.6, GVD is dependent on the wavelength due to the dispersion slope of optical fibre. Dispersion slope matching between transmission fibre and DCF is not always achieved and therefore the dispersion map can differ for different wavelength channels. This is normally the case for transmissions in the C band over NZDSF, where the dispersion map is nearly flat for short wavelengths

whereas for longer wavelengths an increasing dispersion map is obtained (see results of section 4.2.4).

## 2.6. A laboratory tool: the recirculating loop

Most of the laboratory (ultra) long-haul experiments are performed using a recirculating loop. Introduced for optical communications by N. S. Bergano et al. in 1991 [144], it enables the emulation of ultra-long distances while keeping affordable the number of required devices. It also allows measuring the performance of system at different distances. The Recirculating loop consists of three main blocks, namely the transmitter (Tx), the receiver (Rx) and the transmission link, through which signal passes multiple times.

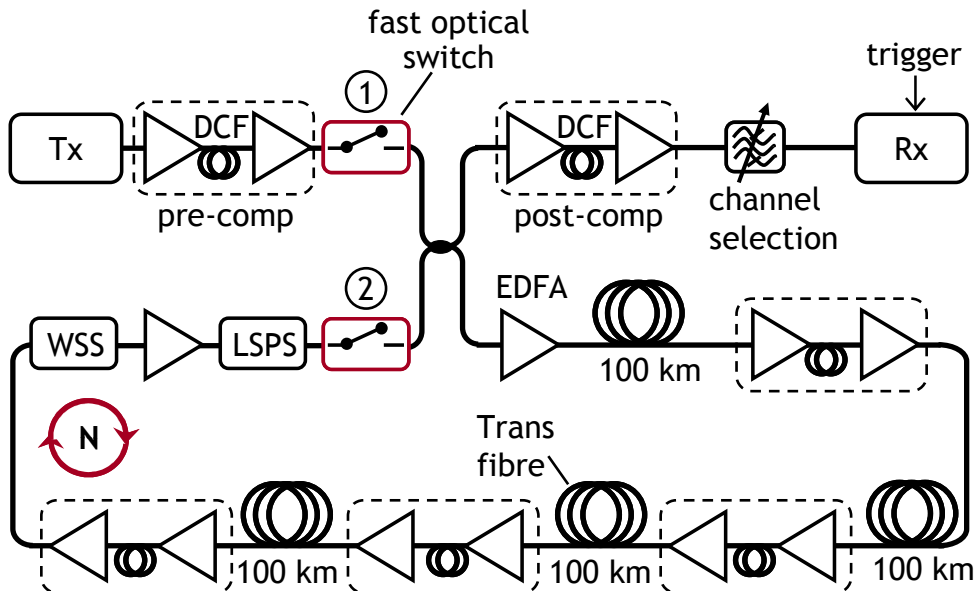


Fig. 2.27: Recirculating loop scheme.

Fig. 2.27 depicts the scheme of a recirculating loop used along this thesis. The signal generated by the transmitter is boosted through a dual-stage EDFA incorporating dispersion compensating fibre DCF for pre-compensation and sent into the recirculating loop. The recirculating loop itself incorporates four 100km-long spans transmission fibre which are separated by dual-stage EDFA including an adapted spool of DCF for dispersion compensation, according to the desired transmission map. A wavelength selective switch (WSS) is also inserted at the end of the loop to perform channel power equalisation and can also emulate optical filtering whereas a loop synchronous polarisation scrambler (LSPS) ensures correct polarisation distribution. The transmission fibre used is either SSMF or NZDSF and dual stage amplifiers can be replaced by hybrid Raman/EDFA amplifiers depending on experiment configuration. At the receiver side, after applying desired post-compensation, the channel under study is selected by a 0.4-nm bandwidth tuneable filter and sent into the receiver.

Three different fast optical switches control the propagation of the signal. Optical switching is normally performed by acousto-optic devices. The recirculating loop operates in three stages, injection, recirculation and measurement. In the injection step, the first switch is “on” while the other is “off”. Therefore optical data

enter into the recirculating loop. Afterwards, the second switch flips to “on” while the first turns “off”. This allows light to recirculate. Light propagates along the recirculating loop during a given time corresponding to a multiple of the time spent on covering one round-trip, which is fixed and known. Once the signal has propagated over the desired distance, the measurement starts according to the trigger. Afterwards, this cycle is repeated.

## **2.7. Summary**

In this chapter, conventional optical transmission systems for long-haul distances are discussed. Such systems consist of a transmitter, a receiver and a transmission link as any other communication system. Transmitters transform electrical data into the optical domain whereas receivers do the opposite. Many different modulation formats can be used to encode the information in the optical field. This chapter deals with three of them: OOK, BPSK and QPSK. OOK encodes information in the intensity of the optical field. It is the simplest modulation format and has been the format of choice for commercial optical transmission systems for decades. It is easy, and thus cheap, to generate and to detect. However, its tolerance against optical noise and nonlinearities is relatively poor.

BPSK in turn consists in encoding the information on two different phase-levels and outperforms OOK noise sensitivity by about 3 dB. At the receiver side, it requires being optically demodulated before opto-electrical conversion because photodiodes are inherently insensitive to the optical phase. The disadvantage of (D)BPSK is therefore the more complex transmitter and receiver. QPSK is another phase modulation format, which encodes information on four phase-levels instead of two. Thus, each transmitted symbol contains two information bits. As a result, the symbol rate of QPSK signals is half the total bit rate and the spectrum width is halved with respect to BPSK and OOK. The tolerance to optical noise of QPSK is the same as BPSK, for a given bit rate. In contrast, the tolerance to chromatic dispersion, PDM and optical filtering are enhanced thanks to the narrower spectrum. The main drawback of (D)QPSK is the transmitter and receiver complexity. Two independent data tributaries can be encoded within the two orthogonal polarisations of the optical field through polarisation division multiplexing. Polarisation division multiplexing is exploited by polarisation-diversity coherent receivers, discussed in Chapter 3, with neither need of additional components nor loss of noise sensitivity, as demonstrated experimentally.

Systems transmission-capacity can be also increased by the use of WDM, where multiple channels at different wavelengths are multiplexed and transmitted simultaneously over the same link. A transmission link itself consists of cascaded fibre spans with optical amplifiers in-between. Each optical amplifier adds ASE to the signal, degrading thus the OSNR. The OSNR at the end of the link improves with the increasing launch power at each span. Nevertheless, a too high launch power excites nonlinear effects which degrade the performance. Thus, a trade-off exists between the OSNR at the end of the link and nonlinear effects generated along the transmission line.

Today’s conventional long-haul systems also use periodically discrete dispersion compensation through DCF. The tolerance to residual dispersion at the

end of the link depends on different parameters such as modulation format and baud rate. Dispersion management is normally optimized to reduce nonlinear impairments, as chromatic dispersion is strongly related with different nonlinear effects arising from Kerr effect. Most of the laboratory (ultra) long-haul experiments are performed using a recirculating loop, which enables the emulation such systems while keeping affordable the number of required devices.

# ***Chapter 3. Coherent detection: the come-back***

Coherent detection relies on detecting a signal through the beating with a reference frequency carrier, commonly supplied by a local oscillator. It has firstly attracted a strong interest from the research community in the 1980's as a mean to enhance the receiver sensitivity. At that time, EDFA were not yet developed and no pre-amplification was done at the receiver side. Optical detection was therefore mainly limited by thermal noise of the photodiodes and electrical amplifiers. A local oscillator much more powerful than the signal allowed for coherent amplification. This can improve the receiver sensitivity up to 20 dB compared to direct detection without pre-amplification [145] because optical detection was no longer limited by thermal noise but by shot noise. Nonetheless, the interest on coherent detection decreased with the introduction of EDFA. Compared with coherent detection, direct detection in conjunction with EDFA pre-amplification gives very similar performance without most of the shortcomings of coherent detection.

A renewed interest arises nowadays about coherent technologies. The recent development of high-speed digital electronics for signal processing and, especially, of analog-to-digital converters (ADC) [146][147], has opened the possibility of using powerful algorithms able to compensate for signal distortions incurred along the fibre-optic transmission, mainly chromatic dispersion and PMD. Thus, today's coherent receivers enjoy the high sensitivity of coherent detection with the added benefits of digital signal processing and are a very likely solution for the next generation high bit-rate transponders (beyond 40 Gb/s).

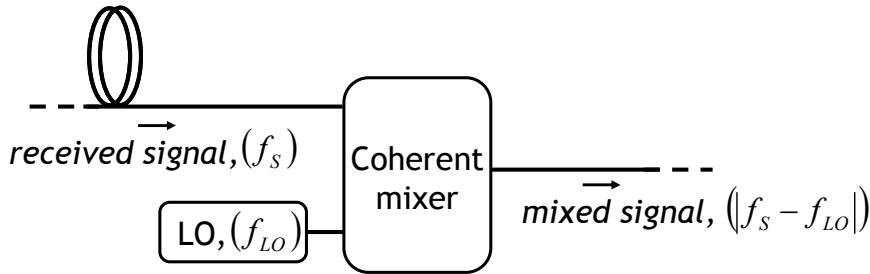


Fig. 3.1: Coherent receiver scheme.

Depending on the required frequency difference between the local oscillator and the signal, one can talk about homodyne, heterodyne or intradyne receivers. Homodyne reception requires the local-oscillator frequency to be strictly locked in frequency and phase (up to a multiple of  $2\pi$ ) of the received signal and gives optimal receiver sensitivity [145] (Fig. 3.2-a). The main constraint is therefore that the frequency and phase of the local oscillator must be controlled and adjusted continuously, which is traditionally done with a phase-locked loop (PLL). The first optical transmission experiment using homodyne detection with an optical PLL was conducted by Maylon in 1984 [148]. Nevertheless, homodyne detection is difficult to realize because of the stringent linewidth requirements for the signal and the local oscillator which are difficult to meet with semiconductor lasers.

In contrast, heterodyne receivers use an intermediate frequency higher than the signal bandwidth (Fig. 3.2 b),  $\omega_{IF} = |\omega_s - \omega_{LO}| = 2\pi f_{FI}$ , to detect the signal so as the frequency of the local oscillator is no longer equal to the one of the signal. This method presents the advantage of relaxing the constraints on the linewidth of the lasers, which makes it easier to implement than homodyne detection. Nonetheless, heterodyne detection requires a receiver bandwidth at least twice the symbol rate [149], i.e. double compared to homodyne detection. The implementation for high bit-rate operation is therefore challenging. Moreover, the sensitivity of a heterodyne detector is at least 3 dB worse compared to homodyne detection, since the effective energy of a heterodyne-detected signal is half of the signal effective energy with homodyne detection [150][151].

Finally, one talks about intradyne detection when the frequency of the local oscillator is *approximately* the same as the frequency of the signal (Fig. 3.2 c). The frequency mismatch between the signal and the local oscillator is recovered in the digital domain by processing the baseband signal so as there is no need of adjusting the local-oscillator frequency and phase. The maximum tolerable frequency-difference is therefore determined by the signal processing. Besides, a phase-diversity receiver is essential as the local oscillator is not phase-locked. Davis et al. showed the first experiment involving phase diversity in 1986 [152]. Intradyne detection aims to detect the in-phase and quadrature components of the signal and therefore a 90° hybrid is required [153]. Both components of the (baseband) optical field can be transferred to the electrical domain by analog-to-digital converters (ADC); thus, the same receiver can operate with any kind of optical modulation format. Moreover, any phase-drift can be compensated through digital signal processing, as firstly shown by Derr in 1991 [154]. Nevertheless, the correct operation of this scheme depends on the fluctuations of the signal SOP. Okoshi et al. introduced polarisation-diversity (heterodyne) receivers to avoid any active polarisation-control in 1983 [155].

Moreover, polarisation-diversity receivers offer the potential of detecting polarisation division multiplexed signals without any additional component. Thus polarisation-diversity receivers can be considered as multiple-input multiple-output receivers (MIMO). Okoshi et al. were also the firsts, in 1987, to demonstrate a receiver combining intradyne detection with polarisation diversity in which all the characteristics of the optical field (without polarisation multiplexing) were translated to the electrical domain [156].

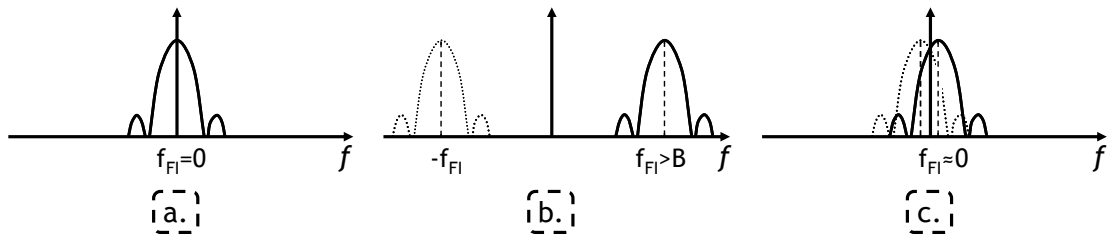


Fig. 3.2: Spectra scheme of (a) homodyne, (b) heterodyne and (c) intradyne coherent detection. The solid lines show the positive frequency components of the intermediate frequency spectrum whereas dashed lines show the negative one.

Today's coherent receivers, as the one discussed here, use on one hand, intradyne polarisation-diversity detection to convert the full optical field (i.e. amplitude, phase and polarisation) to the electrical domain and on the other hand advanced algorithms to compensate for transmission impairments. This requires the detection and digitalisation of four signals, i.e. the in-phase and quadrature components for two arbitrary, but orthogonal, polarisation states.

### 3.1. Receiver sensitivity

One of the main advantages of coherent receivers is its extremely good noise sensitivity. Compared with the widely used (interferometric) differential detection in which the reference is the preceding (distorted) symbol, coherent receivers benefit from a pure reference signal, the local oscillator (assuming ideal local oscillator with no phase noise).

The better sensitivity of coherent detection compared to differential detection can be illustrated with differentially-encoded BPSK signals, also known as DBPSK or DPSK. The differential receiver essentially consists of a Mach-Zehnder filter with differential delay of one symbol period,  $T_s$ , two photodetectors (one for each output branch of the Mach-Zehnder filter) and a circuit integrating the difference of the photodetector currents over time  $T_s$ , as shown in Fig. 3.3-a. Consequently, assuming an additive white Gaussian noise (AWGN) channel, the estimated differentially-decoded sequence is  $\hat{s}_d[k] = r(t) - r(t - kT_s)|_{t=kT_s}$ , where  $r(t)$  is the analog received signal and the BER [157]:

$$BER_{DBPSK} = \frac{1}{2} \exp\left(-\frac{E_b}{N_0}\right) \quad (3.1)$$

where  $E_b$  is the energy per bit and  $N_0$  is the noise power spectral-density. The scheme of the coherent receiver is shown in Fig. 3.3-b. It is much more complex than the

differential one and it will be explained in sections 3.2 and 3.3. After a threshold decision, a BPSK signal is obtained with BER of:

$$BER_{BPSK} = \frac{1}{2} erfc\left(\sqrt{\frac{E_b}{N_0}}\right) \quad (3.2)$$

according to [66]. Differential decoding is performed logically afterwards in the digital domain with two consecutive estimated BPSK symbols so as the estimated differentially-decoded sequence is  $\hat{s}_d[k] = \hat{s}[k] - \hat{s}[k-1]$ , where  $\hat{s}[k]$  is the estimated BPSK sequence at the instant  $k$ . One differentially-decoded symbol turns out to be correct when the two consecutive BPSK symbols are detected either correctly or wrongly, both at the same time. The error probability is consequently  $P_{error\_d} = 1 - [P_{error}^2 + (1 - P_{error})^2]$ , where  $P_{error\_d}$  is the error probability of the differentially-decoded sequence,  $\hat{s}_d[k]$ , and  $P_{error}$  is the error probability of the BPSK sequence,  $\hat{s}[k]$ . This results in a BER for  $\hat{s}_d[k]$  of [158]:

$$BER_{DBPSK} = erfc\left(\sqrt{\frac{E_b}{N_0}}\right) \cdot \left[1 - \frac{1}{2} erfc\left(\sqrt{\frac{E_b}{N_0}}\right)\right] \quad (3.3)$$

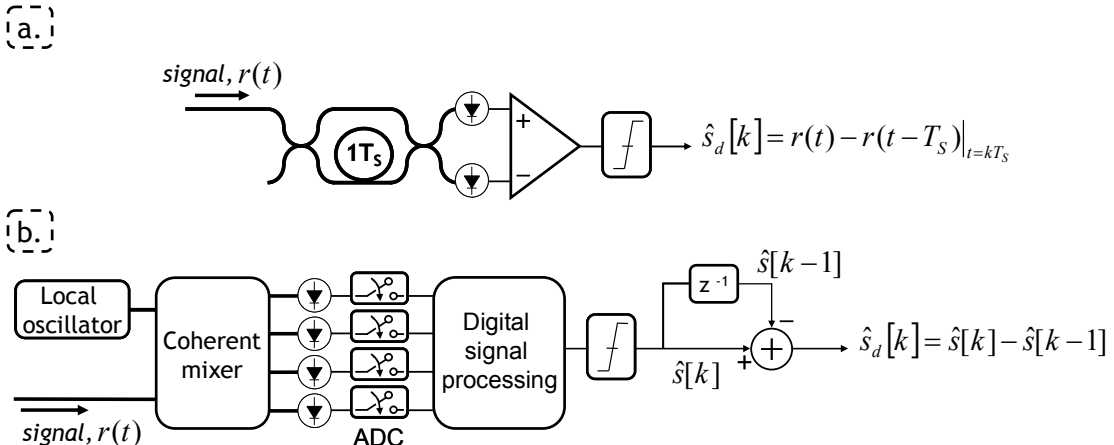


Fig. 3.3: (a) Differential and (b) coherent receiver scheme for differentially-encoded BPSK signal.

Fig. 3.4 shows the receiver sensitivity of the different detection schemes for a (D)BPSK signal at 21.4 Gb/s in terms of performance as a function of the signal to noise ratio (SNR),  $E_b/N_0$ , and as a function of the OSNR (Fig. 3.4 left and right respectively). The relation between SNR and OSNR is [159]:

$$OSNR / 0.1nm = \frac{n_{state} \cdot R_s [GHz]}{12.5} \cdot \left(\frac{E_b}{N_0}\right) \cdot \frac{1}{2} \quad (3.4)$$

where  $R_s$  is the symbol rate,  $n_{state}$  is the number of symbols and 12.5 corresponds to the historically used measure-bandwidth of the optical spectrum analyser (OSA), 0.1 nm. Practical implementations of coherent detection usually involve (logical-) differential decoding to avoid the errors due to the phase ambiguity or induced by cycle slips in the digital carrier phase estimation process (explained in Section 3.3.d). This translates in a degradation of sensitivity corresponding to 0.55 dB in the OSNR

requirement at  $10^{-3}$  BER compared to ideal coherent detection, as shown in Fig. 3.4. This degradation becomes smaller as the  $Q^2$ -factor increases since the errors induced by differential decoding are less significant. ( $Q^2$ -factor is defined in appendix A). However, differentially-decoded coherent detection exhibits an improvement in terms of required OSNR for a given BER compared to interferometric detection. More precisely, it brings a 0.6-dB OSNR requirement improvement at a  $10^{-3}$  BER.

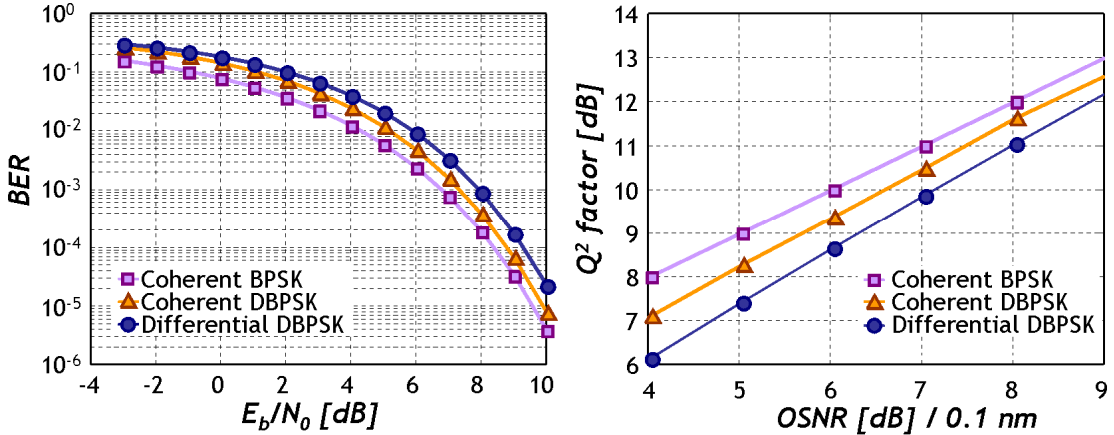


Fig. 3.4: Noise sensitivity of BPSK at 21.4 Gb/s detected through a coherent receiver ▲ with and ■ without differential encoding and ● detected through a differential receiver with differential encoding (courtesy of Dr. Adrian Voicila).

### 3.2. Polarisation diversity coherent mixer

The polarisation diversity receiver I have used throughout this thesis is realised in free-space. This section explains the architecture and operation of such coherent mixers. The emitted optical field,  $\vec{E}_S(t)$ , can carry information on its two orthogonal polarisations,  $\hat{v}$  and  $\hat{h}$  using polarisation-division multiplexing. Assuming that this field is phase-modulated and neglecting the AWGN added to the signal, it can be expressed as follows:

$$\vec{E}_S(t) = E_{Sv}\hat{v} + E_{Sh}\hat{h}, \text{ or} \\ \vec{E}_S(t) = \sqrt{P_{Sv}} \exp(\omega_S t + \varphi_{Sv}(t) + \varphi_{nv}(t)) \hat{v} + \sqrt{P_{Sh}} \exp(\omega_S t + \varphi_{Sh}(t) + \varphi_{nh}(t)) \hat{h} \quad (3.5)$$

where  $\omega_S=2\pi f_S$  is the central frequency of the laser,  $|E_{Sv}|^2+|E_{Sh}|^2$  is the total power of the field,  $P_{Sv}$  and  $P_{Sh}$  are the powers of the fields,  $\varphi_{Sv}(t)$  and  $\varphi_{Sh}(t)$  are the modulated phases, and  $\varphi_{nv}(t)$  and  $\varphi_{nh}(t)$  represent the phase noise along the two orthogonal polarisations.

The state of polarisation (SOP) of the signal changes randomly when propagating through the optical fibre, as through most of the optical devices. In its most general form the Jones matrix is denoted through [24],

$$\vec{E}_R(t) = \begin{bmatrix} \cos \theta & -\sin \theta \\ \sin \theta & \cos \theta \end{bmatrix} \cdot \begin{bmatrix} \cos \varepsilon & j \sin \varepsilon \\ j \sin \varepsilon & \cos \varepsilon \end{bmatrix} \cdot \begin{bmatrix} \exp(j\phi/2) & 0 \\ 0 & \exp(-j\phi/2) \end{bmatrix} \cdot \vec{E}_S(t) \quad (3.6)$$

where  $\theta$ ,  $\varepsilon$  and  $\phi$  are random independent real variables, and  $\vec{E}_R(t)$  is the received signal. The above decomposition of the unitary Jones matrix transformation corresponds to the following chain of transformations in Stokes space: a first rotation around the  $S_1$  axis by an angle  $\phi$ , a second rotation by an angle  $2\varepsilon$  around  $S_2$  and a final rotation by an angle  $2\theta$  around  $S_3$ . Detailed description of polarisation transformations can be found in [24] and [160]. Anyhow, a polarisation-diversity receiver (schematised in Fig. 3.5) is then critical in a fibre-optic communication system with inherently randomly varying polarisation to make the receiver-sensitivity independent of the signal SOP [161]. Such a receiver requires the detection of both the in-phase and quadrature components of the two arbitrary, but orthogonal, polarisation states (a total of four signals) to convert the full optical field (i.e. amplitude, phase and polarisation information) into the electrical domain.

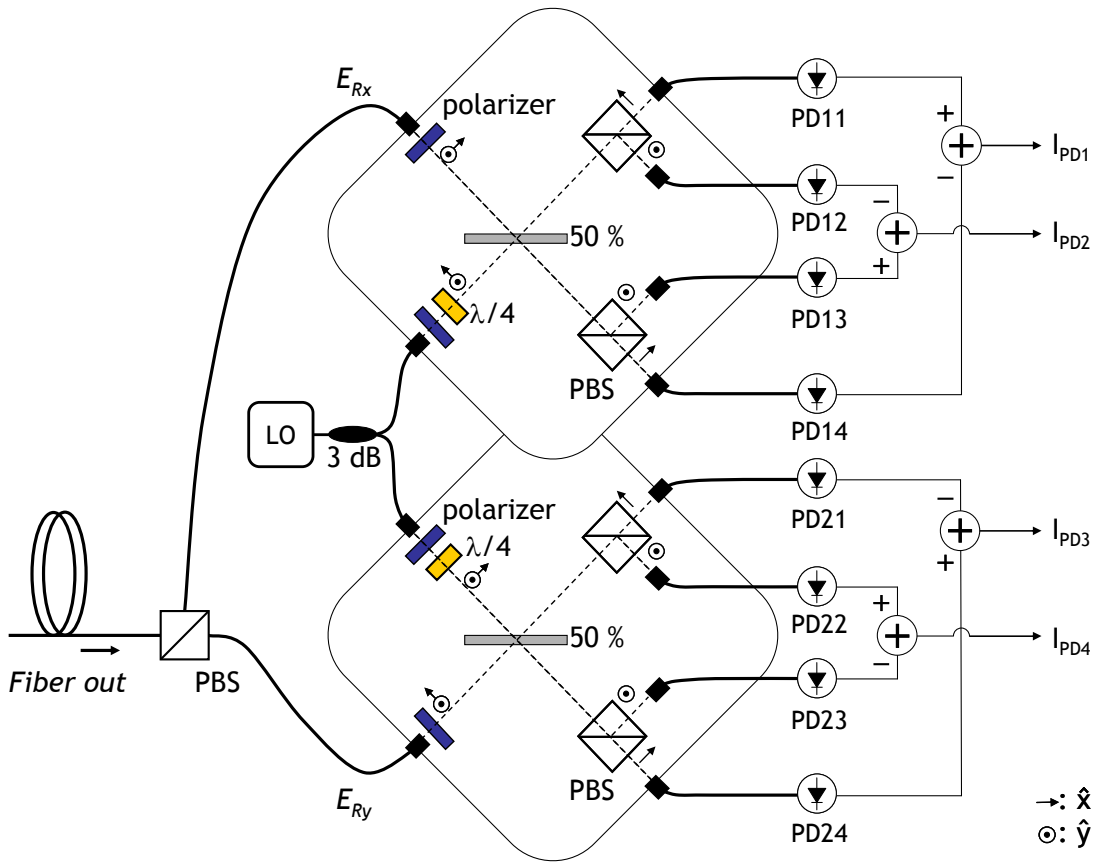


Fig. 3.5: Polarisation diversity coherent receiver realisation

Polarisation-diversity coherent receivers are usually composed of a polarisation beam splitter (PBS) followed by two  $90^\circ$ -hybrids (or coherent mixers) and a local oscillator, as shown in Fig. 3.5. First, a PBS splits up the received signal into two arbitrary, but orthogonal, polarisation components  $E_{Rx}$  and  $E_{Ry}$ ,

$$\vec{E}_R(t) = E_{Rx} \hat{x} + E_{Ry} \hat{y}, \text{ or}$$

$$\vec{E}_R(t) = \sqrt{P_{Rx}} \exp(\omega_R \cdot t + \varphi_{Rx}(t) + \varphi_{nx}(t)) \hat{x} + \sqrt{P_{Ry}} \exp(\omega_R \cdot t + \varphi_{Ry}(t) + \varphi_{ny}(t)) \hat{y} \quad (3.7)$$

where  $\hat{x}$  and  $\hat{y}$  are the polarisation axes of the PBS,  $\omega_R=2\pi f_R$  is the central frequency of the laser (and matches with  $\omega_S$ ),  $P_{Rx}$  and  $P_{Ry}$  are the powers of the fields at the input of the coherent mixers,  $\varphi_{Rx}(t)$  and  $\varphi_{Ry}(t)$  are the modulated phases, and  $\varphi_{nx}(t)$  and  $\varphi_{ny}(t)$  represent the phase noise along the two orthogonal polarisations. The polarisation components  $E_{Rx}$  and  $E_{Ry}$  are indeed the result of an arbitrary rotation of the two polarisation components at the transmitter,  $E_{Sv}$  and  $E_{Sh}$ . Each of the polarisation components is then fed into a 90° hybrid and mixed with the output of a LO laser. Particularly, the polariser rotates the linear polarisation aligned with a given PBS axis into a linear polarisation half the way ( $\pi/4$ ) between both PBS axes, whereas each reflection induces a phase-offset of  $\pi/2$ . The half mirror and the PBS reduce also the amplitude of the optical field by a factor  $1/\sqrt{2}$ . Therefore the optical field, corresponding to the signal, at each output of the coherent receiver can be denoted as:

$$\begin{cases} E_{Out11} = \frac{1}{2} E_{Rx} \exp\left(j\frac{\pi}{2}\right) \\ E_{Out12} = \frac{1}{2} E_{Rx} \exp(j\pi) \\ E_{Out13} = \frac{1}{2} E_{Rx} \exp\left(j\frac{\pi}{2}\right) \\ E_{Out14} = \frac{1}{2} E_{Rx} \end{cases} \quad \begin{cases} E_{Out21} = \frac{1}{2} E_{Ry} \\ E_{Out22} = \frac{1}{2} E_{Ry} \exp\left(j\frac{\pi}{2}\right) \\ E_{Out23} = \frac{1}{2} E_{Ry} \exp(j\pi) \\ E_{Out24} = \frac{1}{2} E_{Ry} \exp\left(j\frac{\pi}{2}\right) \end{cases} \quad (3.8)$$

On the other hand, the local oscillator is free-running and should be tuned with the transmitter laser within an approximate frequency range of several hundred megahertz. The allowable frequency mismatch depends on the signal processing algorithms that are used for carrier phase estimation, which are discussed in section 3.3.d). Besides, the product between the transmitter+receiver linewidth and the baud-rate defines the maximum allowable linewidth of the local oscillator for an optimum operation. This product should be lower than  $1.3 \cdot 10^{-4}$ , according to [162], and corresponds to a 1.4–MHz linewidth when operating at 10.7 Gbaud. This is the reason why an external cavity laser (ECL), with a linewidth of several hundreds of kiloHertz, is commonly used instead of a distributed feedback laser (DFB), which presents a linewidth of several MegaHertz. The 3-dB coupler splits the linearly-polarised light of the local oscillator in two (reducing the amplitude of the optical field by a factor  $1/\sqrt{2}$ ), and each beam is fed into one coherent mixer. The polarisation of each beam becomes circular after passing through the polariser and the quarter-wave plate ( $\lambda/4$ ), so that each beam can be denoted as:

$$\begin{aligned} \vec{E}_{LO}(t) &= \frac{1}{2} E_{LO} \left( \exp\left(j\frac{\pi}{2}\right) \hat{x} + \hat{y} \right), \text{ or} \\ \vec{E}_{LO}(t) &= \frac{1}{2} \sqrt{P_{LO}} \exp(\omega_{LO}(t) + \varphi_{nLO}(t)) \left( \exp\left(j\frac{\pi}{2}\right) \hat{x} + \hat{y} \right) \end{aligned} \quad (3.9)$$

where  $\omega_{LO}(t) = 2\pi f_{LO}$  is the central frequency of the local oscillator,  $P_{LO}$  is the output power of the local oscillator, and  $\varphi_{nx}(t)$  represents the phase noise. Considering the

reflexions inside the coherent mixer, the field corresponding to the local oscillator at each output of the receiver is:

$$\begin{cases} E_{LO11} = E_{LO24} = \frac{1}{2\sqrt{2}} E_{LO} \exp\left(j\frac{\pi}{2}\right) \\ E_{LO12} = E_{LO23} = \frac{1}{2\sqrt{2}} E_{LO} \exp\left(j\frac{\pi}{2}\right) \\ E_{LO13} = E_{LO22} = \frac{1}{2\sqrt{2}} E_{LO} \exp(j\pi) \\ E_{LO14} = E_{LO21} = \frac{1}{2\sqrt{2}} E_{LO} \exp(j\pi) \end{cases} \quad (3.10)$$

Thus the photocurrent in each photodiode if we consider single-ended photodiodes is  $I_{PDmn} = R \cdot (E_{Out\_mn} + E_{LOmn}) \cdot (E_{Out\_mn} + E_{LOmn})^* + \eta_{sh}(t)$ , where  $R$  is the photodiode responsivity, and  $\eta_{sh}(t)$  is the shot noise associated with the direct-current component. Neglecting the shot noise, these photocurrents can be approximated by:

$$\begin{cases} I_{PD11} \propto \frac{1}{4} P_{Rx} + \frac{1}{8} P_{LO} + \frac{1}{2\sqrt{2}} \sqrt{P_{Rx} P_{LO}} \cos(\Delta\omega \cdot t + \phi_{Rx}(t) + \phi'_{nx}(t)) \\ I_{PD12} \propto \frac{1}{4} P_{Rx} + \frac{1}{8} P_{LO} - \frac{1}{2\sqrt{2}} \sqrt{P_{Rx} P_{LO}} \sin(\Delta\omega \cdot t + \phi_{Rx}(t) + \phi'_{nx}(t)) \\ I_{PD13} \propto \frac{1}{4} P_{Rx} + \frac{1}{8} P_{LO} + \frac{1}{2\sqrt{2}} \sqrt{P_{Rx} P_{LO}} \sin(\Delta\omega \cdot t + \phi_{Rx}(t) + \phi'_{nx}(t)) \\ I_{PD14} \propto \frac{1}{4} P_{Rx} + \frac{1}{8} P_{LO} - \frac{1}{2\sqrt{2}} \sqrt{P_{Rx} P_{LO}} \cos(\Delta\omega \cdot t + \phi_{Rx}(t) + \phi'_{nx}(t)) \\ I_{PD21} \propto \frac{1}{4} P_{Ry} + \frac{1}{8} P_{LO} - \frac{1}{2\sqrt{2}} \sqrt{P_{Ry} P_{LO}} \cos(\Delta\omega \cdot t + \phi_{Ry}(t) + \phi'_{ny}(t)) \\ I_{PD22} \propto \frac{1}{4} P_{Ry} + \frac{1}{8} P_{LO} + \frac{1}{2\sqrt{2}} \sqrt{P_{Ry} P_{LO}} \sin(\Delta\omega \cdot t + \phi_{Ry}(t) + \phi'_{ny}(t)) \\ I_{PD23} \propto \frac{1}{4} P_{Ry} + \frac{1}{8} P_{LO} - \frac{1}{2\sqrt{2}} \sqrt{P_{Ry} P_{LO}} \sin(\Delta\omega \cdot t + \phi_{Ry}(t) + \phi'_{ny}(t)) \\ I_{PD24} \propto \frac{1}{4} P_{Ry} + \frac{1}{8} P_{LO} + \frac{1}{2\sqrt{2}} \sqrt{P_{Ry} P_{LO}} \cos(\Delta\omega \cdot t + \phi_{Ry}(t) + \phi'_{ny}(t)) \end{cases} \quad (3.11)$$

where  $\Delta\omega = (\omega_s - \omega_{LO}) = 2\pi\Delta f$ . Balanced photodetection is usually used to filter out direct detection terms ( $P_{Rx}$ ,  $P_{Ry}$  and  $P_{LO}$ ):

$$\begin{cases} I_{PD1} = I_{PD11} - I_{PD14} \propto \frac{1}{\sqrt{2}} \sqrt{P_{Rx} P_{LO}} \cos(\Delta\omega \cdot t + \phi_{Rx}(t) + \phi'_{nx}(t)) \\ I_{PD2} = I_{PD13} - I_{PD12} \propto \frac{1}{\sqrt{2}} \sqrt{P_{Rx} P_{LO}} \sin(\Delta\omega \cdot t + \phi_{Rx}(t) + \phi'_{nx}(t)) \\ I_{PD3} = I_{PD24} - I_{PD21} \propto \frac{1}{\sqrt{2}} \sqrt{P_{Ry} P_{LO}} \cos(\Delta\omega \cdot t + \phi_{Ry}(t) + \phi'_{ny}(t)) \\ I_{PD4} = I_{PD22} - I_{PD23} \propto \frac{1}{\sqrt{2}} \sqrt{P_{Ry} P_{LO}} \sin(\Delta\omega \cdot t + \phi_{Ry}(t) + \phi'_{ny}(t)) \end{cases} \quad (3.12)$$

The resulting fields supply therefore the in-phase and quadrature components along both polarisations. Afterwards the four signals are digitized using analog to digital converters (ADC) operating approximately at twice the baud-rate

### 3.3. Digital signal processing associated to coherent detection

Digital signal processing (DSP) is one essential building block of modern coherent detection. It allows fibre impairments mitigation, polarisation tributaries demultiplexing of PDM signals, and proper operation with an unlocked local oscillator. DSP has been attracting huge interest from the scientific community recently. This thesis focuses on the impact of nonlinearities onto coherent systems and not in a deep study of all the possible algorithms. In that respect, all the results presented in this manuscript have been processed with the algorithm presented in the following paragraphs in order to ease comparisons. This algorithm briefly consists of resampling at twice the symbol rate, digital chromatic dispersion mitigation, polarisation demultiplexing by means of a constant-modulus-algorithm based adaptive equaliser in a butterfly structure, and carrier phase recovery (CPE) using the Viterbi and Viterbi algorithm [172].

Different algorithms from the one used in this work have been proposed to equalise the signal and recover the phase mismatch between the local oscillator and the signal, e.g. least mean squares decision-directed (LMS-DD) [163][164] leading to similar performances [165]. Besides, the powerful DSP capacity of coherent receivers allows also the use of specific algorithms to combat nonlinear propagation effects. Digital nonlinear mitigation using inverse backward-propagation, split-step Fourier algorithm, instead of linear FIR based dispersion-compensation, has been proposed to improve transmission performance [166]. Remarkable improvements have been recently demonstrated but with single channel transmission [167][168].

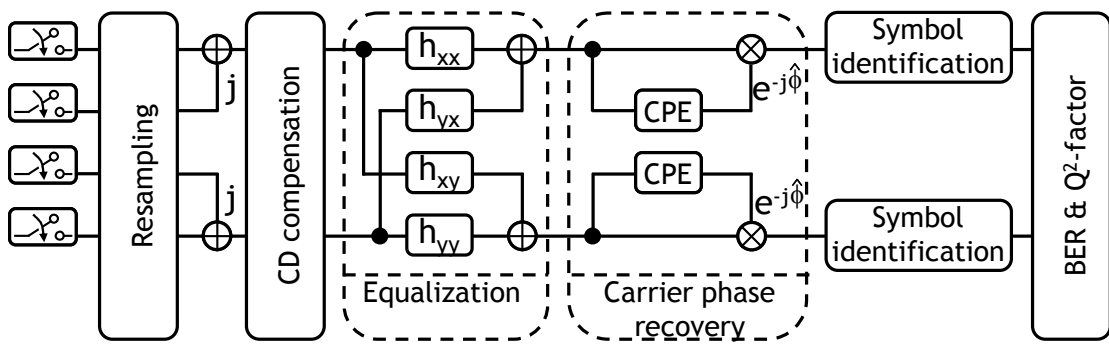


Fig. 3.6: Digital signal processing done in coherent receiver

#### a) Resampling and reconstruction

According to the Shannon-Nyquist criterion, the received signal should be sampled at a rate of at least twice the highest frequency present in the (baseband) spectrum. Practically, in a transponder specially designed for coherent systems, the 3-dB bandwidth of the ADC is roughly 0.5 to 0.8 times the symbol rate and the ADC sampling rate is exactly twice the symbol rate. Nevertheless, sampling heads used in

most of the research experiments have a 3-dB bandwidth of 16 GHz and work at a fixed sampling rate slightly lower than twice the symbol rate. Here, this sampling rate is 50 Gsamples/s for a symbol rate of 28 Gbaud as noted in [169] and [170]. Consequently, digitized signals have roughly 1.8 samples per symbol. In order to have DSP operating at exactly two samples per symbol, the first step is to resample the digital signal using an interpolation technique. Afterwards the baseband signal is reconstructed through the real and imaginary parts along both polarisations given by the photocurrents  $I_{PD1}$ ,  $I_{PD2}$ ,  $I_{PD3}$  and  $I_{PD4}$  so as:

$$\begin{aligned}\hat{E}_{Rx} &= I_{PD1} + j \cdot I_{PD2} \\ \hat{E}_{Ry} &= I_{PD3} + j \cdot I_{PD4}\end{aligned}\quad (3.13)$$

Fig. 3.7 depicts the constellation diagram of both polarisations after resampling and reconstructing the signal 100 Gb/s PDM-QPSK experimental data and the unitary circle with a yellow dashed line. As it can be observed at this step, the constellation diagram of each polarisation carries a mix of both sent polarisation tributaries (represented in Fig. 3.7 in green and violet) on each constellation since the incoming signal presents an arbitrary SOP

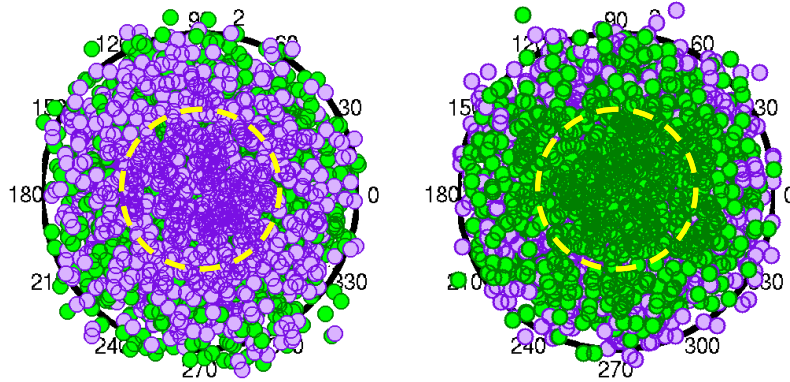


Fig. 3.7: Constellation diagram (of both polarisations) of 100 Gb/s PDM-QPSK after resampling and reconstructing the signal.

### b) Chromatic dispersion compensation

Chromatic dispersion (CD) is a static polarisation-independent phenomenon and then it can be compensated for before equalising and demultiplexing the received signal to recover the two orthogonal polarisation tributaries sent at the transmitter side. Thus, since we roughly know the residual amount of chromatic dispersion, we use the well-known analytical expression of CD to design the filter which compensates for it. This expression is

$$G(z, \omega) = \exp\left(-j \frac{D\lambda^2}{4\pi c} \omega^2\right) \quad (3.14)$$

where  $z$  is the distance,  $\omega$  is the angular frequency,  $j$  is the imaginary unit,  $D$  is the dispersion coefficient of the fibre,  $\lambda$  is the wavelength and  $c$  is the speed of light.

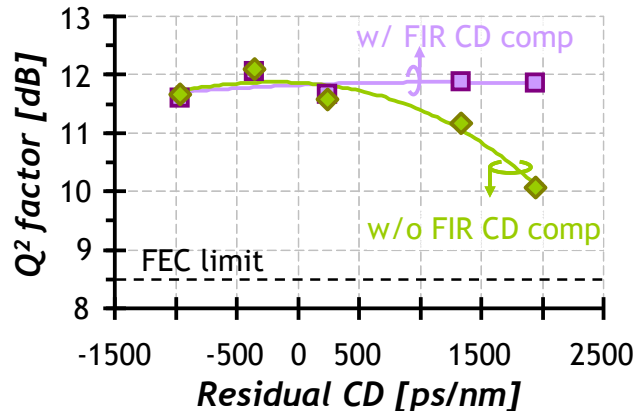


Fig. 3.8: Performance evolution of 40 Gb/s PDM-QPSK as a function of residual chromatic dispersion □ with and ◇ without a FIR filter inserted before the equaliser to compensate for residual chromatic dispersion.

The practical implementation of the digital filter corresponding to such an expression is impossible because its response is not causal and has an infinite duration. Practically, the response is truncated and static finite impulse response (FIR) filters are used. The length of these filters is proportional to the amount of CD to be compensated for [165]. Fig. 3.8 shows the tolerance of PDM-QPSK at 40 Gb/s against residual CD with and without using of a specific FIR filter to compensate it for. As it can be observed, performance remains almost unchanged between -1000 and +2000 ps/nm when the full algorithm, including a CD compensation FIR filter placed before the equaliser, is applied. Thus coherent systems exhibit unparalleled resilience against chromatic dispersion provided complex enough dedicated filters. For practical real-time implementation, the amount of CD compensation will depend on the calculation capacity of the state-of-the-art technologies. At the output of this operation both polarisation tributaries are still mixed, as it can be seen in Fig. 3.9. Therefore the next step is to equalise the signal and demultiplex both polarisation tributaries.

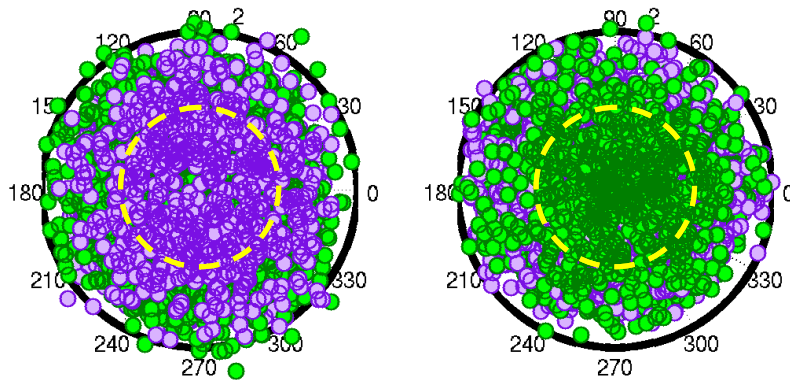


Fig. 3.9: Constellation diagram (of both polarisations) of 100 Gb/s PDM-QPSK after compensating for the chromatic dispersion.

### c) Equalisation and polarisation demultiplexing

A key part of the DSP is to demultiplex the received signal to recover the two orthogonal polarisation tributaries sent at the transmitter side. This can be done

using blind adaptive FIR filters using constant modulus algorithm (CMA) as proposed in [171]. The filters are arranged in a butterfly structure (as seen in Fig. 3.6) and are continuously updated to follow channel perturbations like polarisation-dependent fluctuations, PMD... All these perturbations can be modelled into the Jones matrix of the transmission line. It has to be noted that the two input signals of the block,  $x_{in}$  and  $y_{in}$ , are a mix of the two signals emitted along the two orthogonal states of polarisation of the light. Therefore the task of the equaliser is to estimate the inverse of the Jones matrix (3.5) so as to reverse the effects induced by the channel propagation. The output signal is obtained as follows:

$$\begin{bmatrix} x_{out} \\ y_{out} \end{bmatrix} = \begin{bmatrix} h_{xx} & h_{yx} \\ h_{xy} & h_{yy} \end{bmatrix} \cdot \begin{bmatrix} x_{in} \\ y_{in} \end{bmatrix} \quad (3.15)$$

where  $x_{in}$  and  $y_{in}$  are the input signals,  $x_{out}$  and  $y_{out}$  are the output signals and  $h_{xx}$ ,  $h_{xy}$ ,  $h_{yx}$  and  $h_{yy}$  are the adaptive FIR filters having T/2-spaced complex tap-coefficients (also known as taps). Unless explicitly mentioned, all the results presented in this thesis have been obtained using a 13-tap T/2-spaced equaliser. These coefficients are updated, using the stochastic gradient method, such that:

$$\begin{aligned} h_{xx} &\rightarrow h_{xx} + \mu \varepsilon_x x_{out} \cdot x_{in}^* \\ h_{xy} &\rightarrow h_{xy} + \mu \varepsilon_y y_{out} \cdot x_{in}^* \\ h_{yx} &\rightarrow h_{yx} + \mu \varepsilon_x x_{out} \cdot y_{in}^* \\ h_{yy} &\rightarrow h_{yy} + \mu \varepsilon_y y_{out} \cdot y_{in}^* \end{aligned} \quad (3.16)$$

where  $\mu$  is the convergence parameter,  $x_{in}^*$  and  $y_{in}^*$  are the complex conjugate of  $x_{in}$  and  $y_{in}$  respectively, and the error terms which have to be minimized are given by:

$$\begin{aligned} \varepsilon_x &= 1 - |x_{out}|^2 \\ \varepsilon_y &= 1 - |y_{out}|^2 \end{aligned} \quad (3.17)$$

for unit amplitude signals. At the end of this DSP block, the two output signals,  $x_{out}$  and  $y_{out}$ , are polarisation-demultiplexed and equalised thanks to the estimation of the Jones matrix.

It must be noted here that, an adaptive equaliser using complex tap-coefficients also mitigates for residual chromatic dispersion, as shown in Fig. 3.8. This suggests that a simpler DSP without filter for significant CD compensation inserted before polarisation demultiplexing would be sufficient to provide very good mitigation of residual dispersion impairments in most legacy optical networks relying on dispersion management with periodically distributed dispersion compensating modules. Furthermore, digital equalisation provides unique resistance against PMD for coherent systems, well above the tolerance of today's 10 Gb/s systems [170].

In that respect, I demonstrate the tolerance of PDM-QPSK at 100 Gb/s up to 20 ps PMD. Fig. 3.10 (a) represents the distribution and (b) the cumulative probability of 1000 successively measured Q<sup>2</sup> factor with 8 and 20 ps PMD for 100 Gb/s PDM-QPSK. As a reference, Fig. 3.10 depicts also results obtained with no PMD (<1 ps). Q<sup>2</sup> factor distributions are almost identical whether PMD is emulated or not. Besides, 8 and 20 ps PMD only induce a negligible 0.3-dB extra deviation

compared to the reference curve. This underlines the efficient PMD mitigation of coherent systems, illustrated here for 100 Gb/s PDM-QPSK.

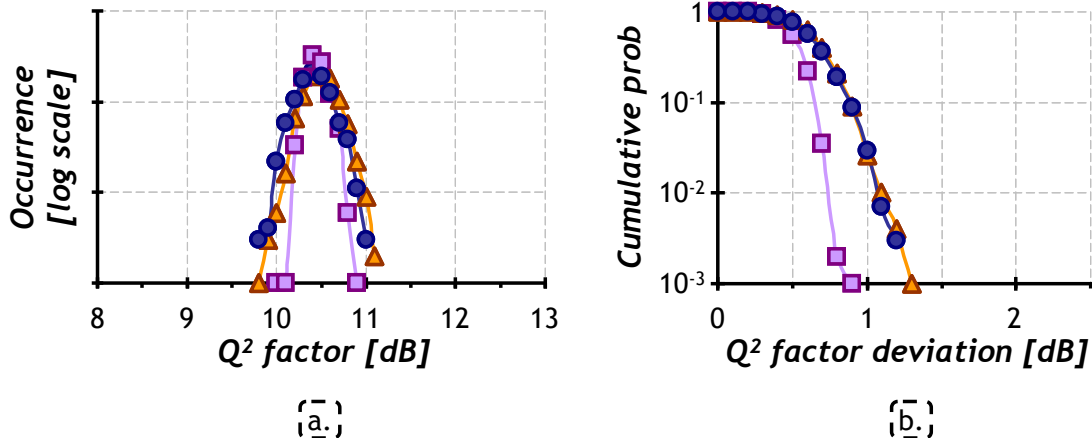


Fig. 3.10: 100 Gb/s PDM-QPSK,  $Q^2$  factor distribution (a) and cumulative probability (b) with  $\blacksquare$  <1 ps,  $\bullet$  8 ps and  $\blacktriangle$  20 ps PMD.

Once the two polarisation tributaries have been demultiplexed by the blind adaptive equaliser, phase-tracking has to be done in the digital domain since the local oscillator is not optically phase-locked onto the received signal. Otherwise, the constellation diagram expected (four clouds located at  $+\pi/4$ ,  $+3\pi/4$ ,  $-3\pi/4$  and  $-\pi/4$ ) would look like a thick circle, as it appears in Fig. 3.11. This phase offset will be recovered by the following block in the DSP.

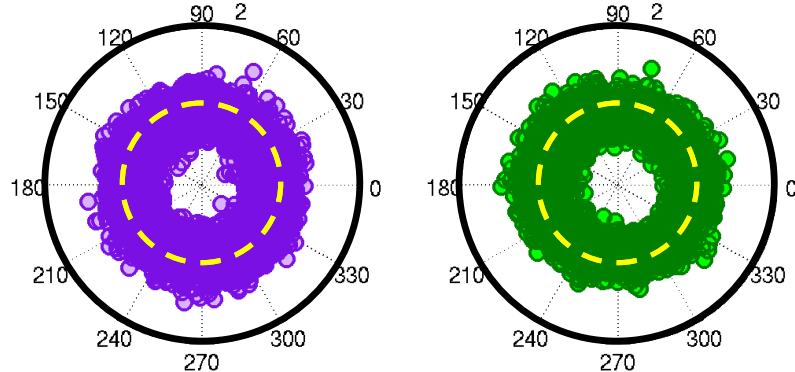


Fig. 3.11: Constellation diagram (of both polarisations) of 100 Gb/s PDM-QPSK after equalising and polarisation demultiplexing.

#### d) Carrier phase estimation

The carrier phase estimation (CPE) is used to recover and subsequently remove the remaining phase mismatch,  $\varphi$ , between the local oscillator and the signal. Since the previous adaptive algorithm acts as a fine clock recovery block as well, the estimation of this mismatch is done on the “central” sample only (while the other is dropped) by using a nonlinear carrier phase tracking algorithm [172] as follows: first, the  $M$ -th power of the complex symbol is taken in order to remove any information encoded in the phase of the signal ( $M$  being the number of phase levels of the modulation, i.e., four for a QPSK modulation). Second, an averaging window of  $N+1$  elements is computed by summing the result over  $N/2$  pre-cursor and  $N/2$  post-cursor symbols.

Then, the argument is taken since we are only interested in the phase. Finally, as shown by the equation below, the resulting phase is divided by  $M$  to correct for the initial elevation to the  $M$ -th power; the result is in the range  $[-\pi, \pi]$ .

$$\hat{\phi}(k) = \frac{1}{M} \arg \left[ \sum_{p=-N/2}^{N/2} x_{out}^M(k+p) \right] \quad (3.18)$$

Subsequent unwrapping is used to be able to follow large time-varying excursions of the signal phase, as for instance when a carrier frequency detuning with respect to the local oscillator is present. At the output of this block, both polarisation tributaries are demultiplexed and the symbols on each polarisation can be identified, as observed in Fig. 3.12

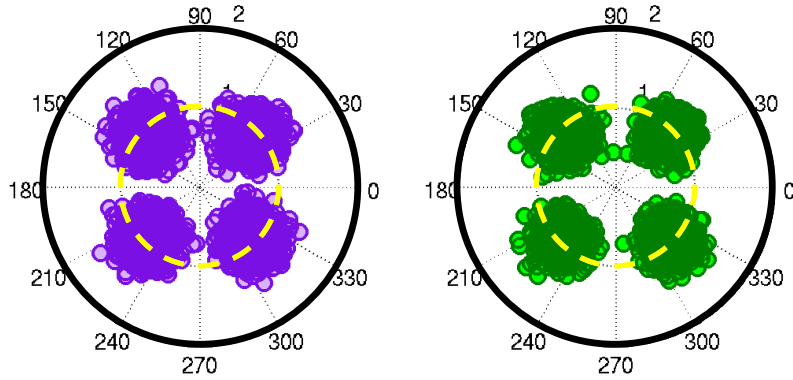


*Fig. 3.12: Constellation diagram (of both polarisations) of 100 Gb/s PDM-QPSK after carrier phase estimation.*

CPE is critical since a correct estimation of the phase, and hence the performance, depends on the number of consecutive symbols considered [173][174]. If the carrier is affected both by zero-mean ASE-induced linear phase noise and by zero-mean (nonlinear) cross-phase modulation (XPM), a large CPE averaging window,  $N+1$ , efficiently averages out both ASE-induced noise and XPM. Thus, after subtracting the estimated phase out of CPE from the carrier, the phase offset is cancelled. However, both XPM and ASE-induced noise are still affecting the carrier. If a small averaging window is used instead, some residual ASE-induced noise will be present at CPE output and its variance will add to the ASE-induced noise already present on the carrier, since ASE is a white (uncorrelated) process. On the contrary, the residual XPM at the CPE output will partly cancel the XPM originally on the carrier. XPM is indeed a correlated process with typically a low-pass spectrum as compared to the distorting (surrounding) signal [175]. Hence a small averaging CPE window results in a lower XPM, at the expense of a larger ASE-induced noise. It is thus clear that window size can be adjusted to lower values when XPM is dominant w.r.t ASE noise.

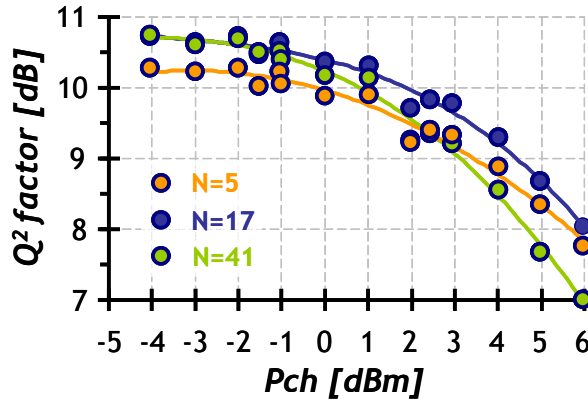


Fig. 3.13: 100 Gb/s PDM-QPSK, Performance dependence on the averaging window used for CPE for after 400 km of SSMF with fixed OSNR by loading noise at the receiver side.

Fig. 3.13 illustrates the performance dependence on the averaging window of 100 Gb/s PDM-QPSK after 400 km of SSMF (more details of system configuration are given in section 1.1). OSNR is intentionally controlled by noise loading at the receiver side so that it is constant while increasing the power and the  $Q^2$  factor reaches the arbitrary reference of  $\sim 10.5$  dB when performance is mainly limited by optical noise (i.e. for powers lower than  $-1$  dB). In contrast, nonlinear impairments degrade the performance for high powers per channel,  $P_{ch}$ . As it can be observed, longer CPE averaging gives better performance for low launch powers as transmission is mainly limited by optical Gaussian noise. For high values of launch power in turn, nonlinear effects become dominant and shorter symbol length of CPE gives better performance since nonlinear-induced phase changes are partially cancelled. An optimal value for both low and high powers can be found sometimes. This optimal CPE length is obtained here at 17 consecutive symbols. Unless explicitly mentioned, all the results presented in this thesis have been obtained with optimised CPE length.

It has to be noted here that, as pointed out in [176], phase estimators perform well when estimated phase can be considered as unbiased in the range of the chosen averaging window, leading to the following condition on the frequency detuning,  $\Delta f$ , between the carrier of the received signal and the frequency of the local oscillator:

$$\Delta f \leq \frac{1}{2(N+1)MT_s} \quad (3.19)$$

where  $T_s$  is the sampling period,  $N+1$  is the averaging window of CPE and  $M$  is the number of symbol states. According to this condition, the maximum tolerable frequency offset is around  $\pm 600$  MHz for 100 Gb/s PDM-QPSK operating at 28 Gbaud. Since the accuracy of typical temperature-stabilized lasers is around  $\pm 1$  GHz, a technique derived from the nonlinear carrier phase tracking algorithm and presented in [176] is usually performed to estimate and remove the frequency detuning,  $\Delta f$ , before processing CPE.

#### e) Symbol identification and bit error ratio calculation

After carrier phase estimation, the digital signal is ready to be processed by the decision block. Threshold decision on each symbol is realized (as represented in Fig.

3.14) while differential decoding is used to avoid catastrophic error propagation in case of cycle slips. Finally, we compare the extracted pattern with the original sequence, and errors are found and counted. This results in a BER. For practical reasons, the measured system performance is usually not expressed in BER but in Q<sup>2</sup> factor. Here, the resulting BER of at least four recordings is averaged before being transformed into Q<sup>2</sup> factors.

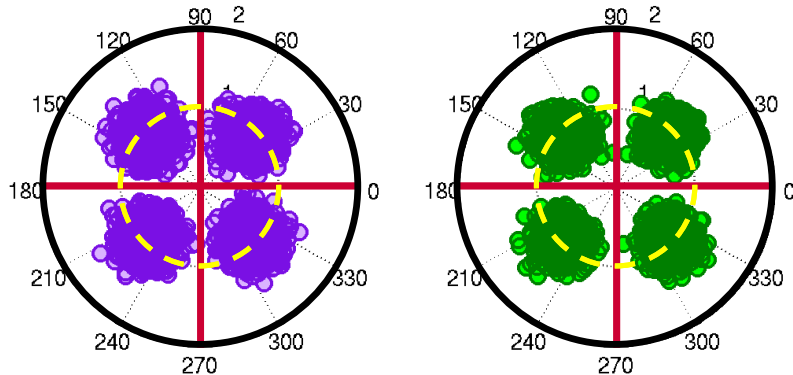


Fig. 3.14: Resulting constellation diagram (of both polarisations) of 100 Gb/s PDM-QPSK with threshold decision.

### 3.4. Summary

A renewed interest in coherent detection has been stimulated by recent progress on high-speed digital electronics for signal processing and on analog-to-digital converters. Coherent detection offers the possibility of detecting signals with optimal noise sensitivity. Besides, recent advances allow combining coherent detectors with digital signal processing and pave the way for the use of polarisation division multiplexing and the compensation or mitigation of linear impairments through suitable algorithms. Thus, today's (digital) coherent receivers enjoy the high sensitivity of coherent detection with the added benefits of digital signal processing. In this chapter, the architecture of the coherent receiver used throughout this thesis, including the algorithms used for digital signal processing have been described. This receiver (coherent mixer and algorithms) are used to process any experimental measurements presented in this chapter and the next ones. The excellent tolerance to chromatic dispersion and to PMD brought by the algorithms applied in digital coherent receivers has been demonstrated experimentally. These tolerances are well above the tolerance of today's 10 Gb/s systems.

The following chapter presents experimental studies involving polarisation division multiplexing of phase-modulated signals detected with a digital coherent receiver at 40 and 100 Gb/s. In this context, I investigate the impact of nonlinear effects occurring along the line and also their interactions with PMD.

# ***Chapter 4. 40-Gb/s systems***

Given that the traffic load currently approaches the maximum capacity of existing 10-Gb/s networks, carriers plan to increase the total capacity of their network infrastructure by increasing channel rates due to the limited bandwidth of optical amplifiers. Their motivation is to respond to the predicted traffic growth of about 50% per year [1]. However, fibre transmission becomes more and more challenging as the bit-rate increases since the tolerance to fibre linear effects is reduced, as discussed in Chapter 2. More precisely, if we consider the same modulation format for a  $n$ -fold increase of the channel bit rate, the sensitivity to optical noise and the maximum tolerable amount of polarisation mode dispersion (PMD) are reduced by a factor  $n$ . At the same time, the minimum tolerable filter bandwidth is increased by the same amount. Moreover, the maximum tolerable amount of chromatic dispersion is reduced by a factor  $n^2$ .

Most carriers do not intend to build specific networks from scratch for increasing the total capacity. Therefore, one likely scenario for the upgrade of existing infrastructures massively carrying 10 Gb/s NRZ channels is to design so-called hybrid systems. In these systems, several channels at higher bit rate (namely 40 or 100 Gb/s) are progressively inserted in wavelength slots with 50-GHz spacing, originally designed for NRZ channels at 10 Gb/s and transmitted over dispersion-managed links, i.e. incorporating periodically dispersion compensating modules to compensate for the accumulated dispersion along the line. Thus channels at 40 or 100 Gb/s will propagate simultaneously with 10 Gb/s NRZ channels over the same fibre.

This chapter focuses on the upgrade of legacy 10-Gb/s systems to 40 Gb/s. Moving from 10 Gb/s to 40 Gb/s over an unchanged 50-GHz channel grid increases the information spectral density (i.e., the number of bits per second transmitted in a unit spectral band) from 0.2 bit/s/Hz to 0.8 bit/s/Hz. Before the rise of digital coherent receivers, the principal concern for the deployment of 40-Gb/s channels was the tolerance to linear effects namely PMD and chromatic dispersion. Different modulation formats using direct (differential) detection have been proposed to meet

this challenge in these so-called hybrid systems at 10/40 Gb/s, namely partial DPSK, phase shaped binary transmission (PSBT) and differential quadrature phase-shift keying (DQPSK). Focussing on linear impairments, DQPSK outperforms the two other solutions [79] thanks to the lower symbol rate and narrower spectrum, as discussed in section 1.1.

More recently, 40 Gb/s PDM-QPSK, associated with coherent detection was praised for its narrow spectrum ( $\sim 20$  GHz, the main lobe) and its excellent robustness to linear impairments, as discussed in Chapter 3 and also shown in [177][178][179][180]. 40 Gb/s PDM-QPSK has a symbol rate of 10 Gbaud and thus benefits of massively developed cost-efficient 10-Gb/s electronics. Thus coherent PDM-QPSK is a potential candidate to upgrade current legacy systems to 40 Gb/s. The first part of this chapter focuses on the investigation of the nonlinear tolerance of 40 Gb/s PDM-QPSK which is a key aspect for the upgrade of legacy 10-Gb/s systems. We first assess the impact of polarisation multiplexing in a single channel scenario and subsequently study the consequences of introducing 40 Gb/s PDM-QPSK in WDM systems over different types of fibres.

Polarisation division multiplexing and coherent detection can be paired with any modulation format. Thus, another option to increase the information spectral density from 0.2 bit/s/Hz to 0.8 bit/s/Hz is PDM-BPSK at 40 Gb/s. When detected with a differential receiver, (singly-polarised) DPSK appears to be more robust against nonlinearities than DQPSK [91]. However, DPSK has two main drawbacks compared to DQPSK: the lower tolerance against linear effects and the larger spectrum ( $\sim 80$  GHz). Picture changes with the introduction of polarisation division multiplexing and coherent detection. PDM-BPSK signals have a baud rate of 20 Gbaud and a spectrum width of 40 GHz. The tolerance to linear effects in turn is brought by DSP done in the coherent receiver. In the second part of this chapter, we investigate and discuss, therefore, the nonlinear tolerance of 40 Gb/s PDM-BPSK in the light of upgrading 10-Gb/s legacy networks.

## 4.1. 40 Gb/s PDM-QPSK

The symbol rate of PDM-QPSK is a quarter of the total bit rate. Thus, 40 Gb/s PDM-QPSK signals have a symbol rate of 10 Gbaud and a spectrum width of 20 GHz. Consequently, it easily fits into the standard 50-GHz grid and uses massively developed cost-effective 10-Gb/s electronics. Moreover, ADC should operate at 20 GSamples/s in order to obtain two samples per symbol relaxing thus practical-implementation constraints. Benefiting from the unparalleled tolerance to linear effects brought by coherent detection, 40 Gb/s PDM-QPSK appears as a potential option to reach the upgrade of current 10-Gb/s legacy systems.

In this context, this section deals with the nonlinear tolerance of coherent 40 Gb/s PDM-QPSK in realistic scenarios. Therefore, the impact on nonlinear tolerance of polarisation multiplexing is first investigated. Next, the tolerance to inter-channel nonlinear effects is discussed either when all channels are 40-Gb/s PDM-QPSK modulated or when the coherent channel is surrounded by 10-Gb/s NRZ channels.

### 4.1.1 Experimental set up

The experiments carried out here involve single-channel transmission, homogenous WDM transmission and also hybrid WDM transmission. Three configurations are thus used successively at the transmitter side as shown in Fig. 4.1-a, b and c. In all configurations, the test channel (at 1546.52 nm) is modulated with PDM-QPSK at 40 Gb/s. On the contrary, the surrounding channels can be either kept continuous-wave (CW), modulated with PDM-QPSK at 40 Gb/s, or modulated with OOK-NRZ at 10 Gb/s corresponding to single-channel, homogenous WDM and hybrid WDM transmissions, respectively.

As depicted in Fig. 4.1, the transmitter consists of eighty-two DFB lasers, spaced by 50 GHz and separated into two spectrally-interleaved combs which are independently modulated. To generate the PDM-QPSK data, the light from each comb is sent to two different QPSK modulators operating at 10.7 Gbaud. The modulators are fed by  $2^{15}$ -1-bit-long pseudo-random bit sequences (PRBS) at 10.7 Gb/s, including forward error correction (FEC) overhead. Polarisation multiplexing is finally performed by dividing, decorrelating and recombining QPSK data through a polarisation beam combiner (PBC) with an approximate 10-nanoseconds delay, yielding PDM-QPSK data at 43 Gb/s. To generate the 10-Gb/s NRZ data required for the hybrid WDM transmission experiment, the light from each comb is sent into a Mach-Zehnder modulator, fed by  $2^{15}$ -1-length PRBS at 10.7 Gb/s. In any case, the two generated combs are passed into low-speed (<10 Hz) polarisation scramblers (PS) and combined with a 50-GHz interleaver.

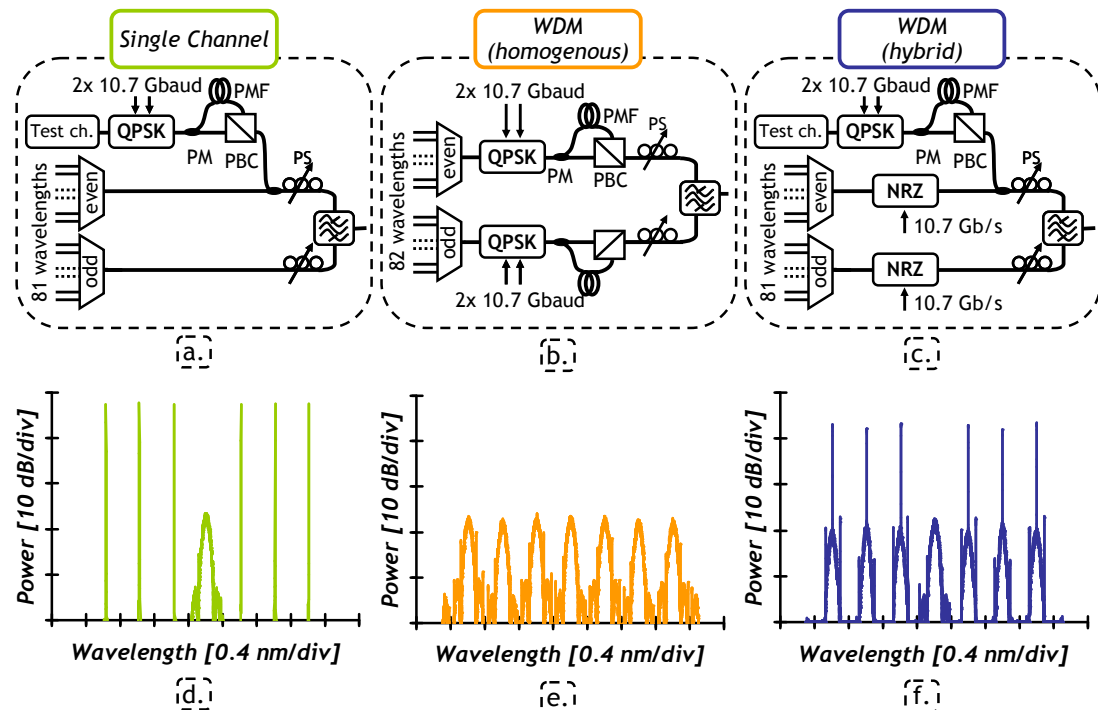


Fig. 4.1: Experimental transmitter set-up and experimental spectra (100-MHz resolution) for three different configurations: (a, d) single-channel, (b, e) homogenous WDM and (c, f) hybrid WDM.

The resulting multiplex is boosted through a dual-stage EDFA incorporating dispersion compensating fibre (DCF) for pre-compensation and sent into the

recirculating loop discussed in section 2.6. The recirculating loop here incorporates four 100-km-long spans of SSMF which are separated by dual-stage EDFA including an adapted spool of DCF for partial dispersion compensation, according to a typical terrestrial transmission map [140]. A wavelength selective switch (WSS) is also inserted at the end of the loop to perform channel power equalisation. The performance is measured after 4 round-trips, i.e. after 1,600 km while varying the power per channel,  $P_{ch}$ , at each fibre input. In all experiments, the launch power of the test channel is set at the same level as all the co-propagating channels. At the receiver side, the channel under study is selected by a 0.4-nm bandwidth tuneable filter and sent into the coherent receiver, discussed in Chapter 3.

#### 4.1.2 Impact of polarisation multiplexing

Polarisation multiplexing does not imply a loss in noise sensitivity, as shown in Fig. 2.17. Nonetheless, the tolerance to nonlinearities is reduced when moving to a polarisation multiplexed scheme owing to the interplay between polarisation tributaries. We first study the impact on nonlinear tolerance of polarisation division multiplexing by comparing 20-Gb/s (singly-polarised) QPSK and 40-Gb/s PDM-QPSK in a quasi-single channel configuration, shown in Fig. 4.1-a. Thus neighbouring channels around the studied channel are kept continuous while ensuring amplifier loading, as seen in Fig. 4.1-d. Singly-polarised QPSK signal exhibits 3-dB better tolerance to optical noise compared to PDM-QPSK, as discussed in section 2.2. Therefore, in order to ease comparisons, the OSNR is maintained constant as the channel power increases by loading noise at the receiver end. The OSNR is set at 16 dB in 0.1 nm when studying the 40-Gb/s PDM-QPSK modulation scheme. This OSNR is intentionally degraded by 3 dB when moving to the 20-Gb/s QPSK scheme. Thus both schemes yield approximately the same  $Q^2$ -factor after propagation (12.6 dB for QPSK and 13 dB for PDM-QPSK), when transmission is mainly limited by optical noise, at low channel power.

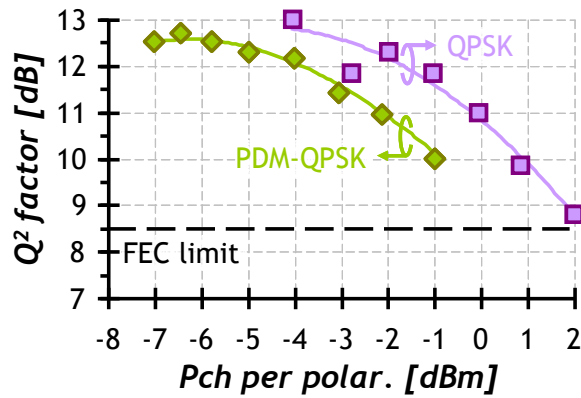


Fig. 4.2: Tolerance to intra-channel nonlinearities after 1,600 km of SSMF.  $\blacksquare$  20 Gb/s QPSK and  $\blacklozenge$  40 Gb/s PDM-QPSK. The symbol rate of both signals is 10 Gbaud. The OSNR is fixed at the receiver by loading noise, so as both schemes give approximately the same performance when the transmission is limited by optical noise, i.e. at low powers.

Fig. 4.2 depicts the results corresponding to this comparison, in terms of  $Q^2$ -factor as a function of the power per channel per polarisation. When the power is

increased, the performance is degraded by nonlinear effects, mainly self phase modulation (SPM)-induced nonlinear phase noise (NLPN). The nonlinear threshold (NLT) is defined as the power leading to a reduction of 2 dB of  $Q^2$  factor at a constant receiver OSNR. Should there be no nonlinear interactions between the two polarisation tributaries, one would expect that the NLT per polarisation of PDM-QPSK at 40 Gb/s be the same as QPSK at 20 Gb/s, i.e. that the nonlinear threshold of 40 Gb/s PDM-QPSK be 3 dB larger than the nonlinear threshold of 20 Gb/s QPSK. Nevertheless, the tolerance to nonlinearities is reduced when moving to PDM signals due to the interplay between both polarisation tributaries, as pointed out in equation (1.36). In fact, the nonlinear-induced phase distortion experienced by each polarisation tributary depends on the power of both polarisation tributaries. As a consequence, PDM signals are more impacted by nonlinearities than singly-polarised signals. Fig. 4.2 shows that the NLT of PDM-QPSK (-1.7 dBm) is approximately 1.5 dB lower per polarisation than for QPSK (0 dBm). This result has been recently confirmed theoretically and numerically by A. Bononi et al [181] and clearly shows that PDM-based channels are more sensitive to intra-channel nonlinear effects than singly-polarised channels.

#### **4.1.3 Tolerance to intra and inter-channel nonlinearities**

I then assess the tolerance of 40 Gb/s coherent PDM-QPSK to cross nonlinearities between channels in a homogenous WDM environment, corresponding to the scheme and spectrum shown in Fig. 4.1-b and e, respectively. Unlike the preceding experiment, the OSNR is no longer controlled at the receiver side. Fig. 4.3-a represents the measured performance versus launch power per channel (comprising both polarisation-tributaries power). As a reference, Fig. 4.3-a also plots the results obtained in a single channel scheme. The optimum  $Q^2$ -factor is found at a power of 0 dBm in the quasi-single channel configuration whereas an optimum power of -3 dBm in WDM configuration is observed. Furthermore, the  $Q^2$  factor is nearly constant while increasing the power per channel from -4 dBm to -2 dBm, despite the 2-dB increase in terms of OSNR. This highlights the poor tolerance of 40 Gb/s coherent PDM-QPSK signals to cross nonlinear effects attributed to the low symbol rate, the  $\pi/2$  phase distance between symbols and polarisation multiplexing [174][182].

The preceding results discussed the nonlinear tolerance under the assumption that all co-propagating channels are 40 Gb/s PDM-QPSK. However, the currently installed WDM systems carry predominantly 10 -Gb/s NRZ channels. As introduced in section 1.2, PDM signals may suffer not only from XPM but also from XPolM arising from neighbour channels. The tolerance to cross nonlinearities induced by 10 -Gb/s NRZ channels is therefore a key parameter to determine its suitability for overlaying existing 10-Gb/s legacy networks.

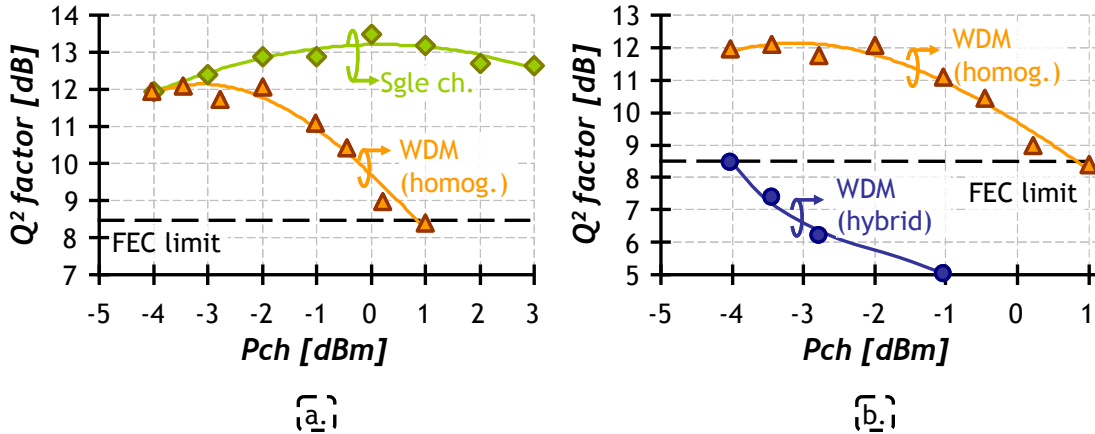


Fig. 4.3: Nonlinear tolerance of 40 Gb/s PDM-QPSK channels after 1,600 km of SSMF. ♦ Single channel configuration, ▲ homogeneous WDM configuration involving only 40 Gb/s PDM-QPSK channels and ● hybrid WDM configuration involving a mix of 40-Gb/s and 10-Gb/s NRZ channels. The symbol rate of all signals is 10 Gbaud.

In this context, I investigate the impact of co-propagating 10-Gb/s NRZ channels onto 40 Gb/s PDM-QPSK channels. We compare the performance of one 40 Gb/s PDM-QPSK channel surrounded either by other 40-Gb/s PDM-QPSK (Fig. 4.1-b and e) or by 10-Gb/s NRZ channels (Fig. 4.1-c and f). Fig. 4.3-b shows the performance evolution in both WDM configurations versus the launch power per channel. Cross nonlinear effects brought by neighbouring NRZ channels degrade severely transmission performance as compared with that observed with 40 Gb/s PDM-QPSK neighbouring channels, as clearly seen in Fig. 4.3-b. Actually, the best Q<sup>2</sup>-factor measured in hybrid configuration is obtained for the lowest launch power, here at -4dBm, and is just at the FEC limit. For comparison, a 2.5 dB increase in performance is found when all channels are PDM-QPSK modulated. These results demonstrate that cross nonlinear effects limit the performance 40-Gb/s PDM-QPSK in WDM legacy systems. This statement is even more evident when 40 Gb/s PDM-QPSK is surrounded by 10-Gb/s NRZ channels. Therefore, countermeasures should be considered to constrain cross nonlinear-induced penalties.

#### 4.1.4 Containing inter-channel nonlinearities in WDM transmission

As discussed in section 3.3, the accuracy of CPE, and hence the system performance, depends on both the nature of the dominant phase noise and the number of consecutive symbols over which the phase is estimated. Therefore, a first option to reduce the impact of cross nonlinearities and improve the performance of a 40 Gb/s coherent PDM-QPSK channel in hybrid 10/40 Gb/s configuration could be to optimise the length of the averaging window when performing the CPE operation.

Fig. 4.4-a shows Q<sup>2</sup>-factor of a 40 Gb/s coherent PDM-QPSK channel versus N in a hybrid 10/40 Gb/s configuration. N designates the number of consecutive symbols over which the phase is estimated. Contrary to homogeneous systems where the optimum CPE length was found to be 9 symbols (Fig. 4.3-a), it is 3 symbols in hybrid systems. Such a reduction of the optimal CPE length unveils the fact that the

performance is here dominated by cross nonlinear effects. As already noted in section 3.3, a consequence of reducing the window of the phase estimator is that additive white Gaussian noise cannot be completely averaged out of the CPE, so that the performance of the estimator is not optimum. The gain of optimising the CPE process is weaker than the encountered penalties and is not sufficient to match the performance of the all-40 Gb/s PDM-QPSK configuration. The difference between these results and other results found in the literature as [174] is attributed to the larger number of surrounding channels and the lower chromatic dispersion used here. Indeed, a too small number of surrounding channels may lead to underestimate the actual penalties brought by 10 Gb/s NRZ co-propagating channels onto coherent ones (as discussed in section 5.2.5); whereas the lower residual chromatic dispersion per span used here -around 30 ps/nm- compared to the larger one -up to 85 ps/nm per span- used in [174] enhances cross nonlinearities.

Another option to reduce the penalties brought by 10 Gb/s NRZ co-propagating channels on the performance of coherent PDM-QPSK channels is to introduce guard-bands between 40-Gb/s PDM-QPSK and 10-Gb/s NRZ channels. I investigate this option by gradually switching off adjacent channels (up to five channels) on both sides of the 40 Gb/s test channel, as depicted in Fig. 4.4-b. As a trade-off between nonlinear penalties and maximum reach for PDM-QPSK and NRZ signals, the launch power per channel is fixed at -1 dBm. This power is within the typical range of operating power of 10 Gb/s NRZ when reaching ultra-long haul (ULH) distances and implies 1-dB performance penalty compared to the optimum performance in an homogeneous WDM 40-Gb/s configuration, according to Fig. 4.3-b.

The results of these measurements are depicted in Fig. 4.4-c with independently-optimized CPE length for each system configuration in terms of performance evolution of the coherent channel while increasing progressively the spacing to the closest neighbour channels on both sides. Ideally, when surrounding channels are far enough from the test one, the performance of the test channel should be the same as in a single channel transmission, i.e.  $\sim 13$  dB of  $Q^2$  factor. When all the channels are 40 Gb/s PDM-QPSK modulated, 2-dB penalty compared to single channel performance is observed when the channel spacing is 50 GHz. This penalty decreases with the channel spacing and is nearly recovered with a guard-band around 150 GHz. On top of that, however, when the PDM-QPSK channel is surrounded by NRZ channels, a performance floor close to the FEC limit is observed even after removing 10-Gb/s channels, as far as 300 GHz away from the PDM-QPSK test channel. It has to be noted here that the power per channel slightly increases while suppressing adjacent channels (by  $\sim 0.5$  dB at the most). Nevertheless, it does not explain the observed performance limitation since intra-channel nonlinearities are not the dominant effect according to the behaviour when all the channels are PDM-QPSK of Fig. 4.4-c and the results of Fig. 4.3-a.

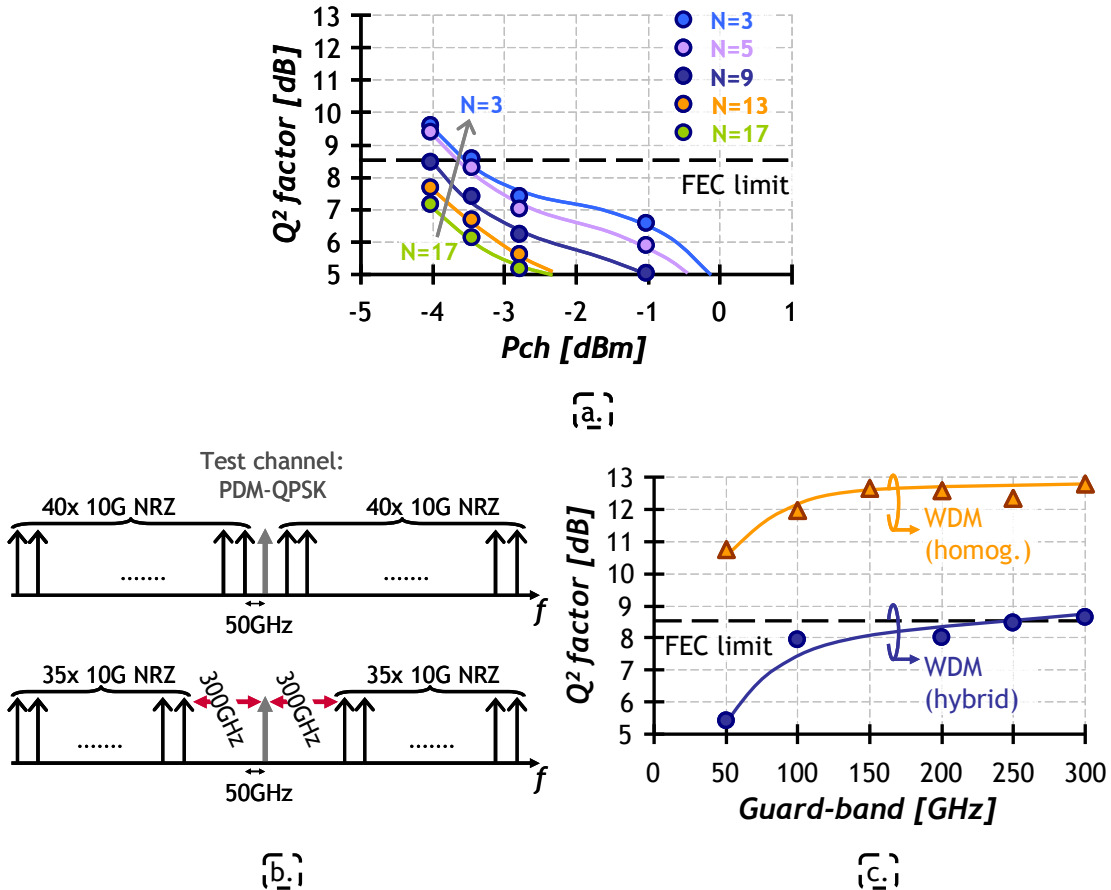


Fig. 4.4: (a) Performance dependence on the CPE averaging window in a hybrid WDM configuration. (b) Channel allocation and (c) performance evolution as a function of the guard-band around the 40-Gb/s PDM-QPSK channel, surrounded either  $\blacktriangle$  by other 40-Gb/s PDM-QPSK channels or  $\bullet$  by 10-Gb/s NRZ channels, when all channels are set at -1 dBm/ch. All measurements have been obtained after 1,600 km of SSMF.

Such a result is attributed to the impact of cross phase modulation (XPM) and also to polarisation scattering induced by cross nonlinear effects brought by surrounding 10-Gb/s NRZ channels, referred to as cross polarisation modulation (XPolM) [183]. In fact, 40 Gb/s PDM-QPSK signals suffer from severe nonlinear interactions coming from co-propagating channels even distant by more than 300 GHz, contrary to what happens in conventional polarisation-insensitive detection, currently used in 10-Gb/s systems [184]. XPolM creates sudden changes of the states of polarisation (SOP) which are possibly faster than the speed of the (digital) polarisation tracking done in coherent polarisation-sensitive receivers [42] and is weakly dependent on the channel spacing [185]. These changes in SOP may translate into amplitude and phase fluctuations deteriorating the performance of polarisation sensitive receivers [186] whereas they would not affect the performance of a polarisation insensitive receiver. However, interactions between nonlinearities and PMD may occur along the transmission changing the picture as discussed in section 4.2.3. Anyhow, the results obtained here indicate that a band-gap wider than 300 GHz between 10 Gb/s and 40 Gb/s channels could be mandatory, which would seriously limit the capacity of hybrid systems.

A third option to contain nonlinearities (not studied in this thesis) would be using the powerful DSP capacity of coherent receivers to apply specific algorithms in order to compensate or mitigate nonlinear propagation effects. DSP-based nonlinear mitigation using inverse backward-propagation, split-step Fourier algorithm, has been proposed to improve the transmission performance [166]. This technique has shown remarkable improvements of the maximum reachable distance in single channel transmission [167]. Nonetheless, when transmission is governed by cross nonlinearities, the benefits of this technique almost vanish [168].

To get further insight on cross nonlinear mechanisms, I study two more possibilities, namely reducing the launch power and removing in-line DCF. Fig. 4.5-a represents performance evolution of the same test-channel while increasing progressively the guard-band around the coherent channel when the launch power per channel is decreased by 3 dB for the hybrid 10/40 Gb/s transmission scheme, i.e. the power per channel is -4 dBm. Cross nonlinearities are weaker as the power of co-propagating channels decreases. Thereby, they induce fewer penalties at -4 dBm than at -1 dBm, as can be observed in Fig. 4.5-a. Nevertheless, even with a 3-dB decrease of channel power, the consequences of XPM are detrimental until the guard-band reaches 250 GHz. In order to reduce the impact of cross nonlinearities, one can think of suppressing DCFs within the line to increase decorrelation between symbols of different from one span to another. I carried out then the same experiment but after removing DCF in-between EDFA of the recirculating loop and setting the power per channel at -1 dBm. The results of this experiment are plotted in Fig. 4.5-b. As it can be observed, nonlinearities induced by co-propagating (10 Gb/s NRZ) channels are now less penalising thanks to a higher residual dispersion per span.

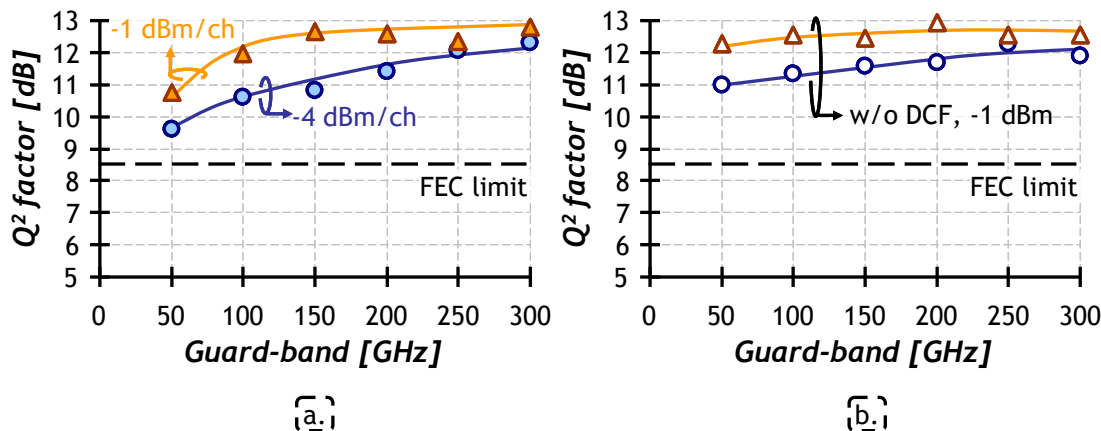


Fig. 4.5: Performance evolution as a function of the guard-band around the 40-Gb/s PDM-QPSK channel after 1,600 km of SSMF. (a) With and (b) without dispersion-management. The test channel is surrounded either by ▲ other 40-Gb/s PDM-QPSK channels or by ● 10-Gb/s NRZ channels.

It would be tempting to constrain distortions from nonlinear effects either by operating at low power per channel (<-4 dBm) or by suppressing DCFs within the line. However, implementing these options in legacy networks implies strong drawbacks and turns out to be unpractical and sometimes even unrealistic. Reducing the operating power would result in a reduction of the maximum achievable transmission distance of the 10 Gb/s channels, as the ONSR at the end of the link

would decrease. As a reference, the typical power per channel used in 10-Gb/s NRZ systems is within the range [-1 dBm; +1 dBm] when reaching ultra-long haul (ULH) distances. Operating at -4 dBm would therefore imply reducing the achievable distance by a factor of two at least. On the other hand, massively deployed 10-Gb/s NRZ channels require chromatic dispersion to be optically-compensated in order to be correctly detected, as discussed in Chapter 2. Therefore, they could not operate over DCF-free systems. Two options could be eventually contemplated, namely optical and electronical dispersion compensation. The two options would imply an extremely complex, and too expensive, receiver for 10-Gb/s operation.

In conclusion, cross nonlinearities, especially brought by co-propagating 10-Gb/s NRZ channels, strongly limit the performance of coherent 40 Gb/s PDM-QPSK. Moreover, optimizing CPE and introducing guard-bands around the test channel is not sufficient to compensate for induced penalties in realistic hybrid 10/40-Gb/s systems. Thereby, 40 Gb/s PDM-QPSK does not seem to be a suitable option for the upgrade of long-haul 10-Gb/s legacy networks.

## 4.2. 40 Gb/s PDM-BPSK

The preceding results have shown that 40 Gb/s PDM-QPSK does not appear appropriate for the upgrade of legacy networks as it suffers dramatically from cross nonlinear effects stemming from 10-Gb/s channels. Hence another solution with similar tolerance to linear effects but with enhanced nonlinear resilience would be desirable. Compared to QPSK format, BPSK is more robust against nonlinearities when detected in a differential receiver [91]. Therefore, we investigate the potential of an alternative solution based on BPSK modulation. This section treats the nonlinear tolerance of BPSK signals combined together with polarisation multiplexing and coherent detection in the context of upgrading 10-Gb/s legacy systems.

40 Gb/s PDM-BPSK signals have a symbol rate of 20 Gbaud and a spectrum width of 40 GHz, i.e. twice those of 40 Gb/s PDM-QPSK. Thereby, 40 Gb/s PDM-BPSK also fits into the standard 50-GHz grid currently used for 10-Gb/s systems, allowing the increase of information spectral density from 0.2 bit/s/Hz to 0.8 bit/s/Hz. On the other hand, however, the higher symbol rate compared to PDM-QPSK makes PDM-BPSK more constraining in terms of bandwidth and speed electronic requirements. Thus the required bandwidth of opto-electronic devices is around 20 GHz whereas ADC should operate at 40 GSamples/s to obtain two samples per symbol.

### 4.2.1 Experimental set up and noise sensitivity

I focus here on two different configurations, namely, homogenous and hybrid WDM transmission, corresponding to Fig. 4.1-b and c. However, coherent channels are modulated here with 40 Gb/s PDM-BPSK. Therefore, the light from a CW laser is BPSK modulated by a MZM modulator fed with a  $2^{15}-1$ -long PRBS at 21.4 Gb/s. Polarisation multiplexing is emulated by splitting the signal along two different paths, delaying one of the two with a polarisation maintaining delay line (PM-DL), and recombining the two paths by means of a polarisation beam combiner (PBC), as depicted in Fig. 4.6-a.

For a given bit rate, PDM-BPSK and PDM-QPSK have theoretically the same sensitivity to optical noise, as discussed in sections 2.1.3 and 2.2. However, in laboratory implementation, 40 Gb/s PDM-BPSK turns out to be slightly better than 40 Gb/s PDM-QPSK (1 dB) in terms of noise sensitivity, as illustrated in Fig. 4.6-b. This is mainly attributed to a better realization of the BPSK transmitter.

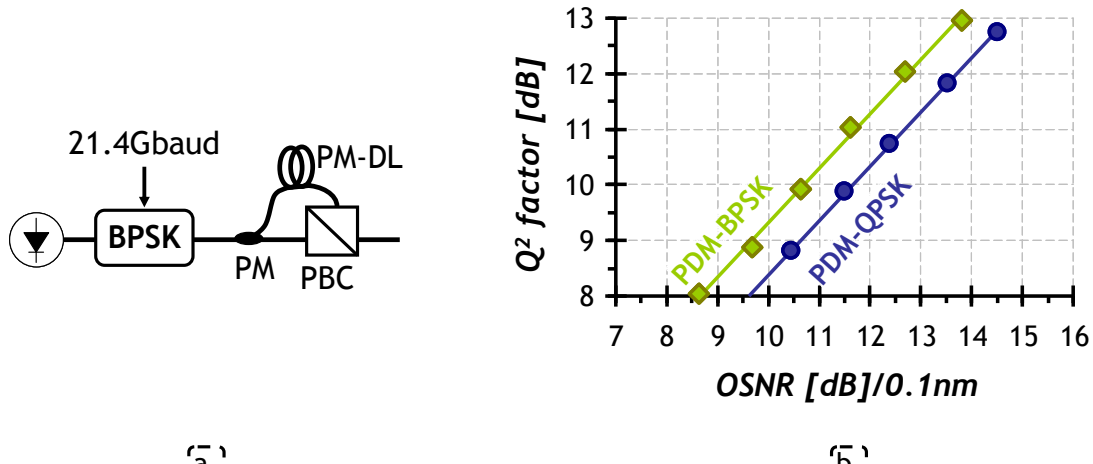


Fig. 4.6: (a) Transmitter scheme and (b) noise sensitivity of ◆ 40 Gb/s PDM-BPSK compared to ● 40 Gb/s PDM-QPSK.

I consider here two different scenarios for 40 Gb/s PDM-BPSK corresponding to two different transmission fibres, namely SSMF and NZDF. Thus, the recirculating loop here incorporates four 100-km-long spans of either SSMF or NZDSF which are separated by dual-stage EDFA including an adapted spool of DCF for partial dispersion compensation, according to a typical terrestrial transmission map. The DCF spools are different for SSMF and for NZDSF. At the receiver side, the channel under study is selected by a 0.4-nm bandwidth tuneable filter and sent into the coherent receiver. The characteristics of SSMF and NZDSF are discussed in section 1.1.2 and summarised in Fig. 2.25. Compared to SSMF, the use of NZDSF can emphasise nonlinear effects due to its low chromatic dispersion. Moreover, NZDSF has strong wavelength-dependent chromatic dispersion which results in different dispersion maps for the different wavelength channels of the multiplex. It is well known that NZDSF systems behave worse for wavelengths close to  $\lambda_0$  (found in our set up at short wavelengths) due to the strength of cross nonlinearities induced by the low residual dispersion per span. This translates usually into a dramatic reduction of the reach of channels at wavelengths around  $\lambda_0$ . In a laboratory environment, besides, NZDSF can be exploited to study different dispersion maps.

### 4.2.2 Impact of cross nonlinearities

Like 40 Gb/s PDM-QPSK, performance and maximum transmission reach of PDM-BPSK is limited by optical noise and nonlinearities, mainly stemming from co-propagating channels. I first investigate the tolerance to nonlinearities of 40 Gb/s PDM-BPSK in a homogeneous WDM configuration, with all channels modulated with 40Gb/s PDM-BPSK (Fig. 4.1-b, but with PDM-BPSK instead of PDM-QPSK), after 3,200 and 4,000 km of SSMF. Fig. 4.7 illustrates the results of these experiments

in which the launch power of the test channel is set at the same level as all the co-propagating channels.

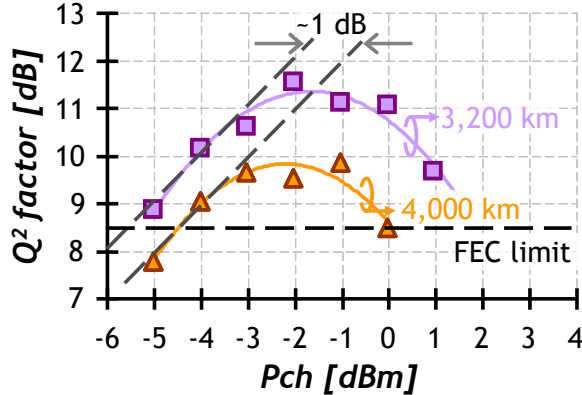


Fig. 4.7: Nonlinear tolerance of 40 Gb/s PDM-BPSK in a homogeneous WDM configuration after □ 3,200 km and after ▲ 4,000 km of SSMF.

The OSNR decreases when moving from 3,200 to 4,000 km according to the ratio between the number of the optical amplifiers (for constant launch power per channel), i.e.  $10 \log_{10}(40/32) \approx 0.97 \text{ dB}$ , as discussed in section 2.4.3. The consequence of this decrease in OSNR is clearly observed in Fig. 4.7 at low channel power (<-3 dBm) for which transmission is mainly limited by optical noise. As it can be seen, performance after 4,000 km is 1 dB lower than after 3,200 km for launch powers lower than -3 dBm. On the other hand, the optimum Q<sup>2</sup> factor obtained after 3,200 km is around 11.3 dB. Linear considerations would consequently predict a drop of the optimum Q<sup>2</sup> factor by 1 dB, according to the decrease of OSNR when moving from 3,200 to 4,000 km. However, on top of optical noise, nonlinearities are also accumulated along the line and they further constrain the performance and the optimum Q<sup>2</sup> factor is found to be around 10 dB after 4,000 km.

Compared to 40 Gb/s PDM-QPSK (Fig. 4.3-a), 40 Gb/s PDM-BPSK is able to reach twice the distance with similar optimum Q<sup>2</sup> factor. Despite its better noise tolerance (due to practical implementation), this better performance comes mainly from a better tolerance to nonlinearities. By having twice the phase distance between symbols than PDM-QPSK, PDM-BPSK tolerates more nonlinear-induced phase distortions. Besides, cross nonlinearities become less penalising with the increasing baud rate, as introduced in section 1.2 and demonstrated (for PDM-QPSK) in section 5.1.

We now focus on legacy systems upgrades and, more precisely, on nonlinearities caused by 10-Gb/s NRZ co-propagating channels (Fig. 4.1-c). I investigate here the nonlinear limitations induced by 10-Gb/s NRZ channels depending on their relative power w.r.t. the 40 Gb/s PDM-BPSK channel. Thus, we compare the performance of one 40-Gb/s PDM-BPSK channel for different powers of surrounding 10-Gb/s NRZ channels after 3,200 km of SSMF. Fig. 4.8 reports the results of these experiments in terms of Q<sup>2</sup>-factor penalty w.r.t. the performance obtained in back-to-back configuration at the same OSNR versus the relative power between the coherent and the NRZ-surrounding channels,  $\Delta P_{\text{ch}}$ . It must be stressed here that the OSNR at the end of the link increases with  $\Delta P_{\text{ch}}$ . Thus, if the Q<sup>2</sup>-factor penalty corresponding to a 1-dB increase in  $\Delta P_{\text{ch}}$  is lower by 1 dB, nonlinear-induced

penalties are weaker than the improvement brought by the OSNR increase and performance consequently improves.

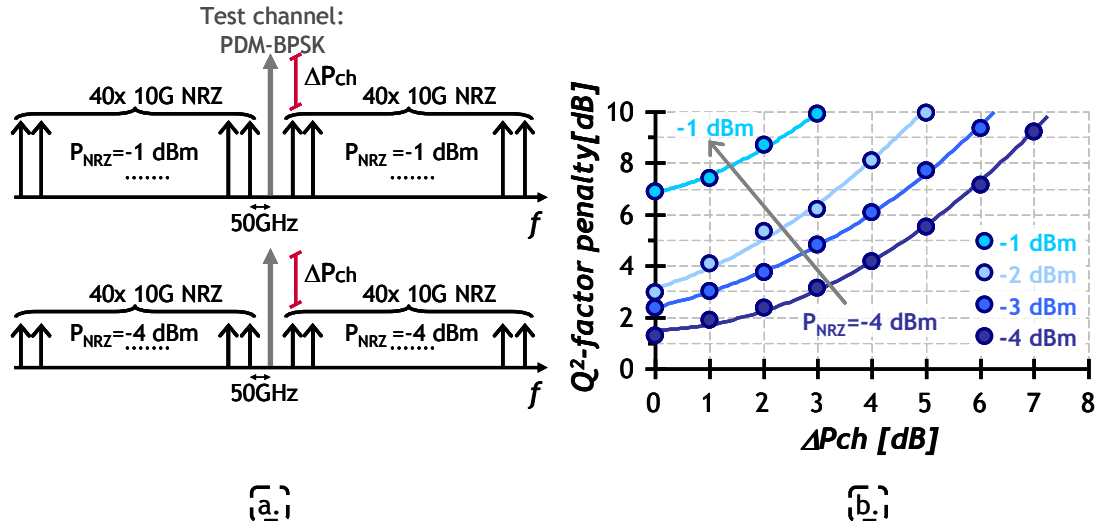


Fig. 4.8: Nonlinear tolerance of 40 Gb/s PDM-BPSK in a hybrid WDM configuration after 3,200 km of SSMF. (a) Experimental channel configuration and (b) impact of 10-Gb/s co-propagating channels.

As a reference, the  $Q^2$ -factor found in a homogeneous WDM transmission (Fig. 4.7, with  $\Delta P_{ch}=0 \text{ dB}$ ) is 0 dB, 0 dB, 0.8 dB and 2 dB for -4 dBm, -3 dBm, -2 dBm and -1 dBm, respectively. Not surprisingly, NRZ co-propagating channels are more penalising than PDM-BPSK channels. Moreover, the magnitude of performance degradation caused by NRZ channels strongly depends on their power, as clearly seen in Fig. 4.8. For low launch power of NRZ channels (-4 dBm), increasing the power of the coherent channel until  $\Delta P_{ch}=3 \text{ dB}$  allows partially recovering the penalties induced by 10-Gb/s NRZ channels, as the nonlinear-induced penalty is lower than the OSNR increase. However, in a more realistic configuration where NRZ channels operate at -1 dBm, around 7 dB of penalty are found when all channels are set to the same power. Here, increasing the power of the coherent channel does not bring significant benefits.

Therefore, depending on the power of 10-Gb/s NRZ co-propagating channels, coherent PDM channels suffer severe nonlinear penalties that are not recovered by increasing the received OSNR. Nevertheless, comparing PDM-QPSK and PDM-BPSK highlights the better tolerance to nonlinearities exhibited by PDM-BPSK. The  $Q^2$ -factor found with 40 Gb/s PDM-QPSK in a hybrid transmission after 1,600 km (Fig. 4.3-b) is already  $\sim 3.5 \text{ dB}$  for -4 dBm and more than 6 dB for -3 dBm, with  $\Delta P_{ch}=0 \text{ dB}$  in both cases. Thus, the penalty suffered by PDM-QPSK is three times larger than that of PDM-BPSK which highlights the better tolerance of PDM-BPSK against nonlinearities. In fact, doubling the system reach with respect to PDM-QPSK, even in presence of 10-Gb/s NRZ channels, is clearly the most undeniable comparative advantage of PDM-BPSK.

### 4.2.3 Further insight on inter-channel nonlinearities: interplay between nonlinearities and PMD

As preceding results demonstrate, the performance of polarisation-multiplexed signals detected with digital coherent receivers is mainly limited by cross nonlinearities. XPolM in particular creates sudden polarisation changes while (digital) polarisation tracking done in coherent polarisation-sensitive receivers is only able to follow slower polarisation evolution. Thus, nonlinear-induced polarisation changes may translate into crosstalk between polarisation tributaries at the receiver side.

One option to reduce this crosstalk could be to use RZ-shaped polarisation tributaries interleaved by half a symbol period, obtaining thus time-orthogonality between polarisation tributaries, as shown in Fig. 4.9. Thereby, the amplitude of the interfering tributary “X” will be weak when the tributary “Y” is sampled at its maximum amplitude. And vice versa for the next sampling instant,  $T_{k+1}$ . Later on, iRZ-PDM-BPSK stands for orthogonal RZ-BPSK polarisation tributaries interleaved by half a symbol period while NRZ-PDM-BPSK refers to the case when orthogonal NRZ-QPSK polarisation tributaries are pulse-to-pulse aligned. Unlike with direct detection schemes, RZ pulse carving does not bring any improvement in noise sensitivity for PDM signals detected with a coherent receiver as digital equalisation already compensates for non-perfectly matched receiver filtering, as demonstrated in Fig. 5.3. However, we do not focus here on the noise sensitivity of 40 Gb/s iRZ-PDM-BPSK but we aim to study its behaviour with respect to nonlinear effects.

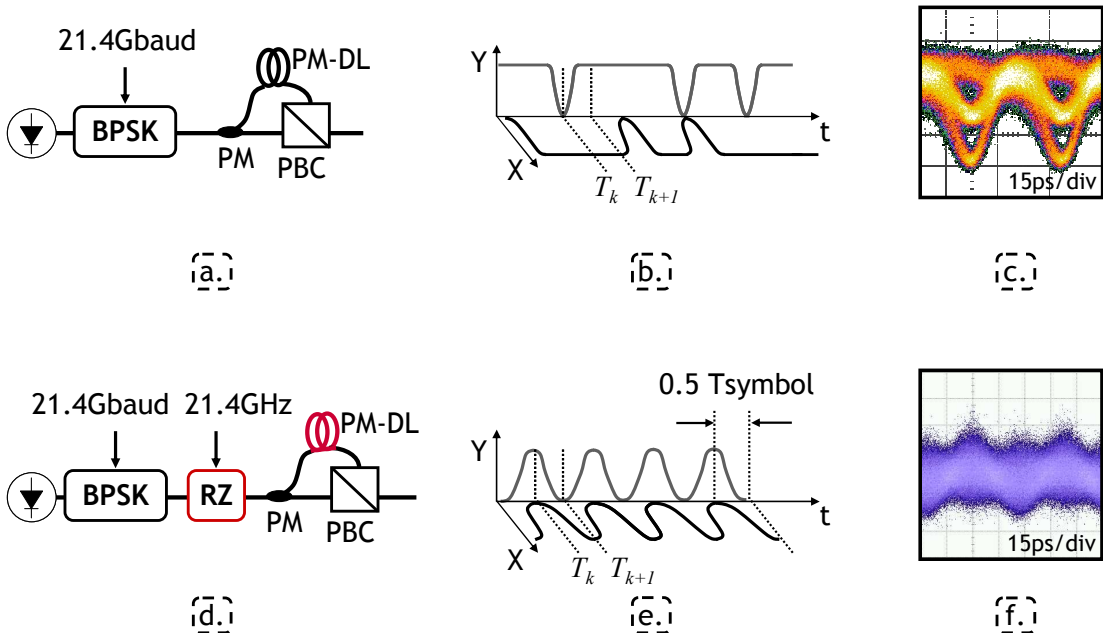


Fig. 4.9: (a, d) Transmitter schemes, (b, e) typical shape of the signal in the time domain and (c, f) experimental eye diagram for NRZ-PDM-BPSK (upper figures) and iRZ-PDM-BPSK (lower figures).

To generate iRZ-PDM-BPSK, BPSK modulators operate at 21.4 Gbaud and are followed by a 50% RZ pulse shaper operating at 21.4 GHz, as depicted in Fig. 4.9-d. Polarisation multiplexing is then performed by dividing, decorrelating and recombining the RZ-BPSK data through a polarisation beam combiner (PBC). Here,

by adjusting a polarisation-maintaining delay line (PM-DL) with appropriate length before the PBC, the two orthogonal polarisation tributaries are interleaved by half a symbol. The corresponding schematic forms of this signal in the time domain and eye diagrams are shown in Fig. 4.9-e and f. When polarisation tributaries are interleaved by half a symbol, a nearly constant channel power with very low peak-to-average power ratio is measured, as shown in Fig. 4.9-f.

### a) Nonlinear tolerance of 40 Gb/s iRZ-PDM-BPSK

I study tolerance to nonlinear effects of 40 Gb/s iRZ-PDM-BPSK by comparing its behaviour with that of NRZ-PDM-BPSK after 4,000 km of SSMF (as in Fig. 4.7). The performance is measured after a homogeneous WDM transmission, i.e. with neighbour channels of the same format according to Fig. 4.1-b (but with [N/i]RZ-PDM-BPSK instead of PDM-QPSK) and the launch power of the test channel is set to the same level as all the co-propagating channels. Fig. 4.10 shows the results of this experiment in terms of  $Q^2$  factor of the test channel versus launch power per channel. Performance is limited by optical noise for low values of launch power (-5 dBm) and both solutions give the same performance as they have the same sensitivity to optical noise. Beyond a certain value of power, however, cross nonlinearities take precedence and performance is degraded as the power increases.

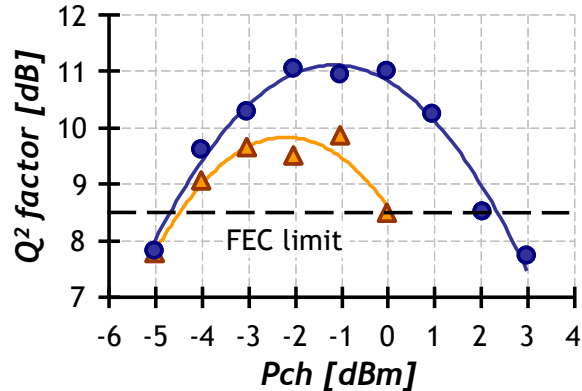


Fig. 4.10: Nonlinear tolerance of ▲ NRZ-and ● iRZ-PDM-BPSK at 40 Gb/s in a homogeneous WDM configuration, i.e. surrounded by channels of the same type. The measurements have been obtained after a 4,000 km of SSMF.

iRZ-PDM-BPSK appears to be more tolerant against nonlinear effects as nonlinearities become penalising for higher launch powers, according to Fig. 4.10. The power corresponding to the optimum performance and the optimum performance itself of iRZ-PDM-BPSK are 1-dB higher compared to NRZ-PDM-BPSK. This noticeable improvement of the tolerance to nonlinearities is not only attributed to the time-orthogonality of polarisation tributaries but also to the RZ pulse-shaping itself, and the smaller depolarisation induced by co-propagating channels. In fact, RZ-interleaving is especially effective when applied to all the channels of the multiplex, as I have demonstrated in [187] for 100 Gb/s PDM-QPSK.

These results prove that combining RZ pulse-shaping with time-polarisation interleaving improves the *average* performance of the system. Now, to get further insight on how nonlinearities impact the performance and on the improvement brought by iRZ, I measure the system performance stability. The channel power is

set at the power corresponding to the optimum performance of iRZ, i.e. -1 dBm, and 2000 random draws of polarisation conditions are measured. In that respect, a polarisation scrambler is inserted at the end of the link. It scrambles at 4 kHz, in the range of the loop repetition frequency ( $\sim 0.5$  kHz); ensuring independent polarisation conditions at each round-trip. It has to be stressed here that the intrinsic PMD accumulated along the link is very small ( $<1$  ps).

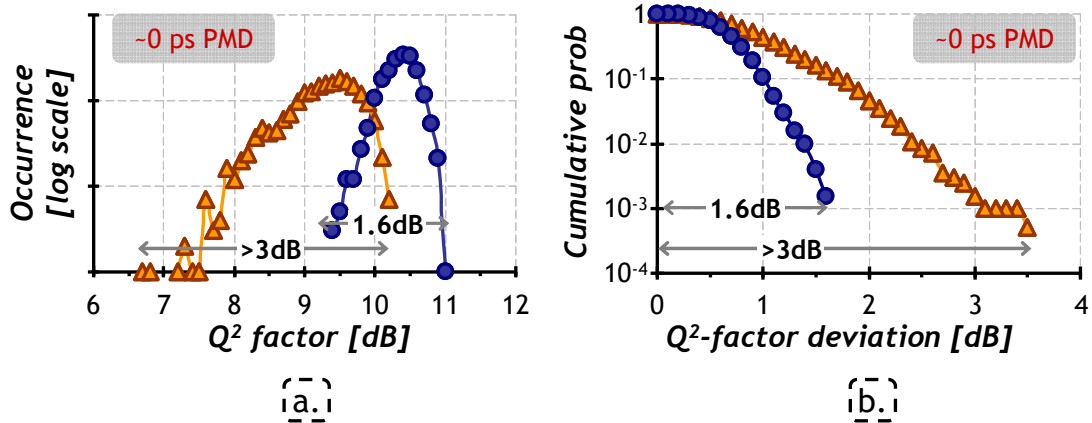


Fig. 4.11: (a)  $Q^2$ -factor distribution and (b) cumulative probability deviation with 0 ps PMD of  $\blacktriangle$  NRZ- and  $\bullet$  iRZ-PDM-BPSK at 40 Gb/s after 4,000 km of SSMF in a homogeneous WDM transmission. The power of all channels is -1 dBm.

Fig. 4.11 depicts the results of these experiments in terms of  $Q^2$ -factor probability density function (a) and cumulative probability deviation from the best performance (b). As it can be observed, NRZ-PDM-BPSK presents a relatively broad  $Q^2$ -factor distribution (Fig. 4.11-a). This translates into a probability of  $10^{-3}$  of having deviation from the best performance greater than 3 dB (Fig. 4.11-b). As previously stated, the PMD along the line is very small ( $<1$  ps) and it does not explain this wide distribution. Indeed, the large  $Q^2$ -factor distribution observed with NRZ-PDM-BPSK can be attributed to inter-channel nonlinearities discussed throughout this chapter. iRZ-PDM-BPSK in turn appears to be less impacted by cross nonlinearities and it improves system performance not only in terms of average  $Q^2$ -factor but also in terms of  $Q^2$ -factor distribution width.

### b) Impact of distributed PMD

One may think that the improvements brought by iRZ will be reduced in the presence of PMD, due to the random differential group delay (DGD) added to the signal. Since the PMD is a linear distortion, FIR filters are supposed to efficiently mitigate it, as demonstrated in section 3.3. Nevertheless, this extra initial DGD could break the time-orthogonality between polarisation tributaries causing a reduction of the improvements brought iRZ. I investigate the impact of distributed PMD onto both NRZ- and iRZ-PDM-BPSK under the same conditions, with the power set at -1 dBm. A 7-ps PMF is inserted at the end of the loop (after the low-speed polarisation scrambler) well in excess of the small PMD accumulated into the transmission fibre spools ( $<1$  ps), as illustrates Fig. 4.12. Therefore, after ten round-trips, the loop behaves very similarly to a ten-section all-order PMD emulator with a PMD equal to  $\sqrt{10}$  times the DGD of the PMF, i.e 22 ps.

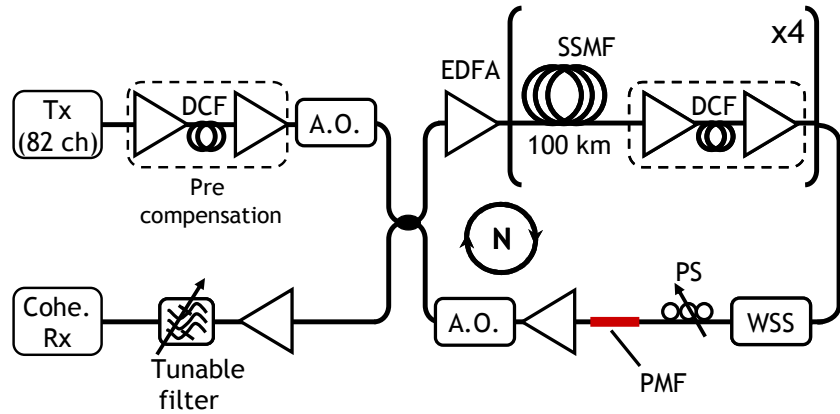


Fig. 4.12: Experimental set up to emulate distributed PMD. The DGD of the PMF is 7 ps.

Like Fig. 4.12, Fig. 4.13 reports the results of these experiments, with 22 ps PMD, in terms of  $Q^2$ -factor probability density function (a) and cumulative probability deviation from the best performance (b). Comparing Fig. 4.12 and Fig. 4.13, we first observe that distributed PMD has induced no noticeable penalty onto the performance iRZ-PDM-BPSK, neither in terms of average nor in terms of cumulative probability deviation from the best performance.

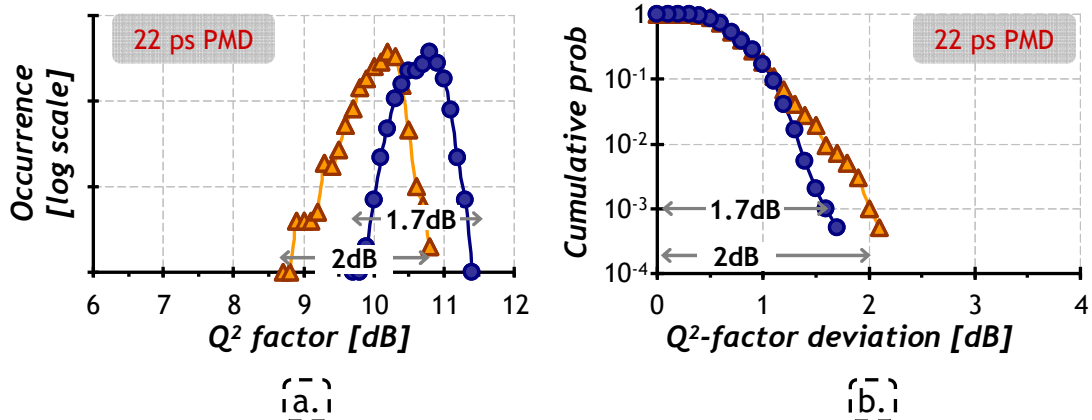


Fig. 4.13: (a)  $Q^2$ -factor distribution and (b) cumulative probability deviation with 22 ps PMD of  $\blacktriangle$  NRZ-and  $\bullet$  iRZ-PDM-BPSK at 40 Gb/s after 4,000 km of SSMF in a homogeneous WDM transmission. The power of all channels is -1 dBm.

On top of these considerations, the effect of distributed PMD turns out to be beneficial for NRZ-PDM-QPSK. The  $Q^2$ -factor distribution of NRZ-PDM-BPSK improves both in terms of average  $Q^2$ -factor (Fig. 4.13-a) and in terms of width or cumulative probability (Fig. 4.13-b). Hence, NRZ-PDM-BPSK behaves similar to iRZ-PDM-BPSK. Compared to the results obtained with 0 ps PMD, the average  $Q^2$ -factor of NRZ-PDM-BPSK improves by about 0.7 dB whereas the deviation from the optimum performance reduces by more than 1 dB. This improvement is attributed to the decorrelation between polarisation tributaries and depolarisation induced by PMD which reduces both the intra-channel interactions between polarisation tributaries and inter-channel XPolM. These results have been recently confirmed through numerical simulations [188]. As it can be noticed, this improvement is smaller for iRZ-PDM-BPSK. This is due to fact that iRZ-PDM-BPSK suffers less from nonlinearities as both polarisation tributaries are

already orthogonal in time and iRZ-PDM-BPSK co-propagating channels induce weaker cross nonlinearities.

In conclusion, the impact of distributed PMD may turn out to be beneficial, reducing thus nonlinear-induced penalties, provided linear PMD is compensated for at the receiver side. Coherent receivers can relatively easily perform this PMD compensation thanks to digital signal processing, as PMD is a linear distortion. Besides, the benefits on the nonlinear tolerance brought by the interplay between nonlinearities and PMD are greater as the signal is more penalised by nonlinearities.

#### 4.2.4 Impact of dispersion map

As introduced in section 2.5, NZDSF systems present a wavelength-dependent dispersion map. The dispersion map is nearly flat, in our test bed, for short wavelengths (close to  $\lambda_0$ ) whereas it increases for longer wavelengths. Consequently, NZDSF systems usually behave worse for short wavelengths than for longer ones as the strength of cross nonlinear effects depends on the residual dispersion per span (RDPS). NZDSF have generally a lower chromatic dispersion compared to SSMF which can enhance the impact of cross nonlinearities. In that context, the recirculating loop incorporates four 100-km-long spans of NZDSF which are separated by dual-stage EDFA including an adapted spool of DCF for partial dispersion compensation. Different types of NZDSF exist as discussed in section 1.1.2. Here, I employ a NZDSF with a chromatic dispersion at 1550 nm of 4.25 ps/(nm·km) and chromatic dispersion slope of 0.08 ps/(nm<sup>2</sup>·km). The transmitter is configured according to a homogeneous configuration (Fig. 4.1-c). Three different channels were measured namely 1535.43, 1546.52 and 1555.34 nm, corresponding to three different dispersion maps with an average residual dispersion per span (RDPS) of -2, 35 and 55 ps/nm per span. The results after 3,200 km are depicted in Fig. 4.14.

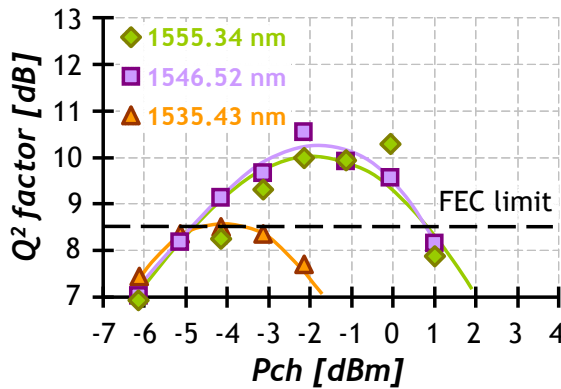


Fig. 4.14: Wavelength dependence of the nonlinear tolerance of 40 Gb/s PDM-BPSK in a homogeneous configuration after 3,200 km of NZDSF. Three different channels were measured at ▲ 1535.43, ■ 1546.52 and ♦ 1555.34 nm, corresponding to three different dispersion maps with an average RDPS of -2, 35 and 55 ps/nm per span, respectively.

The channel at short wavelengths performs worse than the other two due to the higher impact of cross nonlinearities caused by the lower RDPS-induced decorrelation between symbols of different channels from one span to another, as it can be clearly observed. This channel shows an optimum Q<sup>2</sup> factor of around 8.5 dB,

just beyond the FEC limit. The maximum  $Q^2$  factor of the other two channels is 1.5 dB better reaching almost similar performance as over SSMF, as the residual dispersion per span is comparable. In fact, once sufficiently high walk-off is achieved, increasing the residual dispersion per span from 40 to 55 ps/nm neither brings an improvement nor a degradation, as any residual chromatic dispersion at the end of the link is compensated electronically.

These results indicate that an increasing dispersion map is more suitable than a flat one for PDM coherent transmission as it helps reduce the efficiency of cross nonlinearities. This is in compliance with results obtained for OOK formats [140], highlighting thus the compatibility of coherent-based solutions with already deployed networks.

### **4.3. Comparison and summary**

Polarisation multiplexing allows increasing the information spectral density while reducing the requirements on bandwidth and speed of electronics and analog-to-digital converters. Nevertheless, polarisation-multiplexed signals appear to be more sensitive to nonlinear impairments than singly-polarised ones. First of all, the two modulated polarisation tributaries may interact nonlinearly along the transmission limiting the performance in single channel propagation. In a WDM context, coherent polarisation-multiplexed signals may in turn suffer more from inter-channel nonlinearities coming from co-propagating channels located very far in the spectrum caused mainly by cross polarisation modulation (XPolM), contrary to current 10-Gb/s OOK systems. These nonlinearities create sudden changes of the state of polarisation which can be faster than the (digital) polarisation tracking done in coherent polarisation-sensitive receivers. Thus, these changes in the state of polarisation may translate into amplitude and phase fluctuations deteriorating the performance of polarisation sensitive receivers. The impact of these nonlinearities may be reduced by the effect of PMD distributed along the transmission line, provided linear PMD is compensated for at the receiver side. Coherent receivers can relatively easily perform this PMD compensation thanks to digital signal processing, as PMD is a linear distortion

As stated in the preceding sections, 40 Gb/s PDM-BPSK reaches much longer distances than 40 Gb/s PDM-QPSK. I aim here to compare the tolerance to nonlinearities of PDM-QPSK and PDM-BPSK at 40 Gb/s under the same conditions. The test bed relies on NZDSF and both formats are compared in a hybrid configuration where the coherent channel is surrounded by 10 Gb/s NRZ channels (Fig. 4.1-c). The coherent channel is set in the middle of the C band and its power is the same power as the surrounding channels. To obtain a  $Q^2$  factor in the range of 11 dB, the reach of PDM-QPSK is limited to 800 km whereas PDM-BPSK reaches three times this distance, i.e. 2,400 km, in such scenario.

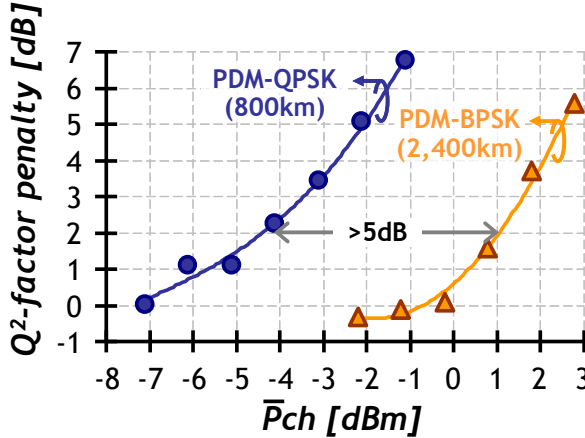


Fig. 4.15: Nonlinear tolerance comparison in a hybrid WDM configuration over NZDSF, in the middle of C-band (1546.52 nm). ● PDM-BPSK and ▲ PDM-QPSK at 40 Gb/s. Power is normalised considering the different transmission distances: 800 km for PDM-QPSK and 2,400 km for PDM-BPSK.

To perform a fair comparison between PDM-BPSK and PDM-QPSK at different transmission distances, I define a relative normalized power w.r.t the reach of PDM-QPSK as:  $\bar{P}_{ch} = P_{ch} + 10 \log_{10}(dist / 800)$ , where  $dist$  is the distance in [km]. Fig. 4.15 represents the results in terms of  $Q^2$ -factor penalty w.r.t. the performance obtained in back-to-back configuration at the same OSNR as a function of the normalised power per channel,  $P_{ch}\bar{P}_{ch}$ . Fig. 4.15 shows that PDM-BPSK is clearly more robust than PDM-QPSK against inter-channel nonlinear effects brought by neighbouring NRZ channels since they become penalising for higher powers. The power corresponding to a 2-dB penalty is around -4.5 dBm for PDM-QPSK whereas for PDM-BPSK, this power is 1 dBm, i.e. more than 5 dB higher. This >5-dB higher nonlinear tolerance combined with the better noise sensitivity explains why PDM-BPSK is able to reach 2,400 km, i.e three times the distance reached by PDM-QPSK. These results highlight the higher tolerance of PDM-BPSK against cross nonlinearities thus confirming the results obtained over SSMF.

	40 Gb/s PDM-QPSK	40 Gb/s PDM-BPSK
Opt./Elec. - Bw	✓ ✓	✓
ADC sampling	✓ ✓	✓
Noise sensitivty	✓ ✓	✓ ✓
NL tolerance	✗	✓ ✓
Potential reach	✗	✓ ✓

Fig. 4.16: Qualitative comparison between PDM-BPSK and PDM-QPSK at 40 Gb/s.

Making a general comparison, it cannot be said that a single modulation format outperforms all others in all aspects. As so, one cannot state that PDM-BPSK is better than PDM-QPSK (or vice versa) for 40 Gb/s operation in absolute terms. The two solutions benefit from the high sensitivity associated to (homodyne) coherent detection and the possibility of compensating for linear impairments thanks

to dedicated DSP. Moreover, both of them allow increasing the information spectral density of today's 10-Gb/s networks from 0.2 to 0.8 b/s/Hz.

PDM-QPSK has two clear advantages compared to PDM-BPSK: the lower symbol rate and the narrower spectrum. The narrower spectrum makes PDM-QPSK inherently more tolerant to narrow optical filtering, which can be used to tightly pack 40 Gb/s PDM-QPSK in ultra-dense WDM configurations with a channel spacing smaller than 50 GHz. Such ultra-dense WDM configurations allows further increasing the spectral efficiency beyond 0.8 b/s/Hz but are, in general, more sensitive to inter-channel nonlinearities due to the small channel spacing. The lower symbol rate of PDM-QPSK in turn relaxes the constraints on the bandwidth and speed requirements of high-speed electronic devices and analog-to-digital converters. This results in an easier and more cost-effective practical implementation. However, PDM-QPSK is relatively vulnerable against nonlinear-induced phase distortions. PDM-BPSK is clearly more tolerant against nonlinearities, even coming from co-propagating channels. The use of PDM-BPSK increases significantly the system reach with respect to PDM-QPSK which is clearly its most undeniable comparative advantage. In conclusion, PDM-QPSK appears to be appropriate for cost-effective solutions reaching short distance, especially over uncompensated links. PDM-BPSK in turn is likely to be the most suitable solution for terrestrial systems covering long distances despite its higher requirements in bandwidth and sampling rate.

# ***Chapter 5. 100-Gb/s systems***

PDM-BPSK outperforms PDM-QPSK in terms of reach and nonlinear tolerance at 40 Gb/s. Nonetheless, PDM-BPSK at 100 Gb/s is not suitable for upgrading standard legacy systems, as it is very challenging to fit into the standard 50-GHz grid due to its broad spectrum ( $\sim$ 100-GHz). Moreover, PDM-BPSK presents stringent requirements on bandwidth and speed of electronic devices and analog-to-digital converters, due its high symbol rate of 50 Gbaud. By having a symbol rate of 28 Gbaud (relaxing thus the requirements on opto-electronics) and a spectrum width of 56 GHz, PDM-QPSK appears here as a better candidate for upgrading 50-GHz based systems. The combination of 100 Gb/s PDM-QPSK with a 50-GHz grid enables long-haul transmission with a 2.0-b/s/Hz information spectral density. Thereby, 100 Gb/s PDM-QPSK could be an appropriate answer to the predicted traffic growth of about 50% per year [1] which corresponds to a potential tenfold increase of traffic over six years.

In the preceding chapter, we have shown that PDM-QPSK at 40 Gb/s is dramatically impacted by inter-channel effects which make it unsuitable to upgrade today's networks. However, consider the general trend of OOK-modulated (direct-detected) channels behaviour against nonlinear effects discussed in Chapter 1. Inter-channel nonlinearities govern the transmission at low symbol rates as pulses of co-propagating channels are large and interact during a significant time inducing higher nonlinear phase-distortions. At higher symbol rates, in contrast, pulses are shorter and therefore pulses of co-propagating channels do not interact for long time, reducing thus the impact of inter-channel nonlinearities. For high symbol rates, intra-channel nonlinearities become dominant as signals are more impacted by chromatic dispersion and inter-pulse interactions are particularly important. Following this reasoning, we investigate PDM-QPSK as a potential candidate to upgrade today's networks at 100 Gb/s although it is not the most suitable at 40 Gb/s.

This chapter deals with the tolerance of PDM-QPSK against nonlinearities, now at 100 Gb/s. In Section 5.1, we give further insight on the evolution of the robustness against cross nonlinearities with the increase of symbol rate, from 10 to 25 Gbaud. Section 5.2 in turn focuses on the suitability of 100 Gb/s to upgrade legacy systems in the presence of 10 Gb/s NRZ co-propagating channels. We treat interactions between nonlinearities and PMD in section 5.3. Finally, we explore green field systems for ultra-long haul distances at 100 Gb/s per channel in section 5.4.

## **5.1. PDM-QPSK: why is it suitable for 100 Gb/s and not for 40 Gb/s?**

PDM-QPSK suffers from strong inter-channel nonlinear impairments at 40 Gb/s severely limiting its performance, as we have demonstrated in Chapter 4. This picture may however change when increasing the symbol rate, as discussed in Chapter 1 with OOK modulated channels.

Compared to 40 Gb/s, PDM-QPSK at 100 Gb/s have a symbol rate nearly 2.5 times higher, i.e 25 Gbaud instead of 10 Gbaud. In this section, I report on the evolution of the behaviour of PDM-QPSK against nonlinearities when moving progressively from 40 Gb/s to 80 Gb/s, and finally to 100 Gb/s under the same experimental conditions.

### **5.1.1 Experimental set up**

Like in Chapter 4, the test bed consists of eighty-two lasers spaced by 50 GHz and separated into two independently-modulated, spectrally-interleaved sets. The test channel is always modulated with PDM-QPSK at 40, 80 or 100 Gb/s. The surrounding lasers can be modulated either with the same format and the same bit-rate as the test channel, or kept continuous. PDM-QPSK data are obtained as in Fig. 4.1-a. However, here, QPSK modulators operate at 10.7 Gbaud, 21.4 Gbaud or 28 Gbaud in order to produce 43, 85.6 and 112 Gb/s PDM-QPSK data, incorporating protocol and FEC overhead.

The resulting multiplex is boosted and propagated through a recirculating loop in the configuration described in section 4.1.1. As in section 4.1.1, the launch power of the test channel is set at the same level as all the co-propagating channels and performance is measured after four round trips, corresponding to a transmission distance of 1,600 km. At the receiver side, a 0.4-nm bandwidth tuneable filter selects the channel under study and sends into the coherent receiver.

### **5.1.2 Nonlinear tolerance evolution with the symbol rate**

Fig. 5.1 reports the performance of the coherent PDM-QPSK test channel versus its power at each fibre input, at 40 (a), 80 (b) and 100 Gb/s (c). The measurements are performed when the neighbouring wavelengths carriers are kept continuous ( $\sim$  single-channel configuration, as in Fig. 4.1-a) or when they are all modulated like the test channel (Fig. 4.1-b). At relatively low power levels, the  $Q^2$  factor increases with power, along with the OSNR. When moving to high power levels, nonlinear effects become stronger and their induced penalties exceed the benefit of the OSNR increase.

The Q<sup>2</sup> factor thereby drops. I define the nonlinear threshold (NLT) as the channel power corresponding to the optimal Q<sup>2</sup> factor.

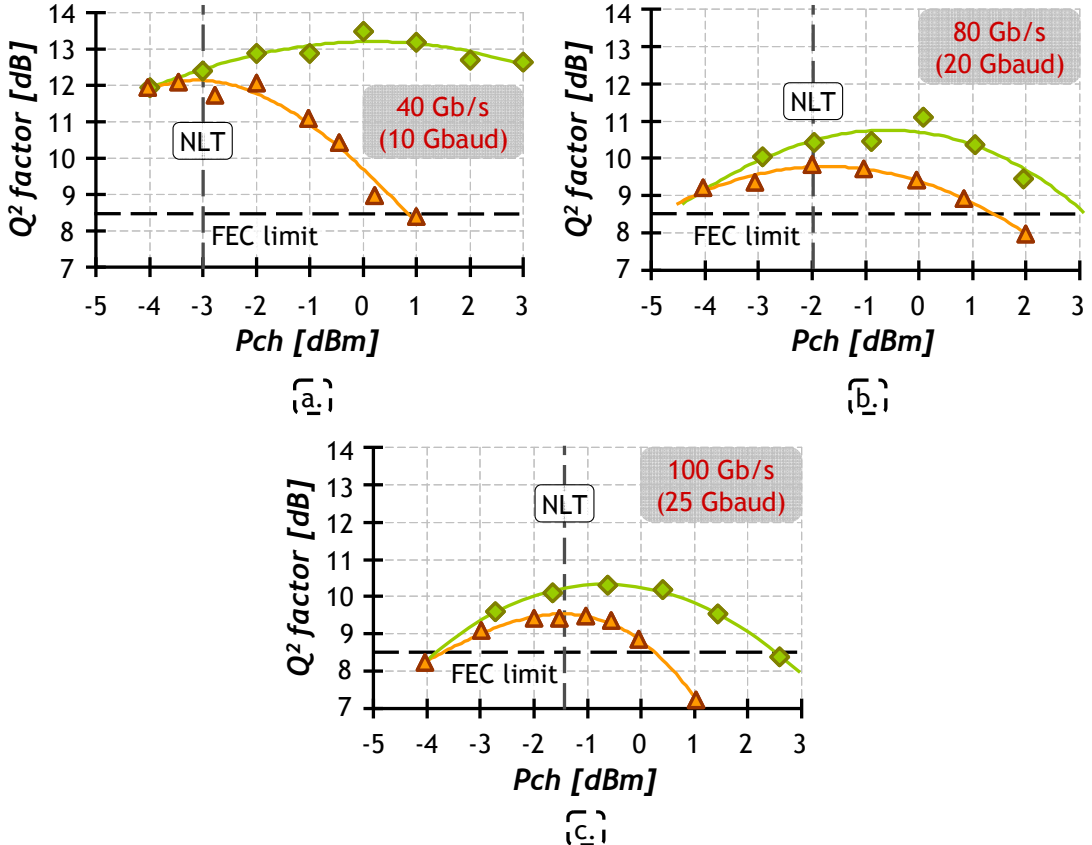


Fig. 5.1: Tolerance to nonlinearities of PDM-QPSK at (a) 40 Gb/s, (b) 80 Gb/s (c) and 100 Gb/s in ◆ single channel and ▲ WDM homogeneous configuration after 1,600 km of SSMF.

Linear considerations would predict a drop of the optimum Q<sup>2</sup> factor when moving from 40 Gb/s to 100 Gb/s according to the ratio between the bit rates, i.e.  $10 \log_{10}(100/40) \approx 4 \text{ dB}$ , due to the worse noise sensitivity, as observed at low channel power (-4 dBm) in Fig. 5.1. However, the impact of neighbour channels onto both the NLT and the optimum Q<sup>2</sup> factor decreases with the increasing symbol rate, reported in Fig. 5.1. The NLT obtained in a single channel configuration is almost unchanged when the bit rate grows from 40 Gb/s to 100 Gb/s. In contrast, NLT increases noticeably in the more realistic configuration of a full PDM-QPSK multiplex, from -3 dBm to -1.5 dBm. This improvement in NLT is mainly attributed to the higher symbol rate which implies a decrease of the walk-off length, discussed in section 1.2.3, thus reducing the strength of cross nonlinearities. As a consequence, the optimum Q<sup>2</sup> factor at the NLT is only reduced by 2.5 dB when moving from 40 Gb/s to 100 Gb/s in presence of WDM nonlinearities. In conclusion, inter-channel nonlinearities are found significantly more penalising at 40 Gb/s than at 80 Gb/s or 100 Gb/s. Thus, coherent PDM-QPSK technologies seem to be more interesting at 100 Gb/s than at 40 Gb/s.

## 5.2. Upgrading legacy systems

In the preceding section, I have demonstrated that the impact of inter-channel nonlinearities becomes weaker as the symbol rate increases in homogeneous WDM configurations, where all channels are PDM-QPSK modulated. However, 100-Gb/s PDM-QPSK channels are likely to propagate over hybrid WDM systems together with massively deployed 10-Gb/s NRZ channels when upgrading legacy systems as most carriers do not intend to build specific networks from scratch for increasing the total capacity of their networks. In this context, nonlinearities stemming from 10-Gb/s NRZ channels may govern the performance of coherent channels, as shown in section 4.1 for PDM-QPSK 40 Gb/s.

I aim here to investigate the suitability of PDM-QPSK at 100 Gb/s to upgrade legacy networks, especially when co-propagating with 10-Gb/s NRZ channels. I get further insight on the impact of cross nonlinearities stemming from neighbours NRZ channels and I also study the potential of two different options to reduce their impact, namely optimising the power of PDM-QPSK channels independently of the power of the 10-Gb/s channels and introducing guard-bands between both types of channels.

### 5.2.1 Experimental set up

Similar to Chapter 4, the test bed test-bed consists of eighty-two lasers spaced by 50 GHz and separated into two independently-modulated, spectrally-interleaved sets. The test channel, at 1546.12 nm, is always modulated with PDM-QPSK, at 40 or 100 Gb/s. On the contrary, surrounding channels can be either kept continuous, PDM-QPSK modulated, at 40 or 100 Gb/s, or NRZ modulated at 10 Gb/s corresponding to single-channel, homogenous WDM and hybrid WDM transmissions respectively.

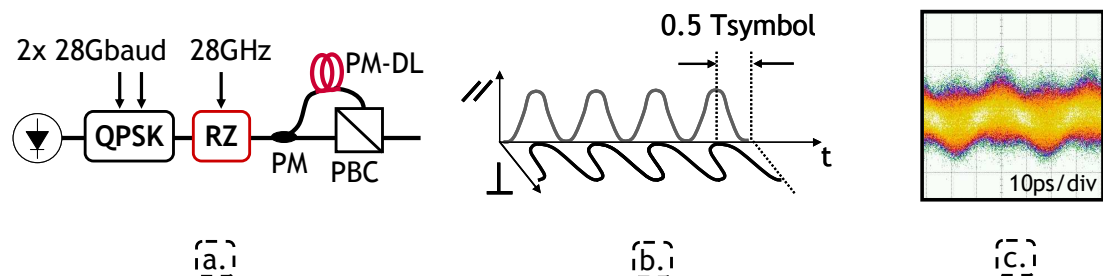


Fig. 5.2: 100 Gb/s iRZ-PDM-QPSK, (a) Transmitter scheme, (b) typical shape of the signal in the time domain and (c) experimental eye diagram.

QPSK modulators operate at 10.7 Gbaud or 28 Gbaud in order to produce 43 and 112 Gb/s PDM-QPSK data, incorporating protocol and FEC overhead. QPSK data are then passed through a 50% RZ pulse carver operating at 28 GHz (resp. 10.7 GHz) in order to produce 28 Gbaud (resp. 10.7 Gbaud) RZ-QPSK signals, as depicted in Fig. 5.2-a. Polarisation multiplexing is finally performed by dividing, decorrelating and recombining the RZ-QPSK data through a polarisation beam combiner (PBC). Here, by adjusting a polarisation-maintaining delay line (PM-DL)

with appropriate length before the PBC, the two orthogonal polarisation tributaries are interleaved by half a symbol yielding iRZ-PDM-QPSK data at 112 Gb/s (resp. 43 Gb/s). The corresponding schematic forms of the signals in the time domain and eye diagrams are shown in Fig. 5.2-b and c. In PDM-QPSK configuration, when polarisation tributaries are interleaved by half a symbol, a nearly almost constant channel power is measured, as shown in Fig. 5.2-c. The recirculating loop here incorporates four 100-km-long spans of NZ-DSF which are separated by dual-stage EDFA including an adapted spool of DCF for partial dispersion compensation, according to a typical terrestrial transmission map [140]. At the receiver side, the channel under study is selected by a 0.4-nm bandwidth tuneable filter and sent into the coherent receiver.

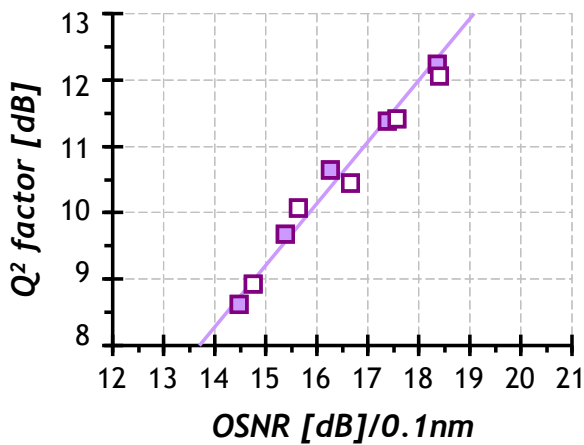


Fig. 5.3: Optical noise sensitivity of PDM-QPSK (empty symbols) and iRZ-PDM-QPSK (full symbols) at 100 Gb/s

As discussed in Chapter 2, the use of RZ pulse carving improves the noise sensitivity of direct detected schemes as the optical filter used is better matched to the RZ rather than to the NRZ spectrum. In contrast, RZ pulse carving does not bring any improvement in noise sensitivity for PDM-QPSK signals since digital equalisation done in coherent receivers already compensates for non-perfectly matched receiver filtering, as shown in Fig. 5.3. Nevertheless, interleaving RZ-QPSK polarisation tributaries increases the tolerance to nonlinearities compared to pulse-to-pulse aligned PDM-QPSK signals, as discussed in section 4.2, for 40 Gb/s PDM-BPSK, and demonstrated in [189] for 100 Gb/s PDM-QPSK. This is especially true when RZ-interleaving is applied to all the channels of the multiplex, as I have demonstrated in [187]. This improvement of the tolerance to nonlinearities is attributed to the RZ pulse-shaping, time-orthogonality of polarisation tributaries and lower depolarisation induced by co-propagating channels that reduce the impact of nonlinear impairments arising from Kerr effect. It must be pointed out that this benefit has not been observed when both polarisations were NRZ-QPSK-interleaved or RZ-QPSK pulse-to-pulse aligned [190], as we have demonstrated in [191] and [192] respectively.

### 5.2.2 Tolerance to nonlinear effects in homogenous WDM systems

I first study the tolerance of 100 Gb/s PDM-QPSK to intra-channel nonlinear effects through a single-channel transmission, i.e. keeping surrounding channels continuous (according to the scheme shown in Fig. 4.1-a). Fig. 5.4-a shows the performance of the test channel (green diamonds) measured after a transmission distance of 1,200 km as a function of the power launch per channel,  $P_{ch}$ . Performance is limited by optical noise for low values of launch power. Therefore,  $Q^2$  factor increases with the power, along with OSNR. The intra-channel effects mainly SPM and NLPN here, arises as soon as the launch power exceeds -1 dBm. However, the performance of PDM-QPSK keeps increasing up to +1 dBm launch power and reaches an optimum  $Q^2$  factor around 12 dB.

Next, I study the behaviour of one 100 Gb/s PDM-QPSK channel surrounded by other 100-Gb/s PDM-QPSK channels, corresponding to transmitter configuration depicted in Fig. 4.1-b. RZ-pulse carving enlarges the spectrum of 100 Gb/s PDM-QPSK resulting in a spectrum width of ~80-GHz. Therefore, one issue of 100 Gb/s PDM-QPSK could be the tolerance to narrow optical filtering stemming from concatenation of several 50-GHz ROADM nodes. I investigate this by emulating three transparent-networks nodes along the transmission. The wavelength selective switch (WSS) inserted at the end of the loop not only performs channel power equalisation but also can emulate optical filtering and crosstalk stemming from nodes in a transparent network. This is done by passing odd and even channels through distinct output ports, introducing an additional optical path to even channels for further decorrelation before recombining them through a 3-dB coupler, as depicted in Fig. 5.4-b.

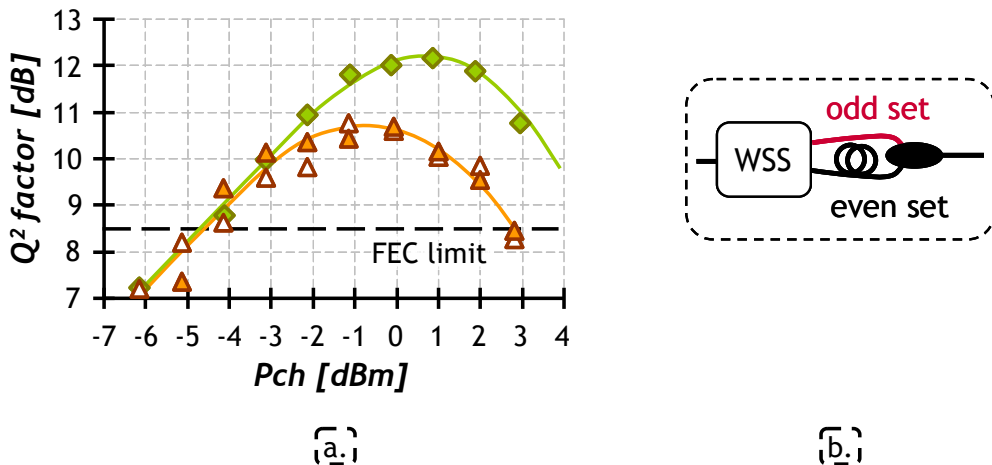


Fig. 5.4: (a) Tolerance to nonlinearities of 100 Gb/s PDM-QPSK after 1200 km of NZDSF in  $\blacklozenge$  single channel and homogeneous WDM configuration  $\blacktriangle$  with and  $\blacktriangledown$  without the emulation of in-line optical filtering and crosstalk. (b) Wavelength selective switch configuration to emulate in-line optical filtering and crosstalk.

Fig. 5.4-a shows the performance evolution of the test channel (orange triangles) versus the power launch per channel in homogeneous WDM configuration. The launch power of the test channel is set at the same level as all the co-propagating. Full orange triangles depict the performance when optical filtering and

crosstalk steaming from nodes is emulated whereas empty triangles depict the results without this emulation. According to Fig. 5.4, neither optical filtering nor crosstalk stemming from three network nodes induce any penalty on the performance of 100 Gb/s. On the other hand, the presence of 100 Gb/s neighbour channels reduces the optimum Q<sup>2</sup> factor of no more than 1.5 dB compared to the single-channel optimum performance. Despite the low chromatic dispersion of the NZ-DSF, the penalty brought by cross nonlinear effects is small due to the relatively high symbol rate (28 Gbauds) which reduces the efficiency of cross nonlinearities [34].

### **5.2.3 Impact of inter-channel effects in hybrid WDM systems**

As discussed in section 4.1, co-propagating 10-Gb/s NRZ channels dramatically limit the performance of coherent 40-Gb/s PDM-QPSK channels. Nevertheless, the tolerance to cross nonlinearities gets better while increasing the baud rate, as pointed out in section 5.1. Thus PDM-QPSK at 100 Gb/s can be a suitable solution for overlaying legacy 10-Gb/s networks while it is not at 40 Gb/s.

The following experiments now focus on the tolerance of PDM-QPSK solutions at 100 Gb/s and 40 Gb/s against inter-channel nonlinear effects in hybrid WDM systems, in which all channels are not modulated with the same modulation format. Thus, I measure the performance of one 100/40 Gb/s PDM-QPSK channel surrounded by 10 Gb/s NRZ channels, corresponding to transmitter configuration depicted in Fig. 4.1-c. It must be stretched that, to compare performance in the same range of Q<sup>2</sup>-factor around 10 dB for the 100-Gb/s channel, the transmission distance was decreased from 1,200 km to 800 km when moving from homogeneous to hybrid WDM configuration.

Fig. 5.5-a shows the OSNR sensitivity for both 100 Gb/s and 40 Gb/s PDM-QPSK. 40 Gb/s shows a 4-dB better noise sensitivity according to the ratio between the bit rates,  $10\log_{10}(40/100)$ . Fig. 5.5-b in turn depicts the tolerance of 100 Gb/s and 40 Gb/s PDM-QPSK to impairments brought 10-Gb/s NRZ co-propagating channels. In order to compare the results obtained with 100 Gb/s and 40 Gb/s PDM-QPSK, which do not exhibit the same tolerance against optical noise, Fig. 5.5-b represents the penalty in terms of Q<sup>2</sup>-factor w.r.t. the performance obtained in back-to-back configuration at the same OSNR. As a reference, I also report in Fig. 5.5-b the results obtained after 1,200 km of single channel transmission at 100 Gb/s (green diamonds). To perform a fair comparison between the curves obtained at different distances, I define a relative normalized power, as in section 4.3, so as:  $\bar{P}_{ch} = P_{ch} + 10\log_{10}(dist/800)$ , where  $dist$  is the distance in [km]. According to Fig. 5.5-b, inter-channel nonlinear effects brought by neighbouring 10 Gb/s NRZ channels reduce transmission distance of 100 Gb/s PDM-QPSK channels from 1,200 km to 800 km. On top of that, cross nonlinearities further limit the performance at 40 Gb/s than at 100 Gb/s.

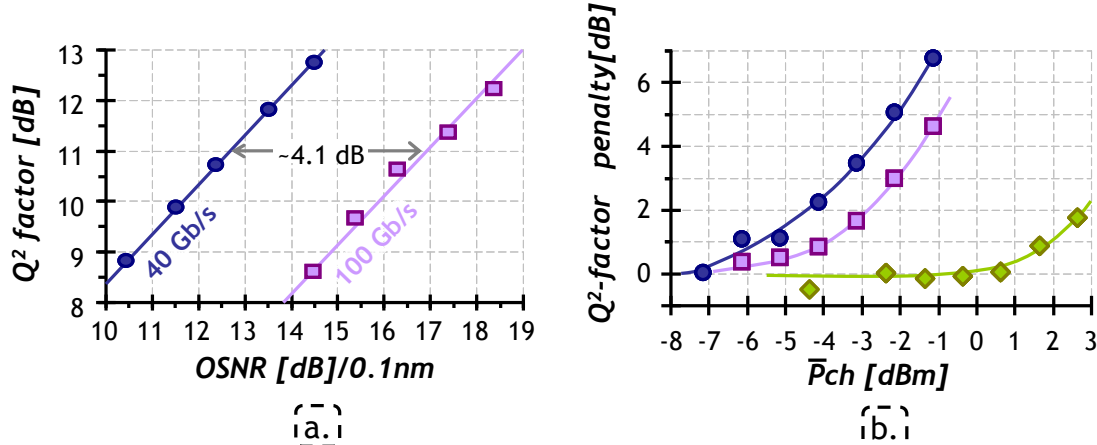


Fig. 5.5: ● 40 Gb/s and ■ 100 Gb/s PDM-QPSK, (a) optical noise sensitivity; and (b) tolerance to nonlinear effects in a hybrid WDM configuration (mixed with 10 Gb/s NRZ) after 800 km of NZDSF. As a reference, the ◆ tolerance to intra-channel nonlinear effects of 100 Gb/s PDM-QPSK after 1200 km of NZDSF is also depicted.

The better behaviour against nonlinearities of PDM-QPSK at 100 Gb/s compared to that at 40 Gb/s is attributed to the equivalent filter of the phase estimation process in the coherent receiver that becomes more effective as the baud rate of the coherent-detected signal increases with respect to that of neighbouring channels [175]. Indeed, the baud rate increase naturally introduces a longer correlation of induced phase noise over consecutive symbols, thus enabling a more accurate recovery of the carrier phase and a reduction of the inter-channel related impairments.

According to preceding results, coherent PDM-QPSK technologies seem to be more suitable at 100 Gb/s as they are more tolerant against inter-channel nonlinearities than at 40 Gb/s. To confirm this statement, we compare the behaviour of 40 Gb/s and 100 Gb/s PDM-QPSK over the commercial Alcatel-Lucent 1626LM WDM platform when surrounded by 10-Gb/s NRZ channels. More precisely, the system configuration relies on a 50-GHz grid and seven spans of SSMF with an average span loss of 22 dB, separated by EDFA incorporating DCF spools according to legacy terrestrial systems. The power of all channels is set to same level.

Fig. 5.6 depicts the behaviour of 40 Gb/s and 100 Gb/s PDM-QPSK versus the launch power per channel,  $P_{ch}$ . PDM-QPSK at 100 Gb/s appears to be more robust than at 40 Gb/s to nonlinearities stimulated by NRZ co-propagating channels as they reveal penalising for higher powers. The optimum  $Q^2$  factor is only reduced by less than 2.5 dB when moving from 40 Gb/s to 100 Gb/s whereas linear considerations would predict a difference of  $\sim 4$  dB according to the worse noise sensitivity, as observed at low channel power (-6 dBm). Focusing on the power range within [-1 dBm, +1 dBm] typically used in 10 Gb/s systems operating over more than 20 spans, results show that 100 Gb/s and 40 Gb/s PDM-QPSK perform similarly, despite its worse noise sensitivity. Hence, inter-channel nonlinearities are found significantly more penalising at 40 Gb/s than at 100 Gb/s also in hybrid WDM systems, where the coherent channel is surrounded by 10-Gb/s NRZ channels.

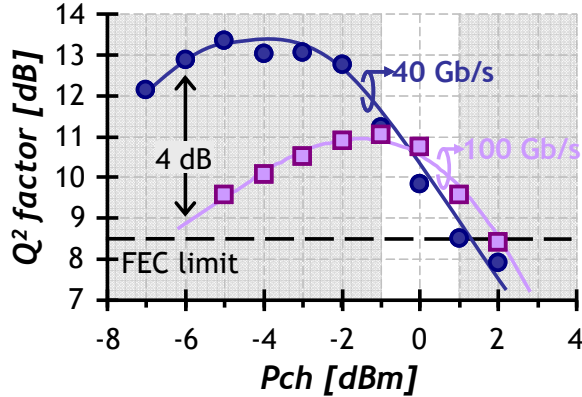


Fig. 5.6: Nonlinear tolerance over the commercial Alcatel-Lucent 1626LM platform when surrounded by 10 Gb/s NRZ channels. The transmission line consists of 7 spans of SSMF with an average span loss of 22 dB. ● 40 Gb/s and □ 100 Gb/s PDM-QPSK.

### 5.2.4 Containing inter-channel nonlinearities in hybrid WDM systems

Next, I study the performance evolution of 40 Gb/s and 100 Gb/s PDM-QPSK over 10-Gb/s systems operating ULH transport. To emulate such systems, the power per channel at each fibre input for all 10 Gb/s NRZ channels is set at the nominal value of -1 dBm and measurements are realised after two round trips of the recirculating loop, i.e. 800 km. According to Fig. 5.5-b, performance of PDM-QPSK channels is impacted noticeably by inter-channel nonlinearities when the power of all channels is set at -1 dBm.

One possibility to improve the performance of coherent PDM-QPSK channels in hybrid WDM configuration would be to optimize the power of the 40/100 Gb/s coherent channel independently of the power of the 10-Gb/s channels. Fig. 5.7-b shows the performance evolution of the test channel while varying its launch power around the nominal value of -1 dBm after 800 km. I choose to represent in x-axis the relative power of the test channel and I set as a reference the nominal power, i.e. -1 dBm. Likewise, y-axis represents the variation of performance compared to that obtained when the power of all channels is the nominal power of -1 dBm.

Below the nominal value, the increase of the launch power enables an increase of the performance. Once the nominal value is reached, only 0.25-dB increase in performance is obtained when increasing the launch power by 3 dB beyond this nominal value of -1 dBm for 100 Gb/s and even less for 40 Gb/s channel. This performance limitation suggests that coherent PDM-QPSK channels suffer severe nonlinear penalties arising from the co-propagating 10 Gb/s NRZ channels [193] that are not recovered by increasing the received OSNR. Therefore, the degree of freedom consisting in optimizing the channel power of the inserted channel almost vanishes in this configuration.

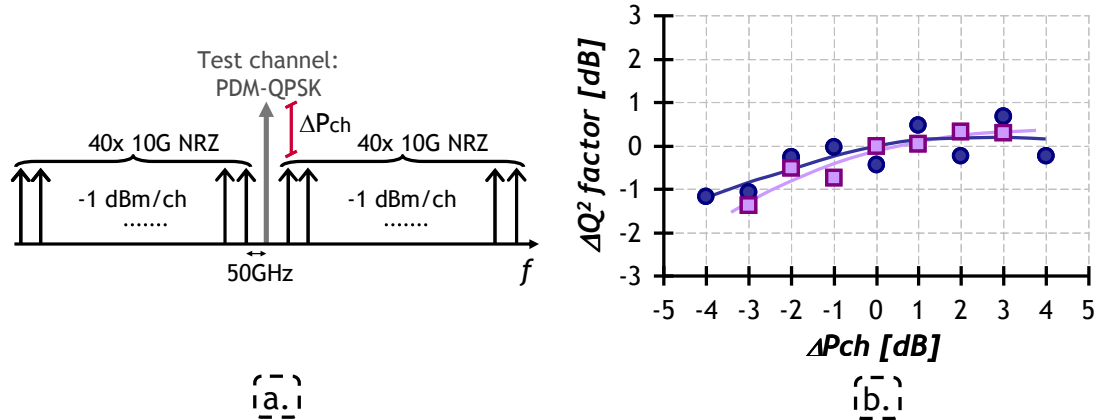


Fig. 5.7: ● 40 Gb/s and ■ 100 Gb/s PDM-QPSK, (a) channel configuration used in the experiment and (b) performance variation of the test channel while varying its launch power w.r.t. the power of 10 Gb/s NRZ channels( fixed at -1 dBm) after 800 km of NZDSF. The nominal power is -1 dBm and the reference  $Q^2$  factor corresponds to the performance obtained when the power of all channels is -1 dBm.

Another option to contain the penalties brought by co-propagating channels on the performance of coherent PDM-QPSK channels in hybrid WDM configuration is to introduce guard-bands between coherent PDM-QPSK and 10 Gb/s NRZ channels. This option was already investigated in section 4.1 to overcome penalties brought by 10 Gb/s NRZ channels onto a coherent PDM-QSPK channel operating at 40 Gb/s over a SSMF based system. However, a limited guard-band of 300 GHz was not sufficient to recover the penalties due to inter-channel effects induced by 10 Gb/s NRZ co-propagating channels in that experiment. Since inter-channel effects appear to be less penalizing when increasing bit rate from 40 Gb/s to 100 Gb/s, I aim here at measuring and comparing the required guard-band for the insertion of a coherent PDM-QPSK channel at both 40 Gb/s and 100 Gb/s with only 1-dB performance penalty.

As depicted in Fig. 5.8-a, I investigate this option by gradually moving away two sets of 20 adjacent channels (up to 1.1 THz) on both sides of the coherent test channel. Ideally, when surrounding channels are far enough from the test one, the performance of the test channel should be the same as in a single channel transmission. The total number of channels is kept constant and the output power of inline amplifiers is set at 15 dBm, corresponding to a launch power of -1 dBm per channel.

To ease comparison between both bit rates, the power of the 40 Gb/s test channel is contained at -5 dBm (i.e. 4 dB lower than that of the 100 Gb/s channel), in order to obtain approximately the same performance in single channel transmission. In the meantime, the power of the 10 Gb/s NRZ channels is kept at -1 dBm to ensure that the test channel at 40 Gb/s experiments the same amount of inter-channel effects as at 100 Gb/s.

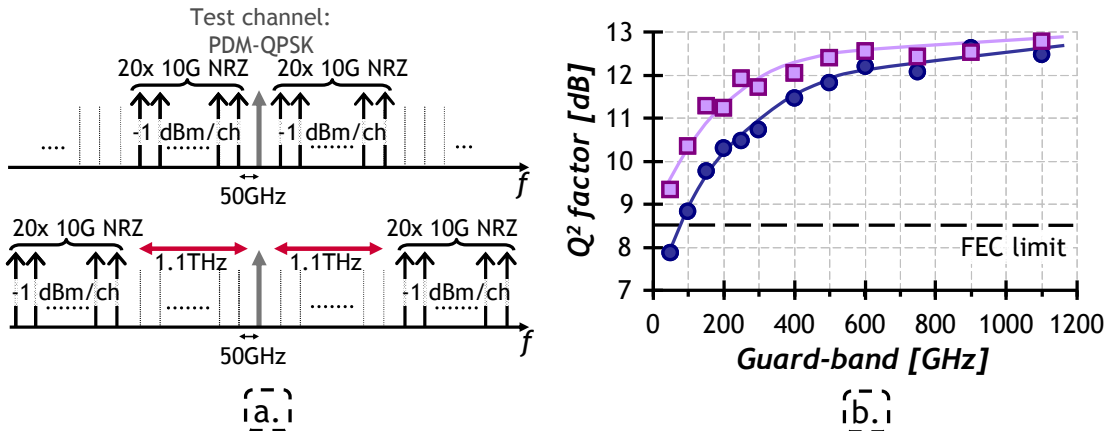


Fig. 5.8: ● 40 Gb/s and ■ 100 Gb/s PDM-QPSK, (a) channel configuration used in the experiment and (b) performance evolution versus guard-band around PDM-QPSK channel after 800 km of NZDSF. The power of all channels is -1 dBm.

The results of these measurements are depicted in Fig. 5.8-b after 800 km for both 40 and 100 Gb/s coherent PDM-QPSK channels. It can be seen in this figure a slow decrease of the performance penalties up to a channel spacing of 1 Thz. This is mainly attributed to XPolM [185][183] (sometimes referred to as polarisation scattering) induced by surrounding 10-Gb/s NRZ channels, as discussed in section 4.1. In fact, PDM-QPSK signals suffer from non-negligible nonlinear interactions even coming from co-propagating channels distant by more than 500 GHz, inline with results obtained with 40 Gb/s PDM-QPSK of section 4.1.

100 Gb/s PDM-QPSK is clearly less impacted by impairments brought by 10 Gb/s NRZ neighbours than 40 Gb/s PDM-QPSK. The largest penalties are induced by the closest adjacent channels, due to the effect of XPM. The maximum penalty is observed, as expected, when no guard-band separate the 10 Gb/s NRZ channels from the test channel, corresponding to a minimum 50-GHz spacing. This penalty is about 4 dB at 100 Gb/s whereas it exceeds 5 dB at 40 Gb/s. This highlights the lower tolerance of the PDM-QPSK at 40Gb/s against inter-channel effects. Moreover, the guard-band required to ensure less than 1 dB penalty in the performance of the 100 Gb/s channel is of 400 GHz, whereas at 40 Gb/s, a 200 GHz-larger guard-band is required, at. 600 GHz. The total transmitted capacity of the system should be drastically reduced to ensure performance of 40 Gb/s PDM-QPSK in a hybrid 10/40 Gb/s WDM system whereas at 100 Gb/s a narrower band gap could be considered. Indeed, a 150-GHz guard-band would provide a beneficial 2 dB improvement of Q<sup>2</sup>-factor margins at 100 Gb/s leading to more than 2.5-dB margins above the FEC threshold ensuring error-free transmission after FEC.

### 5.2.5 Further insight on XPolM: required number of channels

PDM-QPSK signals suffer from inter-channel nonlinearities coming from co-propagating channels located very far in the spectrum, as discussed in the preceding section. This suggests that one can underestimate the actual cross nonlinear interactions experienced by PDM-QPSK channels if only the closest

neighbour co-propagating channels are considered. Hence, nonlinearities experienced by coherent channels may strongly depend on the number of co-propagating channels.

I study here the behaviour of the test channel when varying the number of surrounding 10 Gb/s NRZ channels, as depicted in Fig. 5.9-a. According to typical ULH operation, the power per channel is set at -1 dBm, as in preceding experiments, and is kept unchanged throughout all the experiment. Moreover, the launch power of the 100-Gb/s test channel is set at the same level as 10-Gb/s NRZ channels, i.e. -1 dBm as, since independent power optimisation is worthless. Measurements are realised after 800 km, i.e. two round trips.

When decreasing the number of co-propagating 10-G channels from 82 down to 20, the output power of the amplifiers is successively decreased from 18 to 12 dBm to keep the power per channel to -1 dBm as well as a constant end-of-link OSNR. Below the value of 20 co-propagating 10-Gb/s channels, the output power of the amplifiers is kept at 12 dBm while part of the 10-Gb/s channels are progressively replaced by continuous-wave (CW) channels for constant amplifier loading. When all 20 co-propagating channels are CW, the measure corresponds to the single-channel transmission of the 100 Gb/s coherent PDM-QSPK channel at -1 dBm.

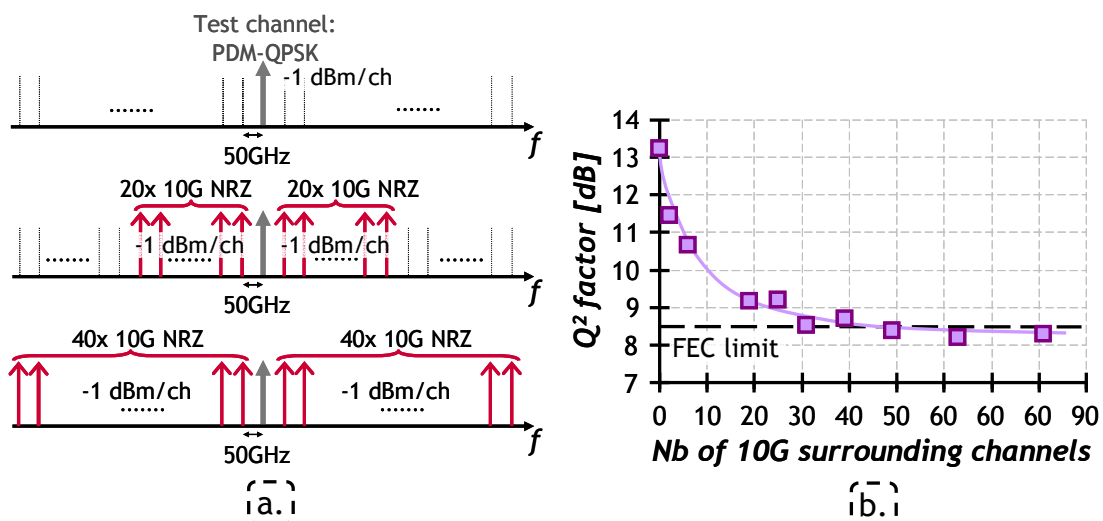


Fig. 5.9: 100 Gb/s PDM-QPSK, (a) experimental channel configuration and (b) performance evolution versus the number of surrounding 10 Gb/s channels after 800 km of NZDSF. The power of all channels is -1 dBm.

Fig. 5.9-b shows the measured performance of the test channel as a function of the number of surrounding 10-Gb/s NRZ channels. Co-propagating 10-Gb/s channels induce a maximum penalty of about 4 dB with respect to single-channel propagation. The performance of the test channel is unchanged (within a 0.5-dB range) only if the number of surrounding channels exceeds 40. In other words, coherent channel suffer from non-negligible interaction coming from channels more than 500 GHz away [186], which confirms results discussed in preceding section. This is mainly attributed to the XPolM which is weakly dependent on frequency spacing [185].

Therefore, measuring the performance of 100 Gb/s coherent PDM-QPSK requires several tens of surrounding WDM channels to be accurate. Indeed, the 2-dB performance variation observed between 5 and 20 surrounding channels indicates that

the performance penalties brought by legacy channels onto 100-Gb/s coherent PDM-QPSK may significantly depend on the test-bed configuration.

### 5.3. Interplay between nonlinearities and lumped PMD

According to the results presented in section 4.2.3, the consequences of interplay between nonlinearities and PMD may differ from the simple addition of both effects separately. In section 4.2.3, PMD was distributed along the line and helped reducing nonlinear impairments thanks to the decorrelation between polarisation tributaries and PDM-induced depolarisation. In contrast, when located in the line, PMD may increase the peak-to-peak power average ratio making the signal weaker against nonlinearities encountered further along the rest of the transmission line. Thus, this section gives further insight on how the tolerance to PMD can be affected by the interplay between located PMD and nonlinearities occurring along the link in 100 Gbit/s PDM-QPSK coherent systems. I also study the dependence on the number of equaliser taps of the PMD tolerance when nonlinear effects are taken into account in order to verify the possibility of reducing the receiver complexity.

#### 5.3.1 Experimental set up

Depicted Fig. 5.10-a, the test bed involves 82 channels modulated with (NRZ-)PDM-QPSK at 100 Gb/s according to the configuration of Fig. 4.1-b. The transmission link here consists of four 100-km-long spans of SSMF, separated by dual stage EDFA, incorporating DCF in-between. The PMD of the line is very small and does not exceed 1 ps. When needed, a PMD emulator (Fig. 5.10-b) can be inserted at the beginning or at the end of the transmission link. It consists of 10 sections of polarisation maintaining fibre (PMF) separated by polarisation controllers, which are driven by a computer to vary the input state of polarisation (SOP) in each PMF. It emulates thus all-order PMD. Two different sets of PMF sections can be used, totalizing either 8 ps PMD or 20 ps PMD.

To ease comparisons, the OSNR is intentionally degraded by loading noise at the receiver end (once and for all in each experiment), so that the Q<sup>2</sup> factor averaged over all the PMD conditions reaches the arbitrary reference of 10.5 dB (corresponding to a BER of  $4 \times 10^{-4}$ ). The channel under study, at 1545.72 nm, is selected by a 0.4-nm bandwidth filter and sent into the coherent receiver.

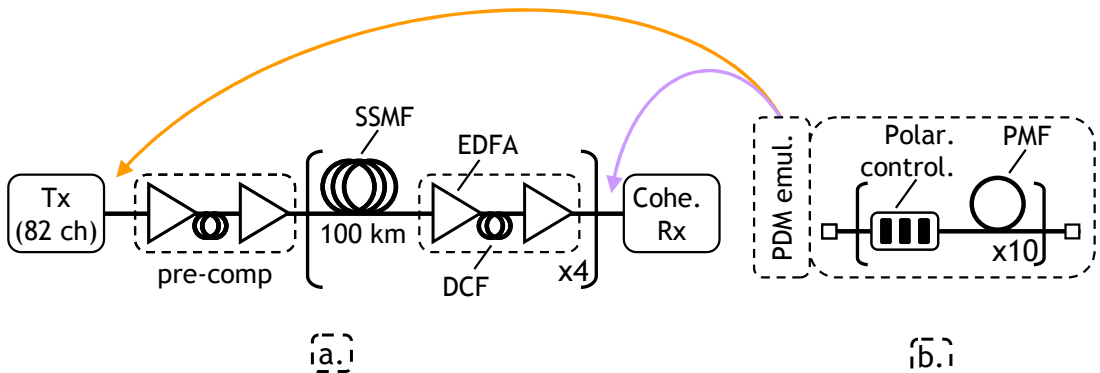


Fig. 5.10: (a) Link configuration and (b) PMD emulator scheme.

### 5.3.2 Impact of nonlinear effects

As a reference, I first record the tolerance of 100 Gb/s PDM-QPSK to nonlinear effects under these conditions without the PMD emulator, i.e. with less than 1 ps PMD in the link. Fig. 5.11 (and Fig. 3.13) shows the results in terms of  $Q^2$ -factor versus the power per channel. Nonlinear impairments arising at high powers per channel,  $P_{ch}$ , degrade  $Q^2$  factor, as expected.

I arbitrarily define here the non linear threshold (NLT) as the value of the power per channel leading to a penalty of 2 dB in terms of  $Q^2$  factor, i.e. 5 dBm, as illustrated in Fig. 5.11. When  $P_{ch}$  is significantly smaller than the NLT, e.g.  $P_{ch}=-1$  dBm, linear impairments dominate and we shall call this propagation regime “linear”, as opposed to when  $P_{ch}=5$  dBm, which we shall refer to as “nonlinear” regime in the following. The next step then is to study the tolerance of 100 Gb/s PDM-QPSK to PMD in both regimes.

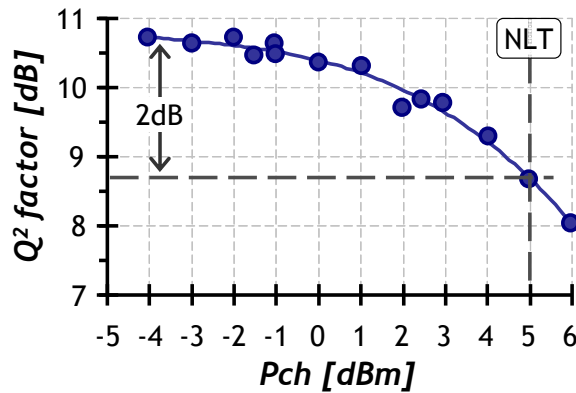


Fig. 5.11: Nonlinear tolerance of 100 Gb/s PDM-QPSK after 400 km of SSMF with fixed OSNR by loading noise at the receiver side. Definition of nonlinear threshold (NLT).

### 5.3.3 Impact of PMD in linear regime

I first assess the impact of PMD in the linear regime, i.e. without significant nonlinear impairments within the line. BER statistics are derived out of 1000 random draws of PMD conditions from the emulator. We compare these statistics when the emulator is located at the transmitter or at the receiver side. Fig. 5.12 represents the probability density function of the  $Q^2$ -factor (a) and the cumulative probability deviation from the best performance (b) obtained when the PMD emulator is located at the receiver side (any performance better than this value has been counted as 0-dB deviation).

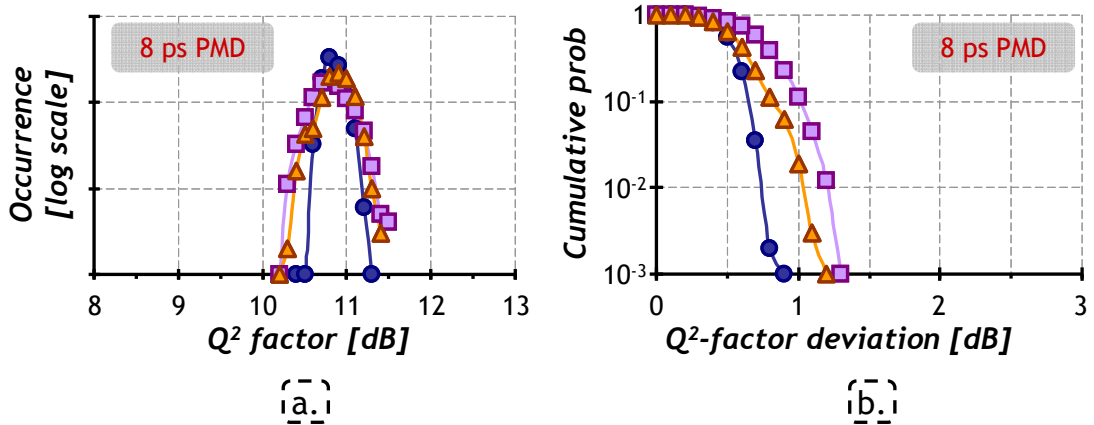


Fig. 5.12: Linear regime, (a)  $Q^2$ -factor distribution and (b) cumulative probability deviation. ● Without in-line PMD, with ▲ 8 ps PMD when the emulator is placed at the transmitter side and ■ 8 ps PMD when the emulator is placed at the receiver side.

Since the PMD is a linear distortion, FIR filters are supposed to efficiently mitigate it, as already pointed out. Fig. 5.12 represents the results obtained in linear regime with 8 ps PMD as well as the reference result obtained without PMD emulation, i.e. <1 ps PMD. The  $Q^2$ -factor distribution is relatively narrow as there are no significant nonlinearities along the line. Moreover, it is almost identical whether the PMD emulator is placed at the beginning or at the end of the link, as expected in linear regime. Besides, compared to the reference curve obtained without PMD a negligible 0.3-dB deviation is observed in Fig. 5.12-b due to the 8 ps PMD. This underlines the efficient mitigation of PMD at 100 Gb/s when it does not interact with nonlinearities along the transmission line.

### 5.3.4 Impact of PMD in nonlinear regime

The picture changes when moving from a linear to a nonlinear regime since nonlinearities present within the line may interact together with PMD and change the behaviour of PDM signals. I then carry out similar experiments in the nonlinear regime for two different values of PMD, 8 ps and 20 ps. For easier comparison with results represented in Fig. 5.12, the  $Q^2$ -factor penalties due to the increase of  $P_{ch}$  are compensated for by increasing the received OSNR. Fig. 5.13 shows the results obtained in nonlinear regime for 8 ps (top) and 20 ps (bottom) PMD. Like Fig. 5.12, Fig. 5.13 represents the probability density function of the  $Q^2$  factor (left) and the cumulative probability deviation (right). When the PMD emulator is located at the receiver side, no noticeable difference is observed in the cumulative probability compared to the linear regime (Fig. 5.12) even with 20 ps PMD, confirming the potential of digital coherent receivers to deal with PMD and mitigate its impact when there is no interplay with nonlinear effects.

In contrast, when the PMD emulator is placed at the transmitter side, about 0.7-dB of extra margin, in terms of OSNR targeted at the end of the transmission, needs to be provisioned for 8 ps PMD to assure the same system performance compared to when the emulator is placed at the receiver side. This extra margin increases to 1 dB when 20 ps PMD are located also at the transmitter side. This highlights the detrimental interaction between PMD and nonlinear effects which is

difficult to unwrap by digital processing in the receiver, and which has been confirmed in [194]. In fact, PMD increases the peak-to-average power ratio of PDM signals, as recently illustrated in [195]. As a consequence, lumped PMD makes 100 Gb/s PDM-QPSK less resistant to nonlinearities occurred along the transmission line. In contrast, when the emulator is located at the receiver end, any additional PMD can be easily separated from the nonlinear effects through dedicated algorithms. Thus, provisioning independent system margins for PMD and nonlinearities can yield a wrong estimation of system outages.

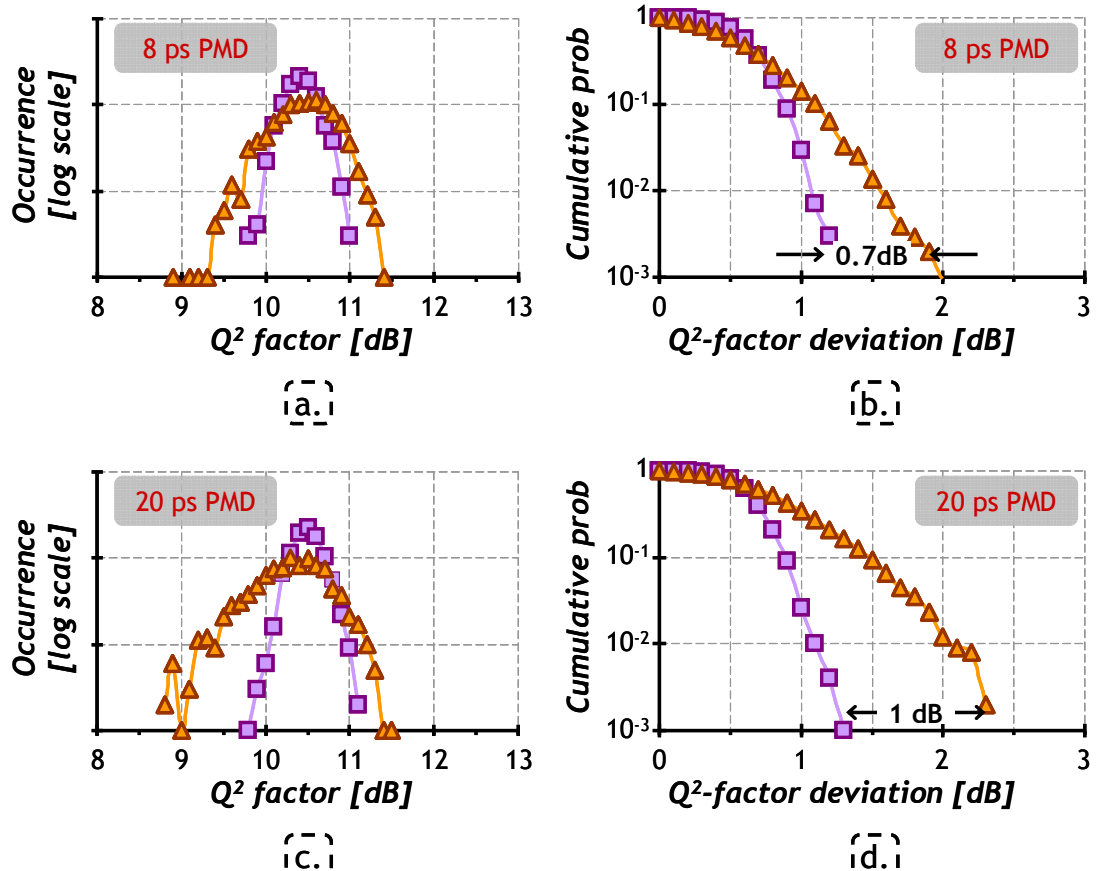


Fig. 5.13: Nonlinear regime,  $Q^2$ -factor distribution (a, c) and cumulative probability deviation (b, d) either with 8 ps (a, b) and 20 ps (c, d) PMD, whether the emulator placed either at the  $\blacktriangle$  transmitter or at the  $\blacksquare$  receiver side.

Since the CPE algorithm and FIR equaliser can be optimized independently (according to what we have observed), it would be tempting to lower the receiver complexity requirements, and thus reduce terminal costs, by decreasing the number of taps used in the equalisation FIR filter. The extra margin required in nonlinear regime when the PMD is generated at the beginning of the link for different equalisation filter tap lengths are shown in Fig. 5.14.

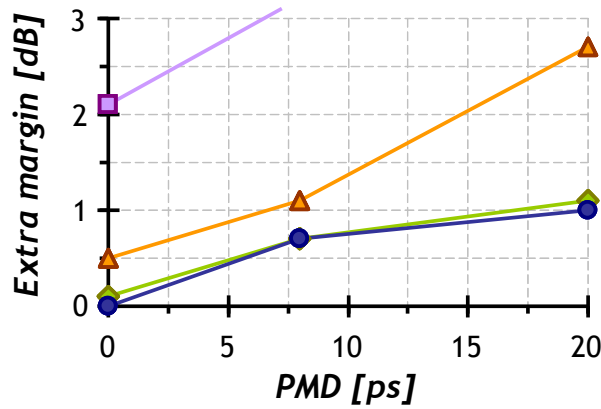


Fig. 5.14: Dependence of  $Q^2$  factor extra margins as function of PMD when using a FIR equaliser with □ 3 taps, ▲ 5 taps, ◆ 9 taps and ● 13 taps.

It can be seen that using small tap-lengths in equalisation requires increasing margins at  $10^{-3}$ . A 3-taps equaliser is not even able to correctly process a signal without PDM. Moreover, an extra margin greater than 2.5 dB is needed for 20 ps of PMD when a 5-tap-length equaliser is used. Besides, nearly no improvement is observed for a number of taps higher than 9.

Thereby, 100 Gb/s PDM-QPSK exhibits excellent tolerance to PMD over dispersion-managed systems when there is no interaction between nonlinear effects and PMD. However, considering nonlinearities and PMD separately would lead to underestimate the required margins when designing a system by up to 1 dB for high PMD amounts at an outage probability of  $10^{-3}$  (with a 13-tap equaliser). Besides, these margins should be increased while decreasing the number of taps used in the equaliser.

## 5.4. Increasing the reach of 100 Gb/s PDM-QPSK

The reach of 100 Gb/s PDM-QPSK remains relatively short compared to the reach of 40 Gb/s PDM-BPSK, for example. The maximum achievable distance of 100 Gb/s can be increased in green field systems by means of an appropriate systems design. The rise of coherent detection and digital signal processing offers new degrees of freedom to optimise systems design. Coherent receivers are able to compensate for digitally huge amounts of chromatic dispersion (at expense of processing complexity). Consequently, they allow for the possibility to realise long-haul transmission without in-line dispersion management instead of using traditional in-line dispersion map. In systems without in-line dispersion management, one can use therefore single-stage EDFA or even hybrid Raman/EDFA amplification, thus improving the noise figure of the amplifier (as discussed in section 2.4.2). Moreover, the impact of inter-channel nonlinearities can be reduced in highly-dispersive links due the decorrelation between symbols of different channels from one span to another. Here, I consider a system specifically designed for 100 Gb/s PDM-QPSK relying in hybrid Raman/EDFA amplification without in-line dispersion management.

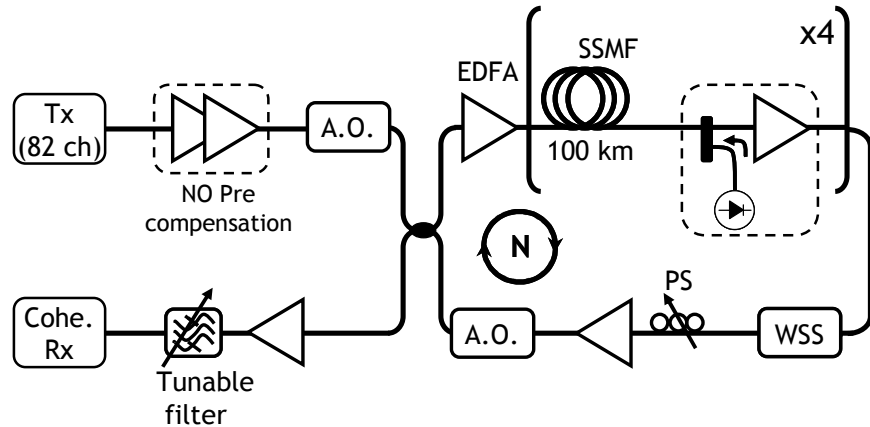


Fig. 5.15: Link configuration with hybrid Raman/EDFA amplification

Depicted in Fig. 5.15, the transmission test bed consists of 82 100-Gb/s PDM-QPSK channels spaced by 50GHz, according to Fig. 4.1-b. The resulting multiplex is boosted through a dual-stage EDFA and sent into the recirculating loop. The recirculating loop incorporates here four 100km-long spans of SSMF. No DCF is used along the line. Chromatic dispersion is fully compensated digitally through DSP in the coherent receiver. Fibre loss is compensated for by hybrid Raman/EDFA optical amplifiers. The Raman pre-amplifier is designed to provide  $\sim 10$  dB on-off gain, thanks to backward-propagating laser diodes at wavelengths 1432 nm and 1457 nm. The performance is measured after six loop round-trips, i.e. after a 2,400 km. The launch power of the test channel is set at the same level as all the co-propagating channels. At the receiver side, the channel under study is selected by a 0.4nm bandwidth filter and sent to the coherent receiver.

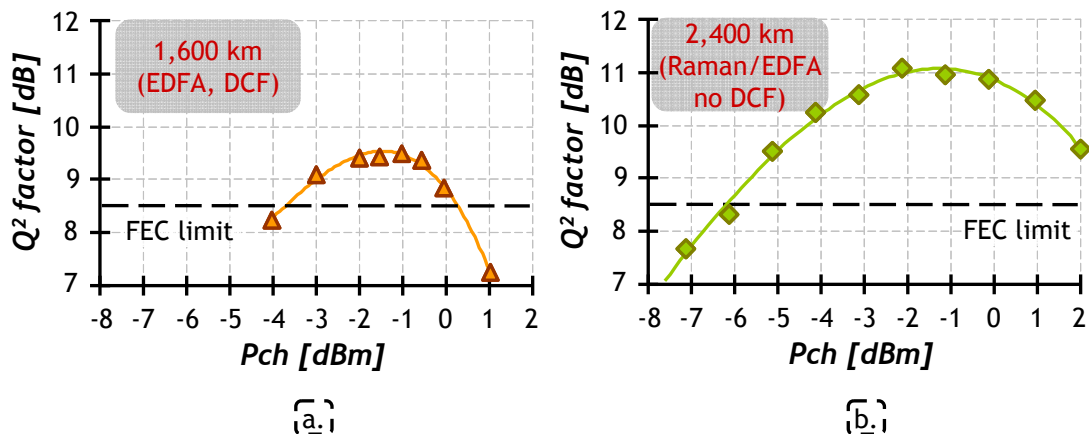


Fig. 5.16: 100 Gb/s PDM-QPSK behaviour, (a)  $\blacktriangle$  after 1600 km of SSMF with EDFA-only amplification and with in-line DCF; and (b)  $\blacklozenge$  after 2400 km of SSMF with hybrid Raman/EDFA amplification and without dispersion management.

Fig. 5.16 depicts the performance comparison of 100 Gb/s PDM-QPSK obtained over a standard link, with EDFA-only amplification and in-line DCF (a), and with hybrid Raman/EDFA amplification without dispersion management (b). As it can be seen hybrid Raman/EDFA amplification allows an increase of the distance from 1,600 to 2,400 km. Focussing in the low power region (-4 dBm), we can observe the benefits on the OSNR brought by hybrid Raman/EDFA amplification. Moving from 1600 km to 2400 km with unchanged EDFA amplification (and with constant

launch power) would imply a reduction of OSNR of  $10\log_{10}(24/16) \approx 1.76 \text{ dB}$  and consequently a decrease of performance. In contrast, we observe here a 2-dB improvement in terms of Q<sup>2</sup> factor after 2400 km thanks to hybrid Raman/EDFA amplification which demonstrates the improvement in OSNR. Moreover, the optimum performance obtained with hybrid/Raman amplification after 2400 km is around 1.5 dB better than after 1600 km with EDFA yielding 2.5 dB margins to industrial operation.

## 5.5. Summary and field trial

As discussed throughout this chapter, coherent PDM-QPSK at 100 Gb/s is a very promising solution to upgrade legacy 10-Gb/s networks for different reasons. As so, it has recently attracted a lot of attention from carriers. First of all, it has a spectrum width of 56 GHz which makes it compatible with the standard 50-GHz channel grid. It allows thus a tenfold increase of information spectral density of today's networks (from 0.2 to 2 b/s/Hz). Besides, it exhibits an excellent tolerance against linear impairments thanks to digital signal processing done in coherent receivers. Before the rise of digital coherent receivers, the principal concern for upgrading systems at 40 Gb/s was the tolerance to linear effects. This fact would have been exacerbated at 100 Gb/s as the tolerance to linear impairments decreases with the increasing symbol rate (for a given modulation format), when signals are combined with direct-detection receivers. Another advantage of PDM-QPSK is that its symbol rate is a quarter of the total bit rate, relaxing therefore the constraints on the bandwidth and speed requirements, and thus the cost of high-speed electronic devices and analog to digital converters. Last but not least, PDM-QPSK is more robust against nonlinearities at 100 Gb/s than at 40 Gb/s thanks to its higher symbol rate, 25 instead of 10 Gbaud. Its superior nonlinear tolerance enables 100 Gb/s PDM-QPSK to offset the 4-dB worse noise sensitivity w.r.t. 40 Gb/s and perform equally when surrounded by 10-Gb/s NRZ channels operating for long-haul distances.

As at 40 Gb/s, PDM-QPSK at 100 Gb/s may suffer (less) from inter-channel nonlinear effects stemming from channels located very far in the spectrum. Hence, measuring accurately the impact of cross nonlinearities onto the performance of 100 Gb/s (and 40 Gb/s) coherent PDM-QPSK requires several tens of surrounding WDM channels, as demonstrated in this chapter. According to the results presented in Chapter 4, the consequences of interplay between nonlinearities and PMD may differ from the simple addition of both effects separately. In this chapter, the impact of located, instead of distributed, PMD was discussed. Located PMD may increase the peak-to-peak power average ratio making the signal weaker against nonlinearities encountered further along the rest of the transmission line. According to the results, considering nonlinearities and PMD separately would lead to underestimate the required margins when designing a system.

As a proof of the suitability of 100 Gb/s PDM-QPSK to upgrade massively-deployed 10-Gb/s networks, we have successfully conducted, together with colleagues from the business unit, a field trial on Telefónica's network in Spain. The chosen route uses Alcatel-Lucent 1626LM platform and measures 1,088 km between Madrid-Sevilla-Mérida, as shown in Fig. 5.17-a. The link relies on SSMF and EDFA-only amplification, and includes five 50-GHz multi-degree ROADM. The 100-Gb/s

PDM-QPSK channel was generated in Madrid and surrounded by two 40-Gb/s P-DPSK channels (with 50-GHz spacing) and three 10-Gb/s NRZ channels. Afterwards, the five channels were inserted among other 42 channels carrying real 10-Gb/s traffic, as illustrated in Fig. 5.17-b. At the receiver side, the 100-Gb/s channel was selected by a filter, sent into the coherent receiver described in Chapter 3 and processed off-line in a computer. The performance stability of the 100 Gb/s channel was measured over more than 24 hours without traffic hit. Fig. 5.17-c reports the results of the long-term measurements in terms of  $Q^2$  factor time-evolution and probability density function. The average  $Q^2$  factor was 10.61 dB, with a standard deviation of 0.16 dB, proof of an excellent stability over the 21,969 measurements done during 24.4 hours.

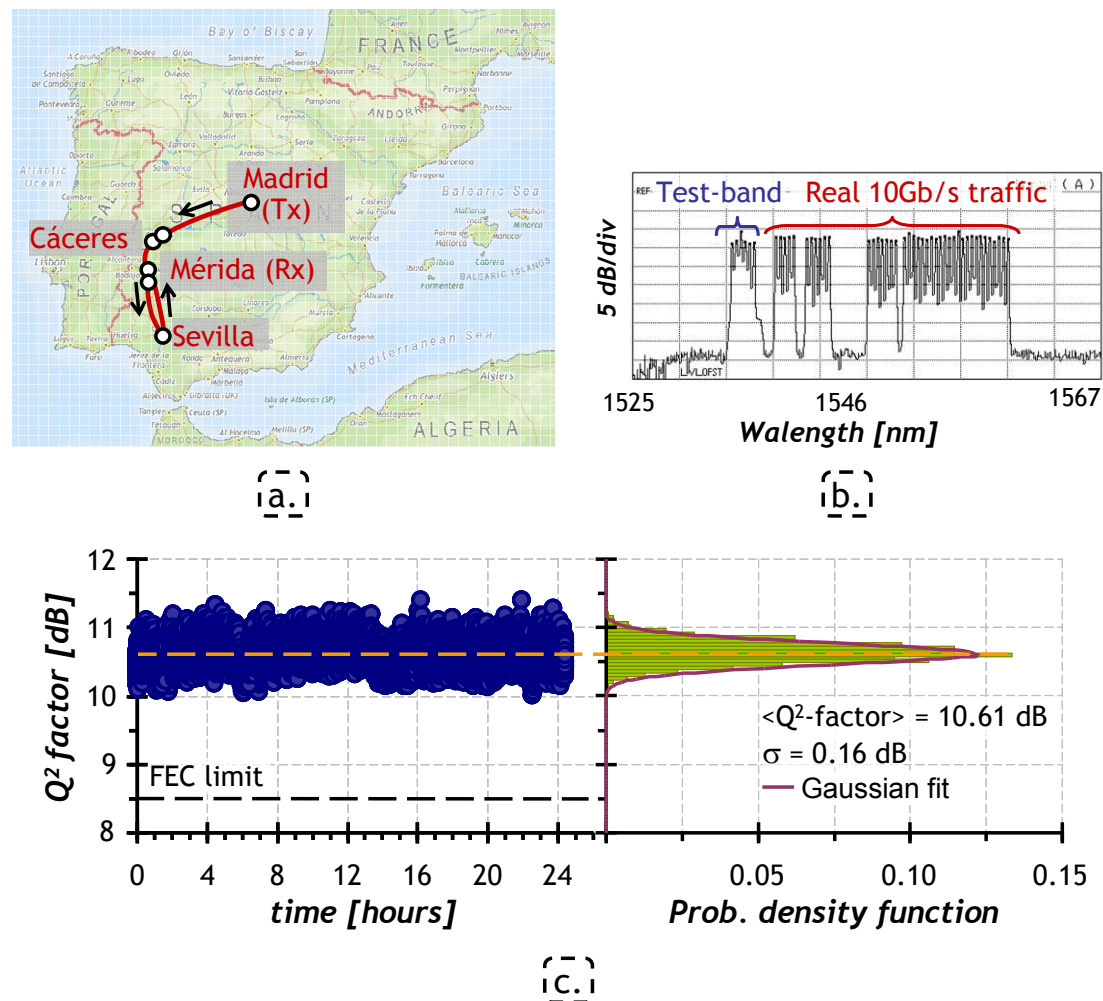


Fig. 5.17: Field trial over 1088-km Telefónica's installation of 1626LM between Madrid-Sevilla-Mérida. The link relied on SSMF and EDFA-only, and incorporated 5 ROADMs along the line. (a) Geographical situation, (b) spectrum allocation, (c)  $Q^2$ -factor evolution over more than 24 hours and probability density function.

This result not only shows the potential of 100 Gb/s PDM-QPSK to upgrade standard 50-GHz systems and to co-propagate with 10 and 40 Gb/s channels but also demonstrates the interest of carriers onto 100 Gb/s technologies. This interest is stressed by the 100 Gb/s ULH-DWDM project driven by the optical internetworking forum (OIF) which has adopted coherent PDM-QPSK to aid the industry in the

development of transceiver technology for transport of 100 Gb/s signals in long distance backbone networks.



# ***Outlook and conclusions***

In this thesis, I have investigated polarisation-diversity coherent detection paired with phase-modulated polarisation-multiplexed signals for long-haul transmissions at 40 and 100 Gb/s. Before the rise of coherent detection, one of the major concerns for the deployment of high bit rate systems ( 40 Gb/s) was the tolerance to linear impairments. However, by providing access to all the characteristics of the optical field (amplitude, phase and polarisation), digital coherent receivers offer the possibility of compensating linear impairments while giving the best noise sensitivity, as we have demonstrated. Coherent receivers can exhibit an excellent tolerance to linear impairments which depends only on signal-processing receiver capability. Besides, combining multilevel phase-modulated signals with polarisation multiplexing allows increasing the information spectral density while reducing the requirements on bandwidth and speed of electronics and analog-to-digital converters. Nevertheless, we have shown that polarisation-multiplexed signals appear to be more sensitive to nonlinear impairments.

First of all, we have emphasized that the two modulated polarisation tributaries interact nonlinearly along the transmission limiting the performance of single channel propagation. Moreover, in a more realistic WDM context, we have evinced that coherent polarisation-multiplexed signals sometimes suffer more from inter-channel nonlinearities coming from co-propagating channels located very far in the spectrum, contrary to current 10-Gb/s OOK systems. Indeed, nonlinearities, such as cross polarisation modulation (XPolM), create sudden changes of the state of polarisation which cannot be followed by the (digital) polarisation tracking done in coherent polarisation-sensitive receivers. We have attributed these changes in the state of polarisation to amplitude and phase fluctuations deteriorating the performance of polarisation sensitive receivers whereas they would not affect the performance of a polarisation insensitive receiver. Although the impact of these nonlinearities can be partially constrained by means of the optimisation of the carrier phase estimation, we have shown that they may strongly limit the system performance. I have also given further insight on the interaction between PMD and

nonlinearities in the context of polarisation-multiplexed coherent systems. Unlike to current 10-Gb/s systems, I have proved that, when distributed, PMD often turns out to be beneficial by reducing these nonlinear-induced penalties, provided linear PMD is compensated for at the receiver side. Digital signal processing in coherent receivers can easily perform this compensation. On the contrary, when lumped in the line, PMD may increase the peak-to-peak power average ratio. This in turn increases the detrimental impact of nonlinearities encountered further in the transmission line.

I have also compared two different coherent solutions which appear as good candidates to upgrade massively deployed 10-Gb/s networks at 40 Gb/s, namely PDM-QPSK and PDM-BPSK. The choice of an adequate modulation format is always a trade-off between characteristics such as OSNR requirement, spectral width and tolerance to narrow filtering, nonlinear tolerance, PMD tolerance and transponder complexity. Hence, one cannot say that one format is better in all characteristics. We have confirmed experimentally that the two solutions benefit from the high noise sensitivity of coherent detection, the potential of compensating for linear impairments by means of suitable digital signal processing, and exhibit the same information spectral efficiency of 0.8 b/s/Hz. PDM-QPSK has a lower symbol rate (a quarter of the bit rate) and thus the constraints on high speed electronics and analog-to-digital converters are relaxed. It is therefore potentially more cost-effective. Nevertheless, as I have emphasized, PDM-QPSK at 40 Gb/s is severely impacted by cross nonlinearities, especially in dispersion-managed systems. PDM-BPSK in turn has a double symbol rate compared to PDM-QPSK, but we have shown that it is much more tolerant against nonlinearities, even stemming from 10-Gb/s channels. Thus, PDM-QPSK could be better suited for cost-effective solutions reaching short distance, especially over uncompensated links. PDM-BPSK in turn is likely to be the most suitable solution for terrestrial systems covering long distances despite its higher requirements in bandwidth and sampling rate.

The picture changes when moving to 100 Gb/s. The spectrum width of PDM-BPSK at 100 Gb/s is of 100 GHz, making its compatibility with the standard 50-GHz grid very challenging. 100 Gb/s PDM-QPSK in turn has a spectrum width of 56 GHz (considering the main lobe width from zero to zero) and is consequently able to fit in the standard channel spacing. It allows therefore a tenfold increase of the total transmitted capacity compared with current 10-Gb/s systems, reaching an information spectral density of 2 b/s/Hz. On top of that, we have highlighted that moving to higher symbol rates increases the tolerance to cross nonlinearities. Hence, our results show that the superior nonlinear tolerance of PDM-QPSK at 100 Gb/s enables to offset the 4-dB higher OSNR requirements w.r.t. 40 Gb/s when upgrading legacy systems with 10-Gb/s channels.

I would also stress here that coherent technology is evolving very fast. When I began this work, three years ago, first experimental demonstrations at 40 Gb/s using coherent detection were still very recent. On the contrary, nowadays, the deployment of coherent-based solutions have already began at 40 Gb/s while field trials, as the one we have conducted together with the colleagues from the business unit and which is reported in section 5.5, prove the suitability of 100 Gb/s to upgrade legacy networks and demonstrate the actual interest of carriers onto 100 Gb/s solutions.

Finally, we have identified that the maximum reach of coherent systems is mainly limited by nonlinearities. Two main options appear to partially overcome this

limitation: the design of dedicated systems in green field and the nonlinear mitigation through digital signal processing. Some recent works have demonstrated promising results with digital nonlinear compensation but with single channel. On the contrary, specific system design has revealed very effective to increase the reach of WDM coherent systems. In this context, the use of uncommon large effective area fibres can reduce the strength of nonlinearities while hybrid Raman/EDFA or Raman-only amplification reduces the noise figure of the amplifiers providing a better OSNR at the end of the transmission line. The fact that there is much room for research in the field of optical fibres, even multi-mode fibres which have a larger effective area, and in the field of digital equalisation opens the door for the optimism that even longer distances with higher capacities could be reached.



# Appendices

## A. Bit error ratio and $Q^2$ factor

The performance of an optical transmission system is often measured in terms of bit error ratio (BER) or  $Q^2$ -factor. The BER is defined as the ration between the number of errors found after decoding,  $N_{errors}$ , and number of detected bits,  $N_{tot}$ :

$$BER = \frac{N_{errors}}{N_{tot}} \quad (A.1)$$

Hence, the lower the BER, the better the system behaves. The most important feature of a digital transmission system is indeed the ability to operate with a sufficient small BER. A transmission is considered “error-free” when BER is smaller than  $10^{-13}$  after propagation.

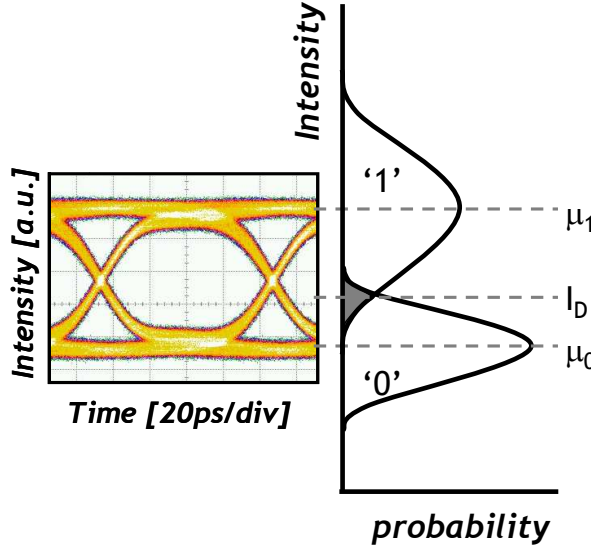


*Fig. A.1: Probability symbol density of a noisy OOK signal*

The Q-factor was first defined to estimate the performance of OOK systems. Fig. A.1 depicts the probability density of the two symbols of an OOK signal, ‘0’ and ‘1’. One can express the optimal decision threshold on a signal degraded by ASE:

$$I_D = \frac{\sigma_0\mu_1 + \sigma_1\mu_0}{\sigma_0 + \sigma_1} \quad (A.2)$$

where  $\mu_0$  and  $\mu_1$  are the mean photocurrents of the symbol ‘0’ and ‘1’, respectively; and  $\sigma_0$  and  $\sigma_1$  are the standard deviations. The Q factor is then defined as:

$$Q = \frac{\mu_1 - \mu_0}{\sigma_0 + \sigma_1} \quad (A.3)$$

The photocurrent of an ideal photodiode can be approximated with a Gaussian distribution for high enough OSNR ( $>10$  dB) and low ISI. Under these assumptions, Q-factor can be used to estimate the BER following the expression [196]:

$$BER = \frac{1}{2} \operatorname{erfc} \left( \frac{Q}{\sqrt{2}} \right) \quad (A.4)$$

where  $\operatorname{erfc}(x)$  is the complementary error function, which for a Gaussian distribution is:

$$\operatorname{erfc}(x) = \int_x^{\infty} \exp(-y^2) \quad (A.5)$$

Throughout this thesis, Q factor is not used to estimate BER but it is used as a conversion of a *measured* BER and expressed in [dB], so as:

$$Q^2 \text{factor} = 20 \log_{10} \left[ \sqrt{2} \operatorname{erfc}^{-1}(2BER) \right] \quad (A.6)$$

$Q^2$  factor in [dB] has the advantage of being proportional to the OSNR. 1-dB increase in OSNR results in  $\sim 1$  dB increase in  $Q^2$  factor, as shown in Fig. 3.4. Fig. A.2 shows the relation between the BER and the  $Q^2$  factor as well as the correspondence of several usual values.

BER	$Q^2$ factor[dB]
$1 \cdot 10^{-2}$	7.33
$4 \cdot 10^{-3}$	8.47
$1 \cdot 10^{-3}$	9.80
$1 \cdot 10^{-4}$	11.40
$1 \cdot 10^{-5}$	12.60
$1 \cdot 10^{-6}$	13.54
$1 \cdot 10^{-7}$	14.32
$1 \cdot 10^{-8}$	14.98
$1 \cdot 10^{-9}$	15.56

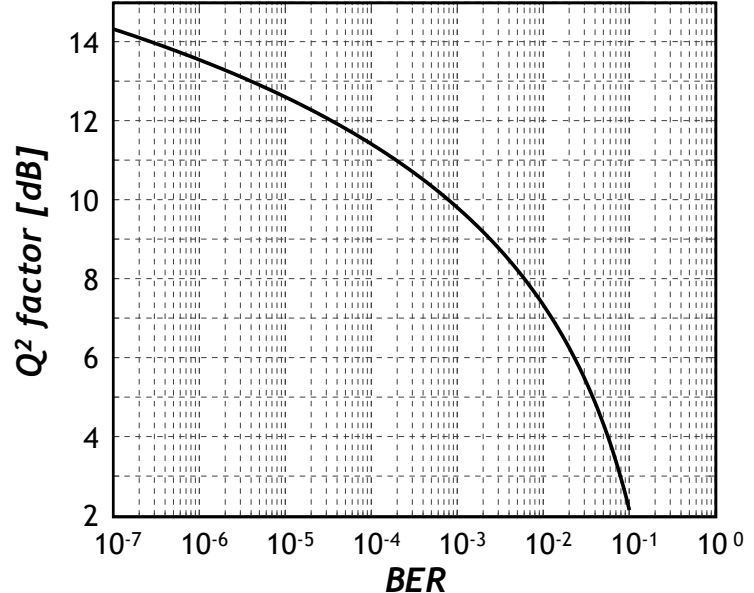


Fig. A.2: Relation between bit error ratio and  $Q^2$  factor.

## B. Capacity increase of unrepeatered submarine systems using 100 Gb/s coherent PDM-QPSK

Unrepeatered transmission systems aim mainly to provide high capacity over long distances with no active elements within the line, consequently reducing the line complexity and the overall system cost. Following this purpose some experiments have already demonstrated high capacities as 2.56 Tb/s [197] over 230 km and 1.28 Tb/s [198] over 402 km with 64 and 32 channels at 40 Gb/s, respectively. The evolution towards 100 Gb/s per channel in unrepeatered systems has been proposed by Du et al. [199] with only 3 channels and over a relatively modest 300-km long distance. Moreover, the total transmitted capacity achieved in this experiment was lower compared with [197] and [198].

We propose to take full advantage of coherent detection and to combine it with PDM-QPSK at 100 Gb/s over an unrepeatered system for the first time, to the best of our knowledge. We transmit a WDM comb of 26 channels over a 50 GHz grid, yielding a spectral efficiency of 2 b/s/Hz, achieving a transmission of a total capacity of 2.6 Tbit/s, over a 401-km long distance over the FEC limit.

### B.1 Experimental set up

Depicted in Fig. B.1, the bed consists of 26 channels spaced by 50 GHz and modulated with 100 Gb/s PDM-QPSK, according to Fig. 4.1. DFB lasers range from 1552.1 nm to 1562.2 nm. The resulting multiplex is passed through a dual-stage EDFA incorporating dispersion compensating module (DCM) which compensates 20% of the total chromatic dispersion of the link. Afterwards the signal is boosted through a high power Erbium-Ytterbium doped fibre amplifier (EYDFA) which delivers up to 30 dBm total power.

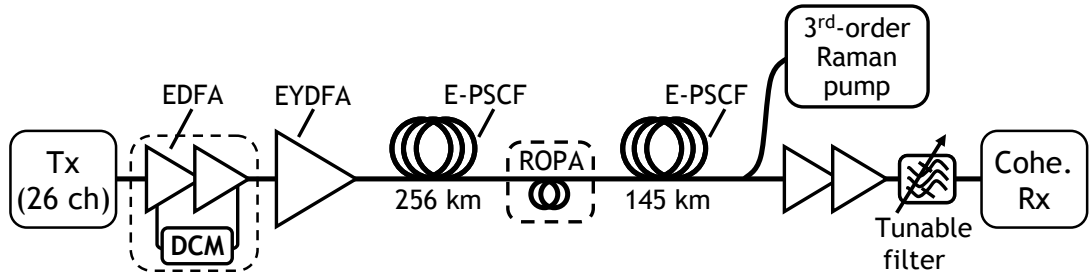


Fig. B.1: Experimental set up

The link consists of two sections of enhanced-pure silica core fibre (E-PSCF) with  $110 \mu\text{m}^2$  effective area separated by a remote optically pumped amplifier (ROPA). The first one is 246-km long and a second one referred to as remote of 145-km long. The total link loss is 66.9 dB at 1560 nm and the total cumulated chromatic dispersion is +8260 ps/nm.

The ROPA is counter-directionally pumped by a Raman fibre laser located at the receiver side and set to deliver 5.5 W at 1276 nm. As described in Fig. B.2, the

energy is transferred progressively from 1276 nm to a wavelength band around 1360 nm and from 1360 nm to a band around 1480 nm, through second-order Raman amplification. Thus, the optical power at 1480 nm is amplified within the fibre of the remote section achieving a maximum around 25 km away from the end of the link. The pump power provided to the ROPA is 5.5 mW (7.4 dBm) for 145-km length remote section. Moreover, signal is further amplified in the remote section fibre thanks to another Raman energy transfer (third-order) from the ROPA pump at 1480 nm to the C-band. The total signal gain provided by this third-order Raman pump is 39 dB. At the receiver end, each channel is isolated from the rest of the multiplex by a tuneable filter and sent to the coherent receiver.

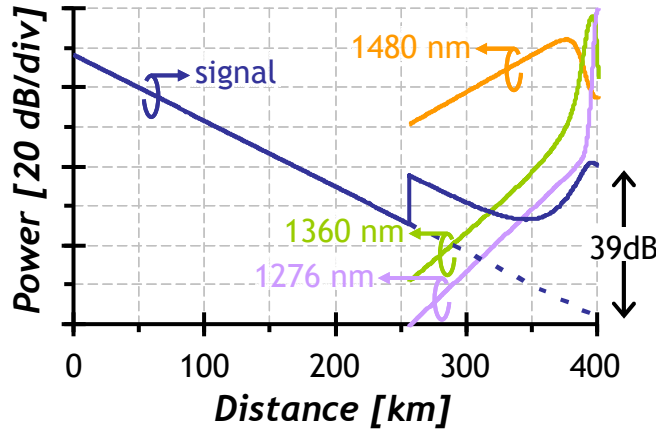
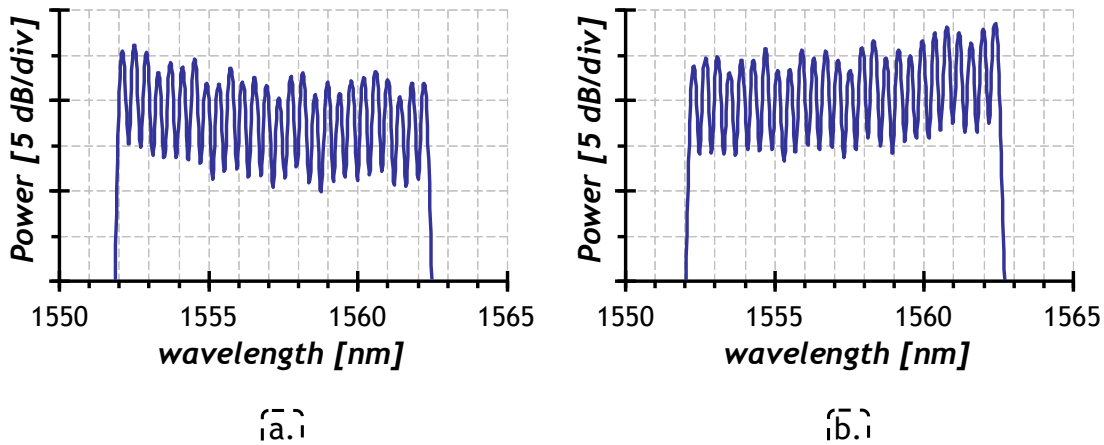


Fig. B.2: Evolution of signal power per wavelength channel and pumps power (1276 nm, 1356 nm and 1480 nm) along the link.

## B.2 Results

The power of all channels is not identical at the input of the link. Indeed, the injected power of channels located at shorter wavelengths is higher than the power of the channels at longer wavelengths. Thus, the spectrum is tilted by 1.8 dB as it can be seen in Fig. B.3-a. The tilt at the input of the link compensates for both inter-channel Raman effect arising in the link fibre and tilted gain spectrum of the remote section [198]. Some remaining tilt is observed on the channel spectrum at the output of the link, as seen in Fig. B.3-b. Nevertheless, the measured OSNR of the channels was well equalised with mean value of 17.1 dB/0.1 nm.



*Fig. B.3: Measured channel spectra (res.=0.2 nm) at link input (a) and output (b) of the link.*

The measured  $Q^2$  factors for the 26 channels are plotted in Fig. B.4. Virtually constant  $Q^2$  factor performance of all channels is obtained thanks to the tilt applied at the input of the link. The average  $Q^2$  factor is 9.1 dB, while the best is 9.5 dB. The worst performing channel gives a  $Q^2$  factor of 8.8 dB, i.e. above the FEC limit yielding  $10^{-13}$  BER after correction, assuming today's commercial 10 Gbit/s FEC techniques with 7% overhead. This would not provide enough system margins for field deployment which requires a performance at least 2-dB above the FEC limit. Repair and aging margins could be obtained by reducing reach by a few tens of kilometres or reducing the number of transmitted channels.

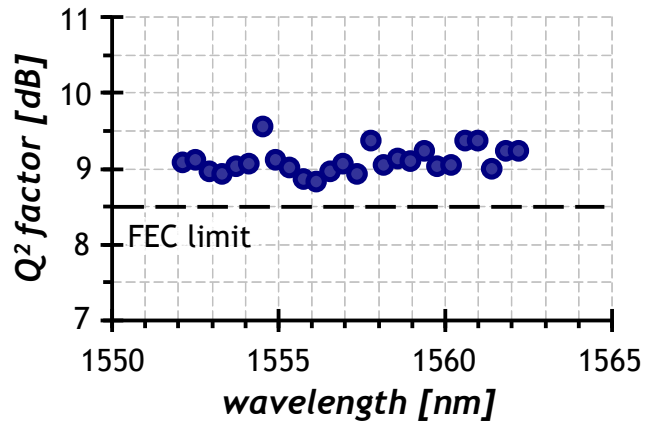


*Fig. B.4: Measured performance of the 26 channels after 401-km long unrepeated transmission.*

### B.3 Summary

A data flow transmission at 2.6 Tbit/s, over a 401-km long unrepeated system, has been experimentally demonstrated. This has been achieved with 26 PDM-QPSK channels at 100 Gb/s detected in a coherent receiver. Channels were spaced by 50 GHZ yielding an information spectral density of 2 bit/s/Hz. Besides, system amplification was performed by a conventional high power booster and a third order remote optically pumped amplifier.

In a practical deployment system, repair and aging margins could be obtained by reducing reach by a few tens of kilometres or reducing the number of transmitted channels. Anyhow, this experiment demonstrates the suitability of coherent solutions for the next generation of unrepeated systems carrying very-high capacities over relatively long distances.



# Bibliography

- [1] Institute of Electrical and Electronics Engineers, “An Overview: The Next Generation of Ethernet,” IEEE 802.3 Higher Speed Study Group–Tutorial, IEEE 802 Plenary, Atlanta, GA, Nov. 12, 2007,  
<[www.ieee802.org/3/hssg/public/nov07/HSSG\\_Tutorial\\_1107.zip](http://www.ieee802.org/3/hssg/public/nov07/HSSG_Tutorial_1107.zip)>.
- [2] K. C. Kao and G. A. Hockham, “Dielectric-Fiber Surface Waveguides for Optical Frequencies,” in *Proc. of Institution of Electrical Engineers*, vol. 113, no. 7, pp. 1151–1158, Jul. 1966.
- [3] S. R. Nagel, J. B. MacChesney, and K. L. Walker, “An Overview of the Modified Chemical Vapor Deposition (MCVD) Process and Performance,” *Journal of Quantum Electronics*, vol. 18, no. 4, pp. 459–476, Apr. 1982.
- [4] E.-G. Neumann, *Single-Mode Fibers*. Springer Verlag, 1988.
- [5] Y. Chigusa, Y. Yamamoto, T. Yokokawa et al., “Low-loss Pure-Silica-Core Fibers and Their Possible Impact on Transmission Systems,” *Journal of Lightwave Technology*, vol. 23, no. 11, Nov. 2005.
- [6] C. F. Bohren and D. Huffman, *Absorption and Scattering of Light by Small Particles*. New York, NY, U.S.A:John Wiley, 1983.
- [7] S. Sudo, M. Kawachi, T. Edahiro, T. Izawa, T. Shioda, and H. Gotoh, “Low-OH content optical fiber fabricated by vapour-phase axial-deposition method,” *Electronics Letters*, vol. 14, 1978.
- [8] K. H. Chang, D. Kalish, and M. Pearsall, “New Hydrogen Aging Loss Mechanism in the 1400 nm Window,” in *Proc. Optical Fiber Communication Conference OFC 1999*, San Diego, U.S.A., Feb. 1999, post-deadline paper PD22.
- [9] *ITU-T G.Sup39, Optical System Design and Engineering Considerations*, Feb. 2006.
- [10] K. Nagayama, M. Kakui, M. Matsui, T. Saitoh, and Y. Chigusa., “Ultra-Low-Loss (0.1484 dB/km) Pure Silica Core Fibre and Extension of Transmission Distance,” *Electronic Letters*, vol. 38, no. 20, Sep. 2002.
- [11] Mathieu Lefrançois, *Étude de technologies avancées pour l'optimisation des systèmes de transmission optique multiplexés en longueur d'onde au débit de 40 Gbit/s*, PhD dissertation, Université Paris-sud, 2007.
- [12] M. Salsi, H. Mardoyan, P. Tran, C. Koebele, E. Dutisseuil, G. Charlet, and S. Bigo “155x100Gbit/s coherent PDM-QPSK transmission over 7,200km” in *Proc. of European Conference on Optical Communication ECOC 2009*, Vienna, Austria, Sept. 2009, paper PD2.5.
- [13] G. P. Agrawal, *Fiber-Optic Communication Systems*, 3rd ed. John Wiley & Sons, 2002.

- [14] G. Keiser, *Optical Fiber Communications*, third edition ed. McGraw-Hill, 2000.
- [15] G. P. Agrawal, *Nonlinear Fiber Optics*, 3rd ed. Academic Press, 2001.
- [16] E.-G. Neumann, *Single Mode Fibers I: Fundamentals*. Springer Verlag, 1988.
- [17] S. Ten and M. Edwards, “An introduction to fundamentals of PMD in fibers,” white paper, available from:  
[<www.corning.com/WorkArea/downloadasset.aspx?id=7827>](http://www.corning.com/WorkArea/downloadasset.aspx?id=7827).
- [18] C. D. Poole, J. H. Winters, and J. A. Nagel, “Dynamical equation for polarization dispersion”, *Optics Letters*, vol. 16, issue 6, pp 372-374, 1991.
- [19] Yann Frignac, *Contribution à l'ingenierie des systems de transmission terrestres sur fibre optique utilisant le multiplexage en longueur d'onde de canaux modulés au débit de 40 Gb/s*, PhD dissertation, École Nationale Supérieur des Télécommunications, 2003.
- [20] G. V. de Faria, M. R. Jimenez, and J. P. von der Weid, “PMD Variations From Factory to Field in OPGW Cabled Fibers,” *Journal of Lightwave Technology*, vol. 18, no. 1, pp. 250–252, Jan. 2006.
- [21] H. Kogelnik and P. J. Winzer, “PMD Outage Probabilities Revisited,” in *Proc. of Optical Fiber Communication Conference OFC 2007*, Anaheim, USA, Mar. 2007, paper OTuN3.
- [22] C. Antonelli and A. Mecozzi, “Theoretical Characterization and System Impact of the Hinge Model of PMD,” *Journal of Lightwave Technology*, vol. 24, no. 11, pp. 4064–4074, Nov. 2006.
- [23] I. P. Kaminow, T. L. Koch, *Optical Fiber Telecommunications IIIA & IIIB*, Academic Press, 1997.
- [24] J. Damask, *Polarization optics in telecommunications*. Springer: New York, 2005.
- [25] H.-C. Ji, J. H. Lee, H. Kim, P. K. J. Park, and Y. C. Chung, “Effect of PDL-induced coherent crosstalk on polarization-division-multiplexed direct detection systems,” *Optics Express*, vol. 17, no. 3, pp. 1169-1177, 2009.
- [26] Z. Wang1, C. Xie, and X. Ren, “PMD and PDL impairments in polarization division multiplexing signals with direct detection,” *Optics Express*, vol. 17, no. 10, pp. 7993-8004, 2009.
- [27] D. Marcuse, C. R. Menyuk, and P. K. A. Wai, “Application of the Manakov-PMD Equation to Studies of Signal Propagation in Optical Fibers with Randomly Varying Birefringence,” *Journal of Lightwave Technology*, vol. 15, no. 9, pp. 1735-1746, Sept. 1997.
- [28] E. L. Buckland and J. W. Boyd, “Electrostrictive contribution to the intensity-dependent refractive index of optical fibers,” *Optics Letters*, vol. 21, no. 15, pp. 1117–1119, Aug. 1996.
- [29] S. V. Chernikov and J. R. Taylor, “Measurement of normalization factor of n<sub>2</sub> for random polarization in fiber,” *Optics Letters*, vol. 21, no. 19, pp. 1559–1561, Oct. 1996.

- [30] L. F. Mollenauer, R. H. Stolen, and J. P. Gordon, “Experimental Observation of Picosecond Pulse Narrowing and Solitons in Optical Fibers,” *Phys. Rev. Lett.*, vol. 44, no. 13, p. 1095–1098, Sep. 1980.
- [31] M. Winter, C.-A. Bunge, D. Setti, and K. Petermann, “A Statistical Treatment of Cross-Polarization Modulation in DWDM Systems,” *Journal of Lightwave Technology*, vol. 27, no. 17, pp. 4064–4074, Sept. 2009.
- [32] R. S. Luís and A. V. T. Cartaxo, “Analytical Characterization of SPM Impact on XPM-Induced Degradation in Dispersion-Compensated WDM Systems,” *Journal of Lightwave Technology*, vol. 23, no. 3, pp. 1503–1513, Mar. 2005.
- [33] G. Bellotti, M. Varani, C. Francia, and A. Bononi, “Intensity Distortion Induced by Cross-Phase Modulation and Chromatic Dispersion in Optical-Fiber Transmissions with Dispersion Compensation,” *Photonics Technology Letters*, vol. 10, no. 12, pp. 733–736, Dec 1998.
- [34] Ting-Kuang Chiang, N. Kagi, T. Fong, M. Marhic, and L. Kazovsky, “Cross-phase modulation in dispersive fibers: theoretical and experimental investigation of the impact of modulation frequency,” *Photonics Technology Letters*, vol. 6, no. 6, pp. 733–736, June 1994.
- [35] L. Prigent and J.-P. Hamaide, “Measurement of Fiber Nonlinear Kerr Coefficient by Four-Wave Mixing,” *Photonics Technology Letters*, vol. 5, no. 9, pp. 733–736, Sept 1993.
- [36] I. P. Kaminow and T. Li, *Optical Fiber Telecommunication, IVA & IVB*, Academic press, 2002.
- [37] R.-J. Essiambre, B. Mikkelsen, and G. Raybon, “Intra-Channel Cross-Phase Modulation and Four-Wave Mixing in Highspeed TDM Systems,” *Electronic Letters*, vol. 35, no. 18, p. 1576–1578, Sep. 1999.
- [38] I. Shake, K. Takara, S. Kawanishi, and Y. Yamabayashi, “Influence of Inter-Bit Four-Wave Mixing in Optical TDM Transmission,” *Electronic Letters*, vol. 34, no. 16, pp. 1600–1601, Aug. 1998.
- [39] A. Mecozzi, C. B. Clausen, M. Shtaif et al., “Cancelation of Timing and Amplitude Jitter in Symmetric Links using Highly Dispersed Pulses,” *Photonics Technology Letters*, vol. 13, no. 5, p. 445–447, May 2001.
- [40] A. Chowdhury, G. Raybon, R.-J. Essiambre, and C. R. Doerr, “Optical Phase Conjugation in a WDM CSRZ Pseudo-Linear 40 Gb/s System for 4,800 km Transmission,” in *Proc. of European Conference on Optical Communication ECOC 2004*, Stockholm, Sweden, Sept. 2004, post-deadline paper Th4.5.6.
- [41] A. Chowdhury, G. Raybon, R.-J. Essiambre et al., “Compensation of Intrachannel Nonlinearities in 40-Gb/s Pseudolinear Systems using Optical-Phase Conjugation,” *Journal of Lightwave Technology*, vol. 23, no. 1, pp. 172–177, Jan. 2005.
- [42] B.C. Collings, and L. Boivin, “Nonlinear polarization evolution induced by cross-phase modulation and its impact on optical transmission systems”, *Photonics Technology Letters*, vol. 12, no 11, p. 1582-1584, Nov. 2000.

- [43] J. P. Gordon and L. F. Mollenauer, “Phase Noise in Photonic Communications Systems Using Linear Amplifiers,” *Optics Letters*, vol. 15, no. 23, pp. 1351–1353, Dec. 1990.
- [44] V. S. Grigoryan, M. Shin, P. Devgan et al., “SOA-based Regenerative Amplification of Phase-Noise-Degraded DPSK signals: Dynamic Analysis and Demonstration,” *Journal of Lightwave Technology*, vol. 24, no. 1, pp. 135–142, Jan. 2006.
- [45] S. L. Jansen, D. van den Borne, C. C. Monsalve et al., “Reduction of Gordon-Mollenauer Phase Noise by Mid-Link Spectral Inversion,” *Photonics Technology Letters*, vol. 17, no. 4, pp. 923–925, Jan. 2005.
- [46] J. Hansryd, J. van Howe, and C. Xu, “Experimental Demonstration of Nonlinear Phase Jitter Compensation in DPSK Modulated Fiber Links,” *Photonics Technology Letters*, vol. 17, no. 1, pp. 232–234, Jan. 2005.
- [47] C. Xu and X. Liu, “Postnonlinearity Compensation with Data-driven Phase Modulators in Phase-Shift Keying Transmission,” *Optics Letters*, vol. 27, no. 18, pp. 1619–1621, Sep. 2002.
- [48] K.-P. Ho and J. M. Kahn, “Electronic Compensation Technique to Mitigate Nonlinear Phase Noise,” *Journal of Lightwave Technology*, vol. 22, no. 5, pp. 779–783, Mar. 2004.
- [49] L. Bangyuan Du, and A. J. Lowery, “Practical XPM Compensation Method for Coherent Optical OFDM Systems,” *IEEE Photonics Technology Letters*, vol. 13, no. 5, pp. 320–322, May 2001.
- [50] A. Bononi, P. Serena and N. Rossi, “Nonlinear signal–noise interactions in dispersion-managed links with various modulation formats,” *Optical Fiber Technology* (2009), doi:10.1016/j.yofte.2009.11.001.
- [51] P. M. Krumrich, R. E. Neuhauser, and G. Fischer, “Experimental Comparison of Raman Thresholds of Different Transmission Fibre Types,” in *Proc. of European Conference on Optical Communication ECOC 2000*, Munich, Germany, Sept. 2000, paper 4.4.1.
- [52] A. R. Chraplyvy, “Limitations on Lightwave Communications Imposed by Optical-Fiber Nonlinearities,” *Journal of Lightwave Technology*, vol. 8, no. 10, pp. 1548–1557, Oct 1990.
- [53] K.-P. Ho, “Statistical Properties of Stimulated Raman Crosstalk in WDM Systems,” *Journal of Lightwave Technology*, vol. 18, no. 7, pp. 915–921, Jul. 2000.
- [54] P. J. Winzer and R.-J. Essiambre, “Advanced Modulation Formats for High-Capacity Optical Transport Networks,” *Journal of Lightwave Technology*, vol. 24, no. 12, pp. 4064–4074, Dec. 2006.
- [55] B. Huissoon, R. J.W. Jonker, P. K. van Bennekom et al., “Cost-Effective Up to 40 Gb/s Transmission Performance of 1310 nm Directly Modulated Lasers for Short- to Medium-Range Distances,” *Journal of Lightwave Technology*, vol. 23, no. 3, pp. 1116–1125, Mar. 2005.

- [56] U. Troppenz, J. Kreissl, W. Rehbein et al., “40 Gb/s Directly Modulated InGaAsP Passive Feedback Laser,” in *Proc. of European Conference on Optical Communication ECOC 2006*, Cannes, France, Sep. 2006, post-deadline paper Th4.5.5.
- [57] Y. Yu, R. Lewen, S. Irmscher et al., “80-Gb/s ETDM Transmitter with a Traveling-Wave Electroabsorption Modulator,” in *Proc. of European Conference on Optical Communication ECOC 2005*, Glasgow, United Kingdom, Sept. 2005, paper OWE1.
- [58] A. H. Gnauck and P. J. Winzer, “Optical Phase-Shift-Keyed Transmission,” *Journal of Lightwave Technology*, vol. 23, n°1, pp. 115-130, Jan. 2005.
- [59] L. Mach, “Über einen Interferenzrefraktor,” *Zeitschr. für Instrumentenkunde*, vol. 12, pp. 89–93, 1892.
- [60] L. Zehnder, “Ein neuer Interferenzrefraktor,” *Zeitschr. für Instrumentenkunde*, vol. 11, pp. 275–285, 1891.
- [61] E.L. Wooten, K.M. Kiss, A. Yi-Yan, E.J. Murphy, D.A. Lafaw, P.F. Hallemeier, D. Maack, D.V. Attanasio, D.J. Fritz, G.J. McBrien, D.E. Bossi, “A review of lithium niobate modulators for fiber-optic communications systems,” *Journal of Selected Topics in Quantum Electronics*, vol. 6, no. 1, pp. 69-82, Jan. 2000.
- [62] W. D. Grover, “Forward Error Correction in Dispersion-Limited Lightwave Systems,” *Journal of Lightwave Technology*, vol. 6, no. 5, pp. 643–654, May 1988.
- [63] K.-P. Ho and C. Lin, “Performance Analysis of Optical Transmission System with Polarization-Mode Dispersion and Forward Error Correction,” *Journal of Lightwave Technology*, vol. 9, no. 9, pp. 1288–1290, Sept. 1997.
- [64] *ITU-T G.975.1, Forward Error Correction for High Bit Rate DWDM Submarine Systems*, Feb. 2004.
- [65] T. Mizuuchi, “Recent Progress in Forward Error Correction and its Interplay with Transmission Impairments,” *Journal of Selected Topics in Quantum Electronics*, vol. 12, no. 4, pp. 544–554, Jul-Aug. 2006.
- [66] J. G. Proakis and D. K. Manolakis, *Digital Signal Processing*, 4th ed. Prentice Hall, 2006.
- [67] A. H. Gnauck, X. Liu, X. Wei, D. M. Gill, and E. C. Burrows, “Comparison of Modulation Formats for 42.7-Gb/s Single-Channel Transmission Through 1980 km of SSMF,” *Photonics Technology Letters*, vol. 16, no. 3, p. 909–911, Mar. 2004.
- [68] H. Sunnerud, M. Karlsson, and P. A. Andrekson, “A Comparison Between NRZ and RZ Data Formats with Respect to PMD-Induced System Degradation,” *IEEE Photonics Technology Letters*, vol. 13, no. 5, pp. 448–450, May 2001.
- [69] A. Klekamp, R. Dischler, and W. Idler, “Impairments of bit-to-bit alternate polarization on non-linear threshold, CD and DGD tolerance of 43

- Gb/s ASK and DPSK formats,” in proc. *Proc. of Optical Fiber Communication Conference OFC 2005*, March 2005, paper OFN3.
- [70] E. A. Golovchenko, N. S. Bergano, C. R. Davidson, and A. N. Pilipetskii, “Modeling vs. Experiments of 16 x 10 Gbit/s WDM Chirped RZ Pulse Transmission over 7500 km,” in *Proc. of Optical Fiber Communication Conference OFC 1999*, San Diego, CA, U.S.A., Feb. 1999, paper ThQ3.
- [71] B. Bakhshi, M. Vaa, E. A. Golovchenko, W.W. Patterson, R.L. Maybach, and N.S. Bergano, “Comparison of CRZ, RZ and NRZ Modulation Formats in a 64 x 12.3 Gb/s WDM Transmission Experiment over 9000 km,” in *Proc. of Optical Fiber Communication Conference OFC 2001*, Anaheim, CA, U.S.A., Mar. 2001, paper WF4.
- [72] F. Seguin and F. Gonthier, “Tunable All-Fiber Delay-Line Interferometer for DPSK Demodulation,” in *Proc. of Optical Fiber Communication Conference OFC 2005*, Anaheim, CA, U.S.A., Mar. 2005, paper OFL5.
- [73] J. Hsieh, C. Ai, V. Chien et al., “Athermal Demodulator for 42.7-Gb/s DPSK Signals,” in *Proc. of European Conference on Optical Communication ECOC 2005*, Glasgow, United Kingdom, Sep. 2005, paper Th1.5.6.
- [74] L. Christen, Y. K. Liz'e, S. Nuccio et al., “Fiber Bragg Grating Balanced DPSK Demodulation,” in *Proc. IEEE/LEOS Annual Meeting*, Montreal, QC, Canada, Nov. 2006, paper WP2.
- [75] M. Kroh, G. Unterbörsch, G. Tsianos, R. Ziegler, A.G. Steffan, H.-G. Bach, J. Kreissl, R. Kunkel, G.G. Mekonnen, W. Rehbein, D. Schmidt, R. Ludwig, K. Petermann, J. Bruns, T. Mitze, K. Voigt, and L. Zimmermann, “Hybrid Integrated 40 Gb/s DPSK Receiver on SOI,” in *Proc. of Optical Fiber Communication Conference OFC 2009*, San Diego, CA, U.S.A., Mar. 2009, paper OMK3.
- [76] D. Penninckx, H. Bissessur, P. Brindel, E. Gohin, and F. Bakhti, “Optical differential phase shift keying (DPSK) direct detection considered as a duobinary signal,” in *Proc. of European Conference on Optical Communication ECOC 2001*, Amsterdam, Nederland, Sept. 2001, paper We.P.40.
- [77] P.J. Winzer, S. Chandrasekhar, and Hoon Kim, “Impact of filtering on RZ-DPSK reception,” *Photonics Technology Letters*, vol. 15, no. 6, pp. 840–842, Jun 2003.
- [78] I. Lyubomirsky and C.-C. Chien, “DPSK demodulator based on optical discriminator filter,” *Photonics Technology Letters*, vol. 17, pp. 492–494, Feb. 2005.
- [79] P. J. Winzer and R.-J. Essiambre, “Advanced Optical Modulation Formats,” in *Proc. of IEEE*, vol. 94, no. 5, pp. 952–985, Jun. 2006.
- [80] C. Wree, J. Leibrich, and W. Rosenkranz, “RZ-DQPSK format with high spectral efficiency and high robustness towards fiber nonlinearities,” in *Proc. of European Conference on Optical Communication ECOC 2002*, Copenhagen, Denmark, paper 9.6.6, Sept. 2002.

- [81] R. A. Griffin, R. I. Johnstone, R. G. Walker, J. Hall, S. D. Wadsworth, K. Berry, A. C. Carter, M. J. Wale, J. Hughes, P. A. Jerram, and N. J. Parsons, “10 Gb/s optical differential quadrature phase shift key (oDQPSK) transmission using GaAs/AlGaAs integration,” in *Proc. of Optical Fiber Communication Conference OFC 2002*, Anaheim, CA, U.S.A., Feb. 2002, p. PD FD6.
- [82] G. Charlet, P. Tran, H. Mardoyan, T. Lefrancois, T. Fauconnier, F. Jorge, and S. Bigo, “151x43Gb/s transmission over 4,080km based on Return-to-Zero Differential Quadrature Phase-Shift-Keying,” in *Proc. of European Conference on Optical Communication ECOC 2005*, Glasgow, U.K., Sept. 2005, p. PD Th4.1.3.
- [83] F. Xiong, *Digital Modulation Techniques*, chap. 4, Artech House, 2002.
- [84] F. Vacondio, A. Ghazisaeidi, A. Bononi, and L. A. Rusch, DQPSK: When Is a Narrow Filter Receiver Good Enough?,” *Journal of Lightwave Technology*, vol. 27, no. 22, pp. 5106–5114, Nov 2009.
- [85] C. R. Doerr, L. Zhang, S. Chandrasekhar, and L. L. Buhl, “Monolithic DQPSK Receiver in InP with Low Polarization Sensitivity,” *Photonics Technology Letters*, vol. 19, no. 21, pp. 1765–1767, Nov. 2007.
- [86] Y. Nasu, M. Oguma, T. Hashimoto, H. Takahashi, Y. Inoue, H. Kawakami, and E. Yoshida, “Asymmetric Half-Wave Plate Configuration of PLC Mach-Zehnder Interferometer for Polarization Insensitive DQPSK Demodulator,” *Journal of Lightwave Technology*, vol. 23, no. 27, pp. 5348–5355, Dec 2009.
- [87] C. Wree, M. Serbay, and W. Rosenkranz, “Toward 1.6 b/s/Hz Spectral Efficiency by Strong Optical Filtering of RZ-DQPSK,” in *Proc. of European Conference on Optical Communication ECOC 2003*, Rimini, Italy, Sep. 2003, paper We4.P.126.
- [88] N. Yoshikane and I. Morita, “160 percent Spectrally-Efficient 5.12 Tb/s (64 x 85.4 Gb/s RZ-DQPSK) Transmission without Polarisation Demultiplexing,” in *Proc. of European Conference on Optical Communication ECOC 2004*, Stockholm, Sweden, Sep. 2004, post-deadline paper Th4.4.3.
- [89] A. H. Gnauck, P. J. Winzer, S. Chandrasekhar, and C. Dorrer, “Spectrally Efficient (0.8 b/s/Hz) 1-Tb/s (25 x 42.7Gb/s) RZ-DQPSK Transmission over 28 100-km SSMF Spans with 7 Optical Add/Drops,” in *Proc. of European Conference on Optical Communication ECOC 2004*, Stockholm, Sweden, Sep. 2004, post-deadline paper Th4.4.1
- [90] M. Serbay, J. Leibrich, W. Rosenkranz, T. Wuth, and C. Schulien, “Experimental Investigation of Asymmetrical Filtered 43 Gb/s RZ-DQPSK,” in *Proc. IEEE/LEOS Annual Meeting*, Montreal, QC, Canada, Nov. 2006, paper WH5.
- [91] G. Charlet, J. Renaudier, P. Brindel, P. Tran, H. Mardoyan, O. Bertran-Pardo, M. Salsi, and S. Bigo, “Performance Comparision of DPSK, P-DPSK, RZ-DQPSK and Coherent PDM-QPSK at 40Gb/s over Terrestrial Link,” in *Proc. of Optical Fiber Communication Conference OFC 2009*, San Diego, USA, Mar. 2009, paper JWA40.

- [92] B. Spinnler, N. Hecker-Denschlag, S. Calabro, C.J. Weiske, E.-D. Schmidt, D. van den Borne, G.-D. Khoe, H. de Waardt, R. Griffim, S. Wadsworth, "Nonlinear Tolerance of Differential Phase Shift Keying Modulated Signals Reduced by XPM," in *Proc. of Optical Fiber Communication Conference OFC 2004*, Los Angeles, CA, U.S.A., Mar. 2004, paper TuF3.
- [93] A. H. Gnauck, P. J. Winzer, and S. Chandrasekhar, "Hybrid 10/40-G Transmission on a 50-GHz Grid Through 2800 km of SSMF and Seven Optical Add-drops," in *Proc. of IEEE*, vol. 17, no. 10, p. 2203–2205, Oct. 2005.
- [94] C. Fürst, J.P-Elbers, M. Camera et al., "43 Gb/s RZ-DQPSK DWDM Field Trail over 1047 km with Mixed 43 Gb/s and 10.7 Gb/s Channels at 50 and 100 GHz Channel Spacing," in *Proc. of European Conference on Optical Communication ECOC 2006*, Cannes, France, Sep. 2006, post-deadline paper Th4.1.4.
- [95] M. Daikoku, I. Morita, and H. Tanaka, "Study of 40 Gbit/s Modulation Format to Upgrade 10 Gbit/s Longhaul Transmission Systems with 50 GHz Channel Spacings," in *Proc. of European Conference on Optical Communication ECOC 2006*, Cannes, France, Sep. 2006, paper Tu4.2.3.
- [96] G. Charlet, H. Mardoyan, P. Tran et al., "Nonlinear Interactions Between 10 Gb/s NRZ Channels and 40 Gb/s Channels with RZ-DQPSK or PSBT Format, over Low-dispersion Fiber," in *Proc. of European Conference on Optical Communication ECOC 2006*, Cannes, France, Sep. 2006, paper Mo3.2.6.
- [97] R. Calvani, R. Caponi, F. Cistemino, US Patent No. 4,817,206, appl. priority data: April 1986.
- [98] E. Dietrich, B. Enning, R. Gross, and H. Knupke, "Heterodyne transmission of a 560 Mbit/s optical signal by means of polarization shift keying", *Electronic Letters*, vol. 23, no. 8, pp 421-2, Dec. 1987.
- [99] J. S. G. Evangelides, L. F. Mollenauer, J. P. Gordon, and N. S. Bergano, "Polarization multiplexing with solitons," *Journal of Lightwave Technology*, vol. 10, no. 1, pp. 28–35, Jan. 1992.
- [100] K. Iwatsuki, K. Suzuki, S. Nishi, and M. Saruwatari, "80 Gb/s Optical Soliton Transmission over 80 km with Time/Polarization Division Multiplexing," *Photonics Technology Letters*, vol. 5, no. 2, pp. 245–248, Feb. 1993.
- [101] M. Nakazawa, K. Suzuki, E. Yoshida et al., "160 Gbit/s Soliton Data Transmission over 200km," *Electronic Letters*, vol. 31, no. 7, pp. 565–566, Mar. 1995.
- [102] H. G. Weber, S. Ferber, M. Kroh et al., "Single Channel 1.28 Tbit/s and 2.56 Tbit/s DQPSK Transmission," *Electronic Letters*, vol. 42, no. 3, pp. 178–179, Feb. 2006.
- [103] A. R. Chraplyvy, A. H. Gnauck, R. W. Tkach et al., "1-Tb/s Transmission Experiment," *Photonics Technology Letters*, vol. 8, no. 9, pp. 1264–1266, Sep. 1996.

- [104] K. Fukuchi, T. Kasamatsu, M. Morie, R. Ohhira, T. Ito, K. Sekiya, D. Ogasahara, and T. Ono, “10.92-Tb/s (273 x 40-Gb/s) Triple-Band/Ultra-Dense WDM Optical-Repeatered Transmission Experiment,” in *Proc. of Optical Fiber Communication Conference OFC 2001*, Anaheim, CA, U.S.A., Feb. 2001, post-deadline paper PD24.
- [105] S. Bigo, Y. Frignac, G. Charlet, W. Idler, S. Borne, H. Gross, R. Dischler, W. Poehlmann, P. Tran, C. Simonneau, D. Bayart, G. Veitih, A. Jourdan', J.-P. Hamaide, “10.2 Tbit/s (256 x 42.7 Gbit/s PDM/WDM) Transmission over 100km Teralight Fiber with 1.28 bits/s/Hz Spectral Efficiency,” in *Proc. of Optical Fiber Communication Conference OFC 2001*, Anaheim, CA, U.S.A., Mar. 2001, post-deadline paper PD25.
- [106] A. Sano, H. Masuda, T. Kobayashi, M. Fujiwara, K. Horikoshi, E. Yoshida, Y. Miyamoto, M. Matsui, M. Mizoguchi, H. Yamazaki, Y. Sakamaki, and H. Ishii, “69.1-Tb/s (432 x 171-Gb/s) C- and enxtended L—Band Transmission over 340 km using PDM-16-QAM modulation and digital coherent detection,” in *Proc. of Optical Fiber Communication Conference OFC 2010*, San Diego, CA, U.S.A., Mar. 2010, post-deadline paper PDPB4.
- [107] G. Charlet, M. Salsi, H. Mardoyan, P. Tran, J. Renaudier, S. Bigo, M. Astruc, P. Sillard, L. Provost, F. Cérou , “Transmission of 81 channels at 40Gbit/s over a transpacific-distance erbium-only link, using PDM-BPSK modulation, coherent detection, and a new large effective area fibre,” in *Proc. of European Conference on Optical Communication ECOC 2008*, Brussels, Belgium, Sep. 2008, paper Th.3.E.3.
- [108] G. Charlet, M. Salsi, J. Renaudier, O. Bertran-Pardo, H. Mardoyan, and S. Bigo, “Performance comparison of singly-polarized and polarisation-multiplexed coherent transmission at 10Gbauds under linear impairments,” in *Proc. of European Conference on Optical Communication ECOC 2007*, Berlin, Germany, Sept. 2007, paper We7.2.2.
- [109] P. J. Winzer and A. H. Gnauck, “112-Gb/s polarization-multiplexed 16-QAM on a 25-GHz WDM grid,” in *Proc. of European Conference on Optical Communication ECOC 2008*, Brussels, Belgium, Sept. 2008, paper We7.2.2.
- [110] S. L. Jansen, I. Morita, T. C. W. Schenk, and H. Tanaka, “121.9-Gb/s PDM-OFDM Transmission With 2-b/s/Hz Spectral Efficiency Over 1000 km of SSMF,” *Journal of Lightwave Technology*, vol. 27, no. 3, pp. 177–188, Feb. 2009
- [111] G. Charlet, M. Salsi, J. Renaudier, O. Bertran-Pardo, H. Mardoyan, and S. Bigo, “Performance comparison of singly-polarized and polarisation-multiplexed coherent transmission at 10Gbauds under linear impairments,” *Electronics Letters*, vol. 43, issue 20, Sept. 27, 2007.
- [112] G. Charlet, J. Renaudier, O. Bertran-Pardo, P. Tran, H. Mardoyan, and S. Bigo, “Performance comparison of singly-polarized and polarization-multiplexed at 10Gbaud under nonlinear impairments”, in *Proc. of Optical Fiber Communication Conference OFC 2008*, San Diego, USA, Feb. 2008, paper OthU8.

- [113] B. Nyman, M. Farries, C. Si, "Technology Trends in Dense WDM Demultiplexers, *Optical Fiber Technology*, vol. 7, no. 4, October 2001, Pages 255-274, ISSN 1068-5200, DOI: 10.1006/ofte.2001.0346.
- [114] E. Desurvire, J. R. Simpson, and P. C. Becker, "High-Gain Erbium-Doped Traveling-Wave Fiber Amplifier," *Optics Letters*, vol. 12, no. 11, pp. 888–890, Nov. 1987.
- [115] R. J. Mears, L. Reekie, M. Jauncey, and D. N. Payne, "Low-Noise Erbium-Doped Fiber Amplifier Operating at 1.54  $\mu\text{m}$ ," *Electronics Letters*, vol. 23, no. 19, pp. 1026–1028, Sep. 1987.
- [116] A. Einstein, "Zur Quantentheorie der Strahlung," *Physikalische Zeitschrift*, vol. 18, pp. 121–128, 1917.
- [117] E. Desurvire, *Erbium-Doped Fiber Amplifiers*. Wiley Interscience, 1994.
- [118] E. Desurvire, D. Bayart, B. Desthieux and S. Bigo, *Erbium-Doped Fiber Amplifiers. Device ans System Developements*, Wiley Interscience, 2002.
- [119] H.A. Haus, "The proper definition of noise figure of optical amplifiers," in *Proc. of Optical Fiber Communication Conference OFC 1999*, San Diego, USA, Feb. 1999, paper ThU3-1.
- [120] R. H. Stolen, E. P. Ippen, and A. R. Tynes, "Raman Oscillation in Glass Optical Waveguide," *Applied Physics Letters*, vol. 20, no. 2, pp. 62–64, Jan. 1972.
- [121] J. Hegarty, N. A. Olsson, and L. Goldner, "CW Pumped Raman Preamplifier in a 45 km-Long Fibre Transmission System Operating at 1.15 $\mu\text{m}$  and 1Gbit/s," *Electronics Letters*, vol. 21, no. 7, pp. 290–292, Mar. 1985.
- [122] M. N. Islam, *Raman amplifiers for telecommunications 1*, Springer Verlag, 2004.
- [123] A. Kobyakov, M. Vasilyev, S. Tsuda, G. Giudice, S. Ten, "Analytical model for Raman noise figure in dispersion-managed fibers," *IEEE Photonics Technology Letters*, vol. 15, no. 1, pp. 1041–1135, Jan. 2003.
- [124] S. Namiki and Y. Emori, "Ultrabroad-Band Raman Amplifiers Pumped and Gain-Equalized by Wavelength-Division-Multiplexed High-Power Laser Diodes," *Journal of Selected Topics in Quantum Electronics*, vol. 7, no. 1, pp. 3–16, Jan-Feb. 2001.
- [125] H. Masuda, E. Yamazaki, A. Sano, T. Yoshimatsu, T. Kobayashi, E. Yoshida, Y. Miyamoto, S. Matsouda, Y. Takatori, M. Mizoguchi, M. Mizoguchi, K. Okada, K. Okada, K. Hagimoto, T. Yamada, and S. Kamei, "13.5-Tb/s (135 x 111-Gb/s/ch) No-Guard-Interval Coherent OFDM Transmission over 6,248 km using SNR Maximized Second-order DRA in the Extended L-band," in *Proc. of Optical Fiber Communication Conference OFC 2010*, San Diego, USA, Feb. 2010, paper PDPB5.
- [126] A. M. Vengsarkar and W. A. Reed, "Dispersion-compensating single-mode fibers: Efficient designs for first- and second-order compensation," *Optics Letters*, vol. 18, no. 11, pp. 924 – 926, 1993.

- [127] L. Grüner-Nielsen, M. Wandel, P. Kristensen, C. Jørgensen, L. Vilbrad Jorgensen, B. Edvold, B. P'alsd'ottir, and D. Jakobsen, "Dispersion-compensating fibers," *Journal of Lightwave Technology*, vol. 23, no. 11, pp. 3566 – 3579, 2005.
- [128] F. Quellette, "Dispersion cancellation using linearly chirped bragg grating filters in optical waveguides," *Optics Letters*, vol. 12, no. 10, pp. 847 – 849, 1987.
- [129] T. Koch and R. Alferness, "Dispersion compensation by active predistorted signal synthesis," *Journal of Lightwave Technology*, vol. 3, no. 4, pp. 800 – 805, 1985.
- [130] A. Yariv, D. Fekete, and D. Pepper, "Compensation for channel dispersion by non-linear optical phase conjugation," *Optics Letters*, vol. 4, no. 2, pp. 52 – 54, 1979.
- [131] C. Lin, H. Kogelnik, and L. G. Cohen, "Optical-Pulse Equalization of Low-Dispersion Transmission in Single-Mode Fibers in the 1.3-1.7-um Spectral Region," *Optics Letters*, vol. 5, no. 11, pp. 476–478, Nov. 1980.
- [132] J. M. Dugan, A. J. Price, M. Ramadan et al., "All-Optical, Fiber-based 1550 nm Dispersion Compensation in a 10 Gb/s, 150 km Transmission Experiment over 1310 nm Optimized Fiber," in *Proc. of Optical Fiber Communication Conference OFC 1992*, San Jose, U.S.A, Feb. 1992, post-deadline paper PD14.
- [133] J.-C. Antona, S. Bigo and S. Kosmalski, "Nonlinear index measurements of various fibre types over C+L bands using four-wave mixing," in *Proc. of European Conference on Optical Communication ECOC 2001*, Amsterdam, Nederlands, 2001, We.L.1.2.
- [134] T. Georges, "Extended Path-Averaged Soliton Regime in Highly Dispersive Fibers," *Optics Letters*, vol. 22, no. 10, p. 679–681, May 1997.
- [135] R. I. Killey, H. J. Thiele, V. Mikhailov, and P. Bayvel, "Reduction of Intrachannel Nonlinear Distortion in 40-Gb/s-based WDM Transmission over Standard Fiber," *Photonics Technology Letters*, vol. 12, no. 12, pp. 1624–1626, Dec. 2000.
- [136] A. Sano, Y. Miyamoto, S. Kuwahara, and H. Toba, "A 40-Gb/s/ch WDM Transmission with SPM/XPM Suppression Through Prechirping and Dispersion Management," *Journal of Lightwave Technology*, vol. 18, no. 11, pp. 1519–1527, Nov. 2000.
- [137] M. Shtaif, "Analytical Description of Cross-Phase Modulation in Dispersive Optical Fibers," *Optics Letters*, vol. 23, no. 15, p. 1191–1193, Aug. 1998.
- [138] A. V. T. Cartaxo, "Cross-Phase Modulation in Intensity Modulation-Direct Detection WDM Systems with Multiple Optical Amplifiers and Dispersion Compensators," *Journal of Lightwave Technology*, vol. 17, no. 2, p. 178–190, Feb. 1999.
- [139] Y Frignac, J.-C. Antona, S. Bigo, J.-P. Hamaide, "Numerical optimization of pre- and in-line dispersion compensation in dispersion-managed systems at 40

- Gbit/s,” in *Proc. of Optical Fiber Communication Conference OFC 2002*, San Jose, U.S.A, Feb. 2002, paper Th.F.F5.
- [140] J.-C. Antona, M. Lefrançois, S. Bigo, G. Le Meur, “Investigation of Advanced Dispersion Management Techniques for Ultra-Long Haul Transmissions”, in *Proc. of European Conference on Optical Communication ECOC 2005*, Glasgow, Scotland, 2005, Mo.3.2.6.
- [141] A. G. Striegler and B. Schmauss, “Compensation of intrachannel effects in symmetric dispersion-managed transmission systems,” *Journal of Lightwave Technology*, vol. 22, no. 8, pp. 1877–1882, Aug. 2004.
- [142] N. Kikuchi, K. Sekine, and S. Sasaki, “Analysis of Cross-Phase Modulation (XPM) Effect on WDM Transmission Performance,” *Electronics Letters*, vol. 33, no. 8, p. 653–654, Apr. 1997.
- [143] T.-K. Chiang, N. Kagi, T. K. Fong et al., “Cross-Phase Modulation in Dispersive Fibers: Theoretical and Experimental Investigation of the Impact of Modulation Frequency,” *Photonics Technology Letters*, vol. 6, no. 6, p. 733–736, Jun. 1994.
- [144] N. S. Bergano, J. Aspell, C. R. Davidson, P. R. Trischitta, B. M. Nyman, and F. W. Kerfoot, “A 9000 km 5 Gb/s and 21,000 km 2.4 Gb/s Feasibility Demonstration of Transoceanic EDFA Systems Using a Circulating Loop,” in *Proc. of Optical Fiber Communication Conference OFC 1991*, Sa Diego, U.S.A, Feb. 1991, paper PD13.1.
- [145] D. J. Maylon, T. G. Hodgkinson, D. W. Smith, R.C. Booth, and B.E. Daymond-John, “PSK Homodyne Receiver Sensitivity Measurements at  $1.5\mu\text{m}$ ,” *Electronic Letters*, vol. 19, no. 4, pp. 144–146, Feb. 1983.
- [146] P. Schvan, D. Pollex, S.-C. Wan, Chris Falt, and Naim Ben-Hamida, “A 22GS/s 5b ADC in  $0.13\mu\text{m}$  SiGe BiCMOS,” in *Proc. IEEE International Solid-State Circuits Conference. (ISSCC)*, San Francisco, CA, U.S.A., Feb. 2006, paper 31.4.
- [147] P. Schvan, J. Bach, C. Falt et al., “A 24GS/s 6b ADC in 90nm CMOS,” in *Proc. IEEE International Solid-State Circuits Conference. (ISSCC)*, San Francisco, CA, U.S.A., Feb. 2008, paper 30.3.
- [148] D. J. Maylon, “Digital Fibre Transmission using Optical Homodyne Detection,” *Electronic Letters*, vol. 20, no. 7, pp. 281–283, Mar. 1984.
- [149] R. A. Linke, B. L. Kasper, N. A. Olsson, and R. C. Alferness, “Coherent Ligthwave Transmission over 150 km Fibre Lengths at 400 Mbit/s and 1 Gbit/s Data Rates using Phase Modulation,” *Electronic Letters*, vol. 22, no. 1, pp. 30–31, Jan. 1986.
- [150] E. Basch and T. Brown, “Introduction to coherent optical fiber transmission,” *IEEE Communications Magazine*, vol. 23, no. 5, pp. 23–30, May 1985.
- [151] G. Nicholson, “Probability of the Error for Optical Hetrodyne DPSK System with Quantum Phase Noise,” *Electronic Letters*, vol. 20, no. 24, pp. 1005–1007, Nov. 1984.

- [152] A. W. Davis, M. J. Pettitt, J. P. King, and S. Wright, "Coherent Optical Receiver for 680 Mbit/s using Phase Diversity," *Electronic Letters*, vol. 22, no. 1, pp. 9–11, Jan. 1986.
- [153] A. W. Davis, M. J. Pettitt, J. P. King, and S. Wright, "Phase Diversity Techniques for Coherent Optical Receivers," *Journal of Lightwave Technology*, vol. 5, no. 4, pp. 561–571, Apr. 1987.
- [154] F. Derr, "Optical QPSK Transmission System with Novel Digital Reciever concept," *Electronic Letters*, vol. 27, no. 23, pp. 2177–2179, Nov. 1991.
- [155] T. Okoshi, S. Ryu, and K. Kikuchi, "Polarization-Diversity Receiver for Heterodyne/Coherent Optical Fiber Communications," in *Proc. Integr. Optics and Optical Fiber Commun. Conf. (IOCC)*, Tokyo, Japan, Jun. 1983, paper 3OC3-2.
- [156] T. Okoshi and Y. H. Cheng, "Four-port Homodyne Receiver for Optical Fibre Communications Compromising Phase and Polarization Diversities," *Electronic Letters*, vol. 23, no. 8, pp. 377–388, Apr. 1987.
- [157] S. R. Chinn, D. M. Boroson, and J. C. Livas, "Sensitivity of optically preamplified DPSK receivers with Fabry-Perot filters," *Journal of Lightwave Technology*, vol. 14, pp. 370-376, Mar. 1996.
- [158] B. Sklar, *Digital Communications: Fundamentals and Applications*, 2nd ed. Prentice Hall PTR, 2001.
- [159] I. P. Kaminow, T. Li, A. E. Willner, *Optical Fiber Telecommunications VA & VB: Systems and Networks*, Academic Press, 2008.
- [160] C. Chen, *Elements of Optoelectronics and Fiber Optics*, 1st ed. Irwin Professional Publishing, 1996.
- [161] S. Tsukamoto, Y. Ishikawa, and K. Kikuchi, "Optical homodyne receiver comprising phase and polarization diversities with digital signal processing," in *Proc. of European Conference on Optical Communication ECOC 2006*, Cannes, France, Sept. 24–28, 2006, paper Mo4.2.1
- [162] E. Ip and J. M. Kahn, "Feedforward Carrier Recovery for Coherent Optical Communications," *Journal of Lightwave Technology*, vol. 25, no. 9, pp. 2675–2692, Sep. 2007.
- [163] N. Benvenuto and G. Cherubini, *Algorithms for Communications Systems and their Applications*, 1st ed. Wiley, 2002.
- [164] P. J. Winzer, A. H. Gnauck, C. R. Doerr, M. Magarini, and L. L. Buhl, "Spectrally Efficient Long-Haul Optical Networking Using 112-Gb/s Polarization-Multiplexed 16-QAM," *Journal of Lightwave Technology*, vol. 28, no. 4, pp. 547–556, Feb. 2010.
- [165] S. J. savory, "Digital filters for coherent detection," *Optics Express*, Vol. 16, Issue 2, pp 804-817, 2008.
- [166] E. Ip, "Nonlinear Compensation Using Backpropagation for Polarization-Multiplexed Transmission," *Journal of Lightwave Technology*, vol. 28, no. 6 pp. 939-951, Mar. 2010.

- [167] D.S. Millar, S. Makovejs, V. Mikhailov, R.I. Killey, P. Bayvel, and S. J. Savory, "Experimental comparison of nonlinear compensation in long-haul PDM-QPSK transmission at 42.7 and 85.4 Gb/s," in *Proc. of European Conference on Optical Communication ECOC 2009*, Vienna, Austria, Sept. 2009, paper 9.4.4.
- [168] S. J. Savory, G. Gavioli, E. Torrengo, and P. Poggolini, "Impact of Interchannel Nonlinearities on a Split-Step Intrachannel Nonlinear Equalizer," *IEEE Photonics Technology Letters*, vol. 22, no. 10, Jan. 1, 2009.
- [169] G. Charlet, J. Renaudier, H. Mardoyan, P. Tran, O. Bertran-Pardo, F. Verluise, M. Achouche, A. Boutin, F. Blache, J.-Y. Dupuy and S. Bigo, "Transmission of 16.4Tbit/s Capacity over 2,550km Using PDM QPSK Modulation Format and Coherent Receiver", in *Proc. of Optical Fiber Communication Conference OFC 2008*, San Diego, USA, Feb. 2008, Paper PDP3.
- [170] C. R. S. Fludger, T. Duthel, D. van den Borne, C. Schulien, E.-D. Schmidt, T. Wuth, J. Geyer, E. De Man, G.-D. Khoe and H. de Waardt, "Coherent Equalization and POLMUX-RZ-DQPSK for Robust 100-GE Transmission", *Journal of Lightwave Technology*, vol. 26, No. 1, Jan. 2008.
- [171] S. J. Savory, A. D. Stewart, S. Wood, G. Gavioli, M. G. Taylor, R. I. Killey, and P. Bayvel, "Digital Equalisation of 40Gbit/s per Wavelength Transmission over 2480km of Standard Fibre Without Optical Dispersion Compensation," in *Proc. of European Conference on Optical Communication ECOC 2006*, Cannes, France, Sept. 2006, paper Th2.5.5.
- [172] A. J. Viterbi and A. M. Viterbi, "Nonlinear Estimation of PSK-Modulated Carrier Phase with Application to Burst Digital Transmission", *IEEE Transaction on Information Theory*, Vol. IT-29, No. 4, pp. 543-551, 1983.
- [173] O. Bertran-Pardo, J. Renaudier, G. Charlet, H. Mardoyan, P. Tran and S. Bigo, "Nonlinearity Limitations when Mixing 40Gb/s Coherent PDM-QPSK Channels with Preexisting 10Gb/s NRZ Channels, " *Photonics Technology Letters*, vol 20, no 15, Aug. 1, 2008.
- [174] D. van den Borne, C. R. S. Fludger, T. Duthel, T. Wuth, E. D. Schmidt, C. Schulien, E. Gottwald, G. D. Khoe and H. de Waardt, "Carrier phase estimation for coherent equalization of 43-Gb/s POLMUX-NRZ-DQPSK transmission with 10.7-Gb/s NRZ neighbours," in *Proc. of European Conference on Optical Communication ECOC 2007*, Berlin, Germany, Sept. 2007, paper We7.2.3.
- [175] M. Bertolini, P. Serena, G. Bellotti and A. Bononi, "On the XPM-induced distortion in DQPSK-OOK and Coherent QPSK-OOK Hybrid Systems," in *Proc. of Optical Fiber Communication Conference OFC 2009*, San Diego, USA, Feb. 2009, paper OTuD4.
- [176] A. Leven, N. Kaneda, U.-V. Koc, and Y.-K. Chen, "Frequency Estimation in Intradyne Reception," *Photonics Technology Letters*, vol. 19, no 6, pp. 366-368, 2007.

- [177] D.-S. Ly-Gagnon, S. Tsukamoto, K. Katoh and K. Kikuchi, "Coherent detection of optical quadrature phase-shift keying signals with carrier phase estimation," *Journal of Lightwave Technology*, vol. 24, no. 1, pp. 12–21, Jan. 2006.
- [178] G. Charlet, N. Maaref, J. Renaudier, H. Mardoyan, P. Tran, S. Bigo, "Transmission of 40Gb/s QPSK with Coherent Detection over Ultra-Long Distance Improved by Nonlinearity Mitigation", in *Proc. of European Conference on Optical Communication ECOC 2006*, Cannes, France, Sept. 2006, paper Th4.3.
- [179] C. Laperle Laperle, B. Villeneuve, Z. Zhang, D. McGhan, H. Sun, and M. O'Sullivan, "Wavelength Division Multiplexing (WDM) and Polarization Mode Dispersion (PMD) Performance of a Coherent 40Gbit/s Dual-Polarization Quadrature Phase Shift Keying (DP-QPSK Transceiver)," in *Proc. of Optical Fiber Communication Conference OFC 2007*, Anaheim, USA, Feb. 2007 paper PDP16.
- [180] J. Renaudier, G. Charlet, M. Salsi, O. Bertran-Pardo, H. Mardoyan, P. Tran, and S. Bigo, "Linear fiber impairments mitigation of 40-Gbit/s polarization multiplexed QPSK by digital processing in a coherent receiver," *Journal of Lightwave Technology*, vol. 26, no. 1, pp. 36–42, Jan. 2008.
- [181] A. Bononi, P. Serena and N. Rossi, "Nonlinear Limits in Single- and Dual-Polarization Transmission," *IEEE/LEOS Summer Topical Meeting 2010*, Acapulco, Mexico, July 2010, invited paper.
- [182] C. Xie, S. Chandrasekhar and X. Liu, "Impact of Inter-Channel Nonlinearities on 10-Gbaud NRZ-DQPSK WDM Transmission over Raman Amplified NZDSF Spans", in *Proc. of European Conference on Optical Communication ECOC 2007*, Berlin, Germany, Sept. 2007, paper Th 10.4.3.
- [183] M.R. Phillips, S.L. Woodward, "Cross-Polarization Modulation: Theory and Measurement of a Two-Channel WDM System", *IEEE Photonics Technology Letters*, vol. 17, no 10, p. 2086-2088, Oct. 2005.
- [184] C. Fürst, J-P. Elbers, C. Scheerer, C. Glingener, "Limitations of dispersion managed DWDM systems due to cross-phase modulation", *IEEE LEOS annual meeting 2000*, Rio Grande, Puerto Rico, Nov. 2000, paper MB3.
- [185] D. van den Borne, N. E. Hecker-Denschlag, G.-D. Khoe, and H. de Waardt, "Cross phase modulation induced depolarization penalties in 2x10Gb/s polarization-multiplexed transmission", in *Proc. of European Conference on Optical Communication ECOC 2004*, Stockholm, Sweden, Sept. 2004, paper Mo.4.5.5.
- [186] J. Renaudier, O. Bertran-Pardo, G. Charlet, M. Salsi, M. Bertolini, P. Tran, H. Mardoyan, and S. Bigo, "Investigation on WDM Nonlinear Impairments Arising from the Insertion of 100Gb/s Coherent PDM-QPSK over Legacy Optical Networks, " *IEEE Photonics Technology Letters*, vol. 21, no 24, p. 1816-1818, Dec. 2009.
- [187] O. Bertran-Pardo, J. Renaudier, G. Charlet, M. Salsi, M. Bertolini, H. Mardoyan, P. Tran, C. Koebel, and S. Bigo, "PDM-QPSK: on the system

- benefits arising from temporally interleaving polarization tributaries at 100Gb/s," *Optics Express*, vol. 17, no 22, pp. 19902-19907, 2009.
- [188] P. Serena, N. Rossi and A. Bononi, "Nonlinear Penalty Reduction Induced by PMD in 112 Gbit/s WDM PDM-QPSK Coherent Systems," in *Proc. of European Conference on Optical Communication ECOC 2009*, Vienna, Austria, 2009, paper 10.4.3.
- [189] O. Bertran-Pardo, J. Renaudier, G. Charlet, P. Tran, H. Mardoyan, M. Salsi, M. Bertolini, and S. Bigo, "Insertion of 100Gb/s Coherent PDM-QPSK Channels over Legacy Optical Networks Relying on Low Chromatic Dispersion Fibres," in *Proc. IEEE Global Telecommunications GLOBECOM 2009*, Honolulu, Hawaii, USA, Dec. 2009, paper ONS.04.1.
- [190] D. van den Borne, S. L. Jansen, E. Gottwald, P. M. Krumrich, G. D. Khoe, and H. de Waardt, "1.6-b/s/Hz Spectrally Efficient Transmission Over 1700 km of SSMF Using 40 × 85.6-Gb/s POLMUX-RZ-DQPSK," *Journal of Lightwave Technology*, vol. 25, no. 1, pp. 222–232, Jan. 2007.
- [191] J. Renaudier, G. Charlet, O. Bertran-Pardo, H. Mardoyan, P. Tran, M. Salsi, and S. Bigo, "Experimental Analysis of 100Gb/s Coherent PDM-QPSK Long-Haul Transmission under Constraints of Typical Terrestrial Networks," in *Proc. of European Conference on Optical Communication ECOC 2008*, Brussels, Belgium, 2008, paper Th 2.A.3.
- [192] J. Renaudier, G. Charlet, O. Bertran-Pardo, H. Mardoyan, P. Tran, M. Salsi and S. Bigo, "Transmission of 100Gb/s Coherent PDM-QPSK over 16x100km of Standard Fiber with all-erbium amplifiers", *Optics Express*, vol. 17, no 7, pp. 5112-5119, March 2009.
- [193] J. Renaudier, O. Bertran-Pardo, H. Mardoyan, P. Tran, G. Charlet, S. Bigo, M. Lefrançois, B. Lavigne, J.-L. Augé, L. Pirou, and O. Courtois, "Performance Comparison of 40G and 100G Coherent PDM-QPSK for Upgrading Dispersion Managed Legacy Systems", in *Proc of National Fiber Optic Engineers Conference NFOEC 2009*, San Diego, USA, Mar. 2009, paper NWD5.
- [194] T.J. Xia, G. Wellbrock, D. Peterson, W. Lee, M. Pollock, B. Basch, D. Chen, M. Freiberger, M. Alfiad, H. de Waardt, M. Kuschnerov, B. Lankl, T. Wuth, E.D. Schmidt, B. Spinnler, C.J. Weiske, E. de Man, C. Xie, D. van den Borne, M. Finkenzeller, S. Spaelter, R. Derksen, M. Rehman, J. Behel, J. Stachowiak, and M. Chbat, "Multi-Rate (111-Gb/s, 2x43-Gb/s, and 8x10.7-Gb/s) Transmission at 50-GHz Channel Spacing over 1040-km Field-Deployed Fiber," in *Proc. of European Conference on Optical Communication ECOC 2008*, Brussels, Belgium, 2008, paper Th.2.E.2.
- [195] M. S. Alfiad, D. van den Borne, S. L. Jansen, T. Wuth, M. Kuschnerov, G. Grossi, A. Napoli, and H. de Waardt, "A Comparison of Electrical and Optical Dispersion Compensation for 111-Gb/s POLMUX-RZ-DQPSK," *Journal of Lightwave Technology*, vol. 27, no. 16, pp. 3590–3598, Aug. 2009.

- [196] N. S. Bergano, F. W. Kerfoot, and C. R. Davidson, "Margin measurements in optical amplifier system," *Photonics Technology Letters*, vol. 5, no. 3, pp. 304 – 306, Mar. 1993.
- [197] T. Miyakawa, I. Morita, K. Tanaka, H.a Sakata and N. Edagawa, "2.56Tbit/s (40Gbit/s x 64WDM) Unrepeateder 230km Transmission with 0.8bit/s/Hz Spectral Efficiency Using Low-Noise Fiber Raman Amplifier and 170pm<sup>2</sup>-Aeff Fiber", in *Proc. of Optical Fiber Communication Conference OFC 2001*, Anaheim, CA, U.S.A., Mar. 2001, paper PDP26-1.
- [198] H. Bissessur, F. Boubal, S. Gauchard, A. Hugbart, L. Labrunie, P. Le Roux, J-P. Hebert and E. Brandon, "1.28 Tb/s (32 x 43 Gb/s) WDM Unrepeateder Transmission over 402 km", in *Proc. of European Conference on Optical Communication ECOC 2003*, Rimini, Italy, Sep. 2003, paper Tu.1.6.3.
- [199] Mei Du, Jianjun Yu, Xiang Zhou, "Unrepeateder Transmission of 107 Gb/s RZ-DQPSK over 300km NZDSF with Bi-directional Raman Amplification", in *Proc. of Optical Fiber Communication Conference OFC 2008*, San Diego, USA, Feb. 2008, paper JThA47.



# Publications

## As first author

- [I] O. Bertran-Pardo, J. Renaudier, H. Mardoyan, P. Tran, G. Charlet, and S. Bigo, “Investigation of Design Options for Overlaying 40Gb/s Coherent PDM-QPSK Channels over a 10Gb/s System Infrastructure,” in *Proc. of Optical Fiber Communication Conference OFC 2008*, San Diego, USA, Feb. 2008, paper OtuM5.
- [II] O. Bertran-Pardo, J. Renaudier, G. Charlet, H. Mardoyan, P. Tran, and S. Bigo, “Nonlinearity Limitations when Mixing 40Gb/s Coherent PDM-QPSK Channels with Preexisting 10Gb/s NRZ Channels,” *IEEE Photonics Technology Letters*, vol. 20, no 15, Aug.1, 2008.
- [III] O. Bertran-Pardo, J. Renaudier, G. Charlet, P. Tran, H. Mardoyan, M. Salsi, and S. Bigo, “Impact of nonlinear impairments on the tolerance to PMD of 100Gb/s PDM-QPSK data processed in a coherent receiver,” in *Proc. of European Conference on Optical Communication ECOC 2008*, Brussels, Belgium, Sept. 2008, paper We3.E.1.
- [IV] O. Bertran-Pardo, J. Renaudier, G. Charlet, P. Tran, H. Mardoyan, M. Salsi, and S. Bigo, “Experimental Assessment of Interactions Between Nonlinear Impairments and to Polarization Mode Dispersion in 100Gb/s Coherent Systems versus Receiver Complexity,” *IEEE Photonics Technology Letters*, vol 21, no 1, Jan.1, 2009.
- [V] O. Bertran-Pardo, J. Renaudier, G. Charlet, M. Salsi, M. Bertolini, P. Tran, H. Mardoyan, C. Koebele, and S. Bigo, “System Benefits of Temporal Polarization Interleaving with 100Gb/s Coherent PDM-QPSK,” in *Proc. of European Conference on Optical Communication ECOC 2009*, Vienna, Austria, Sept. 2009, paper Th.9.4.1.
- [VI] O. Bertran-Pardo, J. Renaudier, G. Charlet, P. Tran, H. Mardoyan, M. Salsi, M. Bertolini, and S. Bigo, “Insertion of 100Gb/s Coherent PDM-QPSK Channels over Legacy Optical Networks Relying on Low Chromatic Dispersion Fibres,” in *Proc. IEEE Global Telecommunications GLOBECOM 2009*, Honolulu, Hawaii, USA, Dec. 2009, paper ONS.04.1.
- [VII] O. Bertran-Pardo, D. Mongardien, P. Bousselet, P. Tran, H. Mardoyan, J. Renaudier, and H. Bissessur, “Transmission of 2.6-Tb/s using 100Gb/s PDM-QPSK Paired with a Coherent Receiver Over a 401-km Unrepeatered Link,” *IEEE Photonics Technology Letters*, vol. 21, no 23, Dec.1, 2009.
- [VIII] O. Bertran-Pardo, J. Renaudier, G. Charlet, M. Salsi, M. Bertolini, H. Mardoyan, P. Tran, C. Koebele, and S. Bigo, “PDM-QPSK: on the system benefits arising from temporally interleaving polarization tributaries at 100Gb/s,” *Optics Express*, vol. 17, no 22, pp. 19902-19907, 2009.

- [IX] O. Bertran-Pardo, J. Renaudier, G. Charlet, M. Salsi, P. Tran, H. Mardoyan and S. Bigo, "Digital Signal Processing in Coherent Receivers for 100 Gb/s Ultra Long-Haul Applications," *OSA Topical Meeting 2010, Signal Processing in Photonic Communications (SPPCom)*, Karlsruhe, Germany, June 2009, invited paper SPWA3.
- [X] O. Bertran-Pardo, J. Renaudier, G. Charlet, P. Tran, H. Mardoyan, M. Bertolini, M. Salsi, and S. Bigo, "Demonstration of the benefits brought by PMD in polarization multiplexed systems," in *Proc. of European Conference on Optical Communication ECOC 2010*, Torino, Italy, Sept. 2010, to be published.

## As co-author

- [XI] G. Charlet, M. Salsi, J. Renaudier, O. Bertran-Pardo, H. Mardoyan, and S. Bigo, "Performance comparison of singly-polarized and polarisation-multiplexed coherent transmission at 10Gbauds under linear impairments," in *Proc. of European Conference on Optical Communication ECOC 2007*, Berlin, Germany, Sept. 2007, paper We7.2.2.
- [XII] M. Salsi, J. Renaudier, G. Charlet, O. Bertran-Pardo, P. Tran, and S. Bigo, "Investigation of single channel nonlinear impairments on 40Gb/s coherent Polarization Division Multiplexed QPSK in dispersion managed and uncompensated systems," in *Proc. of European Conference on Optical Communication ECOC 2007*, Berlin, Germany, Sept. 2007, paper Th10.4.2.
- [XIII] G. Charlet, J. Renaudier, H. Mardoyan, O. Bertran-Pardo, F. Cérou, P. Tran, and S. Bigo, "12.8Tbit/s Transmission of 160 PDM-QPSK (160x2x40Gbit/s) Channels with Coherent Detection over 2,550km," in *Proc. of European Conference on Optical Communication ECOC 2007*, Berlin, Germany, Sept. 2007, paper PDP17.
- [XIV] G. Charlet, M. Salsi, J. Renaudier, O. Bertran-Pardo, H. Mardoyan, and S. Bigo, "Performance comparison of singly-polarized and polarisation-multiplexed coherent transmission at 10Gbauds under linear impairments," *Electronics Letters*, vol. 43, issue 20, Sept. 27, 2007.
- [XV] J. Renaudier, G. Charlet, M. Salsi, O. Bertran-Pardo, H. Mardoyan, P. Tran, and S. Bigo, "Linear fiber impairments mitigation of 40-Gbit/s polarization multiplexed QPSK by digital processing in a coherent receiver," *Journal of Lightwave Technology*, vol. 26, no. 1, pp. 36–42, Jan. 2008.
- [XVI] G. Charlet, J. Renaudier, O. Bertran-Pardo, P. Tran, H. Mardoyan, and S. Bigo, "Performance comparison of singly-polarized and polarization-multiplexed at 10Gbaud under nonlinear impairments", in *Proc. of Optical Fiber Communication Conference OFC 2008*, San Diego, USA, Feb. 2008, paper OthU8.
- [XVII] G. Charlet, J. Renaudier, H. Mardoyan, P. Tran, O. Bertran-Pardo, F. Verluse, M. Achouche, A. Boutin, F. Blache, J.-Y. Dupuy, and S. Bigo, "Transmission of 16.4Tbit/s Capacity over 2,550km Using PDM QPSK Modulation Format and Coherent Receiver," in *Proc. of Optical Fiber Communication Conference OFC 2008*, San Diego, USA, Feb. 2008, paper PDP3.
- [XVIII] J. Renaudier, G. Charlet, O. Bertran-Pardo, H. Mardoyan, P. Tran, M. Salsi, and S. Bigo, "Experimental Analysis of 100Gb/s Coherent PDM-QPSK Long-Haul

- Transmission under Constraints of Typical Terrestrial Networks," in *Proc. of European Conference on Optical Communication ECOC 2008*, Brussels, Belgium, 2008, Th 2.A.3.
- [XIX] J. Renaudier, G. Charlet, O. Bertran-Pardo, H. Mardoyan, P. Tran, M. Salsi, and S. Bigo, "Transmission of 100Gb/s Coherent PDM-QPSK over 16x100km of Standard Fiber with all-erbium amplifiers," *Optics Express*, vol. 17, no 7, pp. 5112-5119, Mar. 2009.
  - [XX] J. Renaudier, O. Bertran-Pardo, H. Mardoyan, P. Tran, M. Salsi, G. Charlet, and S. Bigo, "Impact of Temporal Interleaving of Polarization Tributaries onto 100Gb/s coherent transmission systems with RZ Pulse carving," *IEEE Photonics Technology Letters*, Vol. 20, Issue 24, p. 2036-2038, Dec. 2008.
  - [XXI] G. Charlet, J. Renaudier, H. Mardoyan, P. Tran, O. Bertran-Pardo, F. Verluse, M. Achouche, A. Boutin, F. Blache, J.-Y. Dupuy, and S. Bigo, "Transmission of 16.4Tbit/s Capacity over 2,550km using PDM QPSK Modulation Format and Coherent Receiver," *Journal of Lightwave Technology*, vol. 27, issue 3, Feb. 2009.
  - [XXII] S. Bigo, G. Charlet, O. Bertran-Pardo, and J. Renaudier, "Characterization of the Impact of Non-Linear Effects in Coherent Transmission Experiments," *LEOS Summer Topical Meeting 2008*, Acapulco, Mexico, July 2008, paper MC1.1.
  - [XXIII] J. Renaudier, G. Charlet, O. Bertran-Pardo, and S. Bigo, "Long-haul transmission systems involving coherent detection for linear impairments mitigation," *LEOS summer topical meeting 2008*, Acapulco, Mexico, July 2008, invited paper WD1.1.
  - [XXIV] J. Renaudier, O. Bertran-Pardo, H. Mardoyan, P. Tran, G. Charlet, S. Bigo, M. Lefrançois, B. Lavigne, J.-L. Augé, L. Pirou, and O. Courtois, "Performance Comparison of 40G and 100G Coherent PDM-QPSK for Upgrading Dispersion Managed Legacy Systems", in *Proc of National Fiber Optic Engineers Conference NFOEC 2009*, San Diego, USA, Mar. 2009, paper NWD5.
  - [XXV] S. Bigo, G. Charlet, O. Bertran-Pardo, and J. Renaudier, "Overlying coherent-detection channels over direct-detection channels in multi-bit-rate systems," in *Proc. of Optical Fiber Communication Conference OFC 2009*, San Diego, USA, Mar. 2009, paper OtuD1.
  - [XXVI] G. Charlet, J. Renaudier, P. Brindel, P. Tran, H. Mardoyan, O. Bertran-Pardo, M. Salsi, and S. Bigo, "Performance Comparision of DPSK, P-DPSK, RZ-DQPSK and Coherent PDM-QPSK at 40Gb/s over Terrestrial Link," in *Proc. of Optical Fiber Communication Conference OFC 2009*, San Diego, USA, Mar. 2009, paper JWA40.
  - [XXVII] G. Charlet, M. Salsi, P. Tran, M. Bertolini, H. Mardoyan, J. Renaudier, O. Bertran-Pardo, and S. Bigo, "72x100Gb/s Transmission over Transoceanic Distance, Using Large Effective Area Fiber, Hybrid Raman-Erbium Amplification and Coherent Detection," in *Proc. of Optical Fiber Communication Conference OFC 2009*, San Diego, USA, Mar. 2009, paper PDPB6.
  - [XXVIII] J. Renaudier, O. Bertran-Pardo, G. Charlet, M. Salsi, M. Bertolini, P. Tran, H. Mardoyan, and S. Bigo, "On the Required Number of WDM Channels When Assessing Performance of 100Gb/s Coherent PDM-QPSK Overlaying Legacy Systems," in *Proc. of European Conference on Optical Communication ECOC 2009*, Vienna, Austria, Sept. 2009, paper Tu.3.4.5.

- [XXIX] M. Bertolini, M. Salsi, G. Charlet, H. Mardoyan, P. Tran, O. Bertran-Pardo, J. Renaudier, and S. Bigo, "Single-Carrier vs. Dual-Carrier Transmission of 100Gb/s coherent PDM-QPSK over NZ-DSF Fibre," in *Proc. of European Conference on Optical Communication ECOC 2009*, Vienna, Austria, Sept. 2009, paper Mo.2.3.1.
- [XXX] D. Mongardien, P. Bousselet, O. Bertran-Pardo, P. Tran, and H. Bissessur, "2.6Tb/s (26 x 100Gb/s) Unrepeated Transmission Over 401km Using PDM-QPSK with a Coherent Receiver," in *Proc. of European Conference on Optical Communication ECOC'09*, Vienna, Austria, Sept. 2009, paper We.6.4.3.
- [XXXI] J. Renaudier, O. Bertran-Pardo, G. Charlet, M. Salsi, H. Mardoyan, P. Tran, and S. Bigo, "8Tb/s long-haul transmission over low dispersion fibres using 100 Gb/s PDM-QPSK channels paired with coherent detection," *Bell Labs Technical Journal*, vol. 14, no 4, p. 27-45, Dec. 2010.
- [XXXII] M. Salsi, G. Charlet, J. Renaudier, O. Bertran-Pardo, S. Bigo, P. Plantady, and A. Calsat "Recent advances in submarine optical communication systems," *Bell Labs Technical Journal*, vol. 14, no 4, p. 131-147, Dec. 2010.
- [XXXIII] J. Renaudier, O. Bertran-Pardo, G. Charlet, M. Salsi, M. Bertolini, P. Tran, H. Mardoyan, and S. Bigo, "Investigation on WDM Nonlinear Impairments Arising from the Insertion of 100Gb/s Coherent PDM-QPSK over Legacy Optical Networks," *IEEE Photonics Technology Letters*, vol. 21, no 24, p. 1816-1818, Dec. 2009.
- [XXXIV] F. Vacondio, J. Renaudier, O. Bertran-Pardo, P. Tran, H. Mardoyan, G. Charlet and S. Bigo, "Dual- versus single-carrier configuration for 40 Gb/s coherent BPSK-based solutions over low dispersion fibers," in *Proc. of Optical Fiber Communication Conference OFC 2010*, San Diego, USA, Feb. 2010, paper OTuL3.
- [XXXV] J.-P. Faure, B. Lavigne, C. Bresson , O. Bertran-Pardo, A. Carrasco Colomer and R. Cantó, "40G and 100G deployment on 10G Infrastructure: market overview and trends, Coherent versus Conventional technology," in *Proc. of Optical Fiber Communication Conference OFC 2010*, San Diego, USA, Feb. 2010, paper OThE3.
- [XXXVI] G. Charlet, M. Salsi, O. Bertran-Pardo, S. Bigo, P. Plantady, A. Calsat, "Technological challenges for field deployment and upgrade of multi-terabit/s submarine systems," *SubOptic 2010*, Yokohama, Japan.
- [XXXVII] S. Bigo, O. Bertran-Pardo, J. Renaudier, G. Charlet, "Nonlinear Impairments in coherent communication systems", *IEEE/LEOS Summer Topical Meeting 2010*, Acapulco, Mexico, July 2010, invited paper.
- [XXXVIII] J. Renaudier, O. Bertran-Pardo, P. Tran, L. Pierre, H. Mardoyan, G. Charlet and S. Bigo, "Nonlinear Tolerance of Ultra-Densely spaced 100Gb/s Coherent PDM-QPSK channels," in *Proc. of European Conference on Optical Communication ECOC 2010*, Torino, Italy, Sept. 2010, to be published.
- [XXXIX] M. Salsi, G. Charlet, O. Bertran-Pardo, J. Renaudier, H. Mardoyan, P. Tran, S. Bigo, "Experimental Comparison between Binary and Quadrature Phase Shift Keying at 40Gbit/s in a Transmission System Using Coherent Detection," in *Proc. of European Conference on Optical Communication ECOC 2010*, Torino, Italy, Sept. 2010, to be published.

- [XL] T. Zami, A. Morea, J. Renaudier, O. Rival, H. Mardoyan, O. Bertran-Pardo, J.-C. Antona, S. Bigo, “Higher capacity with smaller global energy consumption in core optical networks due to elastic channel spacing,” in *Proc. of European Conference on Optical Communication ECOC 2010*, Torino, Italy, Sept. 2010, to be published.



